Increasing the genetic diversity of cultivated barley: widening the primary gene pool for drought tolerance

Luis Manuel Guadarrama Escobar

Bachelor of Science in Biotechnology

Master of Agricultural Sciences

ORCID identifier: 0009-0009-5983-0010

Submitted in total fulfilment of the requirement for the degree of

Doctor of Philosophy in Agricultural Sciences

March 2025

Faculty of Science

School of Agriculture, Food and Ecosystem Sciences

The University of Melbourne

Abstract

Drought is one of the most significant environmental stressors affecting global agriculture. Crop wild relatives represent a valuable reservoir of drought tolerance, and their integration into primary breeding pools has been proposed through *de novo* domestication. This approach involves introgressing domestication traits from cultivated material while preserving the genetically complex drought adaptation mechanisms of wild relatives. Barley (*Hordeum vulgare* L.) is an ideal model for studying *de novo* domestication through conventional breeding methods due to the absence of crossing barriers between wild (*H. vulgare* ssp. *spontaneum*) and cultivated (*H. vulgare* ssp. *vulgare*) types. Until now, targeted integration strategies to fully harness the potential of wild germplasm for drought tolerance genetic improvement have been underexplored.

This thesis addresses critical gaps in the exploration, evaluation, selection, and integration of barley wild relatives to the cultivated gene pool by developing a holistic framework. This framework combines physiological, agronomic, and data-driven approaches for germplasm exploration and *de novo* domestication. The ultimate goal is to enhance the utilisation of wild genetic diversity in pre-breeding research. This framework was conceived to enhance the identification of drought-adaptive traits while reducing productivity loss under drought conditions and minimising yield penalties in favourable environments. The feasibility of the framework is demonstrated through the field experimental data, highlighting the relationship between a propsed image-based Transpiration Efficiency (iTE) index—derived from hyperspectral and thermal imaging—and agronomic performance, measured by a Tolerance Index (TOL).

A glasshouse phenotyping protocol for assessing drought tolerance was developed and applied to a random set of 120 wild accessions, using a multi-trait analysis combined with unbiased clustering techniques to evaluate and select drought-tolerant candidates. While there were clear treatment effects on canopy temperature depression CTD – a spectral proxy of transpiration – due to varying soil water content, the lack of interaction effects between genotype, treatment and time of measurement highlights opportunities to enhance the precision of current phenotyping methodologies. The multivariate analysis revealed a weak correlation between genetic and phenotypic diversity and allowed the classification of genotypes into distinct phenotypic clusters, providing insights into different drought response profiles.

Robust molecular markers were developed for three barley domestication genes controlling rachis brittleness (*Btr1*), dormancy (*Qsd1*) and awn roughness (*ROUGH AWN1*). These markers were

used for marker-assisted backcrossing (MABC) to facilitate the introgression of domestication traits from cultivated barley into wild backgrounds aiming to preserve genetically complex drought tolerance mechanisms. This process enabled the generation of BC2F3 *de novo*-domesticated lines, providing a valuable resource for further pre-breeding field research and physiological studies.

Finally, phenotypic responses of *de novo*-domesticated lines were characterised in comparison to their parental lines, confirming the feasibility of *de novo* domestication to retain genetically complex traits from wild relatives while improving their agricultural value for cultivation. This research contributes to a broader understanding of how wild germplasm can be leveraged for stress tolerance breeding via *de novo* domestication, offering practical strategies for integrating wild relatives into modern breeding programmes using emerging high-throughput phenotyping technologies.

Declaration

This is to certify that:

i. This thesis comprises only my original work towards the Doctor of Philosophy except where indicated in the preface.

ii. Due acknowledgement has been made in the text to all other material used.

iii. The thesis is fewer than the maximum word limit in length, exclusive of tables, maps, bibliographies, and appendices.

Luis Manuel Guadarrama Escobar
07/03/2025

Preface

This thesis consists of seven chapters, of which four (Chapter 3 to 6) are experimental. Chapter 2 has been published as a *Viewpoint* paper in *New Phytologist* journal (2025 impact factor 9.4), and therefore employs the pronoun "we" in several instances to recognise the contributions of co-authors to the manuscript. The abstract and introduction of this manuscript have been moved to Chapter 1 to reduce overlap in the first two chapters. As the primary author, my contribution to this publication exceeded 70% and included conceptualising the idea, drafting the main manuscript while integrating co-authors' feedback through multiple revisions, designing and refining all figures, and conducting additional investigations to obtain experimental evidence. The original manuscript is included at the end of the thesis, following the appendices.

The citation of Chapter 2 manuscript is as follows:

Guadarrama-Escobar LM, Hunt J, Gurung A, Zarco-Tejada PJ, Shabala S, Camino C, Hernandez P, Pourkheirandish M. 2024. Back to the future for drought tolerance. new phytologist 242(2 p.372-383): 383-372. DOI: 10.1111/nph.19619

Chapters 3 to 7 are designed for publication in international peer-reviewed journals; however, at the time of writing, they remain as *unpublished material in preparation for publication but not yet submitted*. To maintain consistency throughout the thesis, all figures, tables, and supplementary materials have been renumbered sequentially across chapters. Consolidated Reference and Appendix lists are provided at the end of the thesis. All figures presented in this thesis are original creations in collaboration with PhD supervisors and CropGEM members at the University of Melbourne. Finally, as this thesis is structured as a series of intended independent publications, it inevitably resulted in some degree of repetition throughout different chapters.

Acknowledgements

This research was made possible through financial support from the Australian Government Research Training Program (RTP) Scholarship through the University of Melbourne. This thesis would not have been possible without the support, guidance, and encouragement of my supervisory team Dr Allison Gurung, Prof. James Hunt, Prof. Pablo J. Zarco-Tejada, Dr Tomas Poblete Cisterna, and A/Prof. Mohammad Pourkheirandish. Your mentorship, patience, and willingness to provide critical insights and academic guidance have been invaluable throughout my PhD journey. A special thanks to Dr. Peter Aides and Cameron Patrick for their valuable input in statistical analysis on multiple occasions, and to Dr. Abdulqader Jighly and Dr. Osval A. Montesinos-Lopez for their expertise in genomic prediction models. To Dr Jochen Christopher Reif for his assistance with heritability analysis, and Dr Sergey Shabala for his support and endorsement of the ideas relating to plant physiology presented in the published paper. To Tim Rabanus-Wallace for his invaluable support and expertise in bioinformatics. To Ali Kiani-Pouya for his continuous support in the laboratory and glasshouse, as well as for his insightful and challenging discussions that strengthened my ideas.

I am especially grateful to Dr. Allison Gurung and A/Prof. Mohammad Pourkheirandish, whose early belief in my potential gave me the confidence to pursue a PhD to make meaningful contributions in the field of plant breeding. Their unwavering support, and mentorship have made a lasting impact on my academic growth.

I would also like to express my appreciation to Burnley staff—Rowan Berry and Brett Hough—for their technical support of the polytunnels used for plants. To my research colleagues in the CropGEM laboratory for their valuable discussions and support in troubleshooting challenges and generating new ideas. A special mention to Nirmal Raj Rajendran, Lucas Reber, Kelly Rodgers, Claire Huang and Abhijith—thank you for the stimulating discussions, feedback and companionship. To Asha Gould and Marcus Williams for doing an amazing job developing two of the three molecular markers essential for my research and their repeated help throughout many experiments in the field, glasshouse, laboratory.

I extend my deepest gratitude to my family—my mum Dora M. Escobar Juarez, my dad Luis M. Guadarrama-Ortiz, my sister Erika Guadarrama-Escobar, my uncle Juan A. Guadarrama-Ortiz and my aunt Maricela Avalos—for their love and support. To my close friends, Xavier Sanchez, Omar Castrejon, Andrés Culebro, Irving Perez, Erik Buxmann, Ana K. Parra, Violeta Carrillo, José Celada and Sulyn Cárdenas for their patience every time I neglected to respond to messages

or disappeared into my research, and for being amazing friends throughout this journey. My in-laws, Brian and Fiona Dickson, and sister-in-law, Genevieve Dickson, for their kindness, support, and for making me feel like part of the family—thank you for your love, patience, and encouragement. And last but not least, to my wife, Stephanie Dickson, the person who has been my greatest source of strength, my motivation to every challenge, and my constant reminder of what truly matters. Your love, patience, and boundless support have carried me through this journey, and no words can fully capture how much you mean to me. This achievement is as much yours as it is mine.

This thesis is the result of years of collaboration, and I am truly grateful to all who have contributed to its success.

Table of Contents

List of Tables

List of Figures

List of Abbreviations

Abbreviation	Meaning
A	Carbon assimilation
Anth	Anthocyanins
BC	Backcross
BLUE	Best Linear Unbiased Estimate
CAPS	Cleaved Amplified Polymorphic Sequence
CCC	Cophenetic Correlation Coefficient
Chl	Chlorophyll
CID	Carbon Isotope Discrimination
CTD	Canopy Temperature Depression
CV	Cross Validation
CWSI	Crop Water Stress Index
DAS	Days After Sowing
dCAPS	derived Cleaved Amplified Polymorphic Sequence
DW	Dry Weight
FC	Field Capacity
FIGS	Focused Identification of Germplam Strategy
Flav	Flavonoids
FW	Fresh Weight
g_{sw}	Stomatal Conductance to Water Vapour
GBLUP	Genomic Best Linear Unbiased Prediction
GLM	Generalized Linear Model
GRM	Genomic Relationship Matrix
GWAS	Genome-Wide Association Study
h^2	Narrow-sense Heritability
H^2	Broad-Sense Heritability
HI	Harvest Index
iTE	Image-based Transpiration Efficiency
IWBSC	International Wild Barley Sequencing Consortium
L_v	Latent Heat of Vaporization
LMA	Leaf Mass per Area
LMM	Linear Mixed Model
LOOCV	Leave-One-Out Cross-Validation
LWIR	Long-Wave Infrared
MABC	Marker-Assisted Backcrossing
MAE	Mean Absolute Error
MP	Mean Productivity

NBHI	Narrow-Band Hyperspectral Index
NBI	Nitrogen-Balance Index
NPQ	Non-Photochemical Quenching
PC	Principal Component
PCA	Principal Component Analysis
PCR	Polymerase Chain Reaction
PLSR	Partial Least Squares Regression
R_v	Specific Gas Constant for Water Vapour
RBF	Radial Basis Function
RCS	Response to Closing Stimuli
RMSE	Root Mean Square Error
ROS	Reactive Oxygen Species
SEM	Standard Error of the Mean
SIF	Solar-Induced Fluorescence
SNP	Single Nucleotide Polymorphism
SVR	Support Vector Regression
SWC	Soil Water Content
SWIR	Short-Wave Infrared
T	Transpiration rate
T_a	Ambient Temperature
T_c	Canopy Temperature
TE	Transpiration Efficiency
TOL	Tolerance Index
UAV	Unmanned Aerial Vehicle
VCF	Variant Call Format
V_{cmax}	Maximum Rate of Carboxylation
VIF	Variandce Inflation Factor
VPD	Vapour Pressure Deficit
WBDC	Wild Barley Diversity Collection
WUE	Water Use Efficiency

Chapter 1
General Introduction

1.1 Background

The rising global population is projected to reach 10.9 billion by 2100, coupled with dietary shifts towards higher meat consumption, reinforce the demand for sustainable food production (Adam, 2021). These challenges are further intensified by climate change and global warming. Drought stands out as the most damaging abiotic stressor worldwide, causing annual losses of US$80 billion (Razzaq *et al.*, 2021). Despite previous genetic improvements that have improved productivity, yield gains for key crops such as wheat, rice, maize, and barley are slowing down. This indicates potential limitations of current breeding resources and selection strategies (Araus *et al.*, 2018).

1.2 Genetic erosion and vulnerability of modern crops

Ancient farmers selected beneficial traits during the domestication of crops including reduced natural dispersal mechanisms and reduced seed dormancy. These agronomically valuable traits are the result of naturally occurring mutations selected by humans either deliberately or unintentionally. The selected mutations were maintained, leading to a rapid increase in allele frequency with each generation until these traits became fixed within the population. The repeated cultivation of the same genotypes has restricted the diversity in cultivated crops. This bottleneck effect has occurred at different phases during the history of agriculture (Figure 1.1).

Genetic diversity is crucial for crop improvement, as breeders rely on it to enhance yield and resilience to biotic (living) and abiotic (non-living or environmental) stresses. Genetic diversity has two main components: recombination, which involves chromosome shuffling to produce new allele combinations, and DNA mutation, which creates allelic diversity. Modern breeding has extensively relied upon recombination to improve domesticated cultivars via artificial hybridisation programs, however, this relies on diversity already within the cultivated varieties. The occurrence of domestication events in crop species has typically been limited, for example, in barley, grain retention on spike (non-brittle rachis) has been selected twice by two independent groups of ancient farmers during barley domestication. Thus, a chromosomal segment, including the non-brittle rachis and surrounding genes, is limited to only two alleles passed through the domestication bottleneck. Allele diversity of genes located in other loci unlinked to the

domesticated trait (neutral genes) is also limited in domesticated gene pool to a few lines selected and retained during the domestication by early farmers (Doebley *et al.*, 2006). This genetic erosion within the cultivated gene pool negatively impacted the resilience and adaptive capacity of crops, further worsened with agriculture intensification during the Green Revolution in the 1960s (Zhao *et al.*, 2010; He *et al.*, 2015; Khoury *et al.*, 2021). Wild germplasm are an underexploited genetic resource that can potentially improve the resilience and sustainability of agricultural systems.

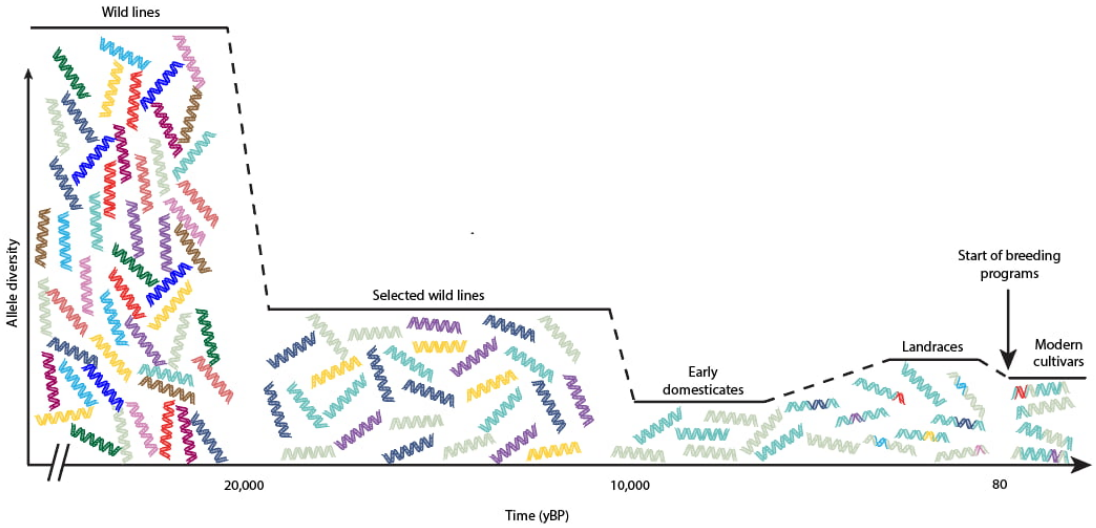

Figure 1.1. Loss of genetic diversity during crop domestication. Genotypes with varying allele diversity are color-coded. Crop domestication led to a significant reduction in allele diversity as ancient farmers selected for plants with spontaneous DNA mutations that provided agronomic benefits (e.g., non-shattering seeds). Although occasional hybridization of early domesticates with wild lines produced landraces, most of the genomic background comes from the early domesticated lines. Modern cultivars arose from chromosome shuffling and recombination of gene alleles selected during domestication. Despite the incorporation of some wild alleles into modern cultivars, the majority of wild diversity remains untapped.

1.3 Germplasm utilisation strategies

Gene banks around the world are responsible for storing seeds of cultivars, landraces, and wild relatives of many agriculturally important crop species (McCouch *et al.*, 2013). However, there is still a significant gap between the availability of stored material and its actual utilisation. Despite the increasing number of entries in gene banks, the number of requests for these materials has not increased proportionally, indicating that available genetic variation is being underutilised (Sharma *et al.*, 2013; Singh *et al.*, 2021).

The identity of gene bank accessions is built upon several descriptors, including passport data (e.g., collection site, growing conditions, soil characteristics), morphological traits, and some agronomic characteristics. While these descriptors aim to provide a comprehensive

characterisation, they do not capture genotype performance under specific environmental conditions. Environmental stresses such as drought vary in timing and intensity across regions, making it impossible to classify gene bank accessions based on drought responses. As a result, detailed characterisation of drought response exceeds the capacity and resources of gene bank curators. This places the responsibility for evaluating these accessions and integrating their genetic resources into breeding programmes on breeders themselves.

Breeders typically use gene bank accessions by developing core collections, which are curated subsets representing the genetic diversity of the entire repositories. Often, these subsets require further refinement to reduce the number of accessions advancing through the breeding pipeline (Xu, 2010; McCouch *et al.*, 2013). For landraces of wheat and barley, the primary strategy for narrowing down candidate accessions—after the initial selection based on genetic diversity metrics and site of origin—involves evaluating yield performance across multiple environments and years. Yield serves the key criterion for assessment (Singh *et al.*, 2021). However, this approach is not directly applicable to wild relatives, as they are not adapted to agronomic use and cannot be evaluated under standard agricultural practices in the same manner as landraces due to non-domesticated traits such as seed shattering Instead, assessing wild relatives requires alternative strategies that consider their adaptive traits, physiological responses, and potential for trait introgression, rather than direct yield performance.

1.4 *De novo* domestication of wild relatives

Early discussions on the use of wild realtives for crop improvement date back to the 1880s with Nikolai Vavilov, a pioneering Russian geneticist and plant breeder whose work on the origin and development of cultivated plants laid the foundation for exploring the potential of diverse germplasms in plant breeding (Hummer & Hancock, 2015). Since then, the employment of wild relatives in modern breeding has been most successful in transferring traits controlled by one or a few major genes, particularly disease resistance, through backcrossing methods(Mammadov *et al.*, 2018; Mishina *et al.*, 2023). However, the intricate physiological and molecular mechanisms of drought responses and the linkage drag of traits detrimental to agriculture complicate the traditional trait introgression via conventional breeding (Khadka *et al.*, 2020).

Drought responses involve complex molecular mechanisms. Many drought tolerant plants (xerophytes) use Na+ as an inexpensive osmoticum to maintain normal stomatal function under mild water stress (Kang *et al.*, 2016; Xi *et al.*, 2018). Under severe stress, plants not only optimise water use efficiency by reducing stomatal aperture but also decrease stomatal density to prevent unproductive water loss (Shabala, 2013; Bertolino *et al.*, 2019; Robertson *et al.*, 2021). This can

be accompanied by changes in leaf wax composition (Hasanuzzaman *et al.*, 2023b), increased root suberisation (Kim *et al.*, 2022), and alterations in aquaporin expression (Maurel *et al.*, 2015; Shekoofa & Sinclair, 2018). All these processes are controlled by a variety of signalling molecules and transcription factors, complicating the already challenging germplasm evaluations; especially during the initial screening of numerous gene bank accessions.

Grain dispersal is one of the most prevalent traits in wild grasses and cereals that contributes to linkage drag. This occurs when the stem holding the grains weakens and fractures upon maturity, leading to grain shattering. While this dispersal mechanism is advantageous in the wild for survival, it poses significant challenges for crop cultivation. To address these challenges, there is a need to develop strategic approaches to efficiently harness the vast diversity of drought response mechanisms found in unexplored wild genetic resources.

The concept of *de nov*o domestication was recently formalised as a targeted breeding strategy to widen the primary breeding pool and ameliorate the loss of genetic diversity in modern cultivars (Fernie & Yan, 2019; Langridge & Waugh, 2019). *De novo* domestication is an accelerated version of the artificial selection exerted by humans that spanned millennia. This method uses molecular techniques to incorporate domestication genes into the wild relatives, offering breeders access to the wild genetic background as only a few genes are modified in the process. *De novo* domestication is particularly advantageous for quantitative traits such as drought tolerance, which are controlled by numerous interacting genes with small additive effects and operating within complex genetic networks. Although counterintuitive due to the long history of selective breeding for high yield and quality crops, *de novo* domestication is aimed to develop an intermediary pre-breeding material to incorporate into more advanced breeding programs. Although mentioned in literature, evidence regarding the preservation of quantitative traits from wild species, while eliminating undesirable traits, remains largely speculative.

Barley is one of the most important grain crops globally, after maize, wheat, and rice, often chosen for cultivation in marginal lands. Consequently, it is also one of the crops most affected by drought stress worldwide (Al Abdallat *et al.*, 2014; Honsdorf *et al.*, 2014; He *et al.*, 2015). The diploid nature of barley, the availability of a reference genome sequence and recently released pan-genome data (Jayakodi *et al.*, 2020; Jayakodi *et al.*, 2024), full sexual compatibility with its immediate wild ancestor (*Hordeum vulgare ssp. spontaneum*), and its close relationship with wheat, make it an ideal model crop suitable for genetic studies with wild relatives in cereals. The absence of crossing barriers between wild and cultivated barley facilitates *de novo* domestication, in which genes responsible for favorable agronomic traits selected during domestication (e.g., non-shattering seeds) can be introgressed from cultivated barley to wild through conventional crossing methods.

1.5 High-throughput phenotyping for evaluation and selection

The value of wild relatives for *de novo* domestication and subsequent use in pre-breeding research cannot be fully realised without a clear understanding of the mechanisms they employ to avoid or tolerate drought, as well as the genetic factors underlying these traits. This challenge is further compounded by the complexity of evaluating and selecting from a large and diverse germplasm. High-throughput imaging technologies, including hyperspectral and thermal imaging, offer a powerful solution by enabling the rapid, non-destructive assessment of physiological traits associated with drought responses, facilitating the identification of key adaptive mechanisms at scale.

Hyperspectral imaging techniques used in the field (Camino *et al.*, 2019; Zarco-Tejada *et al.*, 2021) are not directly transferable to controlled environments as it requires extensive optimisation and specific experimental setups. Scanner-like hyperspectral sensors depend on incident solar radiation or an artificial light source with a complete spectrum to ensure accurate images of spectral reflectance. Thermal sensors, by contrast, capture entire frames in a single snapshot and require minimal optimisation compared to hyperspectral sensors, making them well-suited for high-throughput measurements in glasshouse environments not specifically designed for imaging applications.

1.6 Research aims

The central question of this thesis is how drought tolerance mechanisms in wild barley relatives can be leveraged for mechanistic exploration and pre-breeding research. This is addressed by refining evaluation, selection, and breeding strategies through the integration of phenotypic, physiological, and molecular approaches. These efforts are further strengthened by a data-driven perspective to harness the extensive information generated through high-throughput phenotyping.

The specific objectives are: (1) to develop a targeted exploration framework for drought tolerance that complements conventional yield-based selection using high-throughput imaging techniques; (2) to evaluate drought-tolerant candidate genotypes using multi-trait analysis and use unbiased selection clustering techniques; (3) to assess the relationship between genetic and phenotypic diversity in wild germplasms; (4) to design molecular markers for marker-assisted backcrossing (MABC) of wild with cultivated barley; (5) to generate pre-breeding *de novo*-domesticated material from wild × cultivated barley crosses; (6) to characterise *de novo*-domesticated lines'

phenotypic responses relative to parental lines; and (7) to investigate the effects of *de novo* domestication on quantitative traits of interest.

Significant outcomes include the establishment of a core set of wild genotypes capturing most phenotypic variation from multivariate analysis, the development of molecular markers applicable across diverse wild and cultivated populations, and the creation of *de novo* domesticated barley lines suited for future field research under standard agricultural conditions.

1.7 Thesis outline

Chapter 1 describes the background and research aims of the study.

Chapter 2 is structured as a literature review, examining historical and contemporary approaches to breeding for drought tolerance. It outlines key physiological mechanisms underlying drought adaptation, mainly focusing on those traits amenable to high-throughput phenotyping in large populations. The chapter introduces the concept of high-throughput phenotyping and explores how advancements in remote sensing enable the acquisition of spectral proxies for drought-related traits, with a focus on improving transpiration efficiency (TE). Beyond summarising existing research and defining key concepts central to this thesis, the chapter also proposes a conceptual framework for the systematic exploration of wild relatives in field and glasshouse experiments. This framework integrates high-throughput imaging, machine learning-based clustering, and data science approaches to enhance the selection of drought-tolerant wild material. Furthermore, evidence supporting the feasibility of this approach is provided from the re-analysis of published and unpublished field data. This chapter has been published in *New Phytologist* journal (DOI: 10.1111/nph.19619).

Chapter 3 describes the development of a phenotyping method to characterise wild barley genotypes based on spectral traits under glasshouse conditions. In this pilot study, plants are subjected to varying irrigation regimes, and evaluated using canopy temperature as an indirect measure of transpiration rates, in addition to photosynthetic and non-photosynthetic pigments, and biomass accumulation. The optimised conditions are then applied to the full set of 126 accessions in the next chapter.

Chapter 4 assesses genetic and phenotypic diversity of a collection of 120 wild barley accessions and six cultivated lines focusing on traits outlined in Chapter 2. Through an extensive multi-trait analysis, this chapter establishes a detailed set of criteria for selecting candidate genotypes for two main purposes: i) detailed physiological studies to understand the underlying biological

processes driving the observed responses and ii) to enhance the breeding pipeline by identifying genotypes with desirable agronomic traits for drought tolerance genetic improvement.

Chapter 5 describes the development of molecular markers designed to differentiate between the wild and cultivated alleles of three genes controlling key domestication traits: rachis brittleness (*Btr1*), seed dormancy (*Qsd1*), and awn roughness (*ROUGH AWN1*). These markers are then applied in a Marker-Assisted Backcrossing (MABC) scheme to introgress cultivated alleles into several wild barley backgrounds. Each breeding cycle incorporates genotypic screening to select progeny carrying the targeted cultivated alleles, ensuring the efficient transfer of domestication traits into wild barley lines.

Chapter 6 assesses the *de novo*-domesticated barley lines in comparison to their wild and cultivated parental lines, focusing on spectral traits associated with transpiration and photosynthesis. The primary emphasis is on the retention of genetically complex (quantitative) traits inherited from wild relatives. This chapter offers insights into the feasibility of *de novo* domestication as a strategy to preserve key wild phenotypes through conventional breeding approaches.

Chapter 7 concludes the thesis with a general discussion, summarising key findings, limitations of the study and future research directions.

Chapter 2
Literature review

2.1 Selection criteria for breeding drought-tolerant cereals

Traditionally, crop improvements in arid environments have emphasized yield increase with limited knowledge of physiological and molecular mechanisms involved (Bacon, 2004; Singh *et al.*, 2021). However, the growing unpredictability of weather patterns due to climate change negatively affecting yield heritability reduces the effectiveness of cultivar selection, especially under field drought conditions (Abdolshahi *et al.*, 2015). The future of crop improvement thus relies on traits with stable heritability – those with genetic factors explaining most of the phenotypic variation – under well-watered and drought conditions.

Using yield performance as the primary selection criterion in wild relatives may inadvertently favour early flowering genotypes adapted to Mediterranean climates, which avoid rather than tolerate drought. However, future yield improvements are expected from plants with prolonged reproductive stages that maximize growth and dry matter partitioning during the critical period of grain number determination, and/or exhibit stay green phenotypes (Gregersen *et al.*, 2013; Flohr *et al.*, 2018; Slafer *et al.*, 2023). Gaining a deeper comprehension of drought response is essential to unlock tolerance mechanisms present in wild relatives, particularly because certain wild lines do not exhibit short life cycles as an adaptation to drought. Drought tolerance mechanisms may not be immediately evident in these genetic resources, and rigorous scientific investigation is required.

2.1.1 Transpiration efficiency

Transpiration efficiency (TE) is closely connected to plant physiological processes, making it a promising trait with higher heritability to maintain a high level of carbon assimilation (A) per unit of water transpired (T) (Equation 2.1). TE is a subcomponent of water use efficiency (WUE) – the ratio of grain or biomass accumulated per total water evapotranspiration over the crop life cycle (French & Schultz, 1984) – and can be measured at either the crop or the leaf scale. In contrast to WUE, TE is less prone to the long-term environmental effects, such as variable evaporation and soil characteristics.

$$TE = A/T \qquad \text{(Equation 2.1)}$$

Unlike yield and harvest index (HI) that have been continuously used in modern breeding since the 1960s to estimate drought tolerance (Long *et al.*, 2015), the full potential of TE for plant breeding remains untapped. This is primarily due to the logistical challenges associated with measuring TE on a large scale.

2.1.2 High transpiration efficiency

High transpiration efficiency is desirable for improving drought tolerance in rainfed crops. A plant exhibiting high transpiration efficiency (TE) generates a greater amount of biomass per unit of water transpired, in contrast to a plant with lower TE. Due to logistical challenges, TE is typically measured using indirect methods. For instance, Carbon Isotope Discrimination (CID) provides a high-throughput surrogate of TE for inferring transpiration efficiency in large scale phenotyping experiments (Farquhar & Richards, 1984). CID is based on the differential diffusion of CO_2 isotopes (^{13}C and ^{12}C) through stomata, where ^{13}C is incorporated into the Calvin Cycle by Rubisco at a slower rate compared to ^{12}C. CID offers a valuable time-integrated inference of transpiration efficiency, reflecting the long-term equilibrium between carbon gain and water loss. Since carbon isotopes are stable, it enables sampling without concern of negative effects of short-term environmental fluctuations. Due to this time-integrated nature, CID has found most of its success in selecting genotypes that consistently exhibit high TE throughout their lifecycle. However, these lines generally show yield penalties in environments where yield is less constrained by water supply (Condon & Richards, 1992; Bacon, 2004). This dualism has sparked an ongoing discussion among researchers debating the relative importance of high versus low transpiration efficiency for improving cereal crops (Handley *et al.*, 1994; Blum, 2009; Hughes *et al.*, 2017).

2.1.3 Low transpiration efficiency

Low transpiration efficiency is traditionally considered undesirable for dry environments. A plant with low TE produces less biomass for the amount of water it transpires, compared to one with high TE. Surprisingly, low TE (measured as CID) has been observed in wild barley (*Hordeum vulgare* L. ssp. *spontaneous*) accessions from dry regions, which suggest mechanisms that compensate for the higher water loss or exploit environmental context to achieve high TE (Handley *et al.*, 1994). For instance, TE is highly sensitive to vapor pressure deficit (VPD) and can vary threefold in response to seasonal changes in this climate variable; a response of much greater magnitude than that due to genetic variation (Kar *et al.*, 2020). Wild lines with apparent low TE may in fact have growth and development patterns adapted to endemic seasonal cycles of VPD, and achieve relatively high TE within their local environmental context as a result. Low TE could also be an indication of ephemeral adaptation to maximize carbon uptake following

sporadic rainfall (Handley *et al.*, 1994). Hypothetically, accessions that exhibit low TE under low VPD or well-watered conditions but can promptly switch to high TE at the onset of high VPD or drought stress are ideal candidates for agriculture. Wild barley may possess important stomata regulation mechanisms in response to various environmental stimuli. Comprehensive investigations are required to understand the underlying mechanisms which may exist.

2.2 New frontiers for improving transpiration efficiency

2.2.1 1. Optimum TE under non-stressed conditions

Adjustable pores located in the leaf surface called stomata are vital in managing water loss and carbon uptake in plants. Alterations in stomatal conductance (g_s) affect CO_2 and H_2O differently (Figure 2.1). Water loss through stomata is more than a hundred times higher than carbon uptake (Bacon, 2004). Typical CO_2:H_2O ratios in C_3 and C_4 plants are 1:600 and 1:450, respectively; with C_4 species exhibiting greater efficiency due to Kranz-like anatomy. This inherent dominance of water loss to carbon uptake in C_3 and C_4 plants, largely determined by the concentration gradients and diffusion coefficients of both gases, makes water transpiration (T in) more sensitive to changes in stomatal conductance. Although low stomatal conductance generally reduces carbon assimilation by limiting the diffusion of CO_2 into the carboxylation site, a moderately low supply of CO_2 from the atmosphere can also increase the gradient and driving force of CO_2 diffusion into the leaf interior, while the gradient and driving force for outward H_2O diffusion remains constant. Given the differences in gradient and driving forces of both gases involved in this exchange process, there must exist a lower threshold of g_s where carbon assimilation is only marginally decreased while transpiration is significantly reduced. This has been observed in *Arabidopsis* and barley with reduced stomata density (Hepworth *et al.*, 2015; Hughes *et al.*, 2017), and the same phenomenon could be achieved through an increased sensitivity to closing stimuli (Aliniaeifard & van Meeteren, 2014).

Reduced stomatal density and increased sensitivity to closing stimuli are beneficial traits mainly under non-stressed conditions to reduce the unproductive water losses. However, plants with these characteristics may still experience negative effects on carbon assimilation under severe stress via non-stomatal inhibition (Yang *et al.*, 2021). Overproduction of molecules such as Reactive Oxygen Species (ROS) via the chloroplast Mehler reaction can inhibit carbon assimilation by damaging the photosynthetic machinery and compromising the capacity for carbon fixation (Havrlentová *et al.*, 2021). Appropriate phenotyping methods are then required to distinguish genotypes with high TE while maintaining relatively steady levels of photosynthetic capacity.

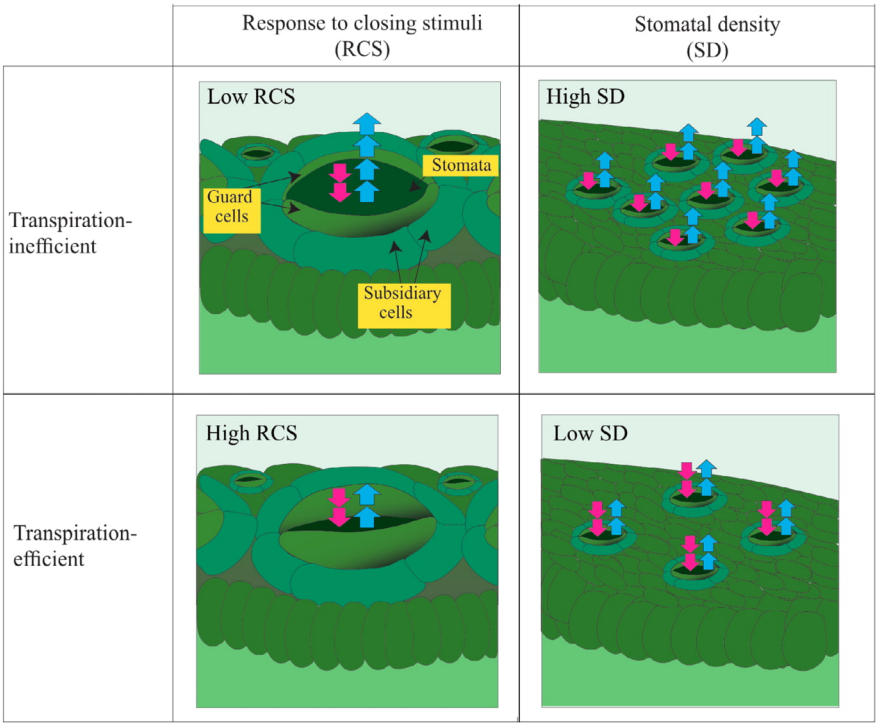

Figure 2.1. Influential factors on transpiration efficiency (TE). Response to closing stimuli (RCS) and stomata density (SD) in a leaf. The top row presents a Transpiration-inefficient genotype with low RCS and high SD, while the bottom row shows a Transpiration-efficient genotype with high RCS and low SD. Pink arrows denotes CO_2 uptake; blue arrows indicate H_2O transpiration. Reduced stomatal conductance, achieved via high RCS or low SD, increases the CO_2 concentration gradient, maintaining CO_2 uptake rate despite significant reductions in transpiration. In the Transpiration-efficient genotype (bottom row), CO_2 uptake remains constant (equal pink arrows), while transpiration halves (fewer blue arrows) relative to the Transpiration-inefficient genotype (top row).

2.2.2 Sustained carbon fixation under drought stress

Carbon assimilation and carbon fixation are closely related yet distinct processes in plant physiology. The differentiation between these two concepts is crucial in order to optimize transpiration efficiency under drought scenarios and use it as a target trait in plant breeding. Carbon assimilation (A) is the broad process of converting atmospheric CO_2 into organic compounds, while carbon fixation is the specific process of converting CO_2 into organic molecules through enzyme-catalyzed reactions in photosynthesis. The carbon assimilation rate is not solely dependent on the capacity for carbon fixation; it is also significantly influenced by the availability of CO_2 in the carboxylation site. Unlike carbon assimilation, carbon fixation can remain stable even when stomata close, preventing CO_2 diffusion, provided the photosynthetic machinery remains intact. Thus, sustained carbon fixation capacity under drought stress does not equal a sustained rate of carbon assimilation. The ability of a plant to sustain carbon fixation under conditions of water scarcity is a crucial trait for retaining crop productivity. By preserving

photosynthetic activity during periods of limited water availability, plants can rapidly resume growth and recover upon rehydration.

The capacity for carbon fixation is typically measured as V_{cmax}, a critical component when carbon assimilation is Rubisco-limited (Sharkey *et al.*, 2007). V_{cmax} represents the maximum catalytic rate at which the enzyme Rubisco can carboxylate ribulose-1,5-bisphosphate (RuBP) under conditions of saturated intercellular CO_2 concentration. V_{cmax} is derived from A-Ci curves obtained through gas exchange measurements, and is characterized by the initial slope of these curves in combination with a photosynthetic model that accounts for both the carboxylation and oxygenation activities of Rubisco, as well as RuBP regeneration (Farquhar *et al.*, 1980).

Understanding the relative changes in the components of transpiration efficiency is a crucial aspect to identify genotypes with high transpiration efficiency through sustained carbon fixation. In theory, plants can achieve high transpiration efficiency by either i) maintaining A while T decreases, or ii) reducing T to a greater extent than A (Equation 2.1). The first approach—where A remains relatively constant compared to a non-stressed baseline—appears advantageous as it seemingly preserves productivity. However, this strategy may not be optimal, particularly under severe drought conditions that depend on water reserves from off-season precipitation. The maintenance of carbon assimilation in this scenario occurs through continued CO_2 diffusion into the leaf, but it inadvertently results in substantial water losses. Consequently, plants adopting this strategy will deplete their water reserves more rapidly compared to those that more efficiently modulate stomatal closure. In contrast, the scenario where T is reduced more significantly than A is a more viable strategy under severe drought conditions. This approach involves maintaining a degree of carbon fixation despite reductions in carbon assimilation and transpiration due to decreased stomatal conductance. It represents a balance between conserving water and sustaining photosynthetic activity (Figure 2.2).

Employing CID as a proxy of TE has limitations in identifying genotypes with sustained carbon fixation capacity as it does not provide insights on the relative contributions of A and T, but rather integrates the effects of stomatal and non-stomatal inhibitions into a single value (Farquhar & Richards, 1984; Condon *et al.*, 2002; Sexton *et al.*, 2021). Furthermore, since the heritability of CID significantly decreases under dry conditions (Richards, 2022), breeding selection criteria are generally constrained to performance under well-irrigated conditions, thus overlooking the negative impacts on carbon fixation capacity under drought stress. The deployment of advanced imaging technologies could provide the means to distinguish alterations in carbon-to-transpiration relationship, essential for selecting genotypes that sustain photosynthesis under drought stress.

2.3 High-throughput phenotyping

The pursuit of more efficient, scalable, and precise methods for assessing changes in TE under drought scenarios underlines the need for innovations in phenotyping technologies. Traditional approaches for examining key physiological processes, such as transpiration rates and carbon fixation, rely heavily on labour-intensive measurements, often limiting the scope and scalability of germplasm evaluations. For instance, transpiration rate traditionally requires direct measurements of stomatal conductance (g_s) using handheld porometers. Similarly, creating A-Ci curves to derive V_{cmax} is time-consuming, taking more than half an hour per curve, and impractical for extensive germplasm evaluations. Remote sensing techniques offer high-throughput and precise options for estimating plant physiological properties, including transpiration rate and V_{cmax} (Camino *et al.*, 2019). These non-destructive techniques can be used at different developmental stages to monitor the progression of plants' responses to drought stress and allow crops to be phenotyped in replicated field trials at an unprecedented scale and resolution.

2.3.1 Thermal imaging

Thermal imaging consists of collecting the thermal infrared spectral region to derive vegetation canopy temperature. The differences in canopy temperature between genotypes can suggest differences in transpiration rates. The Crop Water Stress Index (CWSI) is a valuable tool for quantifying plant transpiration rates by assessing stress levels against established wet and dry baselines in field conditions (Gonzalez-Dugo *et al.*, 2019). Thermal imaging from aerial platforms has become increasingly vital in plant breeding because it enhances the accuracy of measuring CWSI, making it more stable against temporal fluctuations. This improvement increases the heritability of CWSI when contrasted with stomatal conductance measured by handheld porometers (Deery *et al.*, 2016), making it an effective trait for germplasm phenotyping.

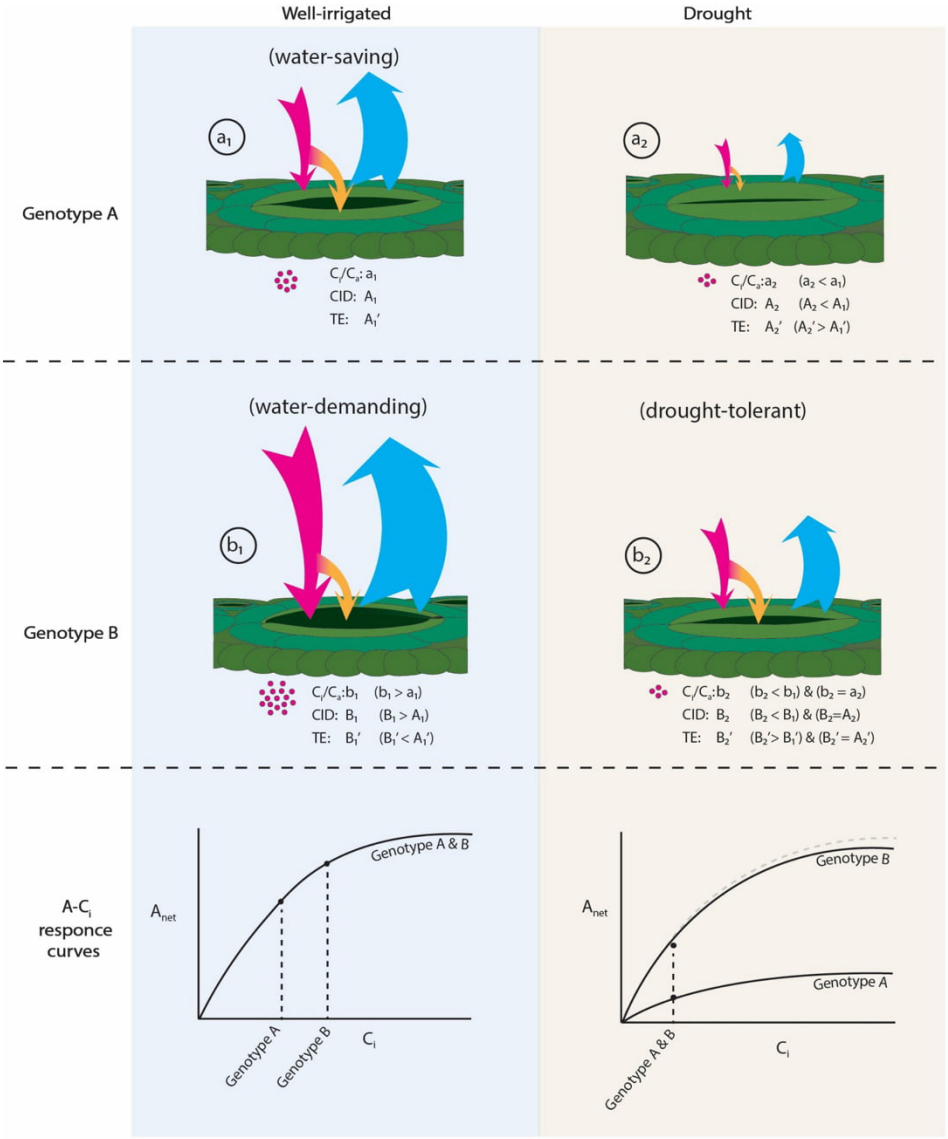

Figure 2.2. Impact of severe drought on two hypothetical genotypes. Under well-irrigated conditions, both genotypes exhibit equivalent carbon fixation capacity (V_{cmax}; orange arrows) but differ in carbon assimilation (A; pink arrows) and transpiration (T; blue arrows). Selections based on Carbon Isotope Discrimination (CID) are generally conducted under well-irrigated conditions given the trait's higher heritability. In this example, Genotype A will be selected based on CID, which exhibits higher TE than Genotype B. Under severe drought, stomata close, increasing both Genotype A and B's transpiration efficiency. The increase in transpiration efficiency occurs due to the significant decrease in transpiration (T) than the reduction in carbon assimilation (A). This increase in TE is accompanied by changes in the ratio between intercellular and ambient CO_2 (C_i:C_a ratio) reflected in CID. Genotype B maintains a robust carbon fixation capacity, while Genotype A achieves the same C_i:C_a ratio via lower stomatal conductance. Differences in carbon fixation capacity are captured via the initial slope of A-C_i curves (bottom row). Under drought conditions, Genotype B's curve and slope closely resemble those observed under well-irrigated conditions, whereas Genotype A's curve and slope exhibit notable deterioration. Genotype B modulates stomatal conductance more efficiently in response to short-term changes in water availability and other environmental stimuli, including vapor pressure deficit (VPD). This increased responsiveness allows Genotype B to effectively minimize water losses while maintaining high productivity under severe drought.

While canopy temperature can provide valuable insights into the impact of drought stress on the transpiration component of TE, interpretations of field-measured CWSI as proxy of transpiration rates should be approached cautiously. A lower CWSI, indicative of a genotype with higher transpiration rates, does not inherently imply that the genotype uses water inefficiently. Low values of CWSI may also result from enhanced access to subsoil water resources, facilitated by the presence of deep root systems. In this scenario, despite the plant's ability to partially close stomata as a survival mechanism, their effective water uptake allows them to continue transpiring at relatively higher rates than less adapted genotypes. The challenge thus lies in differentiating plants that transpire more when water is scarce from plants that transpire more because they have better access to subsoil water. This ability to maintain higher transpiration rates while still conserving water through stomatal closure can be advantageous for the drought-tolerant plant genotypes as it enables them to continue essential physiological processes. To avoid potential confounding effects of deep rooting and transpiration rates, it is advisable to develop phenotyping platforms that account for the above shortcomings. For instance, thermal imaging from field trials can be complemented with appropriate stress management in glasshouse experiments. Comparing the extent to which genotype differences are consistent between the field and glasshouse, can suggest whether a low canopy temperature is due to higher water accessibility through deep rooting or differences in stomata density and aperture.

2.3.2 Hyperspectral imaging

Hyperspectral imaging, also known as imaging spectroscopy, is a method that uses high spectral resolution cameras to create images by capturing the reflected radiation at multiple narrow and contiguous spectral bands. Traits with strong absorption signals such as Leaf Mass per leaf Area (LMA) and non-photosynthetic pigments have been used in models such as Partial Least Square Regression (PLSR) to empirically derive V_{cmax}, a critical component of photosynthetic capacity when carbon assimilation is Rubisco-limited (Serbin *et al.*, 2012; Dechant *et al.*, 2017; Xiaoyu *et al.*, 2022). However, these empirical models have limited transferability to other species or environmental conditions since the information obtained is not directly related to leaf photosynthesis and are affected by canopy structural and background effects (Suarez et al., 2021).

The development of sophisticated sensors with higher spectral resolution has allowed detection of the relatively weaker absorption signatures of important photosynthetic and non-photosynthetic constituents, such as Chl*a*, Chl*b*, carotenoids, anthocyanins, and xanthophylls (Jacquemoud *et al.*, 2009; Ustin *et al.*, 2009). The latter pigments represent a major mechanism for non-enzymatic ROS scavenging and allows plants to reduce detrimental effects of hydroxyl radicals – the most

aggressive form of ROS (Bose *et al.*, 2014; Demidchik, 2015). Mechanistic radiative transfer models, such as the Soil-Canopy Observation of Photosynthesis and Energy (SCOPE) (van der Tol *et al.*, 2009), enables the establishment of a direct relationship between the spectral reflectance captured by an imaging spectrometer and the absorption of these photosynthetic constituents and V_{cmax}. This allows for a more robust determination of plants' carbon fixation capacity than site-specific empirical relationships (Camino *et al.*, 2019; Suarez *et al.*, 2021). Although measured and model-estimated V_{cmax} have yielded a high linear relationship (Camino *et al.*, 2019), it is important to highlight that the objective is not to achieve absolute quantification of V_{cmax}, which is more accurately determined using low throughput gas exchange systems. Instead, the focus lies on the insights gained from the relative changes in the capacity for carbon fixation under the effects of drought of large germplasms collections. Additionally, like thermal imaging, airborne platforms of hyperspectral imaging offer an even higher throughput phenotyping option than ground-based measurements. Airborne hyperspectral imaging can potentially increase the heritability of V_{cmax} by minimizing the impact of spatial and temporal variability during data acquisition (Gálvez *et al.*, 2019).

2.3.3 An image-based transpiration efficiency index for plant breeding

To quantify the relative changes in the components of transpiration efficiency, we propose combining CWSI and normalized values of V_{cmax} obtained via remote sensing into a unitless image-based transpiration efficiency (iTE) index (Equation 2.2). The CWSI, serving as a proxy for transpiration rate, requires a linear transformation before inclusion within iTE to preserve the assimilation-to-transpiration ratio (A:T) from (Equation 2.1); a metric of carbon acquisition relative to water expenditure. The linear transformation necessary for a positive correlation between CWSI and transpiration rate is accomplished by the expression 1 – CWSI. Higher values of 1− CWSI indicate lower levels of crop water stress, and consequently higher transpiration rates.

$$iTE = V_{cmax} /(1\text{-}CWSI) \qquad \text{(Equation 2.2)}$$

We have tested the validity of the proposed iTE by re-analyzing data from Camino *et al.* (2019) across six wheat varieties at the stem elongation stage (Appendix 2.1). This re-analysis shows the variable nature of iTE among wheat varieties under irrigated and rainfed conditions (Figure 2.3), demonstrating the potential of this index for selecting drought-tolerant genotypes. However, a large population with hundreds of accessions can pose a challenge. The population size may weaken the observed effects of iTE due to the noise in data introduced by the impact of the environment. Several components, including the number of genotypes, replicates, variations introduced by the heterogeneity of natural field conditions, and the intrinsic genetic variation of

the germplasm under evaluation, should be carefully considered during the experimental design. The former two generally represent a trade-off between precision and practicality. Including a large number of genotypes enables the incorporation of a broader spectrum of responses and the identification of potentially valuable genetic material, while increasing the number of replicates enhances the statistical robustness. However, increasing either the number of genotypes or replicates requires a greater allocation of resources. Advanced statistical and spatial modelling can help reduce such trade-offs.

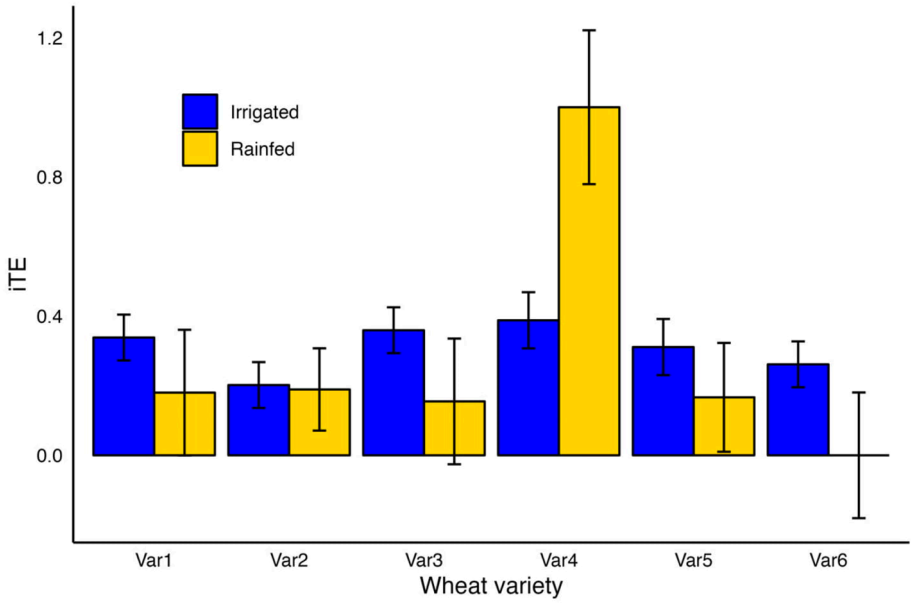

Figure 2.3. Comparative analysis of an image-based Transpiration Efficiency (iTE) index for six wheat varieties (Triticum spp.) under irrigated (blue) and rainfed (yellow) conditions from Camino et al. (2019) dataset. Data are means ± SE. Most wheat varieties show a decrease in iTE from irrigated to rainfed conditions, while Var4 exhibits a pronounced increase, indicating potential adaptation and tolerance of this variety to water scarcity.

The significance of iTE as a trait for drought tolerance improvement lies in the relative changes under drought stress compared to a well-irrigated baseline. Camino *et al.* (2019) successfully demonstrated high correlations between hyperspectrally-derived and ground-based measurements of V_{cmax}. However, to draw robust conclusions about the shifts in iTE across the different irrigation treatments, a sufficient number of whole plots are necessary to integrate the hierarchical structure of split-plot designs into the linear model. An appropriate number of whole plots is tightly linked to the number of factors, treatment levels and replicates of the experimental design. Without an appropriate number of whole plots, the irrigation treatment correlates with the whole plots and the statistical model cannot distinguish variations due to irrigation from those caused by the blocking factor. This is the case of the re-analyzed data from Camino *et al.* (2019). Despite this

limitation in the Camino *et al.* (2019) study, we utilized the combined dataset from irrigated and rainfed plots to illustrate the potential of the relative shifts on iTE and its components as a criterion for selecting drought-tolerant wheat varieties (Figure 2.4).

High relative iTE values under drought, compared to a well-irrigated baseline, indicate that transpiration is reduced more substantially than photosynthetic capacity (Var4). In contrast, lower relative iTE values indicate a genotype undergoing a more significant decline in photosynthetic activity compared to the decrease in transpiration, potentially suggesting the vulnerability of photosynthetic machinery to drought stress (Var6).

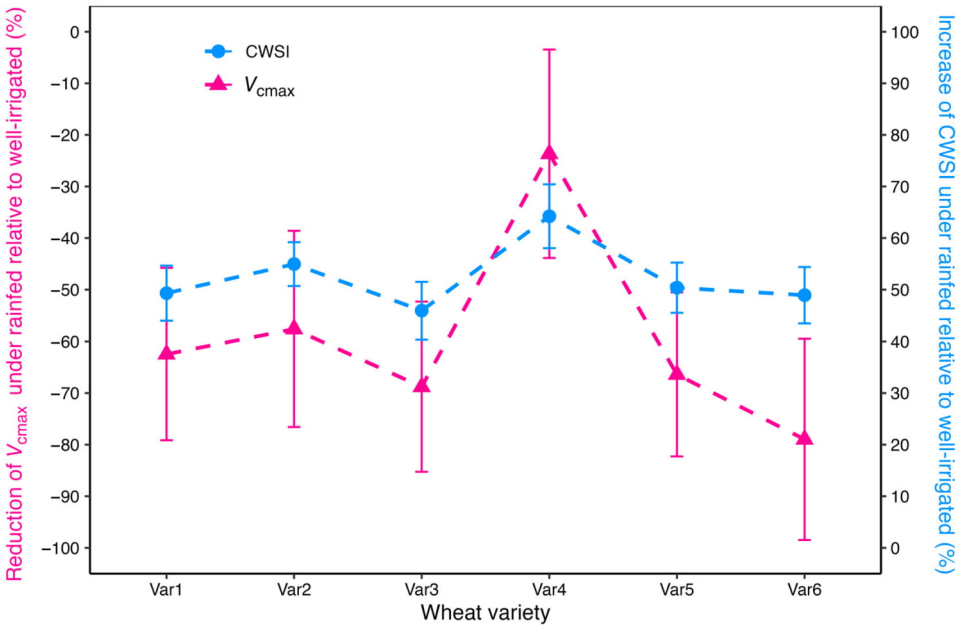

Figure 2.4. Changes of CWSI (blue) and V_{cmax} (pink) to drought relative to well-irrigated conditions across six commercial wheat varieties (Triticum spp.) re-analyzed from Camino et al. (2019). Data are means ± SE. While V_{cmax} typically experiences more than 50% decrease in most varieties, Var4 stands out as an exception, maintaining its carbon fixation capacity with only 23% reduction from optimal conditions, despite the significant increase in CWSI. This suggests a potential tolerance mechanism that retain photosynthetic capacity to some extend under drought stress.

Future research should aim to elucidate the genetic factors underpinning the changes in iTE relative to a well-irrigated baseline. However, the primary significance of iTE in plant breeding lies in its integration with economically relevant traits (Morton *et al.*, 2019). For example, an increase in iTE resulting from a stable V_{cmax} under drought conditions is expected to show a strong correlation with a stress tolerance index derived from the difference between yield under irrigated and yield under drought conditions (TOL index) (Morton *et al.*, 2019). The significant decrease in transpiration during the initial stages of drought stress enables water conservation, while the

plant's sustained photosynthetic capacity allows a better recovery upon rehydration, effectively minimizing crop yield losses. Establishing a correlation between the newly proposed iTE index and a range of tolerance indices thus offers a deeper understanding of how iTE variations translate into practical agronomic outcomes (Figure 2.5).

Notably, low TOL can stem from the lack of responsiveness to stress free conditions if a cultivar has a reduced growth/yield under both rainfed and irrigation. Incorporating other productivity measures, such as Mean Productivity (MP), with TOL can improve the selection criteria for breeding purposes by identifying accessions that achieve low TOL but are also relatively high yielding. This ensures a more accurate and holistic evaluation of their agronomic potential for drought tolerance.

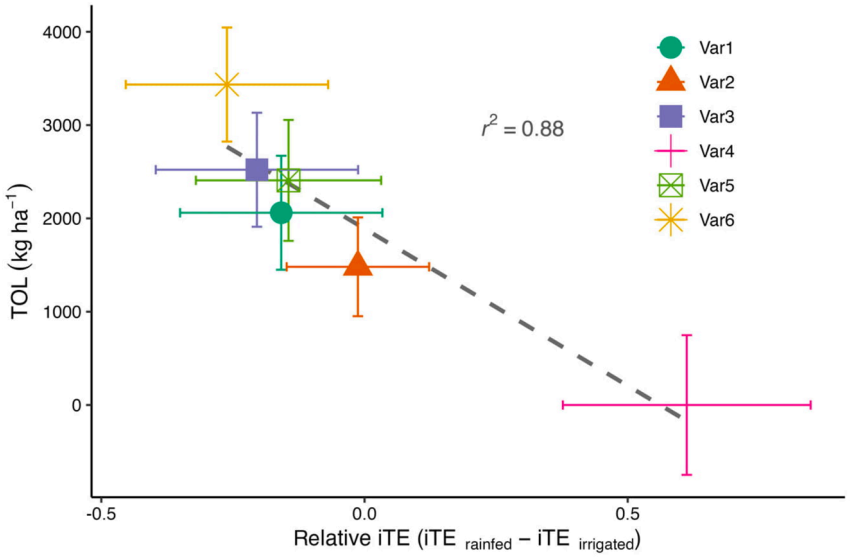

Figure 2.5. Correlation analysis illustrating the relationship between the relative change in iTE from rainfed to irrigated conditions (relative iTE) at the stem elongation stage and the grain yield loss (TOL) for six wheat varieties (Triticum spp.) based on re-analyzed data from Camino et al. (2019). Lower values of TOL and high values of relative iTE are desired for plant breeding. The dashed grey regression line indicates a strong negative correlation, as denoted by the r-squared value of 0.88, suggesting that variations in iTE significantly predict TOL across these varieties. Each variety is represented by a unique symbol and color. Error bars represent ± SE.

The proposed iTE index is primarily intended for screening wild relatives. It addresses the challenge of directly measuring grain yield in the field, which is often impractical due to the inherent grain shattering in wild accessions. Nonetheless, the iTE index has potential applications within cultivated breeding pools. Empirical breeding frequently encounters a dichotomy: i) high yields under optimal conditions yet substantial reductions under drought stress, indicative of high mean productivity (MP) and high yield losses (high TOL) under drought (Morton *et al.*, 2019), versus ii) yield stability under drought stress (low TOL) accompanied by a substantial yield

penalty in well-irrigated scenarios (low MP) (Blum, 2011). Within this framework, elite cultivars with high yields and poor stability might be preferred, if their absolute yield under drought exceeds that of more yield-stable varieties. A deep understanding of the molecular processes that enable photosynthesis to persist under drought stress will lead to the refinement of breeding selection strategies, potentially enhancing the heritability of iTE beyond the limitations imposed by current practices focused exclusively on yield stability (low TOL). This paves the way for integrating the trait of sustained photosynthesis into high-performing elite cultivars. However, before breeders use iTE for crop improvement programs, it is essential to investigate the genetic architecture and heritability of iTE. Comprehensive genomic studies, including Genome-Wide Association Studies (GWAS) and genomic selection models are valuable tools to uncover genetic factors and determine the extent to which iTE can be used for trait introgression in plant breeding.

2.4 Identification and selection of wild candidate accessions

2.4.1 Phenotyping, clustering, and selection

Preliminary screening experiments aim to enhance breeding pools, and traits amenable to high-throughput measurements are essential for evaluating and selecting outstanding accessions within diverse populations. To maximize the use of diverse populations, selection strategies can be built upon unsupervised machine learning methods, like hierarchical clustering, to identify patterns of phenotypic resemblance across different genotypes (Das et al., 2021) (Figure 2.6). Wild accessions may have developed distinct mechanism of drought tolerance. For example, some of them have high transpiration efficiency to modulate stomata conductance at the time of severe drought. However, others with low transpiration efficiency that deplete soil water rapidly probably evolved efficient mechanisms for osmotic adjustment (Handley *et al.*, 1994). Improved osmotic adjustment allows accessions with low transpiration efficiency to withstand longer periods of water scarcity.

Clustering also facilitates a more impartial selection process. By identifying and selecting representative accessions from various clusters, we ensure a broad capture of diverse tolerance mechanisms, moving away from oversimplified classifications based on drought-tolerant versus drought-sensitive or high-yielding versus low-yielding. Such binary classifications risk overlooking valuable genetic material, including accessions with low TE well-suited to arid conditions (e.g. wild barley from desertic regions) (Handley *et al.*, 1994).

Multi-trait evaluations enhance the value of phenotypic diversity assessments as genotypes can be categorized based on the vast variety of responses. For instance, relative changes in iTE offer insights about the balance between transpiration and photosynthetic capacity. However, it is through the collective analysis of iTE, V_{cmax}, CWSI, and TOL that breeders can differentiate

between plants that achieve high iTE either by sustained photosynthesis (type A, Figure 2.6) or significant reductions in transpiration (type C, Figure 2.6). While productivity indices like MP can be considered in comprehensive selection criteria, scientists and breeders should prioritize uncovering and understanding various tolerance mechanisms during pre-breeding research, placing less emphasis in aspects of the plant productivity. This approach is crucial for long-term crop improvement, as it lays the foundation for developing robust drought-tolerant varieties. As the breeding process progresses towards commercialization, breeders will prioritize traits that enhance productivity and marketability, including grain yield and quality.

Multi-trait assessments and clustering can reduce the need for multi-environmental trials. Leveraging existing phenotyping technologies can capture a wide spectrum of response mechanisms within a limited set of growing conditions. Incorporating additional measurements to address and adjust for environmental variations is essential for ensuring accuracy and reliability in the selection process. By integrating environmental data, crop prediction models can reflect genetic potential under varying conditions. The result is a focused and resource-efficient initial screening phase.

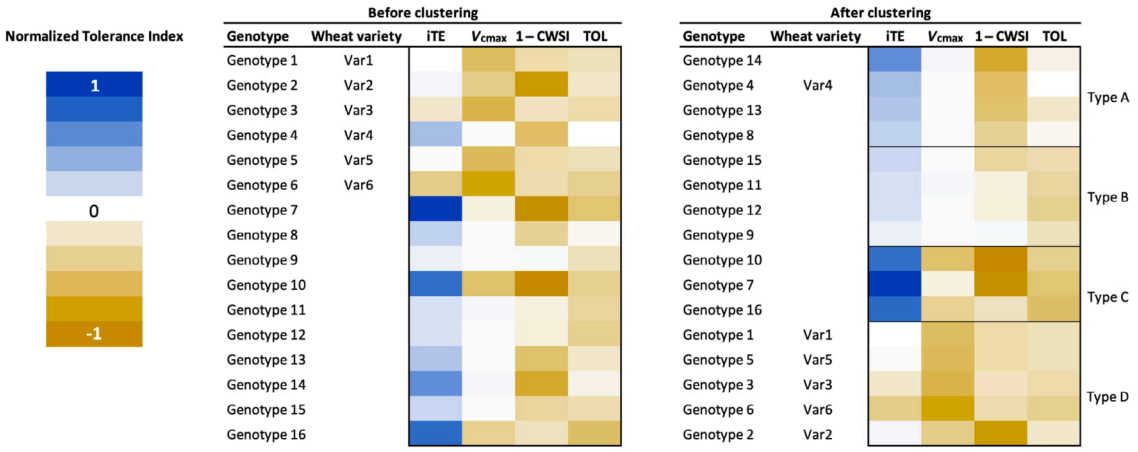

Figure 2.6. Representation of a multivariate clustering analysis involving sixteen genotypes. Traits included in this representation are image-based transpiration efficiency (iTE), carbon fixation capacity (V_{cmax}), canopy temperature-derived transpiration (1-CWSI), and the difference in yield (TOL) between irrigated and drought conditions. The left panel shows unclustered data, while the right panel displays the clustered heatmap representing possible selection criteria. Genotypes have been categorized into Types A-D, reflecting distinct drought response behaviors. Genotypes 1 through 6, corresponding to varieties 1 through 6 (Triticum spp.), are based on experimental data derived from 2016 Santaella experiment (Camino et al., 2019). The data for Genotypes 7 through 16 are hypothetical and have been constructed to illustrate potential grouping into discrete clusters. The color gradient represents a normalized change in multiple traits under drought stress compared to a well-irrigated reference, with blue indicating a 100% increase (+1) and brown indicating a 100% reduction (-1).

2.4.2 Envirotyping

Traditionally, conducting multiple trials under a diverse array of representative environments is considered necessary to confidently select potential candidates for breeding. Given the trade-off between achieving detailed data collection and managing limited resources, researchers usually employ categorical classifications of drought conditions to account for G x E interactions. While there are numerous ways to describe drought events in terms of stress duration, timing and severity, a general classification can be used as transient and prolonged drought. Transient drought events prompt plants to activate short-term adaptive mechanisms such as stomatal closure. In contrast, prolonged drought, characterized by extended water shortages, requires plants to employ long-term survival strategies. This approach facilitates the assessment of G x E interactions within specific drought conditions. However, categorical classifications alone do not fully account for the environmental variation within trial sites and restricts the ability to accurately predict genotypes' performance in different locations.

As technology advances, there are increasingly more low-cost, accurate and rapid methods that allow the systematic quantification of environmental factors, known as envirotyping (Xu, 2016; Resende *et al.*, 2021). Envirotyping enables researchers to include environmental covariates – a quantitative variable used in statistical analysis to account for potential confounding effects or explain variations in the dependent variable – to enhance accuracy of model predictions (Crossa *et al.*, 2022). To gain accurate insights into the impact of drought stress on transpiration efficiency, it is crucial to quantify soil moisture content at various temporal and spatial points within a trial site. This can be achieved through methods such as remote sensing or the utilization of soil moisture probes. While existing techniques for soil moisture measurement primarily serve large-scale hydrological and geosciences research (Liu *et al.*, 2022) or farming decision-making (Maia *et al.*, 2022), developing more suitable approaches tailored for plant breeding is essential. The EM38, an electromagnetic induction instrument, offers a non-invasive and rapid approach for measuring soil moisture at multiple soil depths and soil electrical conductivity (Phathutshedzo-Eugene *et al.*, 2023), making it promising for incorporation in plant breeding research trials. Accurately measuring soil moisture content will enable the removal of confounding effects and help distinguish whether a particularly low transpiration is attributable to the absence of water or to the physiology of the plant.

2.5 Conclusion

The combination of high-throughput image phenotyping and *de novo* domestication constructs a framework where initially, complex but desirable traits for drought tolerance, such as sustained photosynthesis, are integrated into the breeding pool. Subsequently, breeders can fine-tune the

selected lines to meet specific market demands and agricultural needs. This strategy can revolutionize crop development to make it more adaptable to the changing climate and capable of meeting the growing global food demand.

Chapter 3
Development of a high-throughput phenotyping protocol in a glasshouse using thermal imaging

3.1 Introduction

The quest for new genetic sources of drought-tolerance in cereal crops requires the screening and selection of promising genotypes from genetically diverse germplasm. Genotype selection is complicated by the vast array of physiological responses and morphological characteristics of wild relatives (Guadarrama-Escobar *et al.*, 2024). Uncovering drought tolerance in wild germplasm and the data-driven selection of promising candidates requires the development of suitable phenotyping methodologies that address these limitations.

Transpiration rate is a direct measurement of plants' water consumption and a priority trait in drought tolerance research. However, it is one of the most challenging plant traits to measure due to its sensitivity to short-term changes in environmental conditions, including temperature, wind, and humidity. This sensitivity makes selection based on transpiration extremely challenging using classical methods that are time consuming, meaning that plant responses change in between measurement of different lines. This sensitivity requires the development of a high throughput technique to enable numerous measurements in a short time to minimise the impact of environment on transpiration. Remote sensing technologies used as a near instantaneous proxy of plant transpiration can enhance accuracy and have proven useful in both glasshouse and field research (Sirault *et al.*, 2009; Deery *et al.*, 2016; Mulero *et al.*, 2023).

Canopy temperature is closely linked to transpiration, as evaporative cooling from transpiring leaves lowers leaf surface temperature relative to the surrounding air. Monitoring canopy temperature can serve as an indirect measure of transpiration rates and plant water status (Sexton *et al.*, 2021). Under field conditions, high wind speeds significantly increase the amount of water evaporated from the leaf surface, leading to a higher latent heat losses and cooler canopies (Jones, 2014). However, wind speed is not uniformly distributed across a field, introducing spatial variability in transpiration rates and canopy temperature, which can influence the accuracy of canopy temperature measurements. Crop Water Stress Index (CWSI) is typically used as a normalized measure of canopy temperature to account for environmental changes like wind during data acquisition (Camino *et al.*, 2019; Das *et al.*, 2021). CWSI allows for comparable

measures of transpiration rate among a large number of genotypes in the field. In a glasshouse, where wind movements have little impact on transpiration rates, the difference between ambient (T_a) and canopy temperature (T_c) also known as Canopy Temperature Depression (CTD) can be considered an effective index for capturing spatial and temporal variations of canopy temperature. Field testing is generally the preferred approach for breeders conducting germplasm evaluations for breeding purposes, as it provides an accurate representation of the environmental conditions that crops will encounter in agricultural settings. However, studies aimed at investigating drought responses and elucidating underlying mechanisms and genetic factors require precise control of soil water content. Such control is more feasible in a controlled environment than in the field, where soil moisture variability introduces additional complexity. Glasshouses offer semi-controlled environments where external environmental factors can be minimised. The ability to regulate soil water content in a glasshouse setting allows for the controlled imposition of drought stress, yet sparse literature exists on large-scale phenotyping protocols ensuring consistent water content across treatment groups. Maintaining uniform soil moisture levels within each irrigation regime enables researchers to attribute variations in transpiration rates to plant physiology rather than fluctuations in soil moisture. This level of control facilitates a more precise assessment of drought responses and improves the identification of genotypes with adaptive traits.

One of the major differences between the field and in a glasshouse is the scale at which canopy temperature data can be captured. For example, in the field, the high-flying altitude of drones equipped with cameras allow them to capture images of many genotypes within a short time frame and cover a large area in a single frame. Slight changes in position cause minimal perspective differences making alignment and stitching easy to create a comprehensive thermal map of the entire area. In contrast, glasshouses present logistical complications that limit the use of thermal imaging on a similar scale. The height of the camera in conventional glasshouses is restricted to a few metres, and small positional changes can result in significant perspective shifts, making it more challenging to align and stitch multiple images. Due to this height limitation, a camera can only capture a small number of pots at a time, and it requires more images and time to cover the same number of genotypes compared to field imaging. Longer sampling times may introduce a source of environmental variation that negatively impact the identification of the genetic factors affecting the physiological parameter captured by remote sensing camera (Falconer & Mackay, 1996). Although less pronounced, short-term environmental fluctuations in ambient conditions persist within the glasshouse environment. While highly controlled-temperature rooms could reduce such fluctuations, they are typically too small to accommodate the large-scale experiments needed for exploring hundreds of genotypes.

The use of thermal imaging as a proxy of plant transpiration in glasshouses has generally been limited to studies exploring the feasibility of composite traits for assessing phenotypic responses to abiotic stress or investigating the detailed plant physiology of stress responses (Sexton *et al.*, 2021; Mulero *et al.*, 2023). Phenotyping methods applied in these studies are not therefore designed to conduct extensive germplasm explorations and only include a few tens of lines in the phenotyping process.

This chapter addresses the logistical challenges of implementing high-throughput thermal imaging phenotyping in a conventional glasshouse setting lacking an automated irrigation control system. The primary objective is to establish a scalable phenotyping protocol for measuring canopy temperature depression (CTD) under well-watered and drought conditions. The protocol is first tested on a set of seventy-eight pots consisting of twelve genotypes, three replicates and two irrigation treatments, with the aim of refining the methodology for efficient implementation in large-scale experiment involving more than two-hundred pots. A key focus is to determine whether CTD and associated traits, such as biomass accumulation and chlorophyll content, exhibit heritable variations, quantified through broad-sense heritability (H^2) across treatments.

3.2 Materials and methods

3.2.1 Experimental design and glasshouse settings

The phenotyping experiment was conducted at the glasshouse complex of the University of Melbourne, Parkville, Australia (37°47'49.72"S; 144°57'32.08595"E). Thirteen barley lines were grown under well-irrigated and drought conditions with three replicates in a completely randomised design. Three plants per pot were grown in 1.5L-pots. Pot arrangement consisted of a grid pattern of 14 rows by 11 columns (Figure 3.1a). To prevent overlap of plant canopies from different experimental units and maximise the space between them, pots were positioned in alternating positions; all pots were surrounded by an empty space on all sides. The spacing of the pots was configured as follows: 24 cm horizontally, 26 cm vertically, and 17.7 cm diagonally.

The glasshouse temperature settings were configured to control the temperature at which the vents open and the cooling systems activate, rather than maintaining a strict target temperature. The glasshouse temperature was set at 22°C during the day and 15°C during the night. During thermal imaging phenotyping, between 1:00pm and 1:30pm, the cooling system was turned off to prevent wind disturbance, and air temperatures exceeded 22 °C as vents opened completely. The glasshouse temperature during this time was dependent on incoming solar radiation and external ambient temperature.

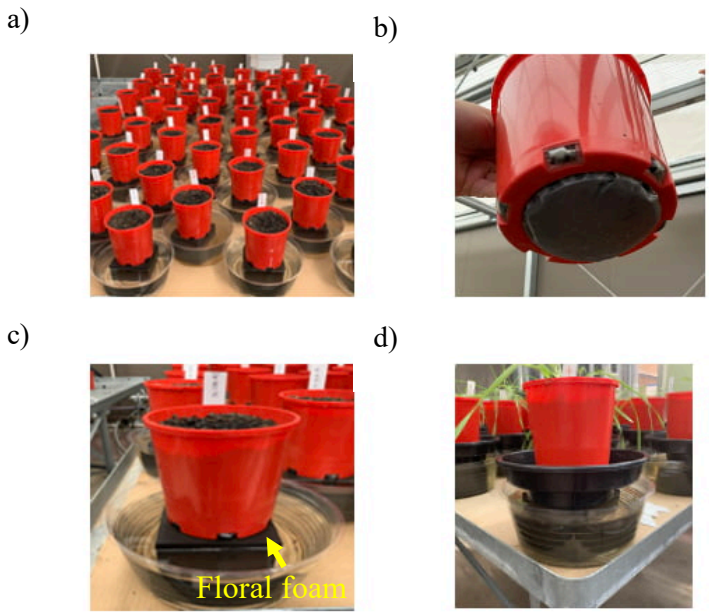

Figure 3.1. Pot configuration and irrigation system used in the experiment. a) Pots arranged in a 14x11 grid in alternating positions; b) a 76-mm hole drilled at the bottom and covered with a 20-micron nylon mesh to prevent roots growing out; c) pot placed on a floral foam within a transparent pot saucer filled with water for capillary irrigation; d) a black pot saucer between the red pot and the floral foam placed at 22 DAS to block water capillary system.

3.2.2 Soil properties

A specialised soil mixture was used to prevent rapid water evaporation which consisted of 70% standard potting mix and 30% clay loam (v/v). The standard potting mix contained 12% washed coarse sand and 88% medium-sized (3-5 mm) pine bark. For each cubic meter of standard mix, several additives were incorporated: 4 kg of Macracote Colonizer Plus (Red) fertilizer with an N:P:K ratio of 15:3:9, enriched with trace elements; 1.5 kg of Saturaid, a soil wetting agent; and 1 kg of dolomite lime. The clay loam component of the mixture had a texture profile of 20.10% sand, 22.10% silt, and 57.80% clay. Pots were filled immediately after mixing to minimise water evaporation and ensure the same initial moisture content in every pot. The gravimetric field capacity (FC) of the final soil mix was 0.64 ml $H_2O \cdot g^{-1}$ dry soil. Each pot was filled with 1,100 g of the final mix with an initial moisture content of 0.44 ml $H_2O \cdot g^{-1}$ dry soil (69 % of FC).

3.2.3 Drought treatment

Anticipating significant variations in phenological development across wild genotypes, traits were measured exclusively during vegetative growth to minimise the influence of phenological differences and ensured data collection occurred within a comparable developmental window. The drought stress treatment was designed according to Marchin *et al.* (2020) with some modifications. Briefly, an 76-mm opening was drilled at the bottom of each pot and covered with

nylon mesh (20-µm, Allied Filter Fabrics, Berkeley Vale, NSW, Australia) (Figure 3.1b) to avoid soil loss. Pots were then placed on a floral foam (OASIS® Noir Ideal Floral Foam Maxlife Brick, Smithers- Oasis, Kent, OH, USA) within a deep pot saucer filled with water (Figure 3.1c). All plants were irrigated by capillary method (Marchin *et al.*, 2020) for 21 days before imposing drought treatment to half of the pots. The well-irrigated half were kept under capillary irrigation for the rest of the experiment to maintain a soil water content between 75-85% of field capacity. Water was replenished every second day. For the other half, drought treatment commenced at 22 days after sowing (DAS) by placing a physical barrier between the floral foam and the base of the pots (Figure 3.1d) to switch the irrigation regime from capillary to manual irrigation. The same set of pots was measured under two different water stress levels: initial reduction to 60–70% field capacity, followed by a further decrease to 30–40% field capacity.

The water content of drought-treated pots was controlled by placing them on a digital scale and adding water from the top until reaching the desired weight. Drought-treated pots were gradually dried by matching the rate of slowest drying pot. Soil water content was measured and recorded every second day from 1- 20 DAS and daily after 21 DAS. The irrigation frequency was determined based on the pot that experienced the quickest soil drying rate and it changed according to the age of the plants as older plants consumed water more rapidly than younger ones.

3.2.4 Phenotyping plant responses to the water stress.

Canopy temperature

To aid image segmentation, a custom matte black-painted cardboard was positioned above the pots to cover the soil, the pot saucers filled with water and the bench (Figure 3.2a) to ensure a uniform background, enhancing the temperature contrast of the canopy. The black-painted cardboard was beneficial for image segmentation. Canopy temperatures were recorded using a thermal camera Model E86 (Teledyne FLIR LLC, Portland, Oregon, USA), with a resolution of 464 x 348 pixels, spatial resolution of 0.9 milliradians, and temperature range of -20 to 120°C. The thermal sensitivity of the camera is <0.04°C at 30°C. The emissivity was set to 0.95. The camera was mounted on a tripod approximately 0.8 m above the plant canopy in a nadir position to achieve a pixel size of 0.72 mm (Figure 3.2b). A video was captured in radiometric IR mode by gliding the thermal camera over the plants. Each pot was distinctly framed within the video, recording at a rate of approximately three frames per second. All pots were systematically measured once within a timeframe of up to 20 min in each phenotyping day (
Table ***3.1***). Images were acquired between 13:00-13:20.

Three radiometric images (r-jpeg format) were extracted from each video recording using FLIR Tools Basic software (Teledyne FLIR LLC, Portland, Oregon, USA). Each pixel effectively contained a temperature reading. A custom script, written in MATLAB 2021b (Mathworks Inc., Natick, Massachusetts, USA), was used to obtain average values of canopy temperature of all pixels within an image (Figure 3.3). The ambient temperature was recorded during canopy temperature measurements using two HOBO data loggers model UX-100-001 (Onset, Cape Cod, Massachusetts ,USA), placed within 1.2 m from the pots. Canopy temperature depression (CTD) was obtained from the difference between the ambient air temperature (T_a) and canopy temperature (T_c) for individual pots (Equation 2.1). CTD contrasts where obtained from the difference between CTD of irrigated and drought treatments for each genotype (Equation 3.2).

$$CTD = T_a - T_c \quad \text{(Equation 3.1)}$$

$$CTD_{contrast} = CTD_{Irrigated} - CTD_{drought} \quad \text{(Equation 3.2)}$$

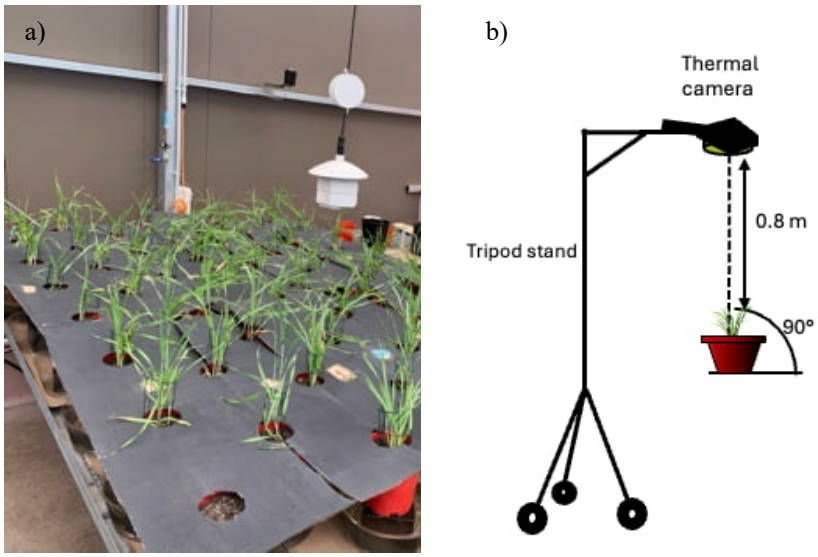

Figure 3.2. Thermal imaging phenotyping preparation, thermal camera and phenotyping stages. a) Black background used to increase image contrast; b) Tripod stand with a thermal camera mounted in nadir position (90° angle) from the pots.

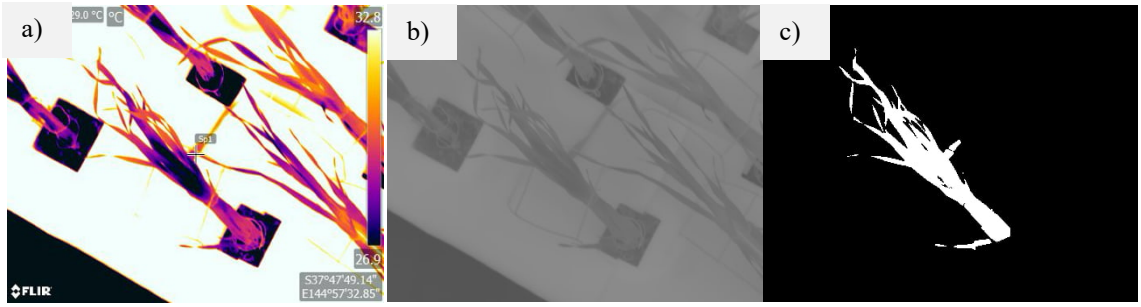

Figure 3.3. Summarised workflow for processing thermal images.a) original radiometric JPEG thermal image displaying temperature distribution, with cooler areas appearing in dark purple and warmer areas in yellow, each pixel containing a temperature value; b) grayscale TIFF image derived from the thermal data; c) binary image segmentation using ImageJ software, isolating plant canopy pixels (white) for temperature analysis.

Chlorophyll content

Plants were measured with a SPAD-502Plus (KONICA MINOLTA, Chiyoda, Tokyo, Japan) at 56 DAS (

Table *3.1*), three days before biomass harvest, to investigate changes in chlorophyll content in response to drought stress. SPAD measurements were carried out on two randomly and fully expanded top leaves per plant and averaged to obtain one value per pot.

Stomatal conductance

Sixty-four observations of stomatal conductance (g_{sw}) were obtained using a handheld porometer Li600P/F (LI-COR Biosciences Inc., Lincoln, Nebraska, USA) at 57 DAS. Measurements were taken between 13:00 - 14:00 PM to minimize physiological variations in transpiration rates that occur throughout the day. For each plant, two to three measurements were taken randomly from the first youngest fully expanded top leaves. The porometer was clamped onto the abaxial leaf surface, and readings were recorded automatically.

Biomass

All above ground biomass for every individual was harvested at 59 DAS (

Table *3.1*) and immediately weighed on a scale to record the individual fresh weight (FW). Collected samples were dried at 70°C for 72 hrs and biomass was re-weighed after the drying treatment to obtain dry weight (DW).

Table 3.1. Summary of data acquisition over the course of the experiment.

Date	**17-Nov**	**21-Nov**	**23-Nov**	**26-Nov**	**28-Nov**	**30-Nov**	**4-Dec**	**6-Dec**	**13-Dec**	**21-Dec**	**22-Dec**	**24-Dec**
Days After Sowing	**22 DAS**	**26 DAS**	**28 DAS**	**31 DAS**	**33 DAS**	**35 DAS**	**39 DAS**	**41 DAS**	**48 DAS**	**56 DAS**	**57 DAS**	**59 DAS**
Canopy temperature	x	x	x	x	x	x	x	x	x	-	x	x
Chlorophyll content	-	-	-	-	-	-	-	-	-	x	-	-

Biomass	-	-	-	-	-	-	-	-	-	-	-	x
Stomatal conductance	-	-	-	-	-	-	-	-	-	-	x	-

3.2.5 Statistical analyses

Canopy Temperature Depression (CTD)

All data processing and statistical analyses were performed with R (version 4.3.2) using packages *lme4* (version 1.1.35.1) (Bates *et al.*, 2015), *emmeans* (version 1.10.0) (Lenth *et al.*, 2024), and *tidyverse* (version 2.0.0) (Wickham, 2014). The strength of CTD and stomatal conductance (g_{sw}) correlation was assessed using Pearson's correlation coefficient (r).

A linear mixed model was applied to CTD data as follows:

$$\boldsymbol{y} = \boldsymbol{X\beta} + \boldsymbol{Zu} + \boldsymbol{e} \qquad \text{(Equation 3.3)}$$

where $\mathbf{y}$ is the response vector of CTD values; $\boldsymbol{\beta}$ is the vector of fixed effects; $\mathbf{u}$ is the vector of random effects; and $\mathbf{e}$ is the vector of residual effects. $\mathbf{X}$ and $\mathbf{Z}$ are the design matrices, corresponding to $\boldsymbol{\beta}$ and $\mathbf{u}$ respectively. The fixed-effect vector $\boldsymbol{\beta}$ partitioned as follows:

$$[\mu\ \boldsymbol{\beta}^{T}{}_{G}\boldsymbol{\beta}^{T}{}_{T}\boldsymbol{\beta}^{T}{}_{D}\boldsymbol{\beta}^{T}{}_{G:T}\boldsymbol{\beta}^{T}{}_{G:D}\boldsymbol{\beta}^{T}{}_{T:D}\boldsymbol{\beta}^{T}{}_{G:T:D}\boldsymbol{\beta}^{T}{}_{Ta}]$$

where i) μ is the overall mean; ii) $\boldsymbol{\beta}^{T}{}_{G}$, $\boldsymbol{\beta}^{T}{}_{T}$, $\boldsymbol{\beta}^{T}{}_{D}$ are the subvectors for the effects of Genotypes (G; accessions), Treatments (T; water stress) and Days after sowing (D; measurement date), respectively; iii) $\boldsymbol{\beta}^{T}{}_{G:T}$, $\boldsymbol{\beta}^{T}{}_{G:D}$, $\boldsymbol{\beta}^{T}{}_{T:D}$ and $\boldsymbol{\beta}^{T}{}_{G:T:D}$ are interaction terms for Genotype:Treatment (G:T), Genotype:DAS (G:D), Treatment:DAS (T:D) and Genotype:Treatment:DAS (G:T:D), respectively; and iv) $\boldsymbol{\beta}^{T}{}_{Ta}$ represents the coefficients of the covariate ambient temperature (Ta), captured with data loggers at the time of thermal data acquisition. The random effects vector $\mathbf{u}$ contains a single factor $[\mathbf{u}^{T}{}_{P}]$ corresponding to Pot ID (P) to account for the hierarchical structure of repeated measurements measured across various DAS. The distribution of the residual effects is assumed to be: $e \sim N(0, \sigma^2 I)$.

Biomass and chlorophyll content

The statistical analysis of biomass data (FW and DW), and chlorophyll content (SPAD values), were performed by fitting a simple linear model using Genotype and irrigation Treatment as factors. The linear regression model for these traits was as follows:

$$\boldsymbol{y} = \boldsymbol{X\beta} + \boldsymbol{e}, \qquad \text{(Equation 3.4)}$$

where $\mathbf{y}$ is the response vector of the trait being analysed; $\boldsymbol{\beta}$ is the vector of fixed effects and $\mathbf{e}$ is the residuals with $e \sim N(0, \sigma^2 I)$. $\boldsymbol{\beta}$ is partitioned into $\boldsymbol{\beta}^{\mathrm{T}}{}_{\mathrm{G}}$ and $\boldsymbol{\beta}^{\mathrm{T}}{}_{\mathrm{T}}$ for the effects of Genotype (G) and Treatment (T). $\mathbf{X}$ is the design matrix corresponding to $\boldsymbol{\beta}$. The p-values were adjusted for multiple testing using the method of Benjamini and Yekutieli (Benjamini & Yekutieli, 2001) and significance of differences between treatments were compared by Tukey HSD test.

Broad sense heritability (H^2)

Variance components were obtained from linear mixed models to estimate the broad-sense heritability (H^2) for each trait (Equation 3.5) (Abdolshahi *et al.*, 2015; Rahman *et al.*, 2021). The estimation process was tailored to the time of the data acquisition for each trait. For Canopy Temperature Depression (CTD), heritability values were calculated for each treatment and Days After Sowing (DAS) separately. For biomass and chlorophyll content measured at the end of the growing season, heritability values were calculated for each irrigation treatment separately.

$$H^2 = \frac{{\sigma_g}^2}{{\sigma_g}^2 + \frac{{\sigma_e}^2}{r}} \qquad \text{(Equation 3.5)}$$

Where ${\sigma_g}^2$ is the genotypic variance, ${\sigma_e}^2$ the residual variance and r is the number of replicates.

3.3 Results

Most of the experimental units of Cultivar-1 either had no germination or showed abnormal growth and were subsequently removed from the analysis.

3.3.1 Soil and ambient temperature conditions in the glasshouse

Manual and capillary irrigation-maintained soil water content across pots within $\pm$ 3.5% FC on days of CTD measurements (Figure 3.4).

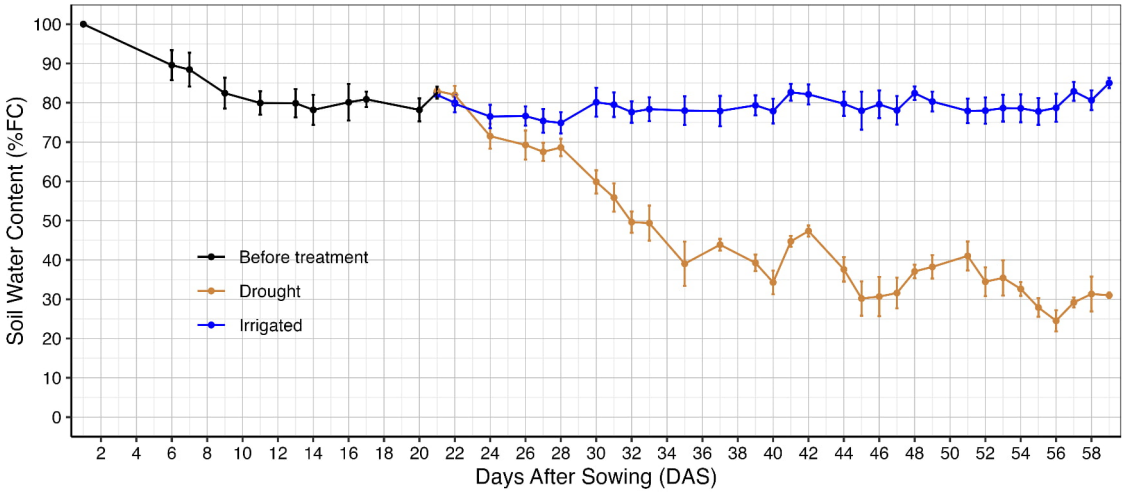

Figure 3.4. Temporal variation in average soil water content (%) within seventy-eight pots over the course of the water stress experiments. The point of divergence between blue and brown lines indicate the starting point of water stress treatment.

3.3.2 Canopy temperature depression and stomatal conductance

Sixty coordinated measurements of Canopy Temperature Depression (CTD) and stomatal conductance to water vapour (g_{sw}) were obtained at 57 DAS when irrigated and drought pots were at 83%FC and 29%FC, respectively. Unlike the rest of CTD measurements in this study, this dataset was collected simultaneously with g_{sw} to establish an empirical relationship between transpiration and canopy temperature. The sixty pots were specifically selected because genotypes in these pots had leaves broad enough to fully cover the measuring aperture of the LI-600P/F, ensuring accurate g_{sw} readings. A linear correlation ($r=0.81$, $p<0.001$) was found between g_{sw} and CTD (Figure 3.5). While there was a clear separation between the CTD distributions of irrigated and drought-treated pots at 57 DAS (Figure 3.6), the correlation plot indicates that some leaves in well-irrigated plants still exhibited low transpiration rates similar to those observed in drought-treated pots.

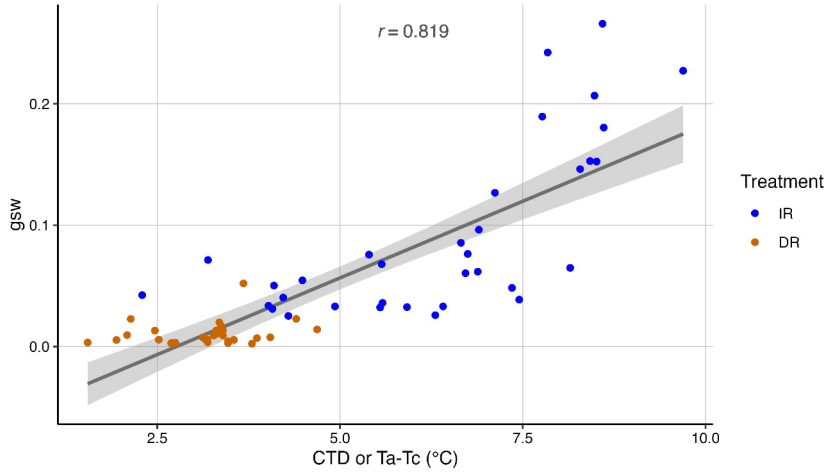

Figure 3.5. Relationship between CTD and stomatal conductance to water vapour (g_{sw}). Temperature measurements were acquired simultaneously with g_{sw}. The correlation was built from measurements taken at 57 DAS.

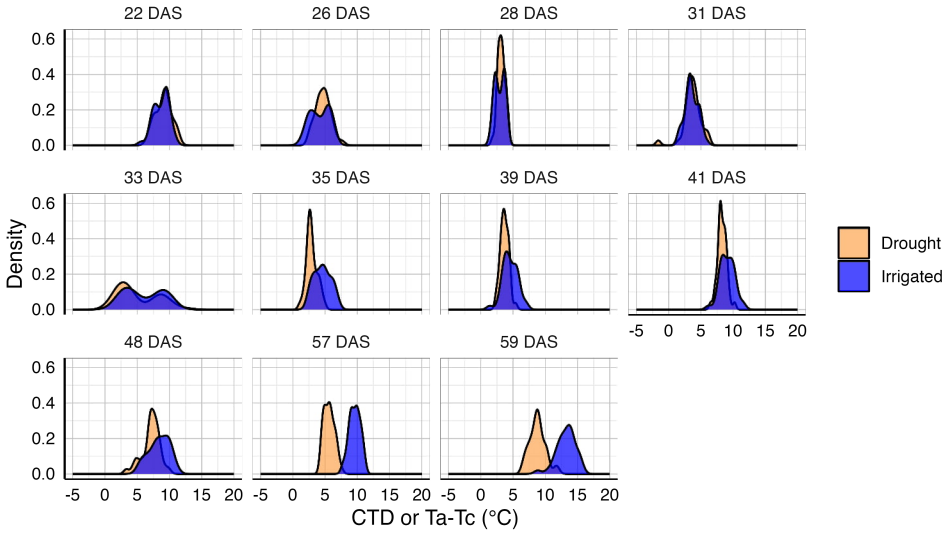

Figure 3.6. Distribution curves of CTD trait between irrigated and drought at different DAS. Using density plots of raw CTD values before linear modelling.

A linear relationship ($r=0.91$, $p<0.001$) was observed between ambient temperature (T_a) and CTD at several DAS for irrigated and drought pots (Figure 3.7). The highest variation in CTD, as indicated by the error bars, was generally observed at the highest mean T_a, suggesting that variations in CTD are more pronounced under higher temperature conditions (Figure 3.7).

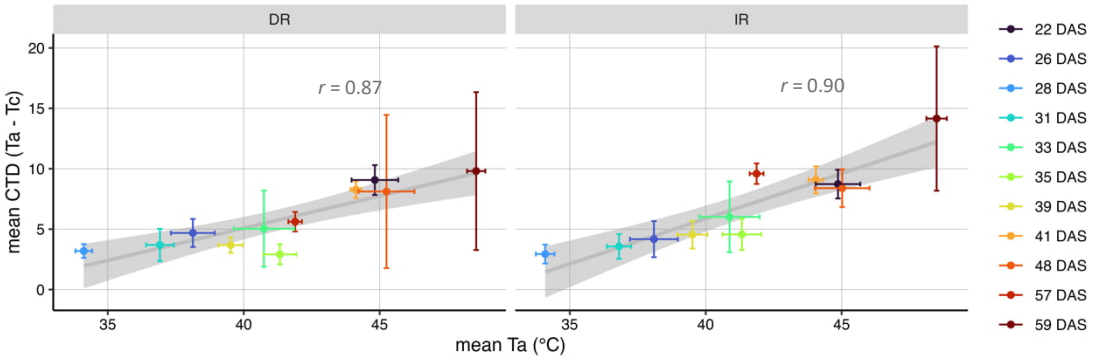

Figure 3.7. Linear relationship between CTD and ambient temperature (T_a) for drought (DR) and irrigated (IR) pots separately.

3.3.3 The effect of drought treatment on measured traits

CTD

The statistical analysis of data collected for canopy temperature depression showed a significant effect of genotype, water stress treatment, DAS, ambient temperature as well as interaction between these factors (Table 3.2). The only interactions that were not found significant within the CTD analysis were Genotype:DAS:Treatment and Genotype:Treatment. CTD at 22, 26, 28, 33 DAS for both irrigated and drought pots showed bimodal distributions, possibly indicating two clusters (Figure 3.6). As expected, CTD differences between irrigated and drought pots – referred to as CTD contrasts – progressively increased as the soil moisture content decreased (Figure 3.6; Table 3.3). Significant treatment contrasts (Equation 3.6) emerged at 33 DAS when irrigated and drought pots were at 78%FC and 49%FC, respectively (Table 3.4), with genotypes WBDC-002, WBDC-020, WBDC-025 and WBDC-048 exhibiting the earliest divergence. Genotype WBDC-025 showed the most pronounced positive CTD contrast on the same phenotyping day (Table 3.4). Genotype WBDC-020 exhibited an unexpected negative CTD contrast at 33 DAS that was statistically significant (Figure 3.8), indicating that the drought-treated pots showed higher CTD values and thus higher transpiration rates compared to their irrigated counterparts. Although other negative CTD contrasts were observed across different DAS and genotypes, these were not statistically significant at p=0.05. Unexpectedly, most of the genotypes that displayed significant CTD contrasts at 33 DAS did not exhibit similar patterns at 39, 41, and 48 DAS, despite the decreasing soil water content during the latter periods.

Table 3.2. Linear Mixed Model (LMMs) analysis of CTD, chlorophyll content (Chl), fresh weight (FW) and dry weight (DW).

	CTD					Chl				
Source of variance	**df1**	**df2⁺**	**F.ratio**	**p-value**		**df1**	**df2**	**F.ratio**	**p-value**	
Genotype	11	47	4.4	<0.001	***	11	48	27.8	<0.001	***
Treatment	1	48	136.2	<0.001	***	1	48	78.4	<0.001	***
Genotype:Treatment	11	47	1.1	0.375		11	48	2.6	0.011	*
DAS	10	393	95.2	<0.001	***					
Ta	1	380	236.8	<0.001	***					
Genotype:DAS	110	478	1.5	0.002	**					
Treatment:DAS	10	478	53.5	<0.001	***					
Genotype:Treatment:DAS	110	478	1.4	0.073						

	FW					DW				
Source of variance	**df1**	**df2**	**F.ratio**	**p-value**		**df1**	**df2**	**F.ratio**	**p-value**	
Genotype	11	48	9.1	<0.001	***	11	48	9.1	<0.001	***
Treatment	1	48	673.3	<0.001	***	1	48	673.3	<0.001	***
Genotype:Treatment	11	48	4.9	<0.001	***	11	48	4.9	<0.001	***

, **,*: Significance at p< 0.05, p<0.01 or p<0.001, respectively. ⁺df2 = denominator degrees of freedom approximated with Satterwaitte's method.*

Table 3.3. Treatment contrasts (IR-DR) for CTD at several DAS.

DAS	**22**	**26**	**28**	**31**	**33**	**35**	**39**	**41**	**48**	**57**	**59**
IR-DR (contrast)	-0.4	-0.45	-0.19	-0.14	0.86	1.71	0.89	0.91	1.45	4.04	4.54
p-value	0.103	0.064	0.449	0.574	<0.001 ***	<0.001 ***	<0.001 ***	<0.001 ***	<0.001 ***	<0.001 ***	<0.001 ***

Table 3.4. Irrigated vs Drought (IR-DR) CTD contrasts.

	Cultivar-2		WBDC-002		WBDC-012		WBDC-019		WBDC-020		WBDC-021	
DAS	IR-DR contrast (°C)	P-value	IR-DR contrast (°C)	P-value	IR-DR contrast (°C)	P-value	IR-DR contrast (°C)	P-value	IR-DR contrast (°C)	P-value	IR-DR contrast (°C)	P-value
22	-0.75	0.387	-0.46	0.593	-0.17	0.845	-1.3	0.128	0.32	0.706	-0.41	0.631
26	-0.92	0.281	-0.29	0.734	0.05	0.956	-0.74	0.385	-0.64	0.452	0.17	0.84
28	-0.62	0.467	0.22	0.798	-0.29	0.734	-0.32	0.708	-0.22	0.795	0.32	0.706
31	-0.35	0.683	0.28	0.747	0.61	0.473	-0.56	0.511	-0.55	0.523	0.41	0.633
33	1.1	0.203	2.88	0.001 ***	1.09	0.201	1.68	0.05	-1.93	0.024 *	-0.72	0.402
35	0.44	0.608	0.69	0.419	3.02	0.000 ***	0.59	0.489	1.64	0.055	1.85	0.031 *
39	0.57	0.501	0.73	0.392	1.62	0.058	-0.05	0.949	3.37	0.000 ***	0.64	0.456
41	0.7	0.415	0.78	0.363	1.63	0.057	-0.05	0.956	3.31	0.000 ***	0.6	0.482
48	1.48	0.084	1.2	0.164	1.25	0.142	1.21	0.158	2.68	0.002 **	3	0.001 ***
57	3.48	0.000 ***	3.65	0.000 ***	2.88	0.001 ***	4.92	0.000 ***	3.65	0.000 ***	3.11	0.000 ***
59	3.8	0.000 ***	2.27	0.008 **	4.77	0.000 ***	4.19	0.000 ***	4.2	0.000 ***	4.25	0.000 ***

(Table 3.4 - continuation)

DAS	WBDC-023		WBDC-025		WBDC-036		WBDC-038		WBDC-048		WBDC-117	
	IR-DR contrast (°C)	P-value	IR-DR contrast (°C)	P-value	IR-DR contrast (°C)	P-value	IR-DR contrast (°C)	P-value	IR-DR contrast (°C)	P-value	IR-DR contrast (°C)	P-value
22	-0.35	0.68	-1.84	0.032 *	1.06	0.216	0.02	0.978	-0.45	0.601	-0.62	0.468
26	-1.01	0.237	-1.26	0.141	-0.26	0.763	-0.81	0.344	0.92	0.28	-0.83	0.329
28	-0.81	0.345	0.06	0.946	-0.14	0.872	0.01	0.989	-0.2	0.812	-0.4	0.64
31	-0.09	0.911	-0.65	0.45	0.29	0.737	-0.68	0.426	-0.38	0.658	-0.16	0.848
33	0.1	0.906	4.27	0.000 ***	0.31	0.716	0.88	0.304	1.91	0.026 *	0.63	0.46
35	-0.12	0.889	2.99	0.001 ***	1.66	0.053	2.55	0.003 **	1.6	0.062	3.48	0.000 ***
39	-0.82	0.335	0.95	0.267	1.53	0.074	0.48	0.574	0.1	0.91	1.41	0.1
41	-0.79	0.356	1	0.241	1.52	0.075	0.47	0.578	0.13	0.876	1.42	0.096
48	-0.06	0.948	1.05	0.221	1.56	0.068	1.22	0.156	0.95	0.268	1.69	0.048 *
57	3.49	0.000 ***	5.14	0.000 ***	4.22	0.000 ***	3.84	0.000 ***	5.17	0.000 ***	4.81	0.000 ***
59	4.05	0.000 ***	5.66	0.000 ***	4.19	0.000 ***	5.72	0.000 ***	4.89	0.000 ***	6.31	0.000 ***

Chlorophyll and biomass traits

Chlorophyll content and biomass are indicators of physiological status such as senescence and agronomic performance. The applied drought stress and phenotyping method caused changes in chlorophyll content, Fresh Weight (FW) and Dry Weight (DW) traits within the panel of genotypes included in this experiment. These significant differences were observed among genotypes ($p < 0.0001$), treatments ($p < 0.0001$), as well as the Genotype:Treatment interactions ($p < 0.01$) (Table 3.2). Chlorophyll content generally increased from irrigated to drought pots except in Cultivar-2 (Figure 3.9), whereas FW and DW decreased under drought for all genotypes (Figure 3.10).

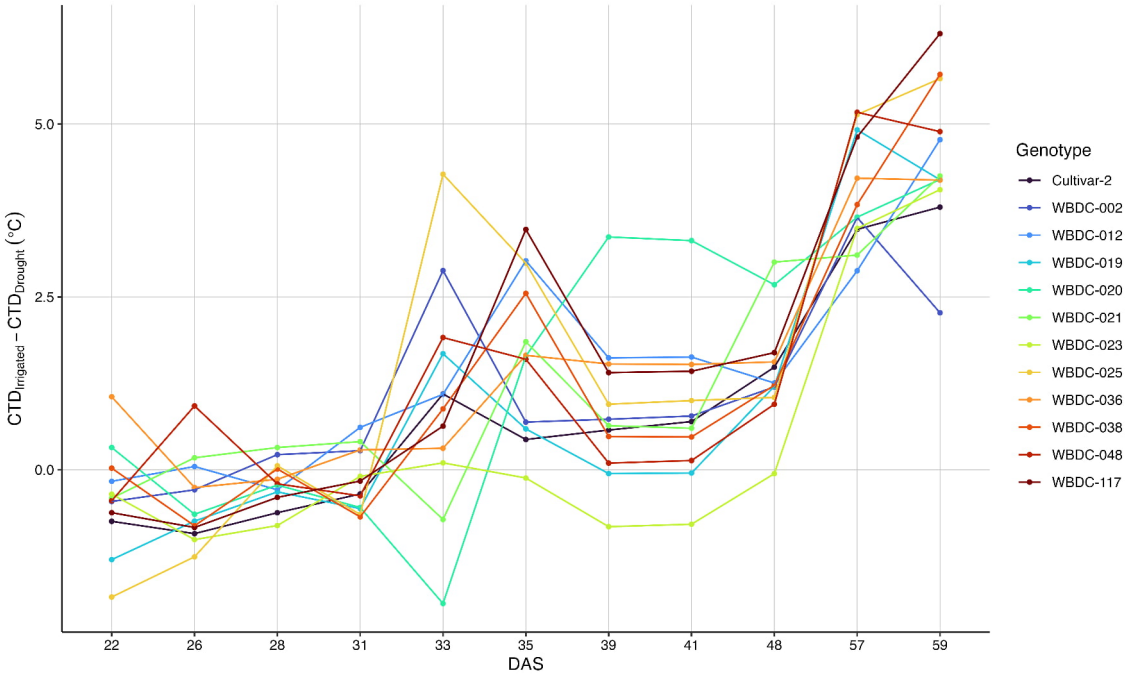

Figure 3.8. CTD contrasts between irrigated and drought treatment across all genotypes and DAS.

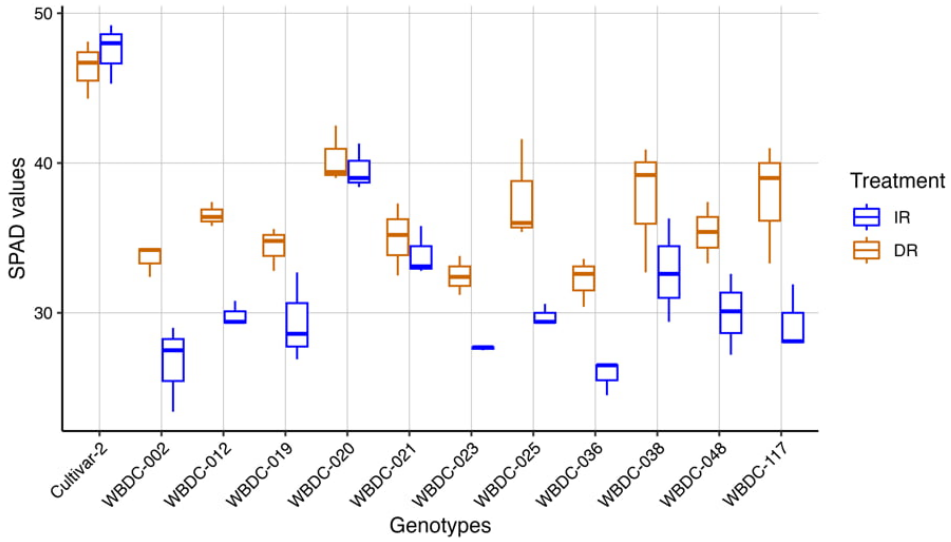

Figure 3.9. Chlorophyll content, as SPAD values, for each Genotype measured at the end of the experiment (DAS = 59).

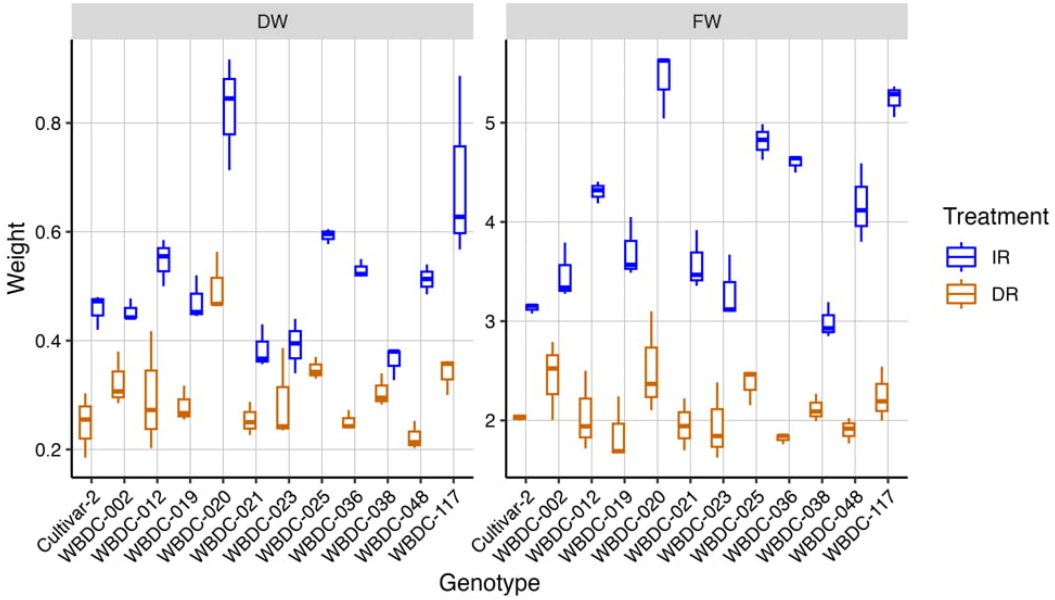

Figure 3.10. Boxplots illustrate the distribution of fresh weight (FW) and dry weight (DW) across genotypes and irrigation treatments.

3.3.4 Broad sense heritability (H^2)

Broad-sense heritability (H^2) quantifies the proportion of total phenotypic variance attributable to different genotypes. Variance components were obtained from linear mixed models using genotype as a random factor to estimate the broad-sense heritability (H^2) for each trait (Equation 3.5). For CTD, heritability values were specifically obtained for each Treatment:DAS combination (Appendix 3.1). For chlorophyll content and biomass, a single H^2 value was obtained for irrigated and drought-treated pots separately at 56 DAS and 59 DAS, respectively.

Heritability for canopy temperature depression (CTD) were highly variable, particularly under drought conditions, indicating a strong environmental influence on this trait. H^2 for CTD ranged between 12% to 75% for irrigated pots and 0% to 82% for drought pots (Appendix 3.2). For irrigated pots, heritability values were observed consistently higher than 40% across most phenotyping days, except for 26 and 48 DAS. In contrast, drought pots displayed lower heritability after 28 DAS once imposed drought. Despite the generally low heritability of CTD for drought-treated pots compared to pots without any water limitation throughout most of the experiment, at 57 DAS – when drought pots were at 29% of field capacity – CTD exhibited moderate H^2 of 42% while 40% in non-stressed pots. Chlorophyll content, Fresh Weight (FW), and Dry Weight (DW) exhibited high broad-sense heritability (H^2) ranging from 48% to 97% (Appendix 3.3). Among these traits, FW in drought-treated plants demonstrated the lowest heritability at 48%. However, DW of drought-treated pots maintained a high heritability of 77%.

3.3.5 Correlation matrix of all measured traits

Correlation matrices were constructed for irrigated and drought pots separately using CTD data from all phenotyping days, SPAD (chlorophyll content), and fresh and dry weight biomass (Figure 3.11). Under irrigated conditions, CTD measurements taken at different DAS exhibited moderate to strong positive correlations ($r>0.5$). As expected, days that were further apart showed weaker correlations, indicating higher variations in transpiration patterns over time and changes in genotype ranking. In contrast, the CTD in drought pots did not display the significant correlation across most DAS. This was expected as it indicates altered transpiration patterns as a result of decreasing soil water content.

Under well-watered conditions, FW and DW exhibited significant correlations with CTD in irrigated pots at 22, 35, 39, 41, and 48 DAS. This association, particularly in the later stages of the experiment, suggests a potential relationship between higher transpiration rates (indicated by higher CTD values) and increased biomass accumulation. The observed correlation may reflect either a causal link between transpiration and biomass production, where increased transpiration supports greater growth, or an indirect effect where greater biomass influences CTD values by reducing heat fluxes contributions from the background. Further investigation is required to determine the physiological basis of this relationship. In contrast, drought-treated pots showed no significant correlation between FW and CTD at any DAS.

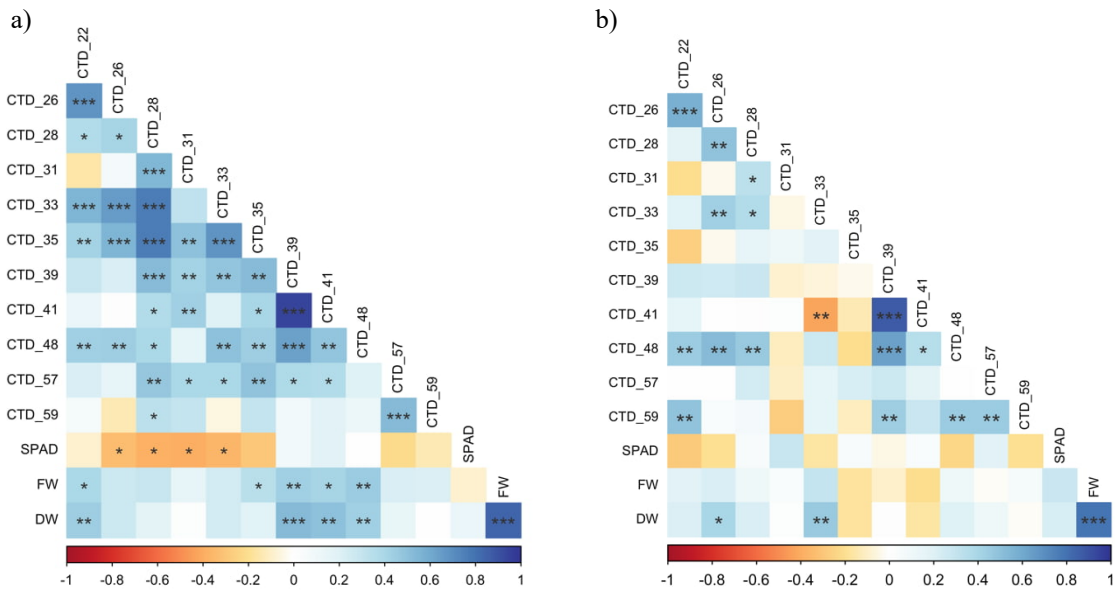

Figure 3.11. Correlation matrices for irrigated (a) and drought (b) pots between CTD at all DAS and FW. Each square represents 36 observations. An asterisk (*) indicates a significant Pearson correlation at $p<0.05$.

3.4 Discussion

3.4.1 CTD as a spectral proxy of transpiration

Transpiration rate reflects the instantaneous water usage of a plant, making it a key trait for assessing drought tolerance. Characterising transpiration patterns across diverse genotypes is critical for phenotyping efforts aimed at selecting candidates for improved water-use efficiency and understanding the genetic basis of drought adaptation.

Up to 99% of transpiration rates under favourable environments are driven by stomatal conductance (Hasanuzzaman *et al.*, 2023a). Open stomata facilitate water losses, leading to evaporative cooling. This cooling effect lowers leaf temperature, creating a negative correlation between canopy temperature (T_c) and transpiration. Consequently, T_c can serve as an indirect proxy for stomatal conductance, provided their relationship is well-characterised under given environmental conditions.

To establish canopy temperature depression (CTD) as a reliable proxy for g_{sw}, a dedicated phenotyping campaign was conducted to validate the relationship between these traits through direct measurements with a handheld porometer. Canopy temperature was recorded using a thermal camera positioned above the plants while stomatal conductance was simultaneously measured with the Li600P/F. This approach enabled precise segmentation of the specific leaf area where stomatal conductance was assessed, ensuring a direct comparison between the two traits.

The need for the extraction of a specific leaf segment arose from the observed temperature heterogeneity within leaves. This yielded a strong correlation between CTD and g_{sw} (r=0.819) which validated CTD as a reliable measure of stomatal conductance (Figure 3.5).

Despite the exponential shape initially observed (Figure 3.5), this apparent relationship is not biologically meaningful as stomatal conductance (g_{sw}) cannot approach infinity when CTD increases due to several physiological and physical constraints that regulate transpiration. While higher g_{sw} enhances evaporative cooling and increase CTD, stomatal opening is physically limited by guard cell mechanics, restricted by water availability, and regulated by boundary layer resistance. Additionally, the latent heat flux is constrained by available radiation energy, meaning that even at maximal stomatal opening, water evaporation from stomata cannot exceed the energy available for vaporisation. As a result, further increases in CTD beyond a certain point do not lead to infinite g_{sw}, but instead may trigger stomatal closure to prevent excessive water loss and hydraulic failure (Grossiord *et al.*, 2020).

The linear relationship between CTD and T_a arises because T_c did not increase proportionally with T_a. This is likely caused by higher evaporation rates from the leaf surface enhanced at a higher ambient temperature. The Clausius-Clapeyron equation provides a mechanistic relationship between saturation vapor pressure as a function of ambient temperature T_a (Equation *3.7*) (Velasco *et al.*, 2009):

$$e_s(T) = e_0 e^{\left(\frac{L_v}{R_v}\left(\frac{1}{T_0} - \frac{1}{T}\right)\right)} \qquad \text{(Equation 3.7)}$$

Where $e_s(T)$ is the saturation vapour pressure in Pa, e_0 is the reference vapour pressure at T_0 = 273.15 K, L_v is the latent heat of vaporization of water in J/kg, R_v is the specific gas constant for water vapour in J/(kg·K), and T is the absolute temperature in Kelvin. This equation describes the exponential relationship between saturation vapour pressure and temperature, illustrating how the capacity of air to hold water vapour increases with temperature (Figure 3.12).

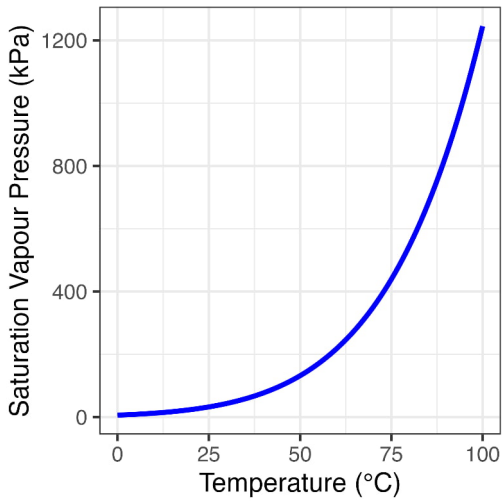

Figure 3.12. Simulated exponential relationship between Saturation Vapour Pressure and ambient temperature (T_a).

The higher VPD caused at higher ambient temperatures thus enhance the evaporative cooling capacity of leaves, preventing T_c from rising at the same rate as T_a. The main implication of this proportionality is that spatial variations of T_a can lead to spurious relationship of CTD with transpiration patterns which can preclude the identification of genetic factors influencing such CTD in response to drought. While CTD itself was intended as a normalisation method to account for spatial variation in ambient temperature that may affect canopy temperature by subtracting the ambient temperature (T_a) from canopy temperature (T_c) (Equation 3.1), the strong positive correlation between CTD and T_a ($r = 0.91$) observed in this study indicates that ambient temperature itself substantially influences CTD and should be therefore be explicitly accounted for in the analysis to enhance the detection of genetic effects.

3.4.2 Assessing genetic variation

The statistical analysis for CTD revealed no significant Genotype:Treatment or Genotype:Treatment:DAS interactions, suggesting that the genotypes in this experiment exhibited similar reductions in transpiration under drought conditions. Significant Genotype:Treatment interactions are desirable as they may indicate variation in physiological responses to different levels of drought severity, while a significant Genotype:Treatment:DAS interaction would suggest time-dependent differences in transpiration regulation under water stress. It has been found that the drought tolerance in transgenic wheat is associated with a prolonged transpiration during water stress compared to the control (González *et al.*, 2019). This highlights the importance of considering temporal dynamics in stomatal conductance and transpiration patterns when assessing genotypic variation in drought responses. The absence of statistical interactions between Genotype, Treatment and DAS in this study may be due to the small number of replicates and

genotypes included in the experiment rather than a lack of inherent phenotypic diversity of CTD responses. Possibly, with a larger and more diverse set of genotypes, more significant Genotype:Treatment interactions will emerge.

3.4.3 Spatial temperature variations influence CTD contrasts

Soil drying is generally expected to increase the $CTD_{contrast}$ (Equation 3.2). Large positive values indicate higher transpiration rates in well-irrigated pots compared to drought-treated ones. Conversely, negative values suggest higher transpiration rates in drought-treated pots compared to irrigated ones. The unexpected negative $CTD_{contrast}$ observed in genotype WBDC-020 at 33 DAS (Figure 3.8) is likely due to differences in spatial microclimates affecting canopy temperature. Although WBDC-020 could be transpiring less under drought conditions, this reduction in transpiration was not reflected as higher $CTD_{contrast}$ due to differences in the locations of the drought pots and the temperature data loggers at the exact moment of data acquisition. For instance, on sunny days, the glasshouse structure creates uneven shading, resulting in lower canopy temperatures for shaded pots compared to those under direct sunlight. In this study, the phenotyping process involved moving the thermal camera around while keeping the pots and temperature data loggers fixed. If a drought-treated pot is shaded while the temperature data logger is exposed to sunlight, the temperature difference between the data logger and the shaded canopy may appear greater than it would be if both, pot and data logger, were shaded. This leads to an overestimation of CTD for that specific pot, giving the false impression of higher transpiration than is actually occurring. Thus, the observed $CTD_{contrast}$ may be more reflective of variations of ambient temperature caused by incoming solar radiation rather than actual genotypic differences in transpiration. This issue should and can be addressed by placing more data loggers to capture spatial variations of temperature more precisely or ensuring a full shaded environment.

3.4.4 Biomass and chlorophyll content for agronomic performance

Fresh Weight (FW), Dry Weight (DW) and chlorophyll content can be used as part of a comprehensive selection criteria for drought tolerance and quantify a genotypes' agronomic value. The experiment design was effective in enabling the identification of significant differences and interactions between irrigated and drought pots in chlorophyll and biomass traits. As expected, drought conditions led to a reduction in both fresh weight (FW) and dry weight (DW). However, whether reduction in biomass was due to stomata contribution alone or changes in the photosynthetic capacity of the plant warrants further investigations.

Chlorophyll content (SPAD values) increased under drought conditions. While drought stress may have reduced chlorophyll biosynthesis, it likely resulted in higher chlorophyll density per unit

area due to reduced leaf growth and thicker leaves in stressed plants (Hasanuzzaman *et al.*, 2017). The observed increase in chlorophyll content could also suggest that the duration of the drought treatment and the overall experiment were insufficient to cause a negative impact. Rapid plant growth and development resulted in a relatively short experiment duration of 59 days from sowing to biomass harvest, compared to typical field experiments. Once Cultivar-2 reached anthesis at 59 DAS, we determined that any further differences in CTD would likely be attributed to variations in phenology, and the increasing contribution of FW biomass to pot weight. Therefore, we proceeded to biomass harvesting. The 38-day period of induced drought was probably too brief to allow for a prolonged and gradual manifestation of chlorophyll reduction, which typically appears as senescence during late reproductive stages in the field.

3.4.5 Selecting optimal growing and CTD phenotyping conditions

CTD measurements differed across phenological stages, which is aligned with the expectation of transpiration rates changing over time with vegetation growth and phenological development (Sobejano-Paz *et al.*, 2020). Daytime temperatures in the glasshouse were maintained at 22°C to accelerate water evaporation and plant transpiration, expediting the onset of drought stress. However, this also accelerated plant development, amplifying phenological differences among genotypes compared to the slower growth and development that would be observed in colder, more natural winter field conditions. This variation in phenology complicates the interpretation of CTD data, particularly in the context of a high-throughput phenotyping protocol aimed at identifying physiological mechanisms associated with drought tolerance. Ensuring that genotypes are assessed at comparable phenological stages is therefore critical for extracting meaningful physiological insights. This is particularly challenging when working with diverse germplasm, where phenological variation among tens or hundreds of lines can introduce significant inconsistencies in drought response assessments through thermal imaging. While early measurements in the experiment could mitigate against phenological differences, phenotyping immature seedlings (e.g., earlier than the 3-leaf stage) may yield inaccurate CTD readings due to small plant size affecting image processing and underdeveloped stomata. Furthermore, in wild germplasm, germination does not occur simultaneously. Assessing plants for drought stress earlier than the 3-leaf stage could result in a significant amount of missing data.

In this experiment, phenological development was not controlled, as large differences among genotypes were not initially expected. However, significant variation in developmental rates can affect the interpretation of CTD data. To account for this, a preliminary experiment to characterise phenological progression across genotypes would be beneficial for estimating an appropriate time point when most genotypes reach a comparable developmental stage. Alternatively, incorporating

a quantitative measure of phenology as a covariate in statistical analyses would help adjust for phenological differences and improve the accuracy of physiological trait comparisons (Celestina *et al.*, 2023).

The results of this experiment suggest that high ambient temperatures (>34°C) during phenotyping may enhance phenotypic differences across genotypes (Figure 3.7). Soil media with high clay loam content (>30%, v/v) possess a high water-holding capacity, which helps prevent excessive water evaporation during CTD phenotyping under these extreme conditions (An *et al.*, 2018). On the other hand, lowering daytime temperatures on non-CTD phenotyping days to below 18°C can slow down phenological development, replicating natural winter conditions to extend the duration of induced drought stress. This approach could lead to more significant phenotype contrasts between irrigation treatments that are less impacted by phenological differences. Given that most glasshouses lack chilling systems and rely on evaporative cooling, conducting drought experiments during winter would lower glasshouse temperatures naturally. However, these lower temperatures in non-CTD phenotyping days could also delay the achievement of target drought levels due to slower soil drying rates in high clay loam content soils. It is therefore recommended to maintain a balance between maintaining low temperatures to delay phenological development and achieving the target drought stress levels.

3.4.6 Heritability

Moderate to high heritability values of potential drought tolerance traits are crucial to exploit the underlying genetics responsible for such mechanisms. In this study, broad-sense heritability (H^2) values for Canopy Temperature Depression (CTD) varied across different days of measurement, indicating fluctuating contributions of genetic and environmental factors to the observed trait variation. On days with moderate to high heritability (H^2) the genetic variance represented a large proportion of the total phenotypic variance, suggesting that measurements on days with less temperature fluctuations, humidity, or soil moisture are more reliable for selecting genotypes with desirable levels of transpiration rates. These results highlight the importance of maximizing genotypic differences by maintaining stable conditions during CTD phenotyping, a challenging task in semi-controlled glasshouse environments.

FW, DW and SPAD showed moderate to high heritability (H^2 > 40%). The moderate heritability in FW of drought pots (H^2= 48%) (Appendix 3.1) indicates some environmental influence in water content since DW of the same treatment group shows high heritability (H^2= 77%). The higher heritability of SPAD, FW, and DW compared to CTD is likely due to the time-integrated nature of these traits, reflecting the cumulative long-term effects of drought stress. The high heritability

of biomass traits observed in this study may be the result of the precise control of soil water content throughout the experiment. Although high heritability of these traits in this experiment suggests that genetic factors are more easily identifiable under this experiment's specific conditions, it does not necessarily indicate that the genetic networks governing biomass and chlorophyll production under drought are less complex. Instead, it reflects the absence of the logistical constraints that CTD faced during sampling.

3.4.7 The impact of biomass on CTD variability

Separating the effects of biomass accumulation and soil water content on pot weights as plants grow has been a long-recognised challenge in drought experiments (Sexton *et al.*, 2021). In the current experimental setup, towards the end of the experiment, above-ground fresh weight biomass represented approximately a 4% difference in field capacity between the pots with the highest and lowest fresh weight (FW). The moderate to low positive correlation ($r<0.3$) between FW and CTD in 39, 41 and 48 DAS under well-irrigated conditions suggests that biomass accumulation had a small but significant influence on CTD measurements when soil moisture was not limiting. However, the lack of correlation under drought treatment suggests that the uncertainty of soil water content introduced by the accumulated biomass was not systematic and did not play a significant part in determining CTD in drought pots (Figure 3.11). This implies that the low heritability values of CTD in drought pots was likely to be caused by random variations in soil water content across pots, which arose from the challenges of maintaining a more consistent soil moisture levels under manual irrigation, and the variations in ambient temperature conditions.

3.4.8 Data acquisition times

Although attempts have been made in the past to develop high-throughput imaging protocols for cereal crops in glasshouses, the scope of these studies is still limited to a few tens of lines per experiment (Grant *et al.*, 2006; Sirault *et al.*, 2009). The phenotyping process in these studies typically involves moving the pots to a specific location for image acquisition. This minimises the spatial component affecting canopy temperature, but it also limits the scope, throughput, and scalability as it takes considerable time to move the pots around. The high-throughput aspect of these methods mostly depends on the short image processing times via automatic segmentation methods (Sirault *et al.*, 2009), yet data acquisition takes hours to complete. Data acquisition in this experiment took 20 minutes for 78 pots, with one photo per pot, significantly reducing the time for CTD measurements and minimizing temporal variations in temperature, relative humidity, and vapor pressure. However, this setup may amplify spatial variations of these factors when the glasshouse structure is highly irregular.

3.4.9 Considerations for scaling up CTD phenotyping under controlled conditions

As plants developed, their increased transpiration rates due to larger leaf area caused the soil to dry out more quickly, requiring more frequent and substantial rewatering to prevent wilting before the next scheduled irrigation. Ideally, tall, narrow pots are more desirable than small pots because they provide soil water profiles closer to those found in the field and are less sensitive to changes in water content due to plant transpiration (Turner, 2019). In large pots, the contribution of biomass growth and transpired water by plants represents a smaller proportion of the total weight of the pots filled with moist soil. With larger pots, more plants can be grown per pot to increase canopy coverage and facilitate image segmentation at early growth stages. However, larger pots are heavier and complicate manual irrigation. Although automated gravimetric irrigation systems present a solution, scaling up CTD phenotyping for germplasm explorations in replicated experiments may involve hundreds, if not thousands, of genotypes, and gravimetric systems are too expensive for this purpose. Non-invasive sensors, which can absorb electromagnetic waves with nearly 100% efficiency (Amiri *et al.*, 2021), could offer a precise and more cost-effective alternative to both gravimetric systems and traditional soil probes for accurately estimating soil water content of hundreds of pots. Precise determination of soil water content can be used as a covariate to model CTD responses more accurately across varying moisture levels, rather than treating them as a categorical factor (e.g., irrigated vs drought).

3.5 Conclusion

This experiment presents a methodology for the precise determination of instantaneous transpiration rate via thermal imaging, specifically tailored for genetic studies, where a significant number of seeds may not be available for all genotypes. Specifically, we investigated how to optimise a phenotyping protocol using thermal imaging, chlorophyll content and biomass traits to characterise barley under irrigated and drought conditions in conventional glasshouses typically available to most researchers. By accurately measuring canopy temperature depression (CTD), researchers can reliably infer transpiration rates, providing valuable insights into mechanisms of plant water usage and drought tolerance that could be harnessed for plant breeding. In this experiment, canopy temperature depression (CTD) – the difference between ambient and canopy temperature – reliably reflected differences in stomatal conductance, validating CTD as a high-throughput spectral proxy of transpiration. However, variations in soil water content and spatial variations of ambient temperature can significantly decrease the contribution of genetic factors of CTD if not carefully controlled. In particular, spatial variations caused by the glasshouse structure, such as uneven shading, can increase environmental variability and decrease trait heritability. We strongly recommend incorporating additional data loggers to monitor temperature

variations more precisely in the glasshouse, which would minimise the risk of underestimating or overestimating CTD. Alternatively, a completely shaded glasshouse could be even more effective in ensuring consistent temperature conditions. Overall, stable ambient conditions during CTD phenotyping are essential for reliable genotype selection based on heritable values CTD. Differences in plant phenology of diverse genotype panels calls for methods that account for and correct CTD at different developmental stages; especially for highly diverse genetic resources such as wild germplasms.

This experiment aims to make the advancements in crop phenomics accessible to a broader scientific community by demonstrating a viable method using thermal imaging. In particular, we here help researchers working in pre-breeding research where the exploration of hundreds of accessions is essential to identifying promising candidate genotypes for drought tolerance.

Chapter 4
Screening wild barley for drought tolerance under glasshouse conditions

4.1 Introduction

Thriving under natural harsh conditions for countless generations, wild relatives are a vast resource of drought tolerance mechanisms and genes (Nevo & Chen, 2010). The successful utilisation of these wild relatives in breeding hinges on selecting the most promising candidates and integrating their unique traits into modern agricultural practices. While genome-wide molecular data provides a comprehensive view of the genetic variation to understand population structure and pointing out redundancies in wild germplasms (Milner *et al.*, 2019). However, genetic information alone does not allow predicting phenotypic performance under stress conditions (Nguyen & Norton, 2020). Integrating genotypic information and phenotypic data offers a powerful tool to assess the potential of diverse germplasms for specific objectives, such as drought tolerance genetic improvement (Darkwa *et al.*, 2020).

Selection activities are generally guided by prior knowledge of agronomic traits that are effective in the target environment. This inherently reduces genetic variation. Breeders prioritise these traits at the pre-breeding stage, anticipating their relevance to commercial breeding (Ivandic *et al.*, 2000; Abdolshahi *et al.*, 2015; Bazzaz *et al.*, 2015; Cai *et al.*, 2020; Bao *et al.*, 2023). While this approach is effective for cultivated germplasm and landraces, it is impractical for wild relatives, as they are not easily grown in field conditions. Given the limited knowledge of these genetic wild resources, selection strategies could be designed to balance both exploratory and applied objectives. In this context, genotype selection strategies for wild relatives can be viewed on a continuum space—ranging from selections focused on detailed molecular analysis of tolerance mechanisms to those prioritising agronomic traits for breeding. Recognising this spectrum is essential for maximising the potential of wild germplasm. A multivariate phenotypic analysis is particularly suited for this purpose.

For drought tolerance assessments, irrigation regimes that supply pots with the same water equally can result in varying soil moisture levels due to genotypic differences in transpiration rates. As a result, distinguishing between the effects of water depletion and plant physiological responses can be challenging. Ensuring similar moisture levels within the same treatment groups could potentially enhance the reliability of physiological measurements, particularly for traits such as canopy temperature depression (CTD), which are highly influenced by soil water availability.

Drought tolerance genetic improvement is particularly challenging due to the intricate relationship between CO_2 and H_2O exchange through the same stomatal pores. The natural response of stomata to close in order to prevent plant desiccation and water depletion inevitably leads to a decrease in biomass and grain yield as CO_2 diffusive resistance increases (Flexas, 2008). Reductions in biomass alone, however, do not reveal whether the overall plant health and ability to photosynthesise is being affected (Flexas, 2008). Photosynthetic and non-photosynthetic pigments, such as chlorophyll (Chl), flavonoids (Flav), and anthocyanins (Anth), can provide insights into the plant functioning under stress conditions (Zarco-Tejada *et al.*, 2018; Zarco-Tejada *et al.*, 2021). Chlorophyll (Chl) is an indirect indicator of photosynthetic capacity and a plant's ability to retain green foliage during stress. Flavonoids and anthocyanins serve as photoprotectors, mitigating light-induced damage into photosynthesis apparatus (Merzlyak *et al.*, 2008). Nitrogen Balance Index (NBI) is an indicator of Carbon/Nitrogen allocation changes due to nitrogen deficiency under stress (Cartelat *et al.*, 2005). These parameters can be optically assessed in a high-throughput fashion with handheld devices or imaging spectroscopy techniques to cover large screening populations (Cerovic *et al.*, 2012; Zarco-Tejada *et al.*, 2018). Coupled with biomass, pigment traits can offer a more comprehensive assessment of plant responses to drought, helping to differentiate between genotypes that experience physiological decline from those that maintain robust photosynthetic function under stress.

A physiology-focused exploration of wild germplasms embraces the trade-off between carbon assimilation and water conservation and opens the door for more complex mechanisms. For instance, an increased efficiency in adaptation of transpiration rates would allow plants to conserve water while sustaining productivity when conditions are favourable by dynamically matching the water supply and demand. This entails closing stomata when water is scarce and keeping them wide open when water is abundant. Theoretically, crops with an efficient adaptive transpiration would still display biomass declines under drought but could potentially avoid the undesired “water-failure” and “yield-penalty” production trajectories (Vadez *et al.*, 2024). Water failure refers to the critical absence of water during the grain filling stages, which can severely impact yield and crop quality. Yield penalty occurs when water is not utilised efficiently throughout the growing season, resulting in excess water remaining in the soil by the end of the season, without translating into grain production (Vadez *et al.*, 2024). The extent of genetic diversity of adaptive transpiration remains elusive due to the current limitations in our ability to measure and identify them at large scale. On the other hand, while the biological significance for survival in natural (non-agricultural) environments is evident, its genetic complexity and agronomic potential remains largely unexplored.

In this study, I conduct a phenotypic analysis of a diverse wild barley genetic pool, focusing on canopy temperature depression (CTD) under varying levels of water deficit to investigate adaptive transpiration. I present a structured approach for the collective analysis and interpretation of canopy temperature, biomass, and spectrally-derived pigment traits, offering a framework for the holistic evaluation of wild populations. To quantify the genetic contribution to these traits, narrow-sense heritability was estimated using the Genomic Best Linear Unbiased Prediction (GBLUP) model, which incorporates genome-wide SNP data to partition phenotypic variance into genetic and residual components. The variance components from a GBLUP model provides insight into the extent to which trait variation is attributable to additive genetic differences. Finally, a combined agronomic, physiological, and phenotypic clustering-based selection strategy was implemented to balance the objectives of selection of wild candidates for mechanistic exploration research and for plant breeding purposes. This approach aims to identify genotypes that maintain productivity under drought while exhibiting valuable adaptive mechanisms, ultimately leading to the selection of a core set of genotypes for pre-breeding research.

4.2 Materials and Methods

4.2.1 Plant material and growing conditions.

The protocol developed in Chapter 3 of this thesis was used to evaluate a pool of 126 barley accessions for drought tolerance, including 120 wild barley genotypes and 6 cultivars (Appendix 4.1). Wild genotypes were sourced from the International Wild Barley Sequencing Consortium (IWBSC), University of Minnesota, USA, along with a VCF file containing whole-genome sequencing variants for 111 out of the 126 genotypes. Three plants per pot were grown in 1.5L pots using the same media as described in Chapter 3. Husks of wild barley seeds were carefully removed manually, and the seeds were immersed in 20 ml of H_2O_2 at 1% for 18 hours the day before sowing.

Glasshouse temperature settings were configured to control the temperature at which the vents open and the cooling systems activate, rather than maintaining a target temperature. The average glasshouse temperature throughout the experiment was 22°C during the day and 15°C during the night. During thermal imaging phenotyping, between 1:00pm and 2:30pm, the cooling system was turned off to prevent wind disturbance, which resulted in higher temperatures than 22 °C despite vents being completely open. The glasshouse temperature during this time highly depended on external conditions such as solar radiation and external ambient temperatures.

4.2.2 Experimental design

The spatial arrangement was similar to the experiment of Chapter 3. Pots were arranged in a 14 x 36 grid with a pot placed in every second location to maximise space utilisation (Figure 4.1). The experiment was divided into three independent trials conducted consecutively in the same glasshouse in 2022; Trial 1 from April to May, Trial 2 from June to July, and Trial 3 from August to September. Each trial contained one replicate for each genotype-by-treatment combination, totaling 252 pots per trial. Pots were arranged in three blocks within each trial to ensure that genotypes were assessed at various spatial locations throughout the glasshouse. Each block contained 42 genotypes under both irrigated and drought, resulting in an incomplete block design. Gendex (Nguyen, 1983) was used to construct a near-optimal alpha-lattice design, maximising genotype pairwise comparisons within each block (Appendix 4.2). To facilitate irrigation, each block was further subdivided into two treatment sub-blocks, one for drought and one for irrigated pots, for a total of six treatment sub-blocks per trial. Irrigation sub-blocks were randomly shuffled across the three trials.

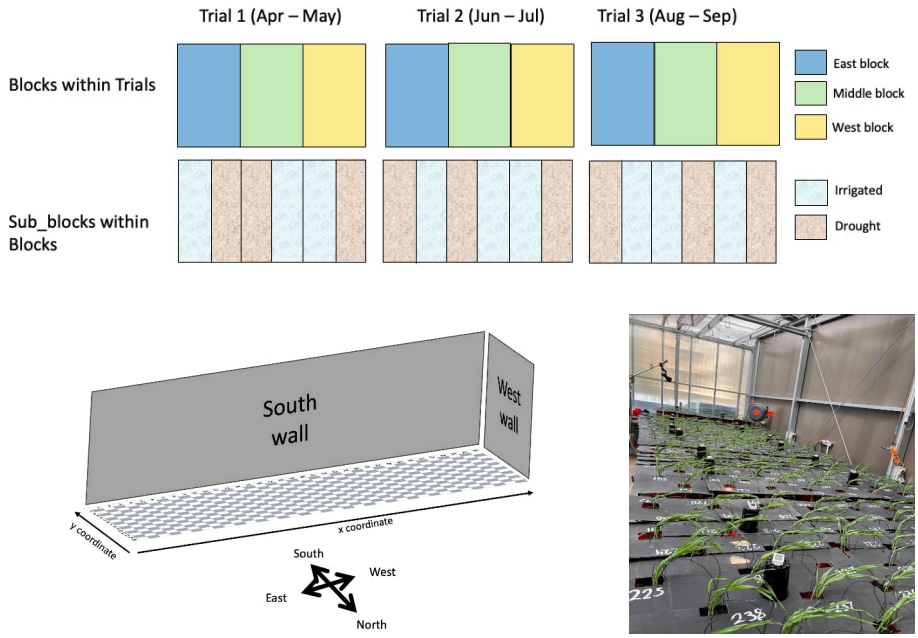

Figure 4.1. Outline of the experimental design and spatial arrangement of pots.

4.2.3 Drought treatment

The drought treatment was conducted using the same method as described in Chapter 3. All plants were initially irrigated by capillarity until 50% of the pots achieved 2-leaf stage, after which drought pots transitioned to manual irrigation by placing a physical barrier between the pot and the floral foam. The well-irrigated half was kept under capillary irrigation for the rest of the experiment and maintained between 90-100% Field Capacity (FC).

The water content of drought-treated pots was controlled by placing them on a digital scale and pouring water from the top until reaching the desired weight. Drought-treated pots were gradually dried by matching the rate of slowest drying pot. The irrigation frequency was determined based on the pot that experienced the quickest soil drying rate and it changed according to the age of the plants as older plants consumed water more rapidly than younger ones. Towards the end of the experiment, irrigation was administered once daily. Historic soil drying data was used to irrigate drought pots one day before each thermal imaging phenotyping campaign to ensure all pots within the same treatment group maintained consistent water content during the time of measurements.

4.2.4 Phenotyping

Primary traits measured in this study included CTD at 3 different levels of water deficit (stages 1, 2, and 3), spectrally-derived pigment traits (Chlorophyll, Flavonoids, Anthocyanins and Nitrogen Balance Index), and above-ground biomass traits (FW and DW).

Canopy temperature depression

Canopy temperature phenotyping was conducted three times during the experiment, referred to as "stages". Stage 1 involved 100% field capacity (FC) vs 100% FC (all pots irrigated), stage 2 involved 100% FC vs. 60% FC (irrigated vs moderate water deficit), and stage 3 involved 100% FC vs. 40% FC (irrigated vs severe water deficit) (Table 4.1). Phenotyping was conducted on sunny days to avoid fluctuations caused by inconsistent lighting conditions, resulting in ambient temperatures during phenotyping ranging between 35°C and 40°C.

The process of canopy temperature (T_c) phenotyping followed a similar procedure detailed in Chapter 3. A custom matte black-painted cardboard was used to cover the soil, pot saucers, and bench to provide a uniform background, enhancing the temperature contrast between the canopy and the background for effective image segmentation. Canopy temperatures were recorded by gliding a thermal camera (Model E86, Teledyne FLIR LLC) over each pot three times within a time frame of 1hr and 30 mins. Three radiometric images were extracted and analysed with a custom MATLAB (Mathworks Inc., Natick, Massachusetts, USA) code to obtain average canopy temperature values. Ambient temperature was recorded using 18 HOBO data loggers (Onset, Cape Cod, Massachusetts, USA) evenly located across the glasshouse, and canopy temperature depression (CTD) was calculated as the difference between ambient (T_a) and canopy temperature (T_c) (Equation *3.1*).

Table 4.1. Summary of data acquisition during the experiment

	Exp1					Exp2					Exp3				
Days After Sowing (DAS)	19 DAS	43 DAS	57 DAS	58 DAS	59 DAS	22 DAS	41 DAS	55 DAS	58 DAS	60 DAS	26 DAS	40 DAS	47 DAS	50 DAS	53 DAS
CTD	✓	✓	✓	-	-	✓	✓	✓	-	-	✓	✓	✓	-	-
Chlorophyll	-	-	-	✓	-	-	-	-	✓	-	-	-	-	✓	-
Anthocyanin	-	-	-	✓	-	-	-	-	✓	-	-	-	-	✓	-
Flavonoids	-	-	-	✓	-	-	-	-	✓	-	-	-	-	✓	-
NBI	-	-	-	✓	-	-	-	-	✓	-	-	-	-	✓	-
Biomass (Fresh and Dry weight)	-	-	-	-	✓	-	-	-	-	✓	-	-	-	-	✓

4.2.5 Statistical analyses

Phenotypic data

Data processing and statistical analysis were performed with R (version 4.3.2) using packages spdep (version 1.2-5) (Bivand & Wong, 2018), lme4 (version 1.1.35.1) (Bates *et al.*, 2015), emmeans (version 1.10.0) (Lenth *et al.*, 2024), tidyverse (version 2.0.0) (Wickham, 2014). Separate models were used for each trait to quantify the effect of drought stress while accounting for several factors of the experimental design such as trial, genotype, sub-blocks, repeated measurements, and spatial location within the glasshouse (Table 4.2). A spatial analysis was performed on each of the primary traits except CTD, by assessing linear trends and spatial heterogeneities in the error terms across models 2 through 7 (Table 4.2). Global Moran's I test was employed to quantify the degree of spatial autocorrelation present in the residuals. A spherical variogram quantified the spatial dependence of residuals, which was used as the variance-covariance matrix (Σ) in linear mixed models 2 through 7. The Akaike Information Criterion (AIC) evaluated whether incorporating spatial covariance improved the model, comparing models with and without this structure to select the best balance between fit and complexity. Principal component analysis was used to examine the variance structure of the entire data set, including primary traits and tolerance indices. Phenotypic and genetic correlation analysis were conducted to assess the relationships between different traits.

Molecular data

A VCF file with whole-genome sequencing information for 111 genotypes was supplied by the International Wild Barley Sequencing Consortium (IWBSC; https://iwbsc.umn.edu), and filtered for biallelic variants using PLINK 2.0 (Purcell *et al.*, 2007). The filtering criteria included a minor allele frequency (MAF) of 0.05, a minimum allele count (MAC) of 100, a per-variant heterozygosity rate of 5%, and a per-variant missing call rate of 1%. After applying these criteria, a total of 881,755 biallelic variants were retained. A sample of 500,000 variants were randomly

selected out of the 881,755 biallelic variants to create the Genomic Relatedness Matrix (GRM) (VanRaden, 2008):

$$GRM = \frac{ZZ^{\mathrm{T}}}{p} \qquad \text{(Equation 4.1)}$$

Where $\boldsymbol{Z}$ is the matrix of the scaled and centred SNP codes and p is the number of SNPs. The $\boldsymbol{Z}$ matrix is defined as:

$$z_{ij} = \frac{x_{ij} - 2p_j}{\sqrt{2p_j(1-p_j)}} \qquad \text{(Equation 4.2)}$$

Where z_{ij} is the element of the $\boldsymbol{Z}$ matrix for individual i and SNP j, x_{ij} is the genotype coding with values 0, 1, or 2 to represent the number of reference alleles. The allele frequency of the reference allele at SNP j is denoted by p_j.

Genotype clustering

Cluster analysis of phenotypic and genotypic data was conducted to understand the extent and structure of genetic diversity in wild germplasms. Following the methodologies of Agre *et al.* (2019) and Darkwa *et al.* (2020), various distance matrices and clustering methods were evaluated to determine the best combination that preserves pairwise distances in the data via the cophenetic correlation coefficient (CCC). Hopkins statistics was used to assess the clustering tendency of the dataset, ensuring that the data exhibited potential for meaningful groupings (Wright, 2022). Distance matrices for phenotypic data included Euclidean, Manhattan, and Gower, while those for genotypic data included IBS, Jaccard, Nei, and Roger. The clustering methods assessed were Ward.D2, Single, Complete, Average (UPGMA) linkage. Mantel's test was employed to evaluate correlations between the selected phenotypic and genotypic distance matrices.

Narrow-sense heritability and genetic correlations

BLUEs for each trait were used in GBLUP models 8 through 14 (Table 2) with a 10-fold cross-validation (CV) to assess prediction accuracy and narrow (h^2) sense heritability using the GRM as a covariance structure. Prediction accuracy was obtained from Pearson's correlation coefficient (r) between predicted and observed values, averaged across all CV partitions. Variance components (σ^2) of the GBLUP model were used to calculate h^2. Genetic correlations among traits were calculated using a multivariate linear mixed model using MTG2 (version 2.22) with its default parameters (Lee & van der Werf, 2016).

Table 4.2. Linear mixed models for estimation of BLUEs, and narrow-sense (h^2) heritability.

Objective	Data source	Model	Group	Trait	Fixed effects	Random effects	Covariates
Estimation of adjusted means per line	Raw data	1	Transpiration	CTD	Trial, Treatment, Genotype, Stage	Sub-block, Pot ID	Ambient temperature
		2	Pigments	Chl	Trial, Treatment, Genotype	Sub-block	x coordinate, y coordinate
		3		Flav	Trial, Treatment, Genotype	Sub-block	x coordinate, y coordinate
		4		Anth	Trial, Treatment, Genotype	Sub-block	x coordinate, y coordinate
		5		NBI	Trial, Treatment, Genotype	Sub-block	x coordinate, y coordinate
		6	Biomass	FW	Trial, Treatment, Genotype	Sub-block	x coordinate, y coordinate
		7		DW	Trial, Treatment, Genotype	Sub-block	x coordinate, y coordinate
Genomic Prediction and narrow-sense (h^2) heritability	Adjusted means from models 1- 7	8	Transpiration	CTD	-	Genotype	-
		9	Pigments	Chl	-	Genotype	-
		10		Flav	-	Genotype	-
		11		Anth	-	Genotype	-
		12		NBI	-	Genotype	-
		13	Biomass	FW	-	Genotype	-
		14		DW	-	Genotype	-

Selection of core set

Traits were filtered based on statistical significance, heritability, and prediction accuracy, retaining those that demonstrated significant differences across irrigation treatments and exhibited moderate to strong genetic control. The thresholds for heritability (h^2) and prediction accuracy (r) were set at 0.2 and 0.3, respectively. Traits meeting or exceeding at least one of these parameters were used for the selection of a core set. Trait values were standardised and integrated into a composite selection criterion.

To facilitate the interpretation, a linear transformation was applied by multiplying each variable by -1 for traits where lower values are more desirable under water-limited conditions, such as low transpiration (low CTD). Traits where higher values indicate better performance, such as the MP index and CTD under irrigated conditions, were left unchanged. The linear transformation ensured that higher values consistently represented better performance across all traits. From an agronomic and physiological perspective, a hypothetical "Attractive candidate" was defined as a point with the highest values for each trait. These represent superior genotypes based on a general view of agricultural success. Conversely a hypothetical "Unattractive candidate" was defined as a point with the lowest values for each trait. These genotypes exhibited traits opposite to those associated with agricultural success, such as low biomass accumulation, and can be treated as negative control for further research for evaluating the effectiveness of selection strategies. Core sets of genotypes were selected from the top 10% and bottom 10% quantiles, based on their proximity to the ideal and unattractive candidates based on the smallest Euclidean distance. The rationale for excluding the middle 80% in this step is to prioritise individuals on two extremes of phenotypic variation. Finally, the selection process also ensured that at least one representative from each phenotypic cluster was included.

4.3 Results

A diverse panel of 126 barley accessions, including 120 wild and 6 cultivated, was assessed based on transpiration, biomass, and pigment traits across three unreplicated trials under controlled glasshouse conditions. Canopy temperature depression (CTD) via thermal imaging showed a significant correlation with stomatal conductance ($p<0.001$). Despite the dormancy breaking treatment, wild barley genotypes exhibited significant differences in gemination and emergence. Seedlings that germinated within a 7-day window from the first seedling emergence were retained for the study. Those germinating outside this window were removed and recorded as missing data to prevent significant biases in trait values due to phenological differences. As a result, Trials 1, 2, and 3 had 12, 21, and 7 pots with missing data, respectively.

Differences in external ambient conditions, such as temperature and solar radiation, between the three consecutive trials influenced the ambient temperature in the glasshouse, leading to variations in soil drying rates across the three trials (Appendix 4.3). The 2-leaf stage was achieved at 19 Days After Sowing (DAS) in the first trial, at 22 DAS in the second trial and at 26 DAS in the third trial. By the end of the three trials, developmental stages between the cultivated and wild material were readily identifiable. All six barley cultivars had consistently achieved heading developmental stage, in contrast to the wild accessions that remained vegetative. No flag leaves were identified in any of the wild accessions.

4.3.1 Spatial analysis and drought effects

Biomass and pigment traits exhibited significant linear gradients along the East-West line of the glasshouse, influencing trait means (Appendix 4.4). Nonetheless, the spatial analyses revealed no significant autocorrelation component ($p>0.05$) in the residuals after accounting for the linear trends in the statistical model (Appendix 4.5). Best Linear Unbiased Estimates (BLUEs), or adjusted means, were spatially adjusted using a linear (deterministic) trend by considering x and y coordinates as covariates in the model and did not include a spatial autocorrelation (stochastic) component.

The distribution of trait values varied across trials (Appendix 4.6). Most traits showed significant differences among genotypes ($p<0.0001$) except for anthocyanin content (Appendix 4.7). Conversely, significant differences between irrigation treatments were only observed in CTD, biomass, and chlorophyll content. No genotype-by-treatment interactions were identified at $p=0.05$ for any of the measured traits.

Mean Fresh weight ranged between 1.45 and 8.37 g plant^{-1} and dry weight ranged between 0.03 and 0.60 g plant^{-1}. Drought stress reduced biomass by an average of 1.28 g plant^{-1}(21%) and 0.07 g plant^{-1}(29%) for fresh and dry weight, respectively. High biomass accumulation of genotypes 080 and 021 was visually outstanding under drought and irrigated conditions, respectively. Genotype 080 under drought outperformed its well-irrigated counterpart in the first two trials, with the drought-treated pot reported as missing in the third trial. Genotype 021 showed the highest biomass under irrigated conditions in all trials. In contrast, genotypes 066 and 111 were significantly smaller than the other accessions, characterised by narrow leaves and reduced overall biomass.

Canopy temperature depression (CTD) ranged from 3.38 to 6.05°C at stage 1, from 3.23 to 7.08°C at stage 2, and from 3.06 to 6.77 °C at stage3. Differences in CTD between irrigation treatments

were highly significant ($p<0.001$) at stage 2 and stage 3. At stage 2, CTD under drought was 14% lower than irrigated, equivalent to a 0.8 °C difference. At stage 3, the difference between treatments increased to 33%, or 1.94 °C.

A slight increase of 4% (0.9 µg cm^{-2}) in response to water deficit was observed only in chlorophyll content while the rest of the pigment traits did not show any significant changes in response to water deficit.

4.3.2 Agronomic and stomata sensitivity indices

In preparation for multivariate phenotypic analysis, nineteen tolerance indices, commonly used in agronomic studies for drought tolerance breeding, were constructed using dry weight biomass under both irrigated and drought conditions. For a complete explanation of these indices refer to Bennani *et al.* (2017) and Morton *et al.* (2019). These indices were then subjected to correlation and principal component analysis (PCA) to understand the relationships among them. The correlation matrix (Figure 4.2a), ordered by hierarchical clustering, revealed distinct grouping of these indices. Cluster 1 included SSI, Red, TOL, and SSPI, while Cluster 2 included MSTIK1, STI, REI, HARM, MP, GMP, and MRP (Bennani *et al.*, 2017). The first two principal components of the PCA biplot (Figure 4.2b) illustrate the direction and magnitude of the trait vectors, indicating that most variables contributed similarly to the principal components PC1 and PC2. They explained together around 87% of the total variation. Notably, DI, DTE, RDI, and SSI are not in any of the main clusters in the correlation matrix but display magnitudes and directions that are nearly opposite to cluster 1, suggesting an inverse but analogous relationship to the traits in that cluster. RDY displays magnitudes and directions that are nearly opposite to those in Cluster 2. One index from each of the main clusters were chosen for their straightforward interpretation: mean productivity (MP) and stress tolerance index (TOL). In addition to agronomic indices, an index for adaptive transpiration, termed Stomatal Sensitivity (SI), was calculated as the difference in transpiration between irrigated and drought conditions (Rischbeck *et al.*, 2017). MP, TOL, SI_stage_2 and SI_stage_3 were included in phenotypic and genetic correlation analyses.

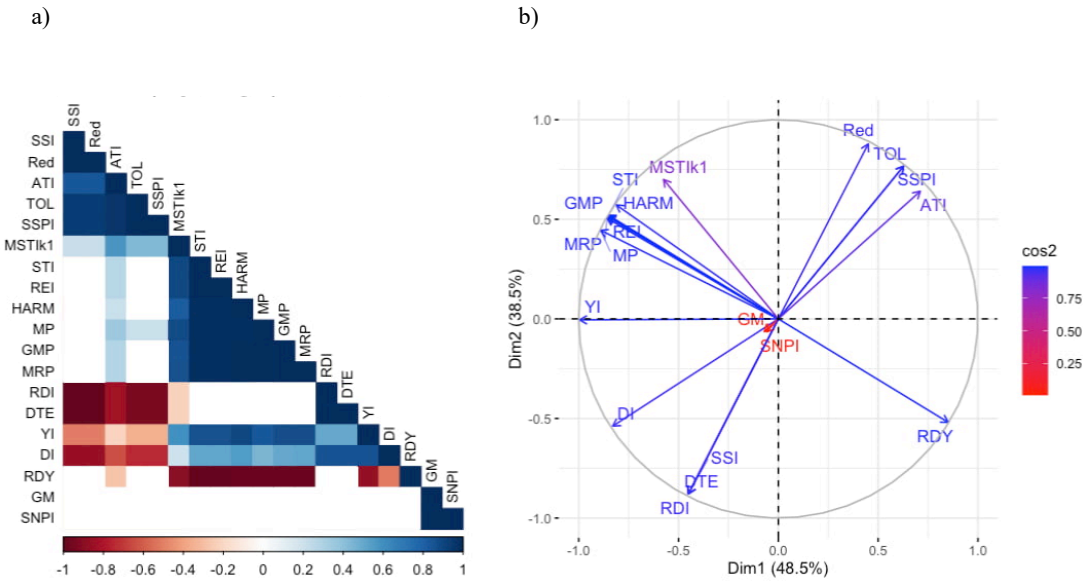

Figure 4.2. Correlation matrix (a) and principal component analysis biplot (b) for the analysis of the relationships between agronomic indices derived from dry weight (DW).

4.3.3 Phenotypic and genetic correlations

The phenotypic and genetic correlation matrices exhibited similar patterns (Figure 4.3). As expected, fresh weight (FW) and dry weight (DW) were highly correlated with canopy temperature depression (CTD) across all phenotyping stages and irrigation treatments at both phenotypic and genetic levels. No significant correlations were found between CTD and TOL. While a significant phenotypic correlation was observed between TOL and SI_stage_2 at p=0.05, this relationship was likely not genetically driven as there was no significant genetic correlation among them. On the other hand, strong phenotypic and genetic correlations were observed between CTD and Mean Productivity (MP). This means that, although reductions in transpiration rate (SI) were not directly linked to variation in biomass losses (TOL) under drought conditions, baseline transpiration (CTD) did have an impact on overall yield potential (MP).

Significant correlations were found among the pigment traits. However, no phenotypic correlations between pigments and CTD, nor between pigments and biomass, were observed, further supported by an absence of genetic correlation. This indicates that the variation in pigment content is largely independent of transpiration rates and biomass accumulation under tested conditions. Despite the crucial role of pigments in plant health protection under stress, they did not appear to be phenotypically or genetically associated with drought responses in this experiment.

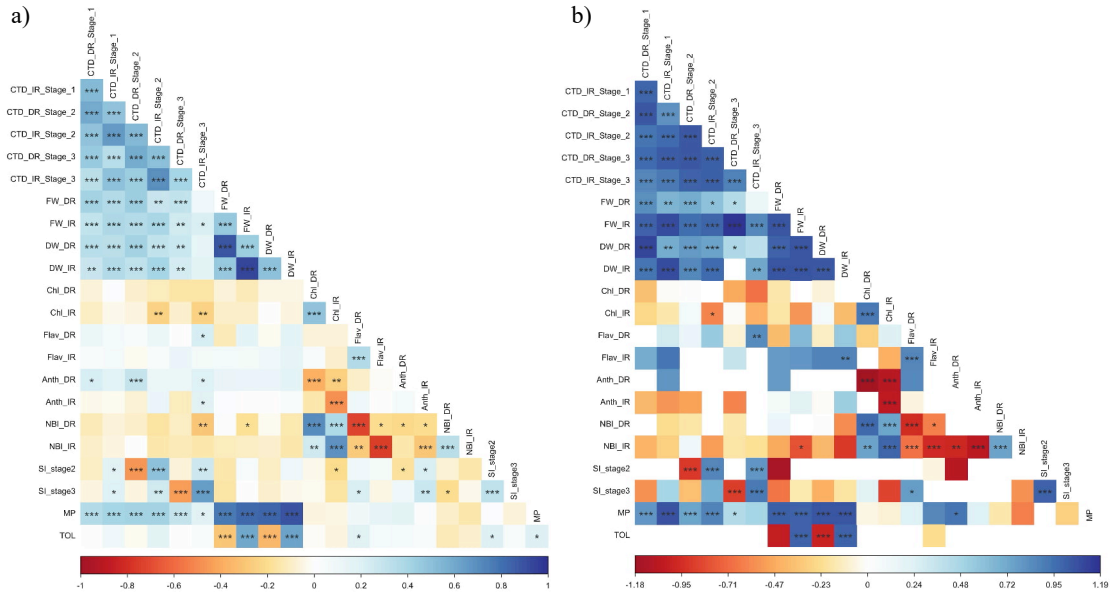

Figure 4.3. Phenotypic (a) and genetic (b) correlation matrices. Phenotypic correlation was calculated based on observed trait values across different genotypes, while genetic correlation was derived from multivariate analysis with MTG2 (Lee & van der Werf, 2016) to assess the underlying genetic relationships between measured traits.

4.3.4 Principal component analysis

Principal component analysis (PCA) of primary traits and agronomic indices indicated that the first three principal components (PC), cumulatively accounted for 50.8% of the total phenotypic variation in the data set (Figure 4.4). PC1 accounted for 26.2% of the total variation with mean productivity (MP) index and biomass under irrigated conditions having the highest absolute contribution and strongest influence. PC2 accounted for 14.7% and was dominated by NBI under drought and SI indices at stage 2 and stage 3. PC3 accounted for 9.9% of the total phenotypic variation where the largest contributions were associated with Dry Weight (DW) and Fresh Weight (FW) under drought conditions.

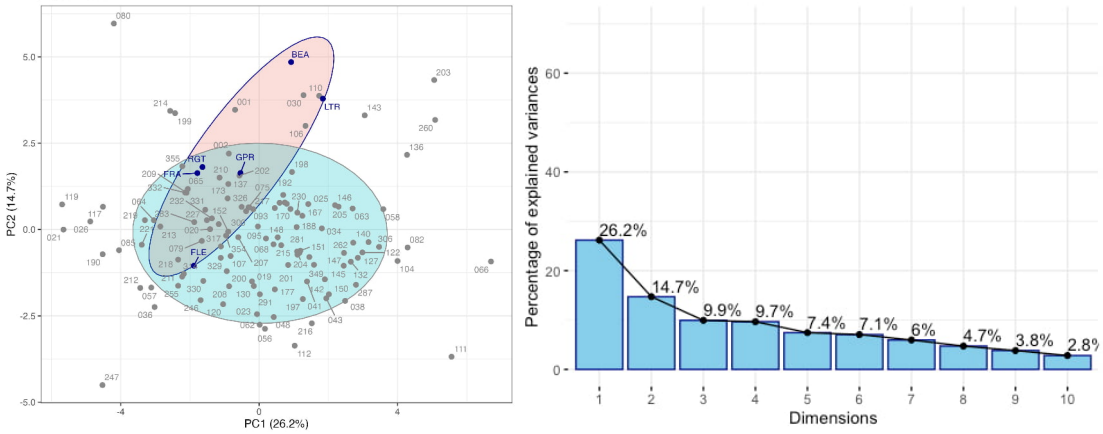

Figure 4.4. Principal component analysis of a diverse barley panel based on 22 traits. a) PC plot illustrates the distribution and genotype clustering in a reduced-dimensional space defined by the first two principal components. b) scree plot showing the proportion of total variance explained by each principal component. Ellipses separate between the cultivated from wild genotypes.

4.3.5 Trait heritability for feature selection

Heritability analysis was conducted to identify and select traits with moderate to strong genetic contributions to the phenotypes for subsequent genotype selection. Narrow-sense (h^2) heritability was calculated on a line-mean basis from the variance components of GBLUP models 15 through 21. Overall, trait heritability ranged from 0% to 97% and prediction accuracies ranged from 0% to 49% (Table 4.3). Biomass traits showed the highest h^2 values with 97%, 93% and 85% for FW of drought pots, MP and DW of drought pots. CTD heritability ranged from 16% to 55% with CTD under drought showing higher heritability than irrigated pots. Pigment traits, TOL, and SI (Stage 2 and 3) showed the lowest heritability values. Cross-validation accuracies (r) were higher for CTD than biomass traits. Heritability thresholds were set at h^2=15% for trait selection. Along with statistical significance between irrigation treatments at $p<0.001$, traits with h^2 above this threshold were used in a composite genotype selection criterion. The selected traits included CTD_DR_Stage_1, CTD_DR_Stage_2, CTD_DR_Stage_3, CTD_IR_Stage_1, CTD_IR_Stage_2, CTD_IR_Stage_3, DW_DR, DW_IR, FW_DR, FW_IR, and MP.

Table 4.3. Statistical analysis, cross-validation accuracy, and narrow-sense (h^2) heritability for trait selection.

Trait group	Trait code	Description	p-value †	Cross-validation Accuracy ††	h^2	Traits for genotype selection
Transpiration	CTD_DR_Stage_1	Transpiration of drought treated pots at 100%FC between 19 and 26 Days After Sowing	<0.0001	35%	34%	Trait 1
	CTD_DR_Stage_2	Transpiration of drought treated pots at 60%FC between 40 and 41 Days After Sowing		44%	55%	Trait 2
	CTD_DR_Stage_3	Transpiration of drought treated pots at 40%FC between 47 and 57 Days After Sowing		49%	53%	Trait 3
	CTD_IR_Stage_1	Transpiration of well-irrigated pots at 100%FC between 19 and 26 Days After Sowing		26%	39%	Trait 4
	CTD_IR_Stage_2	Transpiration of well-irrigated pots at 100%FC between 40 and 41 Days After Sowing		39%	23%	Trait 5
	CTD_IR_Stage_3	Transpiration of well-irrigated pots at 100%FC between 47 and 57 Days After Sowing		37%	16%	Trait 6
	SI_stage2	Stomata sensitivity tolerance index between well-irrigated (100%FC) and drought treated (60% FC) pots	n/a	-	-	-
	SI_stage3	Stomata sensitivity tolerance index between well-irrigated (100%FC) and drought treated (40% FC) pots		8%	6%	-
Biomass	DW_DR	Dry Weight of drought treated pots	<0.0001	26%	85%	Trait 7
	DW_IR	Dry Weight of well-irrigated pots		20%	48%	Trait 8

	FW_DR	Fresh Weight of drought treated pots		25%	97%	Trait 9
	FW_IR	Fresh Weight of well-irrigated pots		20%	33%	Trait 10
	MP	Mean productivity tolerance index	n/a	24%	93%	Trait 11
	TOL	Yield stability tolerance index		-	-	-
Pigment	Anth_DR	Anthocyanin content of drought treated pots	0.404	9%	7%	-
	Anth_IR	Anthocyanin content of well-irrigated pots		0%	2%	-
	Chl_DR	Chlorophyll content of drought treated pots	<0.0001	36%	26%	-
	Chl_IR	Chlorophyll content of well-irrigated pots		21%	26%	-
	Flav_DR	Flavonoid content of drought treated pots	0.6642	25%	16%	-
	Flav_IR	Flavonoid content of well-irrigated pots		-	-	-
	NBI_DR	Nitrogen Balance Index of drought treated pots	0.0141	31%	24%	-
	NBI_IR	Nitrogen Balance Index of well-irrigated pots		13%	16%	-

† Statistical significance between well-irrigated and drought treated pots. No statistical test for tolerance indices as they integrate information of both irrigation treatments.
†† Cross-validation accuracy from a GBLUP model. No cross-validation accuracy (r) and MSE for SI_stage2, TOL and Flav_IR available as there is not enough additive genetic variation that the model can explain, resulting in 0% narrow-sense (h^2) heritability.

4.3.6 Genotype clustering

The Hopkins statistic calculated on the 22 variables, including transpiration, biomass, pigment content, and agronomic indices, was 0.67, while the value for the first three principal components was 0.65. This indicates a moderate clustering tendency across the full dataset, with no significant enhancement observed from dimensionality reduction via principal component analysis. However, when using the 11 traits selected based on statistical significance and heritability, the Hopkins statistic increased to 0.71, indicating a stronger clustering tendency.

The selection of distance matrix and hierarchical clustering methods was assessed using the Cophenetic Correlation Coefficient (CCC) (Agre *et al.*, 2019; Darkwa *et al.*, 2020). Genotypic data was used to benchmark phenotypic similarity with the genotypic similarity across the population and to evaluate how accurately the phenotypic clustering reflected the underlying genetic relationships among the genotypes (Figure 4.5). Table 4.4 shows the CCC from various combinations of dissimilarity matrices and clustering methods using phenotypic and genotypic data. The Average (UPGMA) linkage clustering method consistently produced higher CCC values (>0.67). Among the three dissimilarity matrices for phenotypic traits, the Euclidean distance achieved the highest CCC value of 0.71. The CCC values from molecular data was generally higher than the ones from phenotypic data. A low but significant relationship between the structure of the phenotypic and genotypic distance matrices was observed via Mantel test (0.155; $p<0.001$), indicating that while most of the variation is captured independently by the different types of data, there is some concordance between the phenotypic and genotypic clustering patterns.

No agreement was observed across the Within-Cluster Sum of Squares (WSS), Silhouette method, and Gap Statistic to determine an optimal number of clusters. A cut-off threshold of 6 was applied for a comparative analysis of clustering patterns across all four algorithms. Circular dendrograms in Figure 4.6 show the outcome of the four hierarchical clustering methods. Average and Single linkage formed a large, cohesive cluster, while Ward and Complete Linkage resulted in a more dispersed clustering pattern.

Table 4.4. Comparison of clustering methods and diversity matrices of phenotypic and genotypic data using cophenetic correlation coefficient (CCC).

	Clustering methods			
Dissimilarity matrices	**Ward.D2**	**Single**	**Complete**	**Average (UPGMA)**
Phenotypic data				
Gower	0.38	0.60	0.43	0.68
Manhattan	0.37	0.63	0.46	0.70
Euclidean	0.36	0.69	0.40	0.71
Genotypic data				
IBS	0.80	0.37	0.82	0.84
Nei	0.68	0.71	0.75	0.80
Jaccard	0.68	0.80	0.84	0.88
Roger	0.80	0.48	0.84	0.86

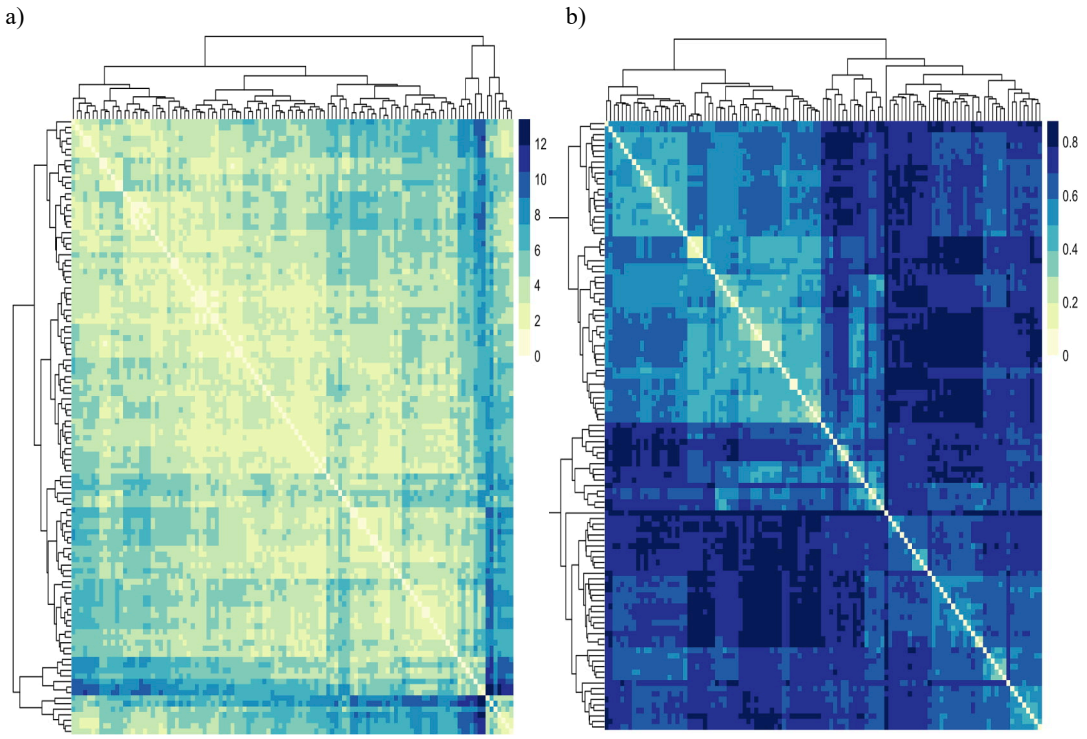

Figure 4.5. Heatmaps representing dissimilarity matrices and hierarchical clustering of genotypes. a) Phenotypic dissimilarity matrix using Euclidean distance. b) Genotypic dissimilarity matrix using Jaccard distance. The colour gradient expresses the dissimilarity levels between 111 wild accessions, with higher values representing greater differences between genotypes. Genotypes with no genotypic information available were excluded.

4.3.7 Selection of a core set of drought-tolerant candidates

Genotypes were classified into distinct groups based on the 11 traits chosen for their statistical significance and moderate to strong genetic control from heritability analysis. Figure 4.7 shows genotypes plotted in a 3D space using the first three principal components (PCs) as coordinates. According to the Ward clustering method, the top 10% of accessions, which had the smallest Euclidean distance to a hypothetical ideal candidate, predominantly belonged to the red and black groups. Genotypes in this top tier included 021, 221, 064, 085, 117, FLE, 247, and 026, listed in descending ranking order. This core set exhibited very high biomass accumulation and mean productivity. The black group, comprising genotypes RGT, 080, 002, and 137, showed average CTD, and above average biomass and mean productivity. In contrast, the bottom 10% of accessions, primarily from the purple and orange clusters, showed significantly different characteristics. The purple group, which included genotypes 066, 111, 260, 127, 025, 112, 063, and 306 in ascending ranking order, was characterised by below-average CTD and very low biomass. The orange group, containing genotypes 203, 104, and 082, exhibited average biomass and very low CTD.

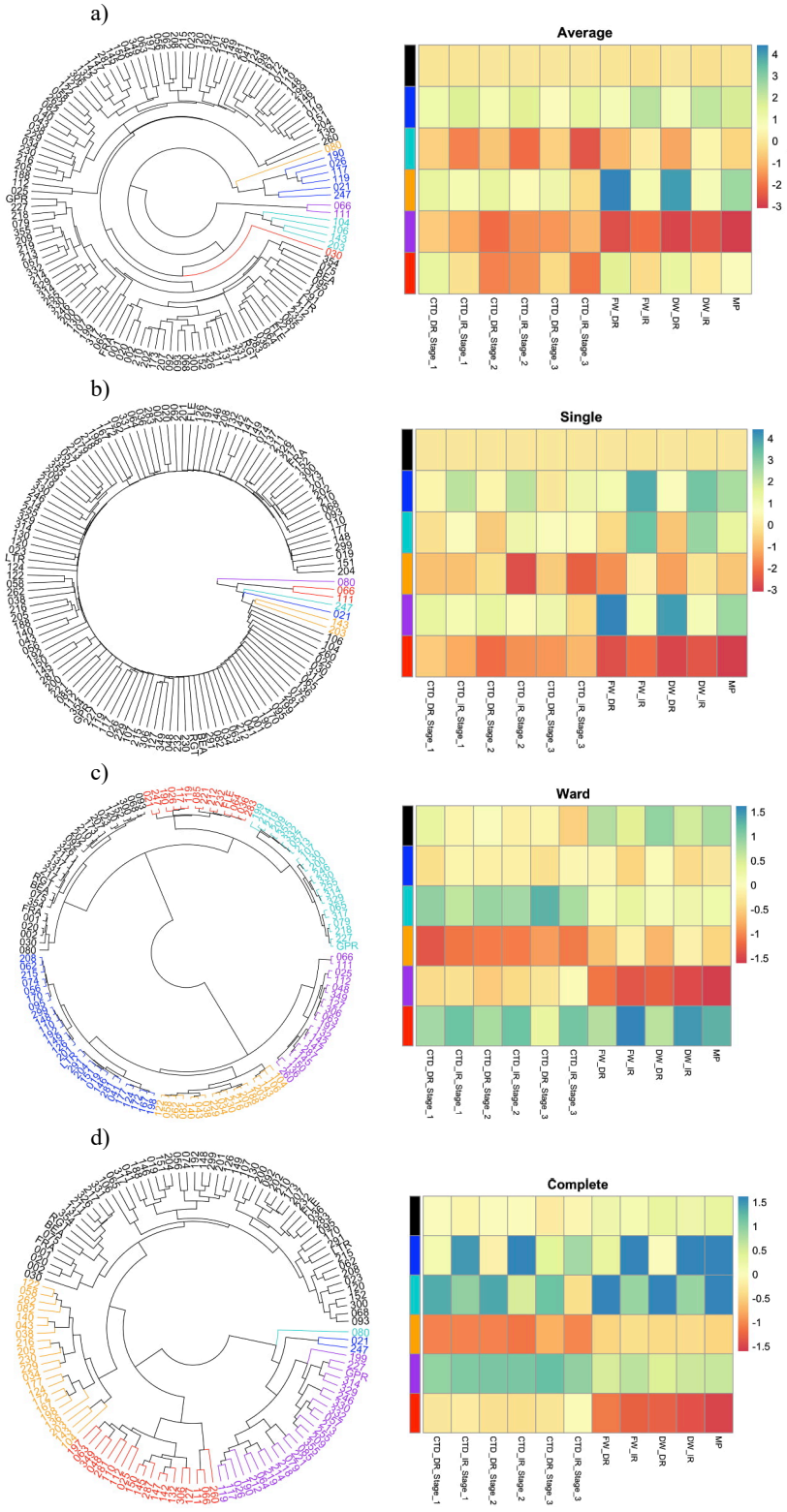

Figure 4.6. Hierarchical clustering of 124 genotypes based on phenotypic data. Clusters are represented by circular dendrograms (left column) and heatmaps of cluster means (right column) using Euclidean distance matrices. Clustering methods shown are: (a) Average linkage, (b) Single linkage, (c) Ward linkage, and (d) Complete linkage.

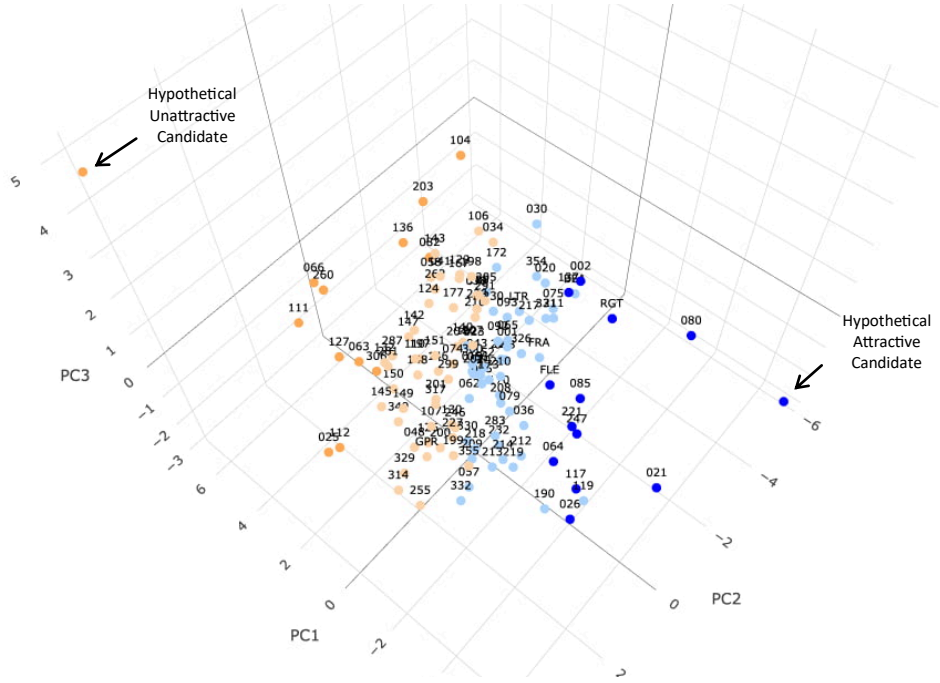

Figure 4.7. Classification of wild and cultivated accessions based on smallest Euclidean distance to a hypothetical ideal candidate. The classification was conducted using eleven traits selected for their statistical significance and heritability. A linear transformation was applied to ensure consistent directionality for desirable trait values. The ideal "attractive" candidate is defined by the highest values for all traits, whereas the least desirable "unattractive" candidate is defined by the lowest values for all traits. Blue and orange colours indicate proximity to the ideal or least desirable candidates, respectively. Coordinates represent the first three principal components.

4.4 Discussion

Wild relatives are a diverse and largely unexploited reservoir of stress tolerance mechanisms and genes (McCouch *et al.*, 2013; Langridge & Waugh, 2019). Developing a comprehensive utilisation strategy is crucial to fully harness these valuable genetic resources. This study explores the drought tolerance potential of wild relatives from three different perspectives: agronomic performance, physiological mechanisms of interest, and data-driven phenotypic clustering analysis. The phenotypic characterisation of a diverse barley germplasm was done by means of transpiration via canopy temperature depression, biomass and pigment traits, where agronomic indices based on dry matter (MP and TOL), and a stomata sensitivity (SI) index were incorporated into the trait set. Trait selection was guided by the statistical significance and heritability analysis, ensuring that only the most relevant traits were used in the process of genotype selection. By comparing many genotypes simultaneously under precise irrigation control this preliminary study provides a benchmark to understand the extent of genetic diversity of CTD, biomass and pigment traits. I also provide a framework for the collective analysis of these traits that will serve as a

foundation for more detailed research, aiming to refine our understanding of the genetic and physiological factors that contribute to drought tolerance in wild relatives of cereal crops.

4.4.1 Drought treatment effects

Biomass and CTD showed the expected decline under drought conditions, but pigment traits did not follow the same downward trend. The lack of significant correlations between pigment and biomass, as well as between pigment and CTD, suggests that there was no evidence of light-induced damage in photosynthesis by the induced water stress treatments. Therefore, reductions of biomass under drought was likely driven solely by decreased stomatal conductance in response to water deficit (Flexas, 2008). Pigment traits were therefore not informative of drought stress tolerance under the tested experimental conditions, although they hold relevance in field environments where drought stress exerts more extreme effects on photosynthesis. The lack of statistically significant genotype-by-treatment interactions further indicates that the imposed stress was probably not strong or prolonged enough to cause significant differences in genotypes' responses to drought. On the other hand, the within-genotype variation was too large as to compromise the detection of subtle phenotypic differences among genotypes. Future drought experiments in controlled environments should aim to create conditions that substantially impact photosynthesis, as variations in the ability of genotypes to sustain photosynthetic activity could amplify the differences in biomass declines among them. This approach would enhance our ability to distinguish between drought-tolerant and drought-sensitive genotypes.

4.4.2 Heritability

Biomass and pigments are time-integrated traits whose values are relatively stable and fixed at the time of sampling. Unlike biomass, CTD is sensitive to short-term environmental fluctuations that can happen during the sampling process. This sensitivity to environmental factors makes it crucial to determine the extent to which CTD measurements are driven by genotypic differences among accessions. Narrow-sense heritability provides this needed metric (Falconer & Mackay, 1996; Visscher *et al.*, 2008). Whole-genome sequencing data available for 111 genotypes allowed for the calculation of narrow-sense heritability (h^2) using variance components from GBLUP models. These models leverage genome-wide molecular marker data to construct a Genomic Relatedness Matrix (GRM).

Interestingly, Flav_IR, SI, and TOL indices, did not exhibit significant phenotypic variance that could be directly attributed to genotype differences. As a result, the GBLUP could not estimate narrow-sense heritability for these traits (Table 4.3), indicating that the observed variability is primarily influenced by measurement errors and/or environmental factors. This aligns with the

lack of genotype-by-treatment interactions from the statistical analysis, indicating that genotypes respond similarly under the studied experimental conditions. On the other hand, higher h^2 under drought for CTD and biomass traits suggest that a substantial portion of the observed variation was attributable to genotypic differences among the accessions (Visscher *et al.*, 2008).

To date, there are no studies of CTD conducted in wild barley populations for the exploration of drought tolerance potential. Most studies using canopy temperature have been in cultivated crops under rainfed field conditions, and only a limited number of them report broad-sense (H^2) or narrow-sense (h^2) heritability to assess the reliability of CTD measurements (Rebetzke *et al.*, 2002; Olivares-Villegas *et al.*, 2007; Andrade-Sanchez *et al.*, 2013; Crain *et al.*, 2017; Sharma *et al.*, 2018; Perich *et al.*, 2020). The heritability values reported across these studies exhibit a broad range, with H^2 ranging from 10% to 90% and narrow-sense h^2 heritability between 38% and 91% (Rebetzke *et al.*, 2013). Interestingly, Rebetzke *et al.* (2013) observed that h^2 in a cultivated wheat population was at its lowest when measurements were taken before irrigation, while Andrade-Sanchez *et al.* (2013) reported a dramatic increase in H^2, from nearly 0% to 70%, after the irrigation system was repaired. This broad range of heritability values underscores the importance of controlling for environmental variability such as soil water content and conducting multiple measurements to ensure the use of accurate and reliable estimates of CTD (Crain *et al.*, 2017; Sharma *et al.*, 2018). The advantage of image-based methods is the ability to collect multiple CTD measurements, enabling the exclusion of unreliable data.

The unexpectedly high heritability of phenotypic traits under drought contrasts with the widely reported decline in heritability for traits such as carbon isotope discrimination (Condon & Richards, 1992; Richards, 2022), and yield (Abdolshahi *et al.*, 2015; Sofi *et al.*, 2019) under irrigation. This reduction in heritability is often attributed to significant genotype-by-environment (GxE) interactions. Although the specific causes of these interactions and the associated low heritability remain unclear, the results of this experiment suggest that the controlled experimental conditions play a crucial role in achieving high heritability under drought. In the field, factors such as initial soil moisture, seasonal rainfall, and soil water holding capacity can lead to uneven variations in soil water content, complicating the identification of genetic components that contribute to plant responses under water depletion (Rebetzke et al., 2002). These environmental differences may explain why some experiments favour cooler canopy temperatures for maintaining yield under drought (Mason & Ravi, 2014; Schittenhelm et al., 2014; Crain et al., 2017; Singh et al., 2022), while others find that warmer temperatures are more advantageous (Rebetzke et al., 2013). When soil water is not fully depleted, genotypes that continue transpiring and maintain cooler canopies often have a yield advantage over those that reduce transpiration

(low CTD). This variability in environmental conditions can reduce the repeatability of experiments, even when trait heritability within a specific trial is high.

The high heritability of transpiration and biomass traits under drought observed in this experiment suggests that the primary obstacle in breeding for drought tolerance may be more related to phenotypic challenges than to genetic complexity (Blum, 2011). Glasshouse phenotyping offers the advantage of controlling both long-term and short-term environmental effects by precisely regulating water content, ambient temperature, wind, and relative humidity. Although there is ongoing concern about the lack of correlation between plant performance under controlled and field conditions (Sales *et al.*, 2022), the impact of drought in agricultural production justify the efforts to understand the underlying causes of these differences. Ensuring the highest possible heritability of CTD when comparing the same genotype panel under controlled glasshouse conditions and in the field will help determine the extent to which glasshouse results are replicable in field conditions. The use of advanced field and glasshouse phenotyping platforms (Perich et al., 2020; Mertens et al., 2023) will be crucial for the investigation of these relationships.

4.4.3 Agronomic-driven genotype selection

The analysis of biomass and agronomic indices allows for the assessment of the barley populations based on economically or societally relevant traits (Morton *et al.*, 2019). High biomass accumulation could suggest high yield potential in the field, while low biomass accumulation typically indicates a reduced capacity for carbon assimilation, which can limit the translocation of assimilates into grain production (Thāpā *et al.*, 2022). Dry weight (DW) offers a direct measure of carbon assimilation independent of water content. Agronomic indices derived from DW in this study, mean productivity (MP) and stress tolerance (TOL), serve as representative metrics for “yield potential” and “yield stability” (Bennani *et al.*, 2017).

An agronomic-driven genotype selection would typically prioritise genotypes with high MP values, as this indicates greater yield potential regardless of irrigation conditions. Meanwhile, low TOL values indicate higher yield stability, reflecting a genotype’s ability to maintain baseline productivity seen under favourable conditions. An ideal candidate displaying both the highest MP and the lowest TOL was not identified in this experiment. In addition, the high narrow-sense heritability of mean productivity indicates that selecting genotypes based on MP alone would be the most effective approach within an agronomic-driven selection framework. Notably, genotypes 080, 021, 026, 119, 117 outperformed all the six cultivars in mean productivity and could suggest yield potential to exploit via plant breeding (Li *et al.*, 2023). In particular, genotypes 080 and 119 outperformed its irrigated counterpart in two out of the three trials. However, measuring water

expenditure is crucial to understanding how these genotypes manage water resources and whether they achieve high mean productivity (MP) while conserving water.

4.4.4 Combining biomass and transpiration to reduce germplasm selection bias

Phenotyping capabilities are the main constraint in the preliminary assessment and selection of promising candidates from diverse germplasms. Preliminary selections are typically conducted using the Focused Identification of Germplasm Strategy (FIGS), where genotype subsets are expected to contain specific characteristics, such as drought tolerance, by leveraging environmental and geographic data from the original collection sites (Khazaei *et al.*, 2013; Street *et al.*, 2016). However, selected accessions are still assessed based on yield or biomass stability as the primary indicators of agronomic success under drought (Cai *et al.*, 2020). Incorporating additional measurements at this stage is often omitted to streamline the exploration and selection process. The results of this study suggest that without a targeted phenotyping approach that integrates both agronomic and physiological indicators, there may be a selection bias favouring genotypes that are stomata-insensitive to drought stress or have low yield potential.

The high phenotypic and genetic correlations of TOL with FW and DW biomass indicate that greater biomass production under irrigated conditions is associated with more significant biomass declines under drought (higher TOL). Consequently, selecting candidates based solely on low TOL, or yield stability, would indirectly favour genotypes with low biomass accumulation. Additionally, the stomatal index (SI) at stage 2 showed a moderate but significant correlation with TOL, suggesting that reductions in biomass are partially due to decreased transpiration under drought. This implies that selection based on yield stability (low TOL) alone could bias the selection towards plants with transpiration that is insensitive to drought (low SI), while selection based on high yield potential (high MP) under favourable conditions would favour plants with high baseline transpiration. Genotypes that are stomata insensitive to water deficits and exhibit high baseline transpiration rates are likely to follow the "water-failure" crop production trajectory in which crops are at risk of water limitation during grain filling (Vadez *et al.*, 2024).

4.4.5 Physiology-driven selection

Adaptive transpiration refers to the ability of genotypes to modulate their water usage in response to varying water availability, optimising water efficiency without compromising productivity. This concept encompasses genotypes that not only adjust their water consumption based on supply but also those that maintain or even enhance productivity with a low transpiration. Efficient stomatal closure is an adaptive mechanism mediated by the abscisic acid (ABA)

signalling pathway (Lim *et al.*, 2015; Agurla *et al.*, 2018), and reduced stomata density has been associated with an increase in transpiration efficiency without negative impacts to biomass accumulation and yield (Hughes *et al.*, 2017). Our ability to exploit natural diversity of these two mechanisms is contingent upon accurately identifying them from large scale phenotyping assessments. Genotypes with low TOL and high SI may indicate stomata responsiveness, while high MP and low CTD may indicated reduced stomata density. In either case, these mechanisms allow plants to sustain biomass production while conserving water.

Given the significant correlations of TOL, MP, CTD and biomass traits, those accessions that significantly deviate from these relationships may possess the above adaptive mechanisms. Under this framework, genotype 080 ranked in the 1st position in MP but ranked 40th in CTD under irrigated and 10th under drought, which may suggest mechanisms that enhance biomass accumulation not being the genotype with the highest transpiration reading. Similarly, although genotype 082 was one of the lowest transpiring genotypes ranking in position 118th based on CTD under irrigation and position 122nd based on CTD under drought at stage 2, it ranked in the 74th position in dry matter accumulation this suggests that 082 compensated for the low transpiration. This type of detailed analysis is impractical for every genotype individually, but it is essential to streamline the process by aggregating those that exhibit similar patterns into response profiles, allowing for more efficient identification of promising candidates for drought tolerance. Notably, genotype 080 was distinctly separated in its own cluster in Complete Linkage hierarchical clustering method, while Genotype 082 was part of the orange clusters in both Ward and Complete Linkage methods (Figure 4.6).

Low biomass accumulation is typically a criterion for excluding genotypes in agronomic selection. However, this characteristic may still be valuable in regions where water conservation is critical (Rebetzke *et al.*, 2013). Genotypes 111 and 066, despite ranking low in mean productivity (MP) and having distinctive narrow leaves, could significantly minimise unproductive water loss while keeping cool canopies. This lower biomass supports sustained transpiration without rapidly depleting water, and the cooler canopies offer protection against light and heat stress (Moore *et al.*, 2021). These accessions may provide a valuable opportunity for cultivation in marginal lands with severe water scarcity and extreme heat.

4.4.6 Clustering-based exploration

A data-driven exploration and selection approach considers the combined influence of multiple traits. Hierarchical clustering, a common technique in exploratory data analysis, is used to identify natural groupings within a dataset (ur Rehman & Belhaouari, 2021). This method organises data points into a nested hierarchy of clusters based on dissimilarity matrices without requiring a

predetermined number of clusters. In a clustering-based selection approach genotypes are treated as unlabelled data without predetermined drought tolerance classifications. By grouping similar observations together in a tree-like structure, hierarchical clustering could reveal distinct genotype profiles from which selections can be made. In addition, genotypes that may not appear as outliers when evaluated on individual traits, could emerge as significant outliers when assessed through a multivariate analysis (ur Rehman & Belhaouari, 2021). Cluster analysis on a diverse breeding pool could yield unexpected combinations of characteristics that could be valuable for breeding programs and/or genetic studies.

The effectiveness of hierarchical clustering is dependent on the underlying structure of the data, which can be assessed using the Hopkins statistic (Wright, 2022). A Hopkins statistic close to 1 indicates a strong tendency for natural groupings within the dataset. Conversely, a value close to 0.5 suggests that the data is uniformly distributed and lacks a clear clustering structure, making it difficult to identify distinct clusters. The increase in *H* statistic observed in this study when using selected traits based on statistical significance and high heritability highlights the importance of using traits that best capture biologically meaningful patterns in the data —a result that was not achieved when using principal components of the entire dataset.

The choice of clustering methods and dissimilarity matrices significantly impacted the resulting groupings. Average and Single Linkage demonstrated highest cophenetic correlation coefficient (CCC) indicating the most accurate representation of pairwise distances between the original data points in the dendrogram (Agre *et al.*, 2019; Darkwa *et al.*, 2020). However, Average and Single Linkage formed large cohesive clusters where only a limited number of genotypes diverged from the primary group, which present challenges for using as an unbiased genotype selection method. The propensity of the Average and Single Linkage to cluster most genotypes into a single cluster was likely due to its inherent averaging process or chaining tendency (Blashfield, 1976). Average Linkage tends to smooth out differences between clusters, leading to the grouping of genotypes together. Similarly, Single Linkage, which connects clusters based on the smallest distance between members, often results in the formation of a single large cluster with minimal differentiation among genotypes. This tendency to form large clusters likely arises from the high phenotypic similarity among accessions. The lack of distinct separation reduces the effectiveness of Average Linkage method for identifying distinc genotype profiles. In contrast, Complete and Ward Linkage methods resulted in a more dispersed clustering pattern, where observations are less likely to group into a single cluster.

Overall, these results show the inherent variability in biological data and the complexity of different clustering algorithms, both of which can significantly impact the outcomes. Nonetheless,

the choice of clustering method for the germplasm exploration can be tailored to the dataset characteristics and specific objectives. In the current experimental context, Complete and Ward Linkage may be more advantageous for general classification purposes, e.g., for choosing representative genotypes for validation studies. On the other hand, Average linkage could be used for identifying significant outliers with unique characteristics that set them apart from the rest of the population. The high degree of similarity observed in the phenotypic distance matrix compared to the genotypic dissimilarity matrix highlights the need for a growing environment that accentuates the phenotypic differences between genotypes and the inclusion of more traits that could improve the clustering tendency and better capture the genetic diversity present in the population.

4.4.7 Genotype selection

Langridge and Waugh (2019) suggested a random selection from a core collection of wild relatives to harness the potential of germplasm collections via *de novo* domestication. Chapter 2 of this thesis proposed a phenotypic selection strategy based on high-throughput spectral images to enable the assessment of drought tolerant candidates from core collections before undertaking the *de novo* domestication process. Building on these studies, genotypes have been categorised based on their Euclidean proximity to a hypothetical ideal candidate within a multidimensional space defined by eleven highly heritable traits. Top 10% of accessions closest to the ideal one represent candidates that are theoretically successful within established physiological and agronomic frameworks. Conversely, the bottom 10% may reveal genotypes with unusual, less understood tolerance mechanisms that could still hold significant agronomic potential. Even if some of these genotypes in this second group are used as negative controls, they are valuable to test and refine our current understanding of drought tolerance mechanisms in wild germplasms within an agronomic context.

4.5 Conclusion

The phenotypic characterisation and candidate selection of diverse germplasms for drought tolerance has historically relied on yield stability as a key drought tolerance index and the most important performance metric. Valuable pre-breeding material would be eliminated at early screening stages based on productivity metrics that either directly or indirectly depend on yield. This study provides a framework for evaluating and selecting genotypes based on a combination of phenotypic traits and genetic data, paving the way for a more informed exploration and selection of wild barley accessions.

The phenotyping platform used lacked the precision needed to detect adaptive transpiration mechanisms with high confidence, as no statistically significant differences or strong genetic control were observed in the reduction of canopy temperature depression (SI index) and biomass (TOL index) under drought conditions. This reflects the current phenotyping limitations and/or the absence of growing conditions that elicit differences in adaptive responses. To better detect this adaptive mechanism, a more severe drought treatment that specifically causes impairments to photosynthesis is needed. In addition, expanding the trait spectrum by including morphological traits, phenological development, photosynthesis capacity metrics and canopy architecture traits may help improve the clustering tendency measured through Hopkins statistic. This could enhance the ability to detect differences and patterns among genotypes that might not be apparent when only a limited set of traits is analysed. Achieving this will require the use of advanced phenotyping platforms equipped with automated irrigation systems to provide consistent drought conditions, enabling researchers to concentrate on trait measurements during the course of the experiment. The core set of wild genotypes selected by agronomic, physiological, and clustering-driven approaches can be used for a validation experiment before embarking on the *de novo* domestication process or the creation of mapping populations for genome-wide association studies (GWAS) to investigate key genes.

Chapter 5
De novo domestication of wild barley via Marker-Assisted Backcrossing (MABC)

5.1 Introduction

De novo domestication has recently gained momentum as an attractive alternative to the overwhelming number of interacting genomic regions potentially involved in drought responses as it only requires dealing with a relatively small number of genes (Langridge & Waugh, 2019). In the last decade, hundreds of QTLs related to drought tolerance have been identified through marker-trait association studies in barley (Mora et al., 2016; Mikołajczak et al., 2017; Ogrodowicz et al., 2017; Kornelia et al., 2018). Since multiple genes of small effect likely interact with one another and with the environment to drive drought responses, it may be more effective to preserve the integrity of genomes from valuable genetic resources while maintaining the complex gene interactions, pathways and networks that confer drought tolerance (Fernie & Yan, 2019; Jian *et al.*, 2022). Before we can evaluate the agronomic characteristics of these genetic treasures under standard field conditions, we first need to adapt them to modern agricultural practices by removing the barriers that prevent cultivation. *De novo* domestication introduces beneficial agronomic traits, non-brittle rachis and reduced dormancy from cultivated plants into wild accessions.

De novo-domestication has been reported in tomatoes (Zsögön *et al.*, 2018) and rice (Yu *et al.*, 2021), but there are no published reports in barley and wheat. Barley is a useful crop model for studying *de novo* domestication and its effects on drought tolerance in cereals, as wild (*Hordeum vulgare* ssp. *spontaneum*) accessions and cultivated (*Hordeum vulgare* ssp. *vulgare*) variates can be crossed using conventional breeding methods due to their full sexual compatibility.

Several genes and QTLs with major effect controlling key domestication-related agronomic traits have been identified in barley (Table 5.1). Many of the mutations responsible for these traits have been experimentally validated (Pourkheirandish *et al.*, 2015; Sato *et al.*, 2016; Milner *et al.*, 2019), offering practical targets for the design of molecular markers for gene introgression via marker-assisted backcrossing (MABC).

Table 5.1 . Major genes and QTLs for essential agronomic traits that enable cultivation in barley.

Trait	Gene/QTL	Agronomic benefit	Mechanism
Non-brittle rachis	*Btr1 / Btr2*	Grain retention after full maturity	Cell wall thickening in disarticulation zone
Reduced dormancy	*Qsd1*	Adequate germination	Build-up of alanine in dormant grain
Smooth awn	*ROUGH AWN1*	Easy handling and increases feed value of straw for livestock	Enzyme involved in activation of cytokinins
Erect growth habit	*AK360532*	Enables harvesting	Possible transcription factor encoding a zinc-ion binding protein
Free threshing	*Thresh-1*	Enables automatic threshing	Possible gene encoding cellulose synthase-like family c and polygalacturonase proteins
Reduced height	*Sdw*	Prevent yield loss through lodging	Metabolic enzyme controlling plant height

De novo domestication via MABC is currently the most viable path for gene introgression to avoid regulatory constraints typically associated with advanced molecular techniques, such as gene-editing (Palmgren *et al.*, 2015; Hanak *et al.*, 2023). MABC involves a series of backcrosses between a wild accession (recurrent parent) and a cultivated variety (donor parent), using molecular markers throughout the breeding process to track and select progeny that contain the cultivated allele for the gene(s) of interest. Multiple backcrosses are needed to increase the contribution of the wild accession's genome, which requires testing and selecting progeny heterozygous for each gene of interest. Once the desired wild genome contribution is achieved, several rounds of self-pollination are conducted to ensure the cultivated allele of the target gene(s) and the rest of the genome are homozygous (Neeraja *et al.*, 2007).

PCR-based codominant markers, such as Cleaved Amplified Polymorphic Sequences (CAPS) and derived-Cleaved Amplified Polymorphic Sequences (dCAPS), can facilitate the MABC to enable breeders to distinguish between homozygous and heterozygous individuals. CAPS and dCAPS amplify specific regions of DNA containing informative polymorphisms between the parental lines, such as single nucleotide polymorphisms (SNPs), insertions, or deletions. CAPS markers require the presence of a natural restriction site in the target polymorphism, while dCAPS markers introduce a primer mismatch to create a new restriction site (Shavrukov, 2016). In barley, codominant markers have been recently developed for *Btr1*, and *Qsd1* (Gould, 2022; Williams, 2022). However, no markers have been reported for the *ROUGH AWN1* locus to facilitate marker assisted selection of smooth awn phenotypes.

The design of robust markers is essential for an efficient MABC program, where the use of highly conserved regions for primer design ensures successful amplification of the target region across diverse accessions. Ensuring cost-effectiveness is crucial for the scalability for large breeding programs involving thousands of progeny tests.

The aims of this chapter are 1) to design a robust, codominant molecular marker for the barley awn roughness gene (*ROUGH AWN 1*), and 2) to develop *de novo*-domesticated lines of wild barley using marker-assisted backcrossing with the *ROUGH AWN 1* marker along with markers for *Qsd1* and *Btr1* to facilitate genotyping and selection at each generation. The resulting pre-breeding material represents the first successful attempt to domesticate wild barley through a targeted molecular approach, providing a valuable resource for breeders to evaluate in field trials under conventional management practices.

5.2 Materials and methods

5.2.1 Plant material and growth conditions

A random cohort of 26 wild barley accessions were selected from the 318 accessions in the Wild Barley Diversity Collection which was collected primarily from the Fertile Crescent. These wild accessions were sourced by the International Wild Barley Sequencing Consortium (IWBSC) (https://iwbsc.umn.edu) and have been self-pollinated for six generations and are highly homozygous. The Australian barley cultivar La Trobe, was used for hybridisation with each wild accessions. Wild accessions are coded as WBDC-020, WBDC-038, WBDC-048, WBDC-066, WBDC-068, WBDC-074, WBDC-075, WBDC-106, WBDC-107, WBDC-108, WBDC-111, WBDC-112, WBDC-117, WBDC-140, WBDC-146, WBDC-172, WBDC-192, WBDC-199, WBDC-200, WBDC-210, WBDC-212, WBDC-255, WBDC-260, WBDC-314, WBDC-317, and WBDC-329. All seeds were sown in seedling trays and vernalised in a controlled temperature (CT) room at 6°C for six weeks. After the six-week vernalisation period, seedlings were transferred into 4L pots and placed in a polytunnel house at the University of Melbourne, Burnley campus, with automatic irrigation where the crossing took place.

5.2.2 DNA extraction

DNA extraction was performed via SDS method on the same day of tissue sampling. Approximately 25-30 mg of fresh tissue from the leaves of the tiller base was directly sampled into 96-well plates and stored in ice immediately. After adding two grinding beads per sample, and 450 µl of DNA extraction buffer (100 mM Tris-HCl, 50 mM EDTA, 500 mM NaCl, 10 mM 2-mercaptoethanol, and 100 µg/ml RNase), the plant tissue was homogenised in a Genogrinder

set at 1250 rpm over four cycles of 45 seconds each. After homogenisation, 60 µl of 10%SDS was added. Plates were inverted 16 times and incubated at 65°C for 60 minutes. This was followed by the addition of 200 µl of 7.5M ammonium acetate, shaking vigorously 16 times, followed by a 60-minute incubation at 4°C. Subsequently, 300 µl of chloroform was added and centrifuged at 4000 rpm for 15 minutes. 150 µl of the aqueous phase was transferred into a new plate containing 100 µl of isopropanol and gently mixed by pipetting up and down. The plate was incubated for 5 minutes at -20°C and centrifuged for 20 minutes at 4000 rpm. The supernatant was discarded, and the DNA pellet was washed with 70% ethanol, followed by another centrifugation for 20 minutes at 4000 rpm. After discarding the supernatant, the plates were dried for 20 minutes to allow ethanol evaporation. The DNA was resuspended in 0.1xTE buffer and stored at 4°C.

5.2.3 Polymerase chain reaction

Each 10-µl PCR reaction consisted of 0.4 µl of forward and reverse primers (10µM), 2 µl 5x MyFi reaction buffer, 5 µl extracted DNA (10 ng/µl), 0.1 µl MyFi Taq DNA polymerase, and 2.1 µl autoclaved MilliQ water. PCR was performed in a T100 Thermal Cycler (BioRad, Hercules, California, USA). PCR cycling conditions consisted of an initial denaturation step of 3 minutes, followed by 35 cycles of 30 seconds for denaturation, 20 seconds for annealing, and 30 seconds for extension. A final extension step was performed for 5 minutes. PCR reaction temperatures were set at 95˚C for denaturation, and 72°C for extension. The annealing temperature differed depending on the analysis: gene sequencing or marker genotyping. On completion of the PCR reactions, plates were held at 12˚C. PCR products were electrophoresed in 3% agarose gel (Bioline, London, England) dissolved in 1xTAE and stained with 0.001% GelRed. 5 µl of PCR product was mixed with 1 µl of 5x loading buffer and loaded onto the gel along with 5 µl of Easy ladder (Bioline, London, England). Electrophoresis ran at 100 volts for 45-50 minutes in 1x TAE buffer.

5.2.4 PCR product purification

PCR product purification was performed with AMPure XP (Beckman Coulter Life Sciences, California, USA). Equal volumes of AMPure XP and PCR product (40 µl each) were mixed thoroughly by pipetting up and down ten times, followed by a 5-minute incubation at room temperature. The mixture was then transferred to a magnetic based plate, SPRIplate 96 for a 2-minute incubation. The solution was carefully aspirated, leaving approximately 5 µl, and discarded. The beads were washed twice with 200 µl of 70% ethanol while plate is still in SPRIplate 96, with each wash involving a 30-second incubation at room temperature before discarding the ethanol. The plate was then dried at room temperature for 5 minutes. Finally, the DNA was eluted by adding 40 µl of 10 mM Tris, mixed by pipetting, and left in the SPRIplate 96

for 1 minute at room temperature. The purified product was transferred to a new plate for sequencing.

5.2.5 *ROUGH AWN1* marker development

Sequence data from nineteen barley pangenome V1 (Jayakodi *et al.*, 2020) accessions FT11 (B1K-04-12), HOR_10596 (Igri), HOR_12046 (Akashinriki), HOR_13170 (Barke), HOR_13821 (Eskishehir), HOR_13942 (Baeza), HOR_3081 (Slaski II), HOR_3365, HOR_7552, HOR_9043, BCC_906 (Morex), HOR_21599 (ICARDA 64 SP), HOR_8148, ZDM02064 (Chiba), ZDM01467 (Du Li Huang), HOR_10350, Hockett, OUN333 (Chame 1), and SFR85-014 (RGT Planet), were used for the design of conserved primers to amplify the *ROUGH AWN1* locus of the studied population (Appendix 5.1). Sequences of barley pangenome V1 accessions were kindly provided by Dr Martin Mascher, IPK Gatersleben, Germany.

ROUGH AWN1 sequencing

DNA sequences of the 19 barley pangenome accessions (Jayakodi *et al.*, 2020) were aligned with MEGA (Tamura et al., 2021) (Appendix 5.2 and Appendix 5.3). PCR primers were designed from fully conserved regions across all accessions around a single nucleotide polymorphism (SNP) at position 1,898 bp within the *ROUGH AWN1* locus (HORVU.MOREX.r3.5HG0502720 gene) (Milner *et al.*, 2019) (Appendix 5.4). PCR primers were retrieved from NCBI Primer Design (https://www.ncbi.nlm.nih.gov/tools/primer-blast/) and synthesized commercially (Sigma-Aldrich, Burlington, Massachusetts, USA). Plant DNA was extracted, and PCR amplification performed as described in sections 4.2.2 and 4.2.3, respectively. PCR amplicons were purified as described in section 4.2.4. DNA concentration of PCR amplicons was quantified using a Nanodrop (Thermo Scientific, NanoDrop products, USA) to ensure a minimum concentration of 30 ng/µL.

PCR amplicons were sequenced bidirectionally via the Sanger method by Macrogen (Seoul, South Korea), with separate runs for the forward and reverse primers. ABI files containing the forward and reverse reads were processed using Sequencher 5.2.4 (Gene Codes Corporation, Ann Arbor, MI, USA). Complementary reads were aligned to generate a consensus sequence for each genotype. Low-quality ends were trimmed, and the resulting high-quality consensus sequences were exported in FASTA format.

Marker design workflow

FASTA files containing high-quality sequenced data were aligned using the MEGA (Tamura *et al.*, 2021). Five additional cultivars from Chapter 3 were included in the alignment as controls: Beast (BEA), Fleet (FLE), Franklin (FRA), Golden Promise (GPR), and RGT Planet (RGT). A

60-bp region flanking the target SNP was entered to dCAPS Finder 2.0 (Neff *et al.*, 2002) to identify restriction endonuclease sites that would either cleave the wild or mutant (cultivated) haplotypes. For CAPS markers, no mismatches were specified, while for dCAPS one mismatch was allowed to introduce new restriction sites. Forward and reverse CAPS primers were designed with NCBI primer design with amplicon sizes ranging from 50 to 200 bp around the target SNP and restriction site. The forward dCAPS primer containing a single nucleotide mismatch was provided by the online tool and was used as a reference to design the corresponding reverse primer with Primer3Plus (https://www.primer3plus.com). Reverse dCAPS primers were selected based on a melting temperature (Tm) within 2-3°C of the corresponding forward dCAPS primer, minimal risk of primer-dimer formation, low hairpin formation, and a GC content between 40-60%. Each primer pair, including forward and reverse primers, represented a distinct marker option.

Post-digestion restriction patterns and fragment sizes were evaluated *in silico*. DNA sequences for each marker were examined using a custom Python script (Appendix 5.5) to identify additional restriction sites along the amplified sequence. Marker selection for subsequent progeny genotyping was determined based on the clarity of the restriction pattern for gel visualisation, as well as the cost and availability of the corresponding restriction enzyme. Endonucleases were sourced from New England Biolabs (Ipswich, Massachusetts, USA; https://www.neb.com/en-au/tools-and-resources/selection-cha+*rts/isoschizomers).

5.2.6 Allele introgression

Crossing technique

Wild and cultivated barley were hybridised via conventional breeding methods in a marker-assisted backcrossing scheme (Figure 5.1). Each crossing cycle consisted of the emasculation of La Trobe cultivar (female parent) by carefully removing the anthers from immature spikes with a tweezer (Figure 5.2) while anthers were still green. Lateral (sterile) spikelets were also removed to prevent pollen formation. Emasculated spikes were then covered with pollination bags. Two to four days post-emasculation, once the stigma on the emasculated parent is ready (Figure 5.2), pollination was carried out by gently rubbing the anthers of the male parent—a wild genotype—onto the stigmas in the emasculated spike. Pollination bags were labelled and secured with a clip and seed was harvested after 3-4 weeks.

Breeding scheme

ROUGH AWN1, Qsd1, and *Btr1* markers were employed for progeny genotyping and selection in a marker-assisted backcrossing (MABC) scheme. This involved a series of crosses between La

Trobe and 26 wild genotypes followed by two rounds of self-pollination (Figure 5.1). Individuals heterozygous for the three target genes were selected at BC1F1 and BC2F1 generations. To prevent a significant reduction in the number of back cross lines with potentially desirable genotypes in the early generations, progeny with one or two homozygous markers were retained if none of the back crosses were heterozygous for all three markers. In BC2F2, progenies were selected based on homozygosity for the cultivated alleles for the three loci. Details of primer sequences, PCR reactions, enzyme digestion conditions and restriction patterns for the three markers employed in each genotyping generation can be found in Appendix 5.6, Appendix 5.7, and Appendix 5.8.

Progeny genotyping

The genotyping protocol underwent multiple rounds of optimisation to minimise enzyme usage. Genotyping was performed in 96-well plates, with each plate containing two replicates of the La Trobe cultivar (homozygous), a wild accession (homozygous), and an F1 hybrid (heterozygous), along with a negative control (empty tube during extraction) to monitor for contamination. DNA extraction was carried out from fresh leaf tissue of young seedlings at 2 or 3-leaf developmental stage, as described in section 5.2.2. *ROUGH AWN1*, *Btr1* and *Qsd1* were amplified in 10 µl PCR reactions (section 5.2.3). Enzyme digestion was carried out in 15 µl reactions containing 10 µl of PCR product, 1.5 µl of 10x rCutSmart buffer (NEB, Ipswich, Massachusetts, USA), 0.07 to 0.1 µl corresponding to 1 unit of restriction enzyme, and the remaining of Milli-Q water adjusted according to the enzyme concentration. Samples were incubated in a PCR machine for 5 hours to ensure full digestion. Incubation temperatures were 37 °C for *HaeIII* and *EcoO109I*, and 65 °C for *Taq1-v2*. 5 µl of digested PCR product was mixed with 1 µl of 5x loading buffer and loaded onto to agarose gel. 4% agarose gel was used for *ROUGH AWN1* and *Btr1*, while a mixture of 3% agarose and 1% MetaPhor agarose (Lonza, Basel, Switzerland) was employed for *Qsd1*. The PCR parameters, restriction enzyme profiles, incubation conditions, and gel electrophoresis specifications for each gene are detailed in Appendix 5.6. Electrophoresis was run in 500 ml gels for 90 minutes at 120 volts in 1xTAE buffer.

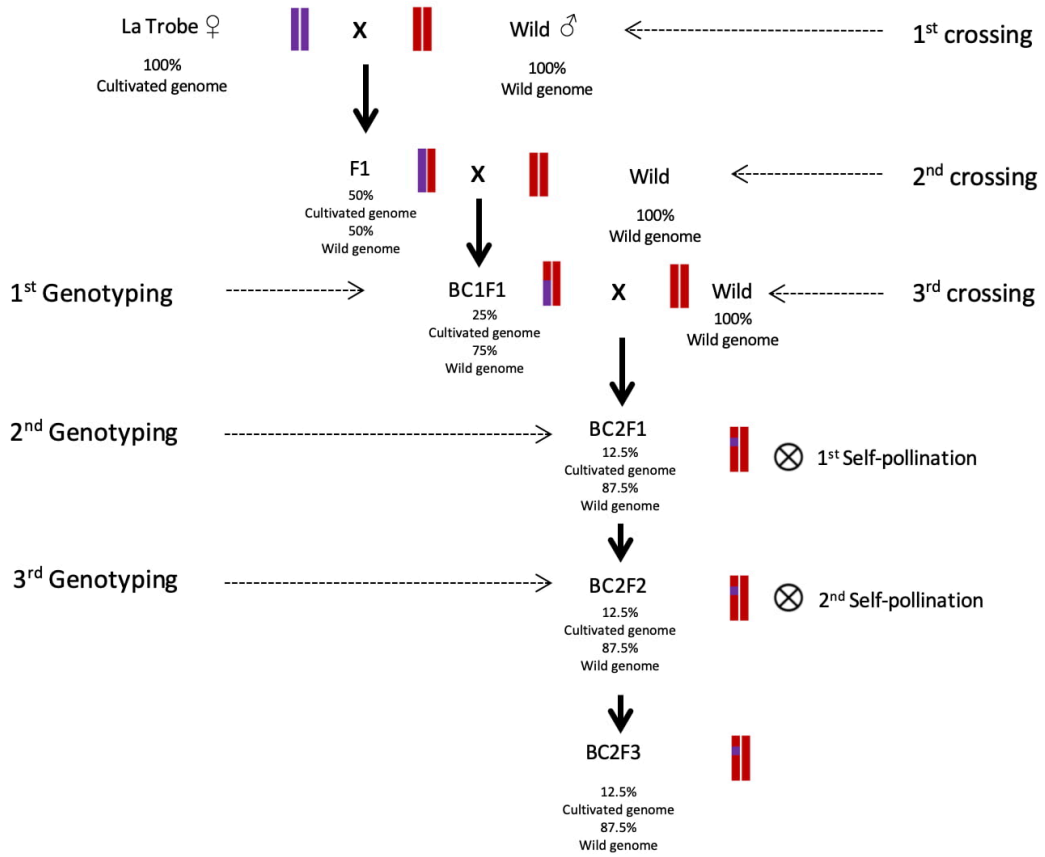

Figure 5.1. Breeding scheme for the introgression of the cultivated alleles for ROUGH AWN1, Btr1 and Qsd1 genes via Marker-Assisted Backcrossing (MABC).

Figure 5.2. Conventional breeding process via emasculation and pollination, and seed development.

5.3 Results

5.3.1 Marker development

Evaluation of the target ROUGH AWN1 polymorphism

To develop a molecular marker that robustly differentiated La Trobe (LTR) from the 26 WBDC accessions at the *ROUGH AWN1* locus, the allelic state of the SNP at position 1,898 within the HORVU.MOREX.r3.5HG0502720 gene reported by Milner *et al.* (2019) was first examined. Multiple primer pairs were designed to amplify the surrounding region of the target

polymorphism. Primer details are provided in the Appendix 5.9. All four primer pairs successfully amplified the region containing the target SNP (Figure 1.1). Among them, primer pair 3 was selected for its maximum length and used to amplify an 897 bp region flanking the polymorphism of interest in the 26 WBDC accessions and the six barley cultivars.

Following Sanger sequencing and quality inspection, the PCR-amplified region revealed that all 26 WBDC accessions carried the wild-type allele (G) at the target position (Figure 5.4). Unexpectedly, FLE, FRA, GPR, RGT cultivars also carried the wild type allele. In contrast, cultivars LTR and BEA exhibited the non-synonymous variant (G>A) at the same site reported by Milner *et al.* (2019). A second informative SNP (A>T) was identified 475 bp downstream from the first polymorphism, located at position 2,373 bp, in a non-coding region within the same gene. The second SNP showed complete differentiation between cultivated and wild accessions (Figure 5.4). Two additional SNPs were identified at positions 1,919 bp and 2,348 bp (Figure 5.4). These polymorphisms did not correlate with awn roughness phenotypes but were considered for the analysis of restriction patterns as they could introduce unintended recognition sites.

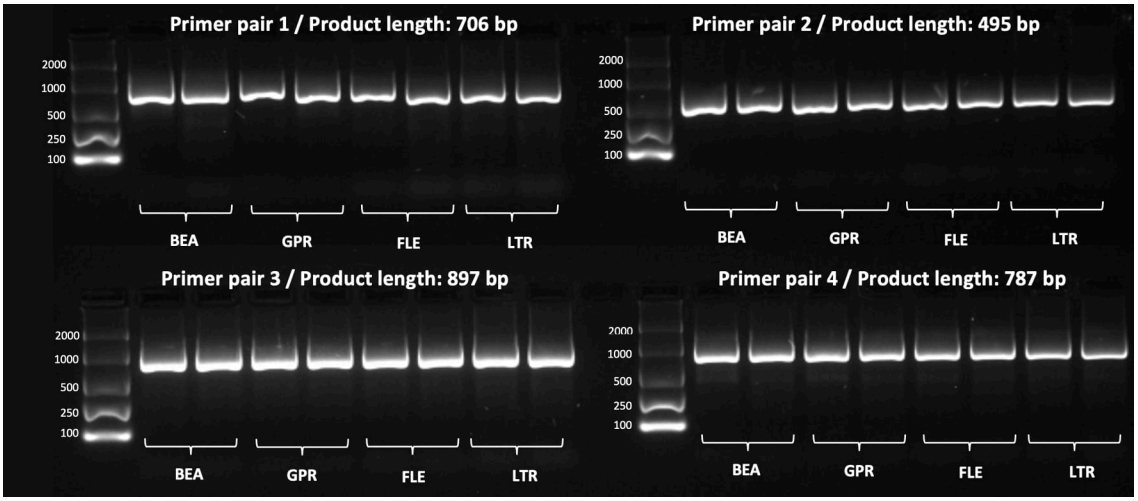

Figure 5.3. PCR amplification of the *ROUGH AWN1* gene using four different primer pairs across four genotypes (LTR, BEA, GPR, and FLE), with two replicates each. A DNA ladder was included on the left side of each group to determine product size.

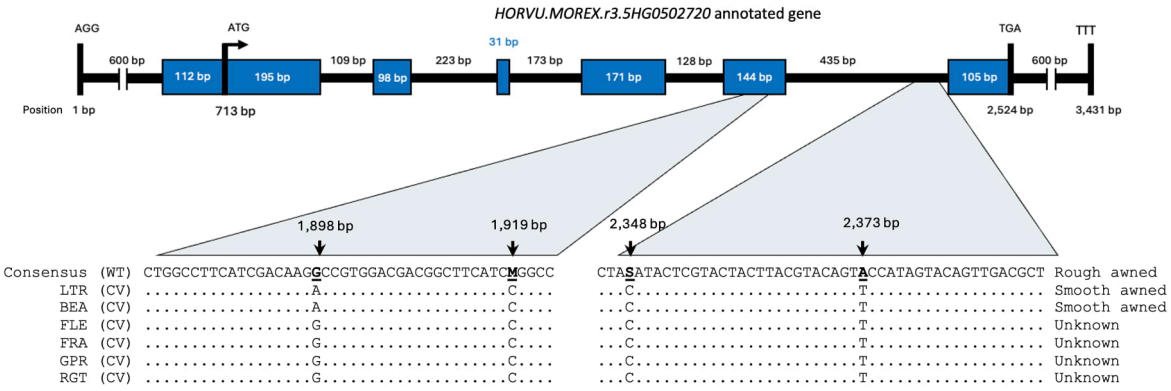

Figure 5.4. Single nucleotide polymorphisms identified from Sanger sequencing results. Two informative SNPs positioned at 1,898 and 2,373 bp within the HORVU.MOREX.r3.5HG0502720 annotated gene showed potential for developing molecular markers. CV: cultivar, WT: wild type. The alignment reference is the consensus sequence for 26 WBDC accessions.

In silico analysis of CAPS and dCAPS candidates

In silico fragment analysis enabled assessment of the viability of candidate markers. For the first informative SNP at position 1,898 bp in HORVU.MOREX.r3.5HG0502720, a total of 8 CAPS and 29 dCAPS polymorphisms were identified within a 60 bp region spanning the target SNP. Nine viable candidate markers with suitable post-digestion restriction patterns were selected, including 7 dCAPS and 2 CAPS markers (coded as M1 to M9) (Table 5.2). For the second informative SNP at position 2,373 bp of the same gene, one CAPS and 17 dCAPS polymorphisms were identified within a 60 bp region spanning the target polymorphism. The restriction pattern produced by the single CAPS polymorphism identified was not suitable for visualisation in gel electrophoresis. From the 17 dCAPS, only 11 of them –all located in the forward strand (+)– contained a sufficiently conserved region across all accessions, enabling the design of primers that amplified a region of suitable length for clear gel visualisation. The reverse strand (-) lacked the necessary sequence conservation for the design of primers that could bind robustly across all accessions. From the 11 options available in the forward strand, only one of them was viable, with a suitable restriction pattern and an affordable restriction enzyme. This candidate was labelled as M10 (Table 5.2). *In silico* digestion with corresponding restriction enzymes did not reveal additional recognition sites introduced by the SNPs at positions 1,919 and 2,348 bp. Among all the options, M4 produced the best balance between restriction pattern and cost, and was therefore selected along with *Btr1* and *Qsd1* markers (Gould, 2022; Williams, 2022) for progeny genotyping.

Table 5.2. Summary of dCAPS and CAPS markers for the SNP at position 1,898 bp within HORVU.MOREX.r3.5HG0502720 gene. The table includes primer sequences, restriction enzyme, cost per unit, and restriction pattern. Mismatches are highlighted in bold for dCAPS, while no mismatches are specified for CAPS.

SNP position	Type	Marker	Primer ID	Restriction enzyme	Recognition pattern	Cost (AUD unit -1)	Primer sequence (5' to 3')	Mismatch	Restriction pattern and total amplicon size
1,898 bp	dCAPS	M1	5HG0502720-F1881	BstNI	CCWGG	$0.04	TGGCCTTCATCGAC**C**AG	A>C	La Trobe: 80+91=171
			5HG0502720-R2032				GGATGGGTGCATGCATGAAA	-	Wild: 15+65+91=171
		M2	5HG0502720-F1878	BslI	CCNNNNNNNGG	$0.12	TGCTGGCCTTC**C**TCGACAAG	A>C	La Trobe: 82 + 100=182
			5HG0502720-R2032				GGATGGGTGCATGCATGAAA	-	Wild: 17+65+100=182
		M3	5HG0502720-F1879	EcoNI	CCTNNNNNAGG	$0.13	GCTGGCCTTC**C**TCGACAAG	A>C	La Trobe: 149
			5HG0502720-R2010				TGTGAAGAGCGAGAGATGGT	-	Wild: 14+135=149
		M4	5HG0502720-F1902	EcoO109I	RGGNCCY	$0.06	TGAAGCCGTCGTCCA**G**GG	C>G	La Trobe: 72
			5HG0502720-R1847				CTGCTGAACGTGGAGGGGTA	-	Wild: 18+54=72
		M5	5HG0502720-F1902				TGAAGCCGTCGTCCA**G**GG	C>G	La Trobe: 108
			5HG0502720-R1811				GATGGCGGATGGATGGGT	-	Wild: 18+90=108
		M6	5HG0502720-F1902b	StuI	AGGCCT	$0.12	ATGAAGCCGTCGTCCA**A**GG	C>A	La Trobe: 70
			5HG0502720-R1848				TGCTGAACGTGGAGGGGTA	-	Wild: 19+51=70
		M7	5HG0502720-F1902b				ATGAAGCCGTCGTCCA**A**GG	C>A	La Trobe: 107
			5HG0502720-R1811				GATGGCGGATGGATGGGT	-	Wild: 19+88=107
	CAPS	M8	5HG0502720-F1801	HpyCH4III	ACNGT	$0.59	TAGCTTTGCTGATGGCGGA	-	La Trobe: 101+42=143
			5HG0502720-R1924				GAAGATGTGGCGCTGGGAT		Wild: 143
		M9	5HG0502720-F1805	BcefI	ACGGC(N)$_{12}$	$2.85	TTTGCTGATGGCGGATGGAT	-	La Trobe: 120+60=180
			5HG0502720-R1966				CTCGAGCTTGTGGACGAGG		Wild: 79+41+60=180
2,373 bp	dCAPS	M10	5HG0502720-F2354	BanI	GGYRCC	$0.03	CGTACTACTTACGTAC**G**GT	A>G	La Trobe: 68
			5HG0502720-R2402				TCCTGCAACCCCAAACGAAT	-	Wild: 17+51=68

5.3.2 Allele introgression via marker-assisted backcrossing

Cultivated alleles were successfully introgressed into wild genetic backgrounds, resulting in 30 backcross lines derived from La Trobe and five wild accessions: WBDC-038, WBDC-068, WBDC-117, WBDC-199, and WBDC-329 (Table 5.3; Appendix 5.10). These BC2F2 plants were self-pollinated to produce BC2F3 bulk seeds, which were used in the phenotyping experiment described in Chapter 6. Each breeding cycle faced challenges such as no seed development after pollination, and unclear genotyping gel bands treated as missing data. A total of 2,202 seeds were genotyped across the three genotyping generations (Appendix 5.11), from which 607 were treated as missing for *ROUGH AWN1*, 594 for *Qsd1*, and 645 for *Btr1*. At BC2F2 genotyping stage, only 12 seeds contained homozygous cultivated alleles for the three markers. However, additional selections at this last genotyping stage were allowed for progenies with one or two heterozygous markers as these loci can be converted to a homozygous state through self-pollination in future generations without the need for further crossing (Table 5.3). By the end of the MABC program, the number of successful LTR/Wild crosses was significantly decreased from 26 F1s to 5 BC2F2 lines.

5.4 Discussion

In cereals, traits such as non-brittle rachis and reduced dormancy were pivotal in transforming wild species into cultivars suitable for planting and harvesting. These traits prevent grain losses caused by seed shattering and ensure timely germination, making them indispensable in modern agriculture and therefore essential targets for *de novo* domestication. On the other hand, while not strictly considered essential for cultivation, yield and stress tolerance benefits are likely the reason why awns have persisted in modern cultivars (Haas *et al.*, 2019). However, bristly awns pose a significant challenge for farmers, especially those growing barley for livestock feed. The difficulty of managing rough-awned varieties has led some farmers to avoid them altogether. Given the yield and stress tolerance advantages of awned varieties (Liller *et al.*, 2017; Haas *et al.*, 2019; DeWitt *et al.*, 2023), it may be more beneficial to retain awns from wild accessions in the process of *de novo* domestication rather than eliminate them entirely. Smooth awns could potentially preserve the photosynthetic benefits while eliminating the nuisances related to awn bristles, improving the practical value of *de novo* domesticated lines.

Table 5.3. Summary of selected *de novo*-domesticated material using *Btr1, Qsd1*, and *ROUGH AWN1* markers for genotyping. Markers were developed by CropGEM research group (University of Melbourne; unpublished data).

	Generation	Donor parent (cultivar)	Wild parent (accession code)	Pedigree	Harvest year	*Btr1*†	*Qsd1*†	*ROUGH AWN 1*†	No. cultivated homozygous alleles
1	BC2F2	La Trobe	WBDC-038	WBDC-038*3/La Trobe_1.1.1	Feb-24	HOC	HOC	HOC	3
2	BC2F2	La Trobe	WBDC-038	WBDC-038*3/La Trobe_1.1.2	Feb-24	HOC	HOC	HOC	3
3	BC2F2	La Trobe	WBDC-038	WBDC-038*3/La Trobe_1.1.3	Feb-24	HOC	HOC	HOC	3
4	BC2F2	La Trobe	WBDC-038	WBDC-038*3/La Trobe_1.1.4	Feb-24	HET	HOC	HOC	2
5	BC2F2	La Trobe	WBDC-068	WBDC-068*3/La Trobe_1.1.1	Feb-24	HOC	HOC	HOC	3
6	BC2F2	La Trobe	WBDC-068	WBDC-068*3/La Trobe_1.1.2	Feb-24	HOC	HOC	HOC	3
7	BC2F2	La Trobe	WBDC-068	WBDC-068*3/La Trobe_1.1.4	Feb-24	HOC	HOC	HOC	3
8	BC2F2	La Trobe	WBDC-068	WBDC-068*3/La Trobe_2.1.4	Feb-24	HOC	HOC	HOC	3
9	BC2F2	La Trobe	WBDC-068	WBDC-068*3/La Trobe_1.1.3	Feb-24	HET	HOC	HOC	2
10	BC2F2	La Trobe	WBDC-068	WBDC-068*3/La Trobe_2.1.1	Feb-24	HET	HOC	HOC	2
11	BC2F2	La Trobe	WBDC-068	WBDC-068*3/La Trobe_2.1.2	Feb-24	HET	HET	HOC	1
12	BC2F2	La Trobe	WBDC-068	WBDC-068*3/La Trobe_2.1.3	Feb-24	HOC	HET	HOC	2
13	BC2F2	La Trobe	WBDC-117	WBDC-117*3/La Trobe_1.1.1	Feb-24	HET	HOC	HOC	2
14	BC2F2	La Trobe	WBDC-117	WBDC-117*3/La Trobe_1.1.2	Feb-24	HET	HOC	HOC	2
15	BC2F2	La Trobe	WBDC-117	WBDC-117*3/La Trobe_1.1.3	Feb-24	HOC	HET	HOC	2
16	BC2F2	La Trobe	WBDC-117	WBDC-117*3/La Trobe_1.1.4	Feb-24	HOC	HET	HOC	2
17	BC2F2	La Trobe	WBDC-117	WBDC-117*3/La Trobe_1.1.5	Feb-24	HOC	HET	HOC	2
18	BC2F2	La Trobe	WBDC-117	WBDC-117*3/La Trobe_1.1.6	Feb-24	HET	HOC	HOC	2
19	BC2F2	La Trobe	WBDC-199	WBDC-199*3/La Trobe_1.1.1	Feb-24	HOC	HOC	HOC	3
20	BC2F2	La Trobe	WBDC-199	WBDC-199*3/La Trobe_2.1.1	Feb-24	HOC	HOC	HOC	3
21	BC2F2	La Trobe	WBDC-199	WBDC-199*3/La Trobe_2.1.2	Feb-24	HOC	HOC	HOC	3
22	BC2F2	La Trobe	WBDC-199	WBDC-199*3/La Trobe_3.1.1	Feb-24	HET	HOC	HOC	2
23	BC2F2	La Trobe	WBDC-199	WBDC-199*3/La Trobe_3.1.2	Feb-24	HET	HOC	HOC	2
24	BC2F2	La Trobe	WBDC-199	WBDC-199*3/La Trobe_3.1.3	Feb-24	HOC	HET	HOC	2
25	BC2F2	La Trobe	WBDC-199	WBDC-199*3/La Trobe_4.1.1	Feb-24	HET	HOC	HOC	2
26	BC2F2	La Trobe	WBDC-199	WBDC-199*3/La Trobe_4.1.2	Feb-24	HET	HOC	HOC	2
27	BC2F2	La Trobe	WBDC-329	WBDC-329*3/La Trobe_1.1.1	Feb-24	HOC	HOC	HOC	3
28	BC2F2	La Trobe	WBDC-329	WBDC-329*3/La Trobe_1.1.2	Feb-24	HOC	HOC	HOC	3
29	BC2F2	La Trobe	WBDC-329	WBDC-329*3/La Trobe_1.1.3	Feb-24	HET	HOC	HOC	2
30	BC2F2	La Trobe	WBDC-329	WBDC-329*3/La Trobe_1.1.4	Feb-24	HET	HOC	HOC	2

† HOC = Homozygous cultivated, HET = Heterozygous

5.4.1 Development of a robust *ROUGH AWN1* marker

Developing molecular markers for a diverse range of accessions is more challenging than for biparental populations. The extensive genetic diversity and sequence variation in barley landraces, wild relatives, and cultivars make it difficult to design robust markers that are effective across diverse germplasms. Ideally, primer design should target highly conserved genomic regions, except for the desired polymorphism. Additional polymorphisms may alter the efficiency of primer binding and potentially introduce unintended restriction sites, reducing the reliability and robustness of the markers for broad applications. Despite these challenges, this study successfully developed molecular markers that effectively capture genetic variation across a diverse range of wild and cultivated barley accessions.

CAPS vs dCAPS

All candidate markers were designed from highly conserved genomic regions flanking the target polymorphisms at 1,898 and 2,373 bp of the HORVU.MOREX.r3.5HG0502720 gene. In general, CAPS offered greater flexibility for primer design than dCAPS and were therefore the first option in the design process. A basic requirement for successful CAPS marker is to amplify a conserved genomic region flanking the target SNP, but the primers are not strictly constrained to be in the proximity of the target SNP. This attribute allowed for some flexibility in selecting the most suitable region for optimal primer design and marker development. In contrast, for dCAPS markers, the amplicon was constrained by the forward primer, which was automatically generated by the dCAPS Finder 2.0 tool, introducing a nucleotide mismatch for the creation of new restriction sites. The position of the forward dCAPS primer is therefore fixed within 20 to 25 bp of the target SNP in either the forward (+) or reverse (-) strands, and only allowed for the design of the reverse primer downstream from the forward primer.

The more effective use of conserved regions for primer design in CAPS markers resulted in clearer and more distinguishable restriction patterns compared to dCAPS. For instance, in M8, the restriction enzyme *HpyCH4III* cleaved the La Trobe allele into fragments of 101 bp and 42 bp, while the wild allele remained uncut at 143 bp (Table 5.2). The difference between the largest cultivated cleaved fragment (101 bp) and the wild uncut fragment (143 bp) was 42 bp, or 29% relative to the largest one. Similarly, for M9, the restriction enzyme *BcefI* cleaved the La Trobe allele into 120 bp and 60 bp fragments. In the wild allele, the 120 bp fragment was further cleaved into 79 bp and 41 bp bands (Table 5.2). The difference between the 120 bp and 79 bp fragments was 41 bp, or 34%. These proportional differences between the uncut fragment and the largest post-digestion fragment—29% for M8 and 34% for M9—highlighted the strong potential for

high-resolution genotyping. In contrast, a similar analysis of dCAPS candidates (M1 to M7 and M10) showed a difference in fragment size of 20% or less. Despite the more suitable CAPS restriction patterns, dCAPS markers were generally better options due to the use of more affordable restriction enzymes suitable for the scale of the genotyping program conducted in this study.

Exon vs intron-located target SNP

Notably, there were more viable marker candidates identified within the genomic region flanking the SNP at 1,898 bp compared to the second SNP at 2,373 bp. Despite both SNPs are within the gene of interest, the first one at 1,898 bp has been identified as a non-synonymous variant responsible for the causal mutation for smooth awn trait (Milner *et al.*, 2019), while the second SNP at 2,373 bp is located within an intronic region of the same gene. M1 to M9 target the SNP at position 1,898 bp, while M10 targets the second SNP at position 2,373 bp. All markers developed from these two polymorphisms completely differentiated wild from cultivated as well as rough from smooth awns within the studied population. However, the difference in the position of the target SNPs renders M1 to M9 more robust than M10. The exon-based SNP at 1,898 bp ensures that the causal mutation directly correlates with the smooth awn trait. In addition, exonic regions tend to be highly conserved under stronger evolutionary pressure (Liu & Zhang, 2022; Monroe *et al.*, 2022; Majic & Payne, 2023), which could ensure a more consistent primer binding in untested barley populations (Shavrukov, 2016). The SNP at position 2,373 bp, located in an intron, exhibited greater sequence variability, making it less suitable for the design of robust primers.

Marker selection for progeny genotyping

The development of a robust *ROUGH AWN1* marker called for a balance between cost-effectiveness and precision for making it available to the wider scientific community working on wild barley *de novo* domestication. Clear and distinct restriction patterns in gel electrophoresis was the main driver for the shortlisting of viable candidates, but the cost of restriction enzymes determined the final selection for progeny genotyping. Based on restriction patterns alone, CAPS represented the most suitable options. However, the corresponding restriction enzymes for CAPS candidates were the most expensive ones; $0.59 and $2.85 per unit for M8 and M9, respectively (Table 5.2). Consequently, dCAPS was identified as the most affordable and scalable option with the cost of the best candidate enzyme EcoO109I (M4) at $0.10 per unit. Therefore, among all dCAPS candidates, marker M4 was selected for genotyping based on the quality of restriction patterns, target SNP located in an exonic region, and lower enzyme cost, representing the option that better ensured the required level of precision without exceeding budgetary constraints.

As the number of genotyping tests increases, enzyme costs may account for a larger portion of the overall expenses. The significantly lower cost of restriction enzyme of the M10 marker ($0.03 per unit) makes it an attractive option for large-scale genotyping experiments with strict budgetary constraints. However, the use of this marker may require an additional phenotyping step to ensure that parental lines exhibit the expected awn roughness and that these phenotypes fully correlate with the genotypes identified by M10. In addition, awn roughness is partially quantitative. It has been suggested that a second independent gene within the 7H locus may be responsible for an additional mutation that reduces barb formation (Milner *et al.*, 2019). It is therefore recommended to verify the allelic state, ± 500 bp of the target SNP, of the *ROUGH AWN1* locus located in chromosome 5H of parental lines before embarking on a large-scale genotyping program. Smooth awn cultivars carrying a polymorphism in the gene located in chromosome 7H may not be distinguishable from rough awn lines using the developed markers in this study.

5.4.2 *De novo* domestication

Ensuring wild background retention

Different factors, such as improper timing of emasculation and pollination, can disrupt the intended contribution of wild genomes by the end of the MABC breeding scheme. In this study, the introgression of cultivated alleles was performed using conventional breeding methods applied uniformly to all plants within a window of 2 to 3 weeks, while balancing the logistical constrains of both emasculation and pollination of up to 15 plants per day. Only 26 crosses were required to generate successful F1 hybrids, but subsequent backcrossing (BC) cycles demanded significantly greater effort. A total number of 150 spikes pollinated per BC cycle to ensure enough progeny carrying the 3 cultivated alleles of *Btr1, Qsd1* and *ROUGH AWN1* genes. However, BC1 and BC2 crossing cycles were unexpectedly more complicated as many spikes failed to set seeds, which suggests that emasculation and/or pollination were conducted outside the optimal window (Lukac *et al.*, 2012). Premature emasculations and delayed crossings of already emasculated spikes were potentially the causes of unsuccessful fertilisation. This large variation among wild accessions in optimal crossing window can alter anthesis timing and increase the risk of unintended self-pollination if the plants have undergone anthesis by the time of emasculation.

Distinguishing between hybridisation and self-pollination in BC1F1 and BC2F1 seeds is challenging as both, successful crosses, and self-pollinated progeny, can display similar heterozygous marker profiles. While the probability of this happening may be low, it could alter the desired genomic contribution of 87.5% and 12.5% for the wild and cultivated parents, respectively (Figure 5.5). The *de novo* domesticated material developed in this research are intended to become the scaffold for the development of new materials and may be subjected to

extensive evaluations. Therefore, it is highly recommended to conduct genome-wide genotyping to confirm that wild genomes represent 87.5% of the total genetic background as originally targeted.

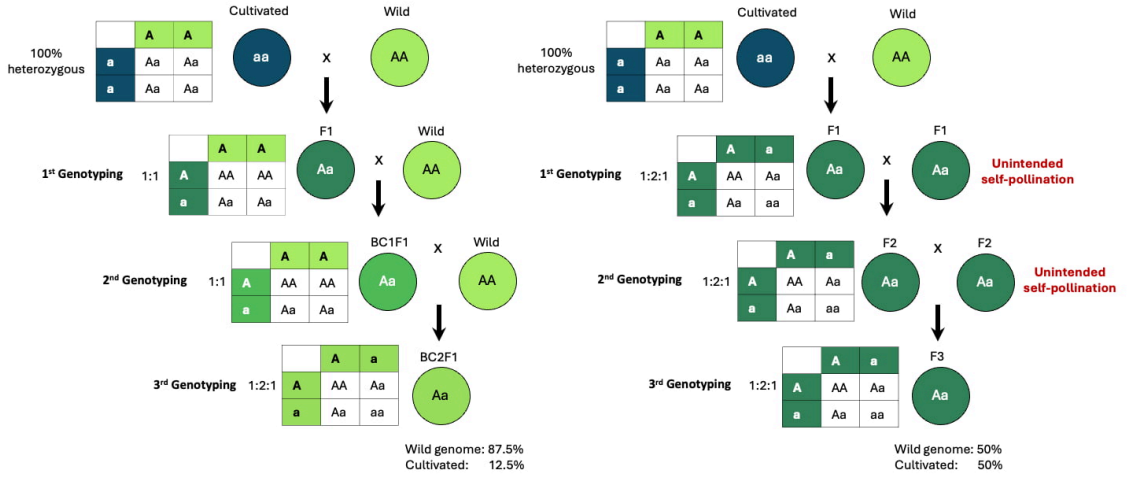

Figure 5.5. Possible outcomes during marker-assisted backcrossing. The goal was to reach the BC2F1 stage (3rd genotyping generation) with heterozygous alleles for all three markers. This BC2F1 underwent subsequent self-pollination to fix the cultivated alleles in a de novo domesticated line carrying most of wild genomic background. However, attaining heterozygous state can arise from two distinct scenarios: (a) The ideal scenario, where successful hybridization occurs between the cultivar and wild accessions in the first and second genotyping generations; (b) Undesired self-pollination events where instead of F1 x Wild and BC1F1 x Wild hybridization, unintended self-pollination occurs at both stages. Both scenarios result in heterozygous alleles by the 3rd genotyping generation, but with differing contributions from the wild and cultivated genomes.

Practical considerations

Considering the practicality of conducting *de novo* domestication through MABC can lead to more efficient strategies for its implementation. It has been proposed that *de novo* domestication could be initiated from a random subset of germplasm collections (Langridge & Waugh, 2019). However, there is only a limited number of lines that can be practically handled for *de novo*-domestication at a time via MABC. Considering the vast genetic diversity and the complexity of *de novo* domestication process, random selections may be highly inefficient for accelerating crop improvement from the utilisation of wild relatives.

The process of *de novo* domestication via MABC in this experiment has proven to be complex and time-consuming, particularly when considering the scale required to efficiently leverage the vast genetic diversity available in gene banks. Considering random segregation of the three genes introgressed in this study, a minimum of 8 seeds was theoretically needed to find one with the three cultivated alleles in heterozygous state, representing a ratio of $1/2^3$ (12.5%). For BC2F2, 64 seeds were required to identify one with all three cultivated alleles in the homozygous state, representing a ratio of $1/4^3$ (1.6%). In practice, these proportions were highly variable. In BC1F1,

for instance, the expected rate for the three heterozygous alleles decreased from 12.5% to 3.7% for WBDC-048 crosses, but increased to 21.6% for WBDC-074. This deviation from the expected rate were due to small number of sample, losses from low success crossing rates, poor germination, and missing data from unclear genotyping gels. This uncertainty increases the number of seeds required to ensure enough viable progeny for genotyping and selection in each LTR/wild combination. The number of required progeny increases exponentially with the addition of more genes for selection, as the combinatorial segregation of alleles complicates the identification of individuals carrying the desired genetic combinations. For six target genes, at least 64 seeds would be required to find one with six domestication genes in heterozygous state in BC1F1 and BC2F1 ($1/2^6$ or 1.6%). In the self-pollination BC2F2 stage, the probability of finding homozygous lines decreases to 1 in 4096 ($1/4^6$ or 0.02%). These constraints highlight the inefficiency of conventional MABC for introgressing multiple domestication loci, particularly when working with large numbers of wild accessions.

To overcome these challenges, gene editing technologies offer a promising alternative to accelerate *de novo* domestication. Unlike MABC, which relies on recombination and selection over multiple generations, gene editing enables the direct modification of domestication genes in a single step, reducing the need for extensive crossing and genotyping of large number of progenies.

5.5 Conclusion

This thesis chapter examined the design process for developing CAPS and dCAPS molecular markers for the barley *ROUGH AWN1* gene, detailing key steps involved in the selection of affordable and robust marker options. Wild and cultivated barley were successfully hybridised and BC2F3 lines carrying smooth awns, reduced dormancy, and non-brittle rachis alleles were selected via marker-assisted backcrossing. To the best of my knowledge, these are the first *de novo*-domesticated barley lines, which can be used as pre-breeding material to enhance the genetic diversity of current barley breeding pools. The introduction of alleles for non-brittleness ensures grain harvestability; reduced dormancy ensures timely germination; and smooth awns increases the value for a future commercialisation. The next step in the evaluation of *de novo* domestication of wild relatives is to assess their agronomic potential and stress tolerance in field and/or controlled phenotyping trials to realise the full potential of the developed pre-breeding material.

Chapter 6
Phenotypic evaluation of *de novo*-domesticated barley lines

6.1 Introduction

In recent years, *de novo* domestication has been explored in economically important crops like potato, wheat, rice, and tomato (Ye *et al.*, 2018; Zsögön *et al.*, 2018; Mirzaghaderi *et al.*, 2020; Yu *et al.*, 2021). However, the main focus of these studies, has been in overcoming obstacles, such as reproductive incompatibilities, technical limitations, and knowledge gaps on the genetic mechanisms underlying domestication genes (Jian *et al.*, 2022). For instance, addressing self-incompatibility in wild potato by introducing the *S-locus* inhibitor (*Sli*) gene has been essential to allow self-pollination and enable the use of wild diploid potatoes for breeding purposes (Ye *et al.*, 2018). In rice, significant efforts have been directed towards establishing reliable transformation and gene editing systems for the *de novo* domestication of allotetraploid wild rice (Yu *et al.*, 2021). As a result, there is limited evidence on the effect of *de novo* domestication on complex abiotic stress responses after the process has been successfully achieved, which is an essential step towards its broader acceptance and implementation for breeding crops resilient to climate change. This chapter therefore investigates the impact of *de novo* domestication on drought-related traits with complex quantitative inheritance and examines the extent to which wild phenotypes are preserved in *de novo*-domesticated lines after the introgression of cultivated alleles of domestication genes such as *Btr1, Qsd1,* and *ROUGH AWN1*. Contrasting phenotypes between the cultivated parent (LTR) and the wild parent would ideally provide a reference framework for this evaluation.

This study also evaluates the relationship between traits that reflect instantaneous processes, such as transpiration rate from thermal imaging, and time-integrated drought response metrics, such as biomass accumulation and water-use efficiency (WUE) within a temporal framework for identifying drought-tolerant candidates. A key objective is to determine how well spot measurements of canopy temperature and photosynthesis as proxies for transpiration efficiency, taken at different time points, align with WUE estimates derived from biomass and total water use.

Additionally, this study examines whether *de novo*-domesticated lines exhibit phenotypic profiles indicative of differences in stomatal response mechanisms compared to their wild and cultivated parents. This is done through the combined analysis of spectral proxies for transpiration and

photosynthesis alongside time-integrated traits like biomass and WUE, integrating multiple physiological parameters to characterise stomatal regulation. While molecular studies have identified key processes governing stomatal aperture and closure (Kostaki *et al.*, 2020; Vialet-Chabrand *et al.*, 2021; Hasanuzzaman *et al.*, 2023a), their application to guide large-scale phenotypic screening remains unexploited.

Finally, this study evaluates whether gas exchange measurements and hyperspectral reflectance data from a portable spectroradiometer can be leveraged to develop empirical predictive models of photosynthetic capacity using supervised machine learning (ML) in a glasshouse experiment. Here, V_{cmax} (the maximum rate of carboxylation by Rubisco), acts as a critical parameter for measuring photosynthetic capacity and it is derived from coding-based curve-fitting routines using A-Ci response curves obtained from gas exchange measurements (Busch *et al.*, 2024). Empirical ML models are developed using Partial Least Squares Regression (PLSR) and Support Vector Regression (SVR), as previously reported in the literature (Dechant *et al.*, 2017; Silva-Perez *et al.*, 2018; Zarco-Tejada *et al.*, 2021). PLSR uses linear combinations of the original wavelengths, known as latent variables, from the entire spectrum of reflectance data as input to predict V_{cmax}. SVR uses the hyperplane that best fits the data points in a continuous space. While SVR is more effective at handling non-linear relationships than PLSR, it is also less effective when the input variables are highly collinear (Ballabio & Sterlacchini, 2012; Jou *et al.*, 2014). To avoid using highly collinear reflectance bands, Narrow-band Hyperspectral Indices (NBHIs) are calculated from highly informative wavelengths that directly correlate with specific plant traits and serve as input for SVR models. An extensive list of NBHIs has been previously reported by Zarco-Tejada *et al.* (2021). By correlating spectral signals with photosynthetic activity, researchers can extend the scope of photosynthetic measurements to track changes in photosynthesis over time for tens or hundreds of plants.

6.2 Materials and Methods

6.2.1 Plant materials, growing conditions and experimental design

The barley lines used in this experiment were the Australian cultivar La Trobe (LTR), three pure wild lines (WBDC-038, WBDC-068, and WBDC-199), and six *de novo*-domesticated lines generated in Chapter 5. The *de novo* domesticated lines were BC2F3 progenies from two distinct lineages collected from each of the three La Trobe/Wild combinations (Figure 6.1).

Husks were removed manually, and seeds were treated with H_2O_2 as per methods in Chapter 2. One to two plants per pot were grown in 1.5L-pots using 70% potting mix / 30% clay loam (v/v) growing media described in Chapter 3 and Chapter 4. Seedlings emerging outside the 7-day

window following the first plant emergence were removed to minimise variation introduced from differences in phenological development. After thinning, each pot retained a minimum of one plant, with most pots containing two plants.

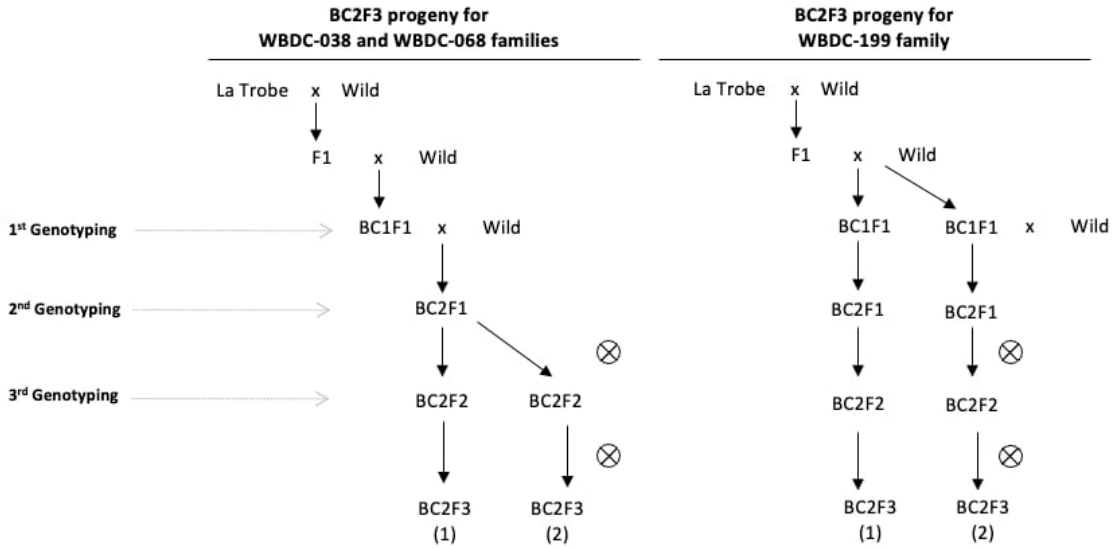

Figure 6.1. Backcrossing scheme used in Chapter 4 to develop de novo-domesticated barley lines. Seeds were separated at BC2F2 stage for LTR/WBDC-038 and LTR/WBDC-068 families and at BC1F1 stage for LTR/WBDC-199 family. Different BC2F3 progeny of the same family are referred to as distinct lineages. BC2F3 seeds were used in a phenotyping experiment along with cultivated and wild parents. Lineage separation for the LTR/WBDC-038 and LTR/WBDC-068 crosses differed from LTR/WBDC-199 cross due to the lack of viable progeny with all three markers in the desired (heterozygous) allelic state first and second genotyping events, corresponding to BC1F1 and BC2F1 generations.

A layer of 250 g of black gravel was added to pots to minimise water evaporation from topsoil during the experiment and a matte black-painted cardboard was positioned at the base of the pots to eliminate signal interference from an irregular surface (Figure 6.2). The gravel and the cardboard were beneficial for enhancing the contrast between the canopy and background pixels, which facilitated the segmentation of thermal images.

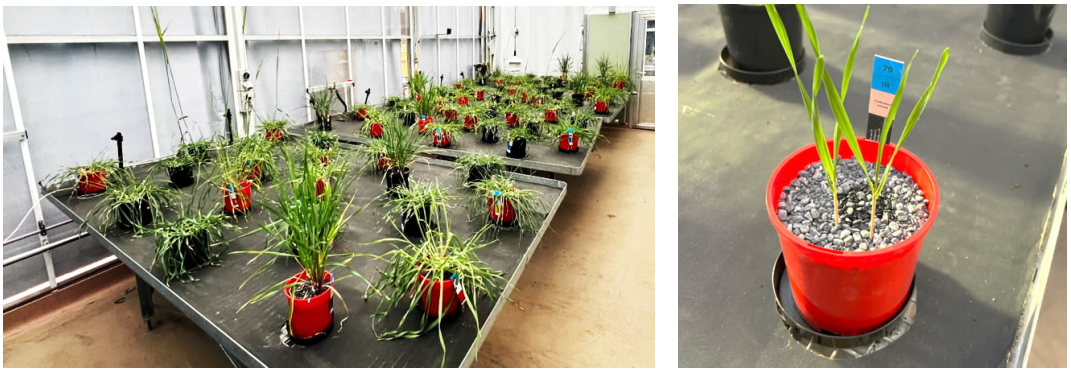

Figure 6.2. Overview of the glasshouse set up showing the arrangement of the pots (left), and the matte black-painted cardboard positioned at the base of the pots to provide a uniform background (right). Example of a pot with a 250 g layer of black gravel added to the topsoil to minimise water evaporation.

To avoid manipulation of leaves in preparation for thermal imaging phenotyping, spacing between pots was increased from 26 cm in previous experiments (Chapter 3) to 40 cm. Plants were grown at 20°C for 58 days with supplemental lighting (Fortimo LED Line, High Flux VO, Eindhoven, Netherlands) at an intensity of 500 µmol m^{-2} s^{-1} measured at the level of plant canopy. A light:dark photoperiod of 12:12 h was maintained throughout the experiment.

Four replicates for each line-by-treatment combination were assessed within the same trial. Pots were distributed in a Complete Randomised Block Design, arranged in a grid pattern of 4 rows by 20 columns, with each set of 5 columns representing a distinct block (Figure 6.3; Table 6.1).

Table 6.1. Line codes, family background and material type of each line included in the experiment.

Genotype	Line	Line Code	Family	Material type
G-1	L-01	Cultivated	LTR	Cultivated parent
G-2	L-02	068_Wild	G068	Wild parent
G-3	L-03	068_BC2F3_1	G068	*De novo*-domesticated / BC2F3 (1)
G-4	L-04	068_BC2F3_2	G068	*De novo*-domesticated / BC2F3 (2)
G-5	L-05	199_Wild	G199	Wild parent
G-6	L-06	199_BC2F3_1	G199	*De novo*-domesticated / BC2F3 (1)
G-7	L-07	199_BC2F3_2	G199	*De novo*-domesticated / BC2F3 (2)
G-8	L-08	038_Wild	G038	Wild parent
G-9	L-09	038_BC2F3_1	G038	*De novo*-domesticated / BC2F3 (1)
G-10	L-10	038_BC2F3_2	G038	*De novo*-domesticated / BC2F3 (2)

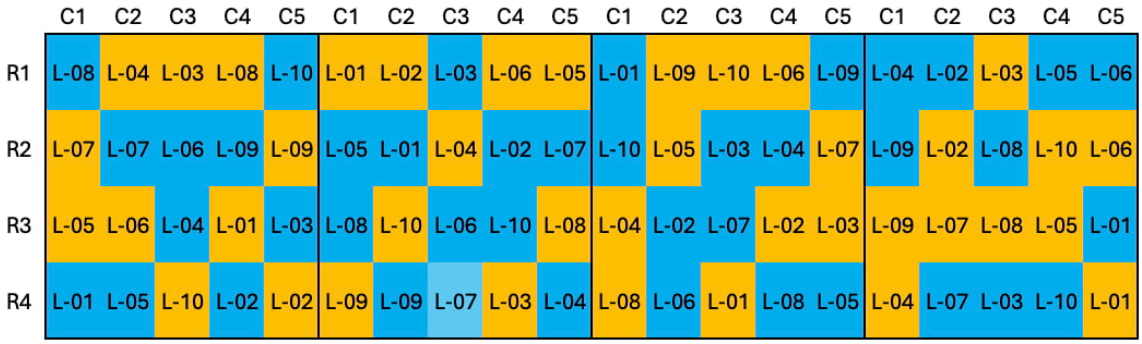

Figure 6.3. Experimental layout for the assessment of de novo domesticated material against their corresponding parents. Lines are coloured by treatment and were randomly distributed across four blocks. Blue represents irrigated pots and yellow represents drought pots.

6.2.2 Drought treatment

Irrigation treatments were applied manually, following the similar irrigation regimes used in Chapters 3 and Chapter 4. Capillary irrigation was not employed in this experiment as the number of pots was optimal to maintain manual irrigation for the two treatment groups, Irrigate (IR) vs Drought (DR). Each pot was placed on a digital scale, and water was added from the top until the pot reached the target weight. Drought-treated pots were gradually dried by matching the rate of slowest drying pot while irrigated pots were maintained between 75% and 85% of Field Capacity (FC). Soil water content was measured and adjusted daily from 16 days after sowing (DAS) and twice a day after 40 DAS (Figure 6.4). The day before thermal imaging measurements, soil water content was adjusted based on each pot's historical drying rate, ensuring that the target percentage of field capacity (%FC) was reached during data collection the following day.

6.2.3 Plant phenotyping

Canopy temperature

Canopy temperature measurements followed the procedure detailed in Chapter 3 and Chapter 4. Canopy temperature was recorded by gliding a thermal camera (Model E86, Teledyne FLIR LLC) over each pot three times within a time frame of 45 min. Three radiometric images were extracted and analysed with a custom MATLAB (Mathworks Inc., Natick, Massachusetts, USA) code to obtain average canopy temperature values per pot. Ambient temperature was recorded using 27 HOBO data loggers (Onset, Cape Cod, Massachusetts, USA) evenly located across the glasshouse, and canopy temperature depression (CTD) was calculated as the difference between ambient (T_a) and canopy temperature (T_c) (Equation 3.1; Chapter 3).

Pigment content

Spectrally-derived pigment traits (Chlorophyll, Flavonoids, Anthocyanins and Nitrogen Balance Index) were obtained with a Dualex Scientific+ (FORCE-A, Orsay, France). Measurements were

taken 2 to 3 days before biomass harvest from two random fully expanded top leaves and averaging the values per pot.

Spectral reflectance

Spectral reflectance was measured using a handheld SpectraPen SP110 (Photon System Instruments, Drásov, CZ), separated in two distinct groups of data. The first group consisted of temporal measurements taken throughout the experiment to track changes over time. For these measurements, reflectance was recorded from two or three of the youngest fully expanded leaves per plant, and an average value was calculated for each pot. The second group comprised leaf reflectance measurements taken alongside photosynthesis assessments to enable the development of an empirical relationship between reflectance data and photosynthetic parameters.

Biomass

Above ground fresh and dry weight biomass were measured as per methods in Chapter 4. Biomass was immediately weighed on a scale to obtain fresh weight (FW). Plants were dried at 70°C for 72 hours and re-weighed to determine the dry weight (DW).

Water use efficiency

Water Use Efficiency (WUE) was calculated as the ratio of above-ground biomass to the total water supplied to each pot throughout the experiment.

Photosynthesis capacity

Photosynthetic capacity was assessed with two gas exchange systems Li6800 (LI-COR Biosciences Inc., Lincoln, Nebraska, USA). For each measurement, the youngest fully expanded leaf from the tagged plant in each pot was clamped into a 3 cm × 1 cm gasket. Inlet CO_2 concentration was increased from 200 µmol mol^{-1} to 1400 µmol mol^{-1} at intervals of 200 µmol mol^{-1} to record internal CO_2 concentration (Ci) and net carbon assimilation (A). The temperature in the chamber was maintained at 25°C. A constant photosynthetic photon flux density of 1500 µmol m^{-2} s^{-1} within the chamber and each leaf was light adapted for 5 min before starting a CO_2 response curve.

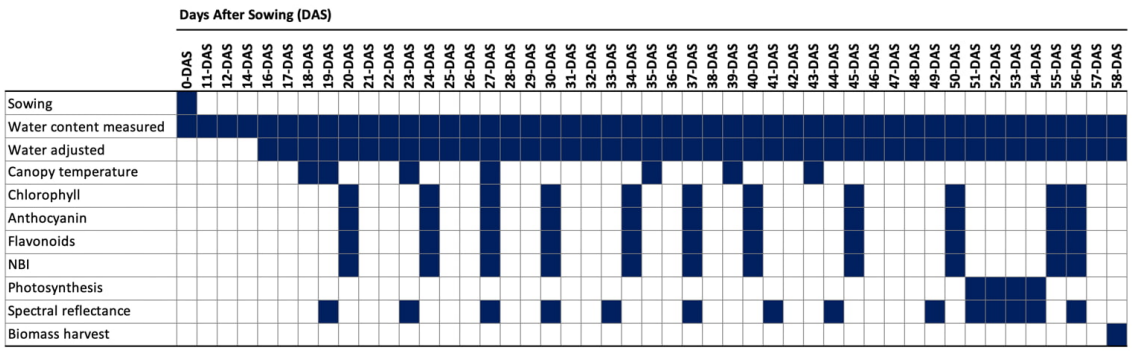

Figure 6.4. Timeline of activities conducted during the experiment for phenotyping experiment including de novo-domesticated lines, along with wild and cultivated parents. Activities conducted include water content measurements, water adjustments, and trait measurements. Blue-shaded cells correspond to the days after sowing (DAS) on which each activity was performed.

6.2.4 Statistical analyses

Linear and machine learning models

Linear models were used in R (version 4.3.2) (Table 6.2), using the *emmeans* package (version 1.10.0) (Lenth *et al.*, 2024) for estimating marginal means and the *tidyverse* package (version 2.0.0) (Wickham, 2014) for data processing. The *lme4* package (version 1.1.35.1) (Bates *et al.*, 2015) was employed to fit linear mixed-effects models, allowing control for confounding variables and testing the significance of effects across treatments, lines, time points, and their corresponding interactions.

Partial Least Squares Regression (PLSR) model was used to predict photosynthetic capacity (V_{cmax}) from spectral reflectance data spanning wavelengths from 400 nm to 793 nm. The PLSR model was implemented with *pls* R package (version 2.8.3), and evaluated using Leave-One-Out Cross-Validation (LOOCV). Predictions were made using varying numbers of latent components (5, 10, 20, and 30).

Sixty-seven Narrow-Band Hyperspectral Indices (NBHIs) were calculated (Zarco-Tejada *et al.*, 2021) and filtered using Variance Inflation Factor (VIF) analysis with R package *fmsb* (version 0.7.6) (Nakazawa, 2018). The selected NBHIs were used as predictors in a Support Vector Regression (SVR) model with a radial basis function (RBF) kernel, and hyperparameter tuning via a grid search to optimise the cost (C) and epsilon (ε) parameters. Model evaluation was conducted using Leave-One-Out Cross-Validation (LOOCV) with one level of each grouping factor (e.g., day or treatment) excluded at a time to identify whether measurements from a particular day or treatment were significantly affecting model performance. Performance metrics for PLSR and SVR models included Mean Absolute Error (MAE), Root Mean Squared Error (RMSE), and coefficient of determination (R^2).

Decision tree models were developed to assess the relative importance of measured traits for classifying samples into families (LTR, G038, G068, and G199), irrigation treatment (IR,DR), lines (L1 to L10) and material type (Wild, Cultivated). A leave-one-out cross-validation (LOOCV) approach was implemented to evaluate the model's performance. The decision tree was trained using the *rpart* R package (version 4.1.23) (Therneau *et al.*, 2015).

Table 6.2. Overview of the statistical models used for data analysis.

Trait group	Predicted trait	Input variables	Model
Transpiration	CTD	Treatment, Line, Stage, Block, Pot number	linear mixed model
Pigments	Chl	Treatment, Line, Stage, Block	Linear model
	Flavonoids	Treatment, Line, Stage, Block	
	Anthocyanins	Treatment, Line, Stage, Block	
	Nitrogen Balance Index	Treatment, Line, Stage, Block	
Biomass	Fresh weight	Treatment, Line, Block	
	Dry weight	Treatment, Line, Block	
Spectral reflectance	NBHIs	Treatment, Line, Stage, Block	
	Photosynthesis	Reflectance data from 400 nm to 794 nm	PLSR
		VIF-filtered NBHIs	SVR
All	Classification group	All traits	Decision tree

Photosynthesis capacity

Carbon assimilation (A) values were normalised to the specific leaf area of each sample before A-Ci curve fitting. Leaf area was measured by photographing the leaves on a white background to facilitate image segmentation using Fiji software (ImageJ, National Institutes of Health, Bethesda, Maryland, USA). The measured area for each sample was then input as a constant into the gas exchange parameter calculations. Two curve fitting routines were conducted with *plantecophys* (version 1.4.6) (Duursma, 2015) and *photosynthesis* (version 2.1.4) (Stinziano *et al.*, 2021) packages to calculate V_{cmax} and J_{max}. The outputs from both packages were compared using correlation analysis to evaluate agreement between the two methods.

6.3 Results

6.3.1 Consistent soil water content for all pots

Irrigation in this experiment was regulated by precisely controlling pot water content rather than applying the same amount of water to all pots. This approach ensured that drought stress was imposed consistently across genotypes (Figure 6.5), preventing undesirable variability in drought

severity that could confound the interpretation of quantitative traits such as canopy temperature depression (CTD), chlorophyll content, and biomass accumulation as the experiment progresses and plants mature. This is particularly relevant when comparing wild, cultivated, and *de novo*-domesticated lines, as genetic differences could influence their transpiration levels under varying water levels.

As expected, significant day-to-day fluctuations in soil water content (SWC) depletion rates were observed. After 35 DAS, the variability in SWC of irrigated pots significantly increased, while the variation of SWC in drought pots remained stable. Although the daily mean varied significantly across different DAS, the SWC was consistently maintained within a range of ±5% around the mean for each day of CTD phenotyping. These fluctuations in SWC highlight the challenges of maintaining consistent water content over time, even in a controlled glasshouse environment.

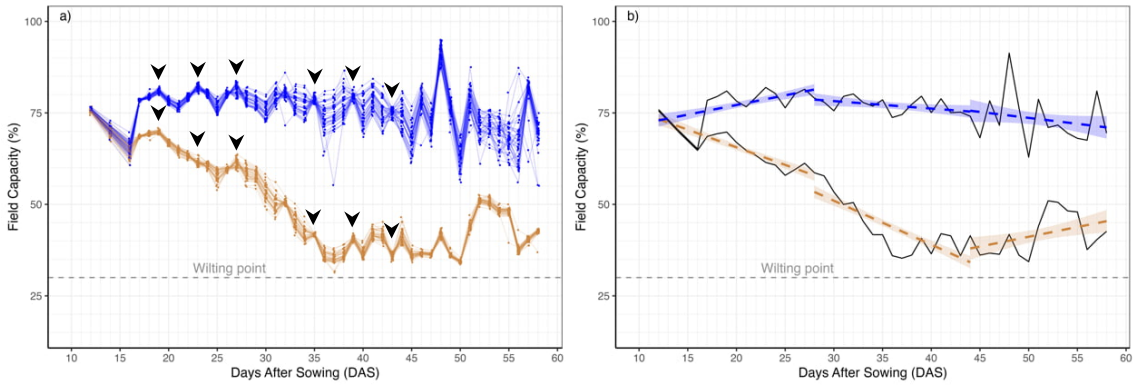

Figure 6.5. Variations in soil water content (SWC) expressed as a percentage of field capacity (%FC) across treatments throughout the experimental period. a) Faded lines illustrate the soil drying trajectories for individual pots. Arrows indicate days of CTD phenotyping campaigns. b) Bold black lines represent the mean %FC values per treatment per day, while dashed lines with confidence intervals indicate linear trends for three distinct DAS intervals (12–28, 29–44, and 45–59). Treatments are distinguished by colour: brown for Drought and blue for Irrigated conditions. The dashed horizontal line marks the wilting point at 30%FC.

6.3.2 Significant effects of drought treatment on measured traits

CTD

Ambient temperature (T_a), DAS, and the two-way interactions Treatment:DAS and Line:DAS had a significant effect on CTD at $p < 0.001$, while the effect of Line was significant at $p < 0.05$ (Appendix 6.1). This indicates that environmental factors, such as temperature and time, drove changes in CTD, which in turn depended on the treatment applied and, to a lesser degree, the genetic background of the lines tested. However, the Treatment:Line and Treatment:Line:DAS interactions were not significant, suggesting similar temporal and treatment responses across

lines. Line 199_BC2F3_2 maintained a distinctive low CTD values under both irrigated and drought conditions compared to the rest of the lines (Figure 6.6).

Biomass and WUE

For FW, DW, and WUE, significant differences were observed among lines ($p<0.001$), while the Treatment:Line interaction was not significant. This indicates that biomass and WUE varied between lines, but the effects of drought on these traits were similar across all of them (Appendix 6.1). Both FW and DW were significantly lower in drought pots. Interestingly, the three wild lines L-02 (068_Wild), L05 (199_Wild), and L-08 (038_Wild) exhibited lower biomass accumulation than La Trobe (LTR), regardless of irrigation treatment (Figure 6.6).

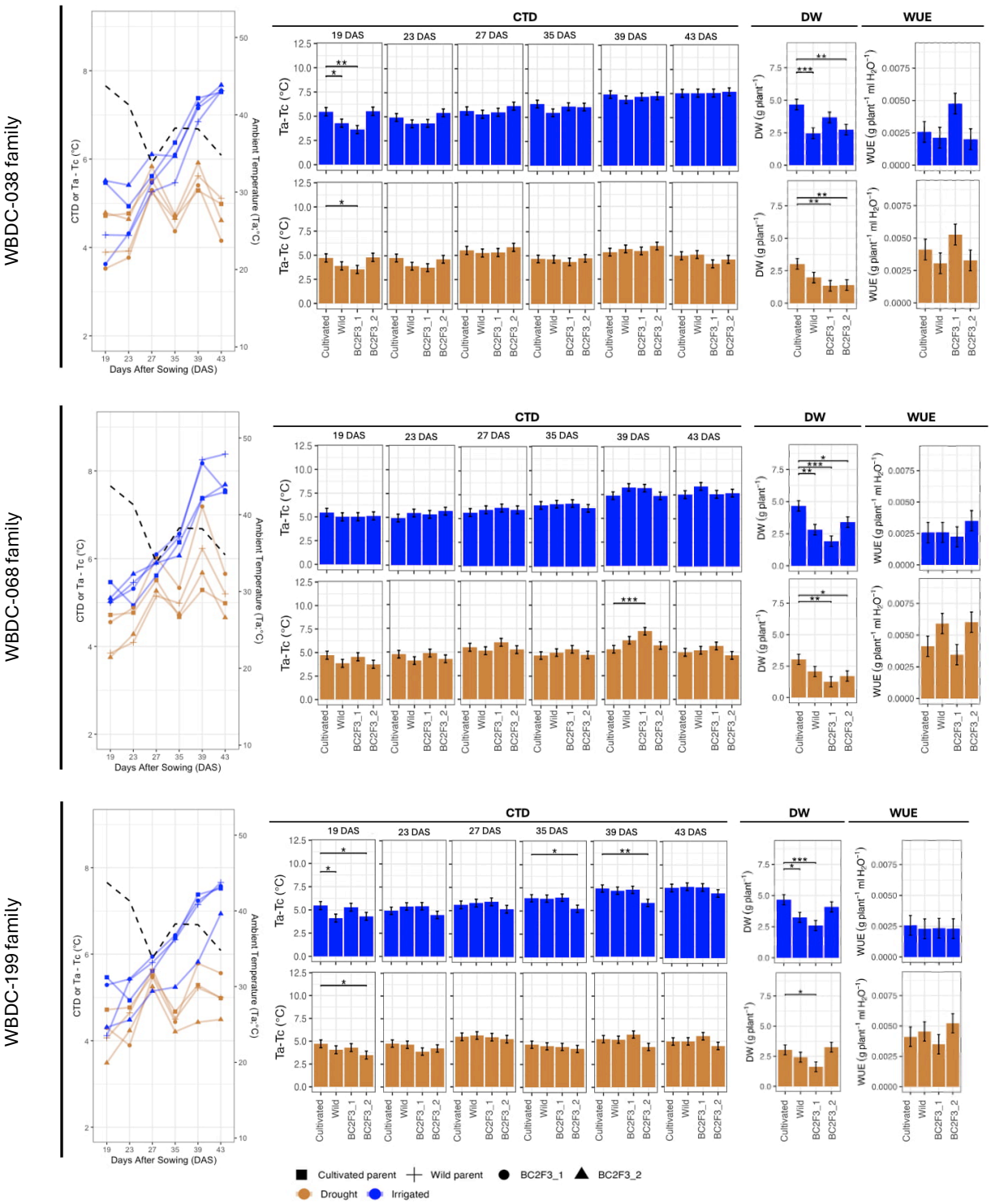

Figure 6.6. Canopy temperature depression (CTD) across three distinct families: WBDC-038, WBDC-068, and WBDC-199, under irrigated (blue) and drought (brown) conditions. Each family contains two de novo-domesticated lines BC2F3_1 (circle) and BC2F3_2 (triangle), along with corresponding cultivated (square) and wild (cross) parents. Left panel shows changes in canopy temperature depression (CTD) taken at 6 stages: 19, 23, 37, 35, 39 and 43 DAS. The dashed line represents the mean ambient temperature (Ta) recorded during canopy temperature acquisition (right y-axis). The right panel shows bar plots representing contrasts of Wild and the two de novo-domesticated lines against the cultivated parent, La Trobe (LTR), for CTD, DW, and WUE. Error bars represent standard errors. Significance differences between lines within each treatment are denoted by asterisks (*p < 0.05, **p < 0.01, ***p < 0.001).

While WUE – biomass divided by total water supplied – was generally higher under drought compared to irrigated pots, no significant differences between La Trobe (LTR) cultivar and the rest of the lines within the same family were observed at p=0.05 (Figure 6.6).

Spectral indices

For pigment and NBHIs, most individual factors— Line, Treatment, and DAS—as well as the two-way interactions among them, had a highly significant effect ($p<0.001$) (Appendix 6.1). Nonetheless, the three-way interaction Line:Treatment:DAS did not show a significant effect. On the final day of pigment and reflectance data acquisition, at 56 DAS, significant differences were evident across these traits (Figure 6.7).

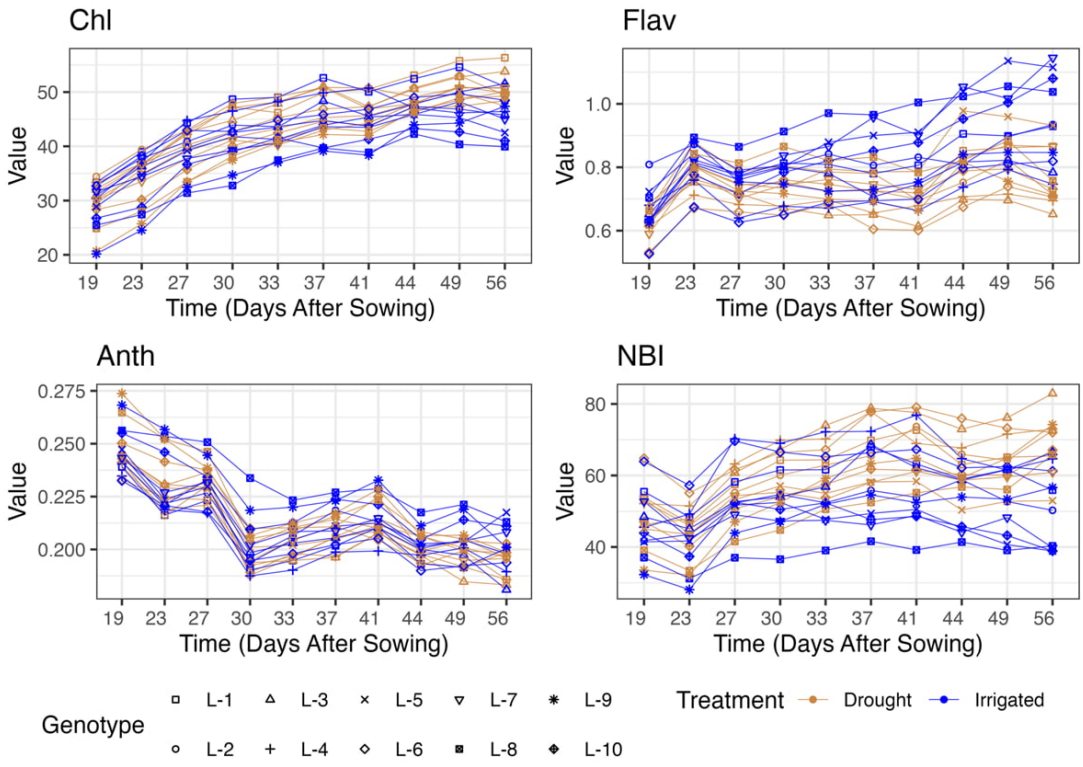

Figure 6.7. Progression of Chlorophyll (Chl), Flavonoids (Flav), Anthocyanins (Anth), and Nitrogen Balance Index (NBI) over time. Each data point shows the estimated marginal means per line for drought (brown) and irrigated (blue) treatments on that specific DAS. Shapes differentiate between lines (L-01 to L-10) as follows: L-01 (Cultivated), L-02 (068_Wild), L-03 (068_BC2F3_1), L-04 (068_BC2F3_2), L-05 (199_Wild), L-06 (199_BC2F3_1), L-07 (199_BC2F3_2), L-08 (038_Wild), L-09 (038_BC2F3_1), and L-10 (038_BC2F3_2).

Time progression of drought responses

An upward trend in canopy temperature depression (CTD) over time was observed across all lines under irrigated conditions, suggesting a potential increase in cooling capacity due to biomass accumulation as plants matured (Figure 6.6). In contrast, CTD remained relatively stable over

time in drought-treated pots, reflecting the reduced evaporative cooling capacity of plants under water-limited conditions.

Dynamic patterns of pigments (Figure 6.7) and NBHIs (Figure 6.8) showed clear differences between irrigated and drought conditions, with the most pronounced variations observed in DNCabxc, CUR, and LIC3. These differences likely reflect the accumulation of metabolic compounds due to plant acclimation to growing conditions under stress and physiological changes associated with plant aging and senescence.

Photosynthesis predictions from spectral data

Photosynthetic parameters V_{cmax} and J_{max} derived from A-Ci curve analyses processed through *photosynthesis* (Appendix 6.2) and *plantecophys* (Appendix 6.3) R packages demonstrated a strong correlation (Appendix 6.4). V_{cmax} from the *photosynthesis* package was chosen for subsequent analyses due to its updated modelling capabilities.

V_{cmax} showed no significant differences between irrigation treatments (Figure 6.9). PLSR and SVR model performances for predicting V_{cmax} from spectral data were low, showing a poor predictive power despite using different number of components and data exclusion in combination with a Leave One Out Cross Validation (LOOCV) (Appendix 6.5).

6.3.3 The effects of *de novo* domestication

For CTD, the phenotyping day 43 DAS, corresponding to the greatest difference in soil water content (SWC) between treatments, was chosen as a critical time point in this experiment to identify pronounced differences between the two parents. For pigments and NBHIs, this assessment is done on the final day of phenotyping for each trait, 56 DAS, when drought stress was expected to reach its peak (Figure 6.4).

For CTD, no significant differences were observed between LTR and each of the wild parents under either irrigated or drought conditions at 43 DAS (Figure 6.6). For pigment traits at 56 DAS, the following contrasting responses between LTR and the wild parent were observed: Chlorophyll (Chl), all families under irrigated and drought conditions; Flavonoid (Flav), family 038 and 199 under irrigated conditions; Anthocyanins (Anth), family 038 under irrigated and drought conditions, and 199 under irrigated conditions; Nitrogen Balance Index (NBI), family 038 under irrigated, and family 199 under both irrigated and drought conditions (Appendix 6.6).

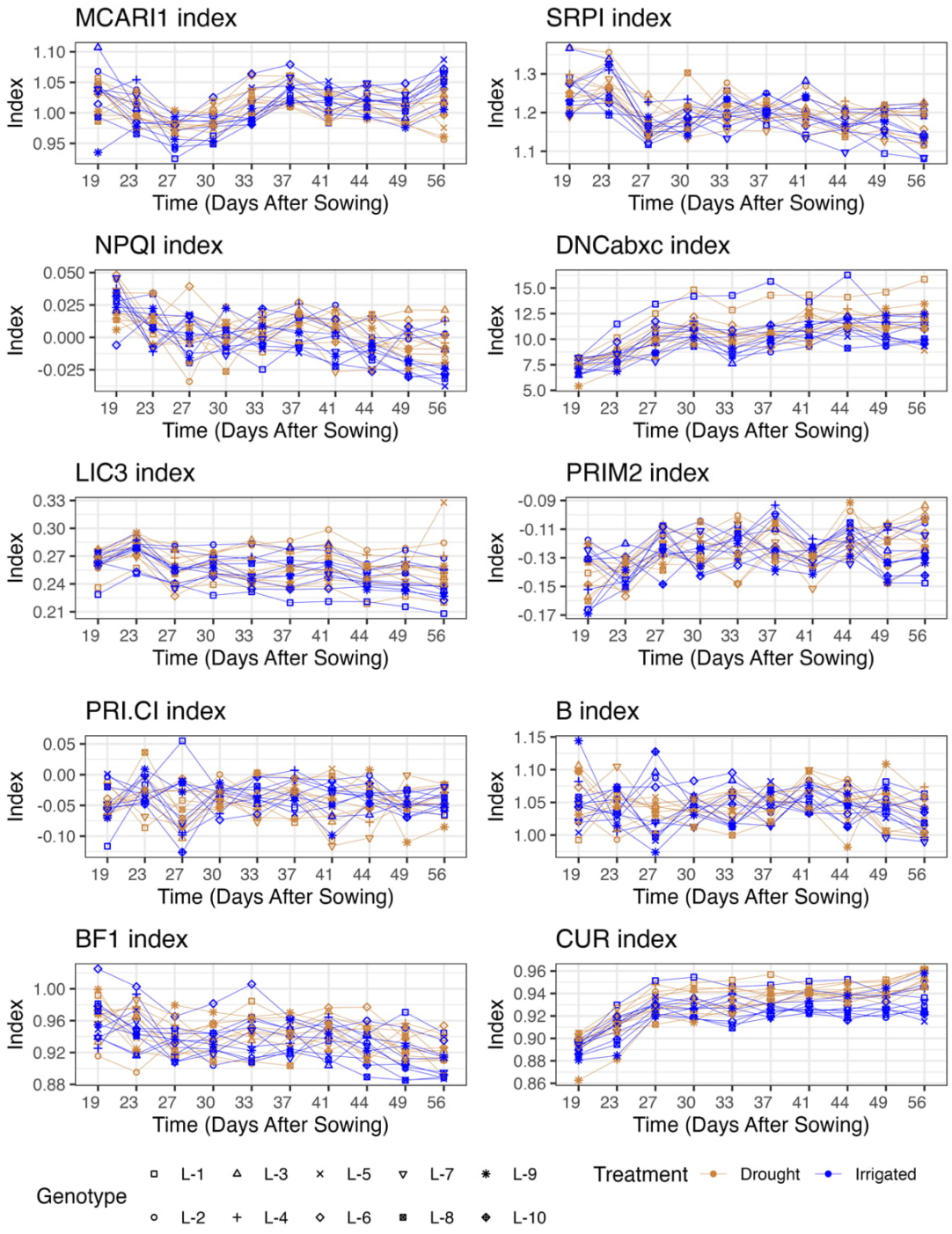

Figure 6.8. Progression of Narrow-Band Hyperspectral Indices (NBHIs) over time. NBHIs were derived from spectral reflectance data captured using the SpectraPen SP110 device. These indices were selected from an initial set of 67 NBHIs after variable filtering using Variance Inflation Factor (VIF) analysis. Each data point shows the estimated marginal means per line for drought (brown) and irrigated (blue) treatments on that specific DAS. Shapes differentiate between lines (L-01 to L-10) as follows: L-01 (Cultivated), L-02 (068_Wild), L-03 (068_BC2F3_1), L-04 (068_BC2F3_2), L-05 (199_Wild), L-06 (199_BC2F3_1), L-07 (199_BC2F3_2), L-08 (038_Wild), L-09 (038_BC2F3_1), and L-10 (038_BC2F3_2).

Similarly, statistically significant differences between LTR and wild lines were observed for the following NBHIs at 56 DAS: MCARI1, family 068 under drought; SRPI, family 038 under irrigated and drought conditions, and family 068 under irrigated conditions; DNCabxc, all three families under drought, and 199 under irrigated conditions; LIC3, family 038 under drought, 068 under irrigated and drought, and 199 under irrigated and drought conditions; BF1, all three families under irrigated conditions; CUR, 199 under irrigated conditions. For biomass, all three families showed difference between LTR and wild for DW under irrigated conditions, but no significant differences were identified under drought conditions. No significant differences were identified between LTR and wild lines for WUE (Figure 6.6).

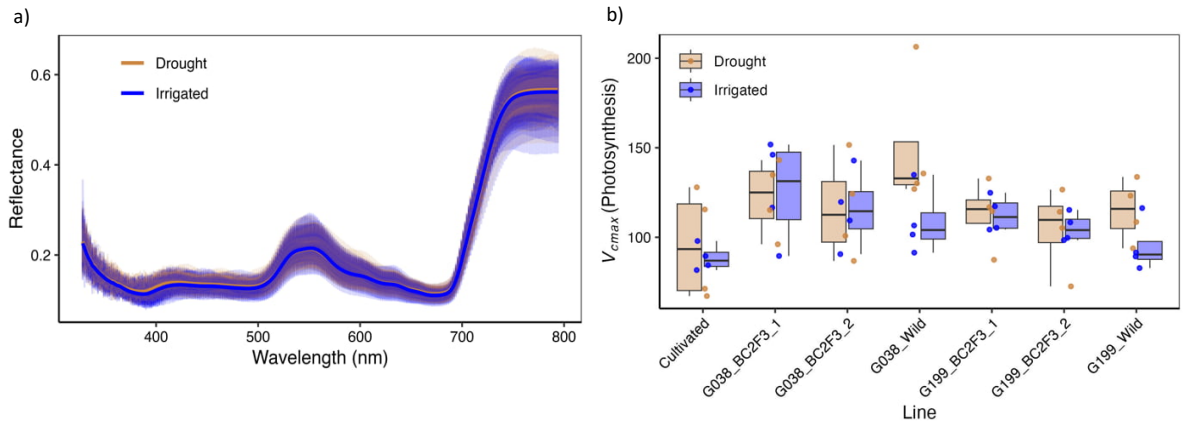

Figure 6.9. Effects of drought stress in reflectance spectra and photosynthesis capacity. Reflectance spectra of individual pots and treatment averaged across all measurement days. Transparent lines represent reflectance data for individual pots while bold lines indicate the mean reflectance values for each treatment; d) Boxplots of Rubisco-limited photosynthetic capacity (V_{cmax}) under drought and irrigated conditions for cultivated, wild, and backcrossed BC2F3 barley lines derived from WBDC-038 and WBDC-199. Brown lines represent drought pots and blue lines represent irrigated pots.

Among pigment traits and NBHIs where LTR and the wild parent were significantly contrasting ($p<0.001$), in 65% of the cases, at least one *de novo*-domesticated line emulated the response of the wild parent, while in the remaining 35% *de novo*-domesticated lines exhibited patterns resembling those of the cultivated parent. Trait/family occurrences where at least one *de novo*-domesticated line closely resembled the wild parent in either drought or irrigated conditions were observed in Chl/038, Chl/068, Flav/199, Anth/038, NBI/038, NBI/199, SRPI/068, DNCabxc/038, DNCabxc/068, DNCabxc/199, LIC3/038, LIC3/068, BF1/038, DW/038, DW/068, and DW/199 (Appendix 6.6 and Appendix 6.7). Occurrences where cultivated and wild lines showed contrasting values but no *de novo*-domesticated lines resembled the wild parent were observed in Flav/038, Anth/199, NBI/199, MCAR1/068, SRPI/038, DNCabxc/199, LIC3/199, BF1/068,

BF1/199, and CUR/199. These results show the variability among *de novo*-domesticated lines in conserving phenotypic traits of the wild parent.

6.3.4 PCA and phenotypic correlation

Principal Component Analysis (PCA) was used to identify major sources of variation in the dataset. The first three principal components (PCs) accounted for 56.9% of the total phenotypic variation in the data set (Table 6.3; Figure 6.10). PC1 accounted for 28.5% of the total variation, with NBI, Flav, Cur, and CTD_Stage_6, having the highest absolute contributions and strongest influence. PC2 explained 15.2% of the variation and was dominated by CTD measured at different time points except for the last DAS. PC3 accounted for 13.2% of the variation, with DW and FW showing the highest contributions.

A phenotypic correlation matrix was used to assess the strength and significance of correlations between traits. Figure 6.11 reveals a strong correlation among CTD at six different time points, indicating their non-random associations, and indicating inherent physiological traits rather than random fluctuations . Fresh weight (FW) and dry weight (DW) biomass exhibited strong positive correlations with CTD at Stage 6 (43 DAS), indicating a potential relationship between canopy cooling capacity observed at later stages and biomass accumulation. Hyperspectral indices such as LIC3, SRPI, and NPQI displayed moderate but significant negative correlations with FW and DW biomass but showed no significant correlation with CTD.

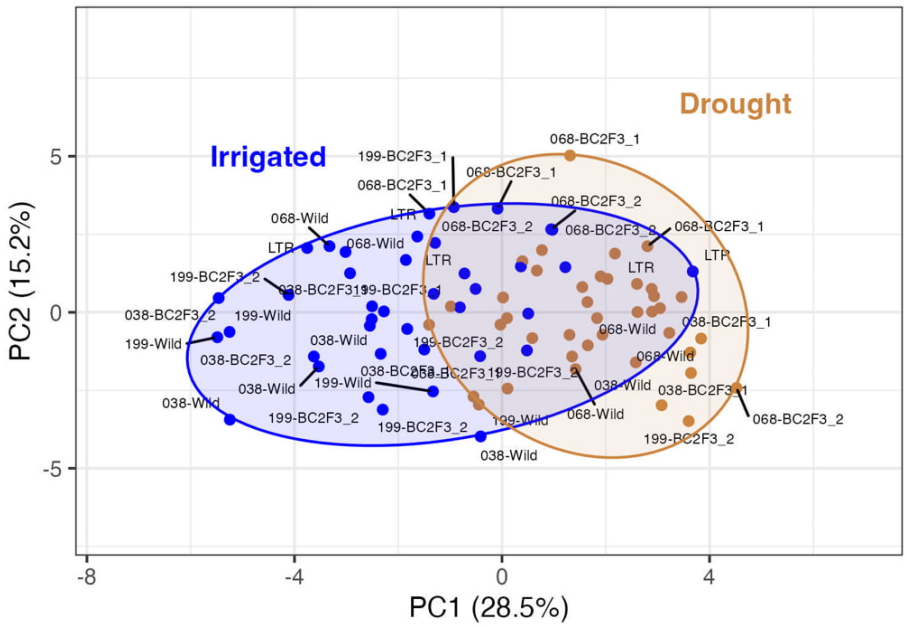

Figure 6.10. Principal Component Analysis (PCA) plot based on all measured traits. Ellipses enclose barley lines under irrigated (blue) and drought (brown) treatments. The plot reveals an overlap between treatment groups.

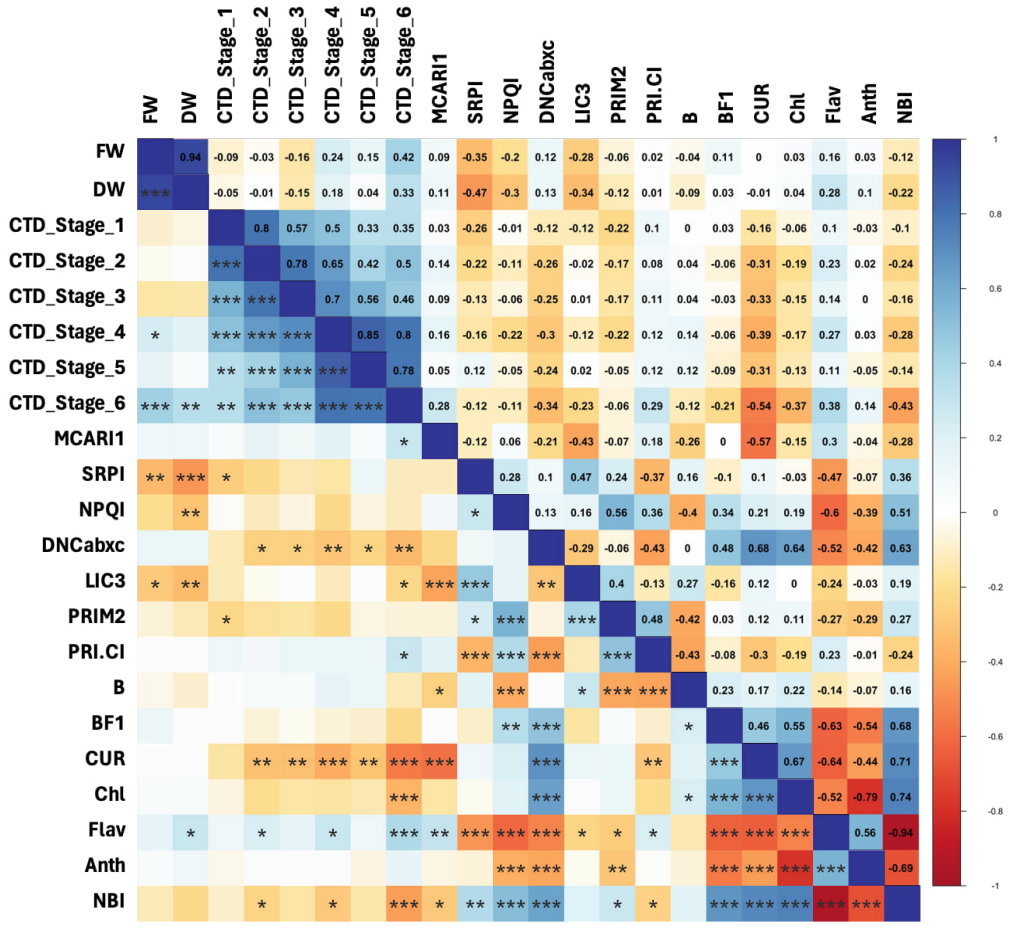

Figure 6.11. Correlation heatmap of pairwise relationships between physiological and biochemical traits across all barley lines and treatments.

Table 6.3. Loadings of the first three principal components (PC1 to PC3) for CTD, biomass, pigments, and NBHIs. Traits are arranged in descending order based on their absolute contribution to each principal component. Percentages indicate the proportion of total variance explained by each PC component.

PC1 (28.5%)			PC2 (15.2%)			PC3 (13.2%)		
Trait	Loadings	Abs. Loadings	Trait	Loadings	Abs. Loadings	Trait	Loadings	Abs. Loadings
NBI	0.346	0.346	CTD_Stage_4	0.357	0.357	DW	0.473	0.473
Flav	-0.324	0.324	CTD_Stage_3	0.348	0.348	FW	0.436	0.436
CUR	-0.322	0.322	CTD_Stage_5	0.335	0.335	LIC3	-0.362	0.362
CTD_Stage_6	-0.293	0.293	CTD_Stage_2	0.334	0.334	SRPI	-0.327	0.327
Chl	0.276	0.276	CTD_Stage_1	0.327	0.327	DNCabxc	0.268	0.268
DNCabxc	0.264	0.264	Anth	-0.308	0.308	PRIM2	-0.253	0.253
CTD_Stage_4	-0.261	0.261	BF1	0.271	0.271	NPQI	-0.248	0.248
CTD_Stage_2	-0.222	0.222	NBI	0.236	0.236	Chl	0.178	0.178
Anth	-0.221	0.221	Chl	0.228	0.228	BF1	0.167	0.167
BF1	0.217	0.217	CTD_Stage_6	0.225	0.225	CTD_Stage_3	-0.150	0.150
CTD_Stage_3	-0.200	0.200	Flav	-0.212	0.212	CUR	-0.129	0.129
CTD_Stage_5	-0.194	0.194	NPQI	0.126	0.126	PRI.CI	-0.127	0.127
NPQI	0.174	0.174	DNCabxc	0.115	0.115	Flav	0.099	0.099
CTD_Stage_1	-0.156	0.156	B	0.106	0.106	CTD_Stage_5	-0.088	0.088
MCARI1	-0.144	0.144	CUR	-0.087	0.087	CTD_Stage_2	-0.083	0.083

SRPI	0.142	0.142	FW	0.038	0.038	MCARI1	0.058	0.058
PRI.CI	-0.118	0.118	LIC3	-0.026	0.026	B	0.050	0.050
PRIM2	0.116	0.116	PRIM2	-0.014	0.014	CTD_Stage_1	-0.048	0.048
DW	-0.097	0.097	DW	-0.012	0.012	CTD_Stage_6	0.037	0.037
LIC3	0.091	0.091	SRPI	-0.010	0.010	Anth	-0.031	0.031
FW	-0.080	0.080	MCARI1	-0.002	0.002	NBI	-0.022	0.022
B	0.051	0.051	PRI.CI	0.001	0.001	CTD_Stage_4	0.012	0.012

6.4 Discussion

6.4.1 DW contribution to data set variability

In this experiment, DW showed significant statistical differences between lines within the same family group (Figure 6.6 and Appendix 6.1). However, its significance to capture variability in the dataset under controlled water regimes appeared subdued despite its biological and agronomic importance. The results of the PCA revealed that DW biomass had a relatively low loading score in PC1 and PC2, while being among the top contributors to PC3 (Table 3.1). PCA disentangles the dataset's underlying structure by identifying traits that dominate variability in distinct orthogonal dimensions (Lever *et al.*, 2017). The relatively low contribution of DW to PC1 indicates that it captured secondary or more subtle patterns of variation in the dataset compared to the primary contributors, which included NBI, Flav, CUR, and CTD_Stage_6, in order of importance.

In the field, differences in stomatal conductance between lines contribute to varying rates of water depletion. Maintaining consistent soil water content (SWC) is almost impossible, making it difficult to isolate changes in transpiration driven solely by plant physiology without the cumulative effects of water depletion. As water levels are not restored to ensure uniform SWC across the same water regime experimental group, different lines may activate stomatal closure mechanisms at varying time points and to a different degree. These variations in SWC determine stomatal conductance and total CO_2 assimilated, ultimately amplifying detectable differences in biomass and grain yield across lines. Consequently, transpiration, biomass and grain yield represent the dominant patterns of variability under field conditions as shown in several multivariate analyses (Ali *et al.*, 2015; Qaseem *et al.*, 2017). As a time-integrated trait, DW compounds the cumulative effects of environmental conditions and plant-soil interactions throughout the growing period, reflecting not only the overall growth performance but also the feedback loop between plant growth and soil water depletion. The minimal contribution of DW variations to PC1 likely reflects the precise regulation of water content across all pots under controlled environmental conditions. Consequently, the strong influence of DW on variation patterns often observed under field conditions did not manifest in this dataset. Instead, the main PC1 contributors were related to photoprotection mechanisms.

Results from this experiment indicate that Flav, Anth, and SRPI (a spectral proxy for the Car/Chl*a* ratio), were generally higher in the wild lines (L-02, L05 and L-08; Table 6.1) compared to LTR (Appendix 6.6). These traits are closely associated with ROS scavenging and energy dissipation in the electron transport chain (ETC), particularly useful for retaining photosynthetic performance under stress (Hasanuzzaman *et al.*, 2020), suggesting that the wild parent possesses physiological mechanisms that enhance acclimation to stress environments.

6.4.2 Pigment traits are highly correlated

The strong correlation observed in NBI with Chl and Flav reflects their mathematical as well as physiological relationships (Cerovic et al., 2012) (Figure 6.11). NBI serves as an indirect indicator of assimilated carbon allocation to either flavonoid biosynthesis or plant growth under N-limited conditions. It is calculated from chlorophyll-to-flavonoid ratio (Chl/Flav) (Cartelat *et al.*, 2005; Cerovic *et al.*, 2012). In this experiment, the observed increases in NBI (Nitrogen Balance Index) over time in drought-treated pots were primarily driven by a rise in chlorophyll (Chl) content, while flavonoid (Flav) levels remained relatively stable. In contrast, NBI in irrigated pots exhibited a less pronounced change. This was due to a concurrent increase in Flav content that offset the rise in Chl as the plants matured. Consequently, NBI values were lower in irrigated pots compared to drought-treated pots at 56 DAS (Figure 6.7). This could suggest healthier drought-treated than irrigated pots since more carbon is allocated to flavonoid production due to nitrogen (N) deficiency (Cartelat *et al.*, 2005). However, higher NBI observed in drought pots may instead reflect a steep increase in chlorophyll density per unit area (Hasanuzzaman *et al.*, 2017) and an unexpected lack of flavonoid accumulation in drought pots, which suggests that imposed stress treatment was not severe or prolonged enough to activate the flavonoid biosynthetic pathways. Flavonoid production often requires both sufficient time and a strong stress signal, such as intense UV-B exposure, to be significantly upregulated (Agati *et al.*, 2012; Ferreyra *et al.*, 2021). The use of a shading screen lowered UV-B radiation and may have contributed to the lack of flavonoid accumulation.

6.4.3 CUR and chlorophyll fluorescence

As opposed to Flav, CUR exhibited a greater increase under drought relative to irrigated conditions. CUR is an optical index related to the curvature of the reflectance spectrum used to monitor changes in reflectance caused by chlorophyll fluorescence, which are independent of pigment levels (Zarco-Tejada *et al.*, 2000a; Zarco-Tejada *et al.*, 2000b). This index is positively correlated with *Fv/Fm*, the maximum quantum yield of photosystem II (PSII) from dark-adapted leaves. Inactivation of PSII through photoinhibition leads to a reduction in *Fv/Fm* (Murchie &

Lawson, 2013), and therefore low CUR values (Zarco-Tejada *et al.*, 2000b). The consistent increase in CUR over time across all lines, with a more pronounced trend under drought conditions, was unexpected and suggests an improvement in the maximum quantum yield of PSII compared to irrigated conditions. However, this response may indicate a transient acclimation to drought stress triggered by the supplemental LED light, increasing capacity of the plant for NPQ to mitigate photoinhibition (Baker & Rosenqvist, 2004). CUR and Flav exhibited a negative correlation (Figure 6.11), indicating that higher flavonoid content acted as an energy escape valve and reduced the reliance on chlorophyll fluorescence for energy dissipation.

A strong negative correlation between CTD at 43 DAS (CTD_Stage_6) and CUR was observed (Figure 11), which suggests that lines with cooler canopy temperatures, and consequently higher CTD values, generally exhibited reduced energy dissipation through chlorophyll fluorescence. Strong correlations between CUR and CTD are likely due to less stomatal limitations to photosynthesis when plants exhibit high stomata conductance, allowing CO_2 to reach the carboxylation site and allowing a greater proportion of energy to be utilised in photochemical quenching rather than being dissipated as chlorophyll fluorescence (Murchie & Lawson, 2013).

Overall, no signs of severe stress to the photosynthesis capacity were observed in this experiment. In addition, most of the pigment and NBHIs related to photosynthetic performance showed no significant correlation with biomass accumulation (FW and DW) under varying water regimes, suggesting that biomass declines across treatments were primarily driven by stomatal limitations to photosynthesis. On the other hand, the variability captured by the main PC1 components did not correlate with the relative importance of various traits for classification across different grouping factors, namely group family (LTR, G038, G068, and G199), irrigation treatment (IR/DR), or lines (L1 to L10) (Appendix 6.8). This suggests that the dominant variation captured by PC1 may be driven by spatial variability of environmental factors or microclimatic differences affecting all plants within the experiment, rather than genetic background or treatment-specific responses.

6.4.4 Photosynthesis predictions from spectral data

Partial Least Squares Regression (PLSR) and Support Vector Regression (SVR) showed limited prediction ability for V_{cmax} from reflectance data, as reflected in the near zero coefficient of determination (R^2). These results differ from previous studies, where Partial Least Squares Regression (PLSR) models demonstrated stronger performance, with R^2 values exceeding 0.6 (Serbin *et al.*, 2012; Dechant *et al.*, 2017; Suarez *et al.*, 2021). The low predictive performance likely stems from small number of observations (56 in total), the narrow spectral range captured

by the SpectraPen SP 110 device (390nm to 793nm), and the absence of significant variation in photosynthesis across samples.

In the study by Silva-Perez *et al.* (2018), approximately 300 observations, representing 55% of the total dataset, were utilised to train the PLSR model. An adequate number of samples for model training is therefore critical in PLSR to establish a robust relationship between spectral data and photosynthesis performance. In addition, several studies have used spectroradiometers with a range capability between 350 and 2500 nm (Dechant *et al.*, 2017; Silva-Perez *et al.*, 2018; Suarez *et al.*, 2021), while in this experiment the spectral range captured by the SpectraPen SP110 device was 400nm to 793nm. Most of the infrared (IR) section of the spectrum, including near infrared (770–1300nm), short wave infrared 1 (SWIR1; 1300–1900 nm), and the short wave infrared 2 (SWIR2; 1900–2500 nm) were not included in the analysis, which likely contributed to the reduced predictive accuracy (Silva-Perez *et al.*, 2018). Moreover, there was likely not enough variation in photosynthesis capacity in response to drought stress, reflected in the lack of significant differences in photosynthetic capacity from gas exchange measurements across irrigation treatments (Figure 6.9b).

6.4.5 *De novo*-domestication for retaining quantitative wild phenotypes

In this experiment, CTD, biomass, pigment content, and Narrow-Band Hyperspectral Indices (NBHIs) displayed continuous distributions, which are characteristic of quantitative traits (Zhang *et al.*, 2009; Yang *et al.*, 2022) (Appendix 9). This continuous variation suggests a complex genetic inheritance in which traits are governed by numerous loci with small additive effects. In most instances where parental lines displayed contrasting values, the phenotypes of BC2F3 lines closely resembled the wild parent. This pattern was more evident for pigment traits (e.g., Chl, Flav, Anth, and NBI) and NBHIs (e.g., DNCabxc, LIC3, and SPRI) in some family groups (Appendix 6.6 and Appendix 6.7).

Recovering the wild phenotype through *de novo* domestication depends strongly on the presence of contrasting phenotypes between the cultivated and wild parents. This was not consistently achieved in this experiment due to the initial random selection of wild lines for crossing. For instance, CTD did not display statistically significant contrasting phenotypes between wild and cultivated parental lines, even at 43 DAS—the time point representing the maximum SWC difference between treatments. This may have precluded the observation of typical *de novo* domestication phenotypic patterns for this trait.

Although *de novo*-domesticated BC2F3 lines carried approximately 87.5% wild and 12.5% cultivated genomic background (Elston & Stewart, 1973) (Figure 6.12), the observed phenotypic patterns may not solely reflect the inheritance of many small additive-effect genes from the wild parent, but could also be the result of major-effect genes, dominance or epistasis. The phenotypic variation observed across BC2F3 lineages within the same family supports this hypothesis. The segregation of different subset of alleles during the MABC breeding process may have distinctively shape trait phenotypes across lineages within the same families (Bernardo, 2016). Additionally, the residual heterozygosity in the BC2F3 lines, resulting from only two self-pollination cycles and leaving approximately 6.25% of their genomes in a heterozygous state, likely influenced trait expression and contributed to deviations from the typical de novo domestication phenotypic patterns highlighted in Figure 6.13.

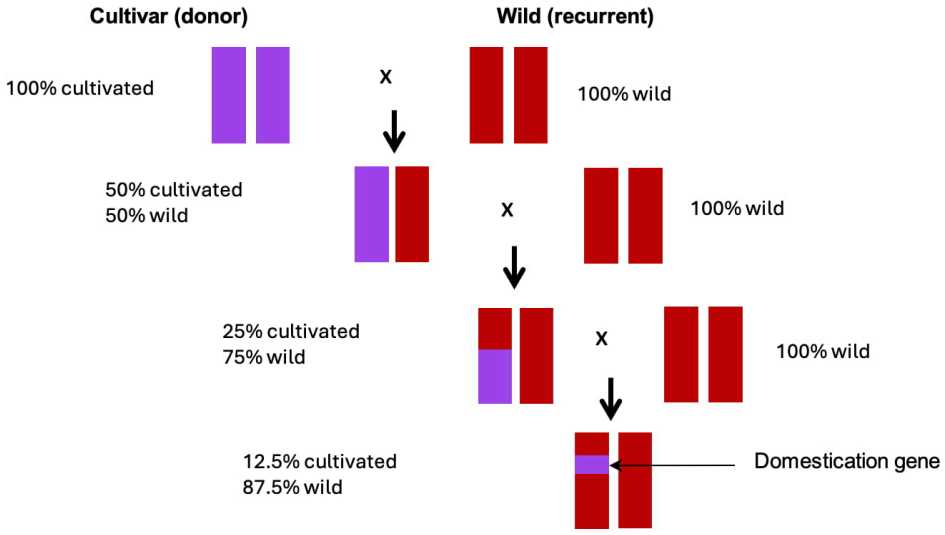

Figure 6.12. Simplified diagram of the Marker-Assited Backcrossing breeding scheme used to develop *de novo*-domesticated lines. A cultivated donor parent (100% cultivated, purple) was crossed with a wild recurrent parent (100% wild, red). Subsequent backcrossing to the wild parent resulted in progeny with progressively reduced cultivated genetic contributions (50%, 25%, and 12.5%), while retaining the domestication gene from the donor parent.

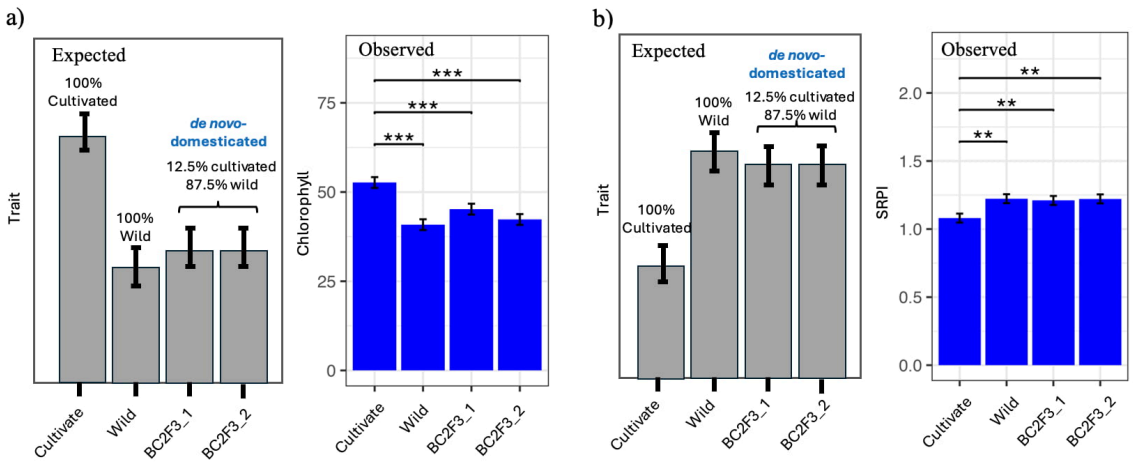

Figure 6.13. Comparison of expected and observed *de novo* domestication phenotypic patterns under two scenarios. a) Traits where the wild parent exhibits lower values, exemplified by chlorophyll content from family 038/IR. b) Traits where the wild parent exhibits higher values, exemplified by SRPI from family 068/IR. In both scenarios, the de novo-domesticated lines closely resemble the wild parent, consistent with their high wild genomic background (87.5%). Significant differences are denoted by *** ($p < 0.001$) and ** ($p < 0.01$). Error bars represent the standard error of the mean (SEM).

6.4.6 Evaluation of *de novo*-domesticated lines for drought tolerance

Optimising stomatal conductance (g_{sw}) is essential for developing plant ideotypes that efficiently regulate water losses under conditions of high vapour pressure deficit (VPD) and elevated wind and temperature. Those lines with optimal stomatal regulation under these conditions could be valuable resources for breeding programmes aimed at enhancing drought tolerance and water-use efficiency without compromising productivity (González *et al.*, 2019; Vadez *et al.*, 2024). In this experiment, the search for differences in stomatal regulation under stress was performed by deconstructing drought tolerance into simpler components, including CTD as a high throughput proxy of transpiration. A key objective was thus to assess whether CTD differences between parental lines (LTR and wild genotypes) and progeny lines (BC2F3 lines) within the same family aligned with variations observed in time-integrated traits like biomass accumulation and WUE.

Data collected across multiple time points revealed that 199_BC2F3_2 line consistently exhibited lower CTD values under both irrigated and drought conditions (Figure 6.6). Despite the absence of statistically significant differences in CTD at the point of maximum difference of SWC between treatment groups (43 DAS), this sustained low CTD observed throughout the experiment could suggest a low basal transpiration relative to the rest of the lines, including those from other family groups. Low basal transpiration is indicative of water conservation as a drought avoidance mechanism expressed under favourable conditions, which is often related to reduced biomass accumulation. Interestingly, DW biomass of 199_BC2F3_2 showed no significant differences compared to LTR, and was significantly higher than 199_Wild and 199_BC2F2_1 under both irrigated and drought conditions (Figure 6.6).

6.4.7 Low CTD did not translate into biomass declines

The lower CTD values and similar biomass of 199_BC2F3_2 compared to LTR suggests high transpiration efficiency (TE)— the instantaneous exchange of water for carbon dioxide through stomata. However, the apparent high TE advantage was not translated into high WUE when calculated as DW divided by total water supplied during the experiment. Instead, WUE of 199_BC2F3_2 was similar to 199_BC2F3_1, 199_Wild, and LTR, which implies that the reduced transpiration observed in CTD measurements did not translate into measurable improvements in a time-integrated trait such as WUE. On the other hand, the higher CTD values observed in the rest of the lines, indicative of high transpiration and fewer stomatal limitations to carbon assimilation (Vialet-Chabrand *et al.*, 2021), did not confer any advantage in DW accumulation by the end of the experiment.

The sustained low CTD values observed in 199_BC2F3_2, coupled with no significant reductions in DW biomass, point to potential physiological adaptations that balance water conservation with carbon assimilation. Reduced stomatal density could be a key factor, as fewer stomata would limit transpiration rates and contribute to lower CTD while maintaining sufficient photosynthetic capacity for biomass production (Hughes *et al.*, 2017). Additionally, non-photochemical quenching (NPQ) mechanisms, which dissipate excess light energy as heat, may have played a role in elevating leaf temperatures and thereby lowering CTD (Trojak & Skowron, 2023; Murakami *et al.*, 2024). These adaptations, while advantageous in conserving water under drought conditions, may not necessarily translate into higher water use efficiency (WUE) over the experiment's duration. However, another plausible explanation is that low transpiration of 199_BC2F3_2, as indicated by low CTD values, occurred only during the periods of data collection, rather than being consistently maintained throughout the entire experiment.

6.4.8 Temperature-sensitive vs temperature-insensitive responses

The observed low CTD values of 199_BC2F3_2 during data collection could be attributed to two potential response mechanisms. First, high temperatures during phenotyping may have activated specific thermosensitive pathways in 199_BC2F3_2, resulting in stomatal closure and consequently reduced CTD values. Alternatively, other lines may have exhibited thermosensitive responses that actively promoted stomatal opening under elevated temperatures, contrasting with the response observed in 199_BC2F3_2. These differing physiological mechanisms likely contributed to the variation in CTD across lines while maintaining comparable WUE and biomass outcomes. In this experiment, ambient temperatures ranged between 33°C and 43°C during CTD acquisition. These are similar temperatures to those used by Xu *et al.* (2024) for testing differences in stomatal responses to high temperatures in *Arabidopsis thaliana*. These high temperatures were

an unintended result from the lack of active cooling to accurately regulate glasshouse temperature during data collection.

Mechanisms coordinating stomatal conductance (SC) in response to environmental stimuli, which may explain the observed results in this experiment, likely involve phototropins (PHOT) and the high-temperature-associated kinase TARGET OF TEMPERATURE 3 (TOT3). PHOT are responsible for mediating blue-light perception signals, while TOT3 regulates plasma membrane H^+-ATPase activity, both of which play key roles in inducing stomatal aperture and adjusting stomatal conductance in response to changing environmental conditions (Driesen *et al.*, 2020; Kostaki *et al.*, 2020; Xu *et al.*, 2024). ABA-mediated signalling pathways, activated under drought conditions sensed by the roots, regulate ion channels to induce stomatal closure (Xu *et al.*, 2024). OPEN STOMATA 1 (OST1), is a SnRK2 protein expressed in guard cells and a positive regulator of ABA signal transduction. OST1 inactivates stomatal opening signalling pathway mediated by TOT3 (Xu *et al.*, 2024). As no mechanisms have been identified that directly induce stomatal closure in response to light and temperature, it is possible that most lines opened stomata in response to these stimuli, whereas line 199_BC2F3_2 may have exhibited insensitivity to temperature-induced stomatal opening, potentially contributing to its observed lower CTD values during data collection. However, this is speculative and further investigation is needed to confirm the underlying mechanisms. Future studies could involve evaluating the expression of temperature and light-responsive genes, such as TOT3 and PHOT, along with ABA-mediated signalling components like OST1, to determine their relative contribution to stomatal conductance regulation in these lines. Additionally, detailed phenotyping of stomatal dynamics under controlled light, temperature, and drought conditions would help validate these hypotheses.

6.5 Conclusion

This study provides the first evidence of *de novo* domestication as an effective approach for retaining genetically complex traits, such as chlorophyll and flavonoids content, from wild relatives. However, the successful retention of these traits directly depends on their genetic architecture, which are likely influenced not only by major additive genetic effects but also by dominance and epistatic interactions.

Photoprotective adaptations, such as chlorophyll fluorescence and flavonoid content for energy dissipation, may play a major role in data variability under highly controlled water conditions. While dry weight (DW) is a key time-integrated trait, and often one the most important performance metrics for agronomic success after grain yield, its reduced influence compared to photoprotective mechanisms as the primary drivers of variability in this experiment highlights

significant genetic diversity in these traits that could be leveraged in breeding programmes. Notably, these variations only become apparent when water content is carefully regulated in all experimental units across irrigation treatments, eliminating the confounding effects of cumulative water depletion, and allowing other physiological differences to emerge.

A candidate *de novo*-domesticated pre-breeding line (199_BC2F3_2) exhibiting potential adaptive strategies advantageous for limited-water environments was identified. Observed from its consistently low canopy temperature depression (CTD) throughout the experiment and comparable dry weight biomass to the La Trobe cultivar, the combined analysis of these phenotypic responses are indicative of physiological adaptations that optimise water use while sustaining biomass productivity. However, further research is essential to elucidate the physiological, molecular and genetic basis of the observed phenotypic responses of line 199_BC2F3_2.

Lastly, the absence of significant differences in water use efficiency (WUE) across genotypes and the non-significant correlations with CTD at different time points underscores the need for integrated approaches that incorporate both instantaneous and time-integrated traits to comprehensively characterise drought adaptation mechanisms.

Chapter 7
General discussion

7.1 Research background and overview

Evidence indicates that wild relatives of cultivated barley may offer adaptive mechanisms to improve drought tolerance in breeding programs (Pham *et al.*, 2019; Barati *et al.*, 2020). *De novo* domestication seeks to utilise these traits while removing unfavourable ones, but retaining quantitative stress response traits remains largely untested. The quantitative nature of drought responses and significant genotype-by-environment interactions hinder the effective use of these mechanisms, suggesting that single-gene transfers may not suffice. To enhance germplasm evaluation, understanding the physiological and molecular bases of drought tolerance is crucial, prioritising traits that improve performance under stress without compromising yields in favourable conditions (Vadez *et al.*, 2024). Current practices rely heavily on genomic and ecological data, often neglecting thorough phenotypic evaluations.

This study established a structured framework for germplasm evaluation, integrating high-throughput hyperspectral and thermal imaging to develop a novel image-based Transpiration Efficiency (iTE) parameter for field exploration of drought-tolerant resources. In addition, a combination of trait responses was proposed and used in a drought experiment under controlled glasshouse conditions to identify phenotypic patterns relevant for breeding and molecular studies. Machine learning clustering algorithms were applied to enable unbiased selections, identifying representative candidates from each cluster while also defining hypothetical ideal candidates based on optimal phenotypic values across multiple traits. This selection strategy facilitated a systematic approach to identifying superior germplasm for mechanistic and pre-breeding research. Following this, molecular markers were developed and applied in marker-assisted backcrossing (MABC) to introgress domestication traits into multiple wild backgrounds. The resulting *de novo*-domesticated lines were then evaluated in a phenotyping experiment alongside their wild and cultivated progenitors to assess the effects of *de novo* domestication on quantitative traits.

7.2 Genotypic vs phenotypic diversity

In the absence of tailored phenotyping methodologies for drought tolerance suited for wild relatives, there appears to be an over-reliance on genetic diversity metrics derived from genomic data, passport information, and ecological data for guiding the selection of subsets of wild

germplasm for breeding and molecular studies (McCouch *et al.*, 2013; Langridge & Waugh, 2019; Stenberg & Ortiz, 2021). While these tools aim to maximise the diversity captured within subsets of genotypes, the results in this study show a substantial gap between the genetic diversity captured and its translation into phenotypic diversity. This discrepancy between genetic and phenotypic diversity was evidenced by the low correlation between genetic and phenotypic dissimilarity matrices (Figure 4.5), which show that genetic diversity did not consistently translate into phenotypic variation despite the high narrow-sense (h^2) heritability of most traits. These findings highlight the need to clearly differentiate between "genetic diversity" and "phenotypic diversity", concepts that are often used interchangeably in the scientific community. Ultimately, the goal is to leverage mechanisms of tolerance through measurable traits rather than merely relying on genetic variation.

7.3 A structured framework for wild germplasms evaluations

This study bridged the breeders' perspective for germplasm selection and evaluation practices with the more controlled, trait-specific approaches used by physiologists and molecular biologists. Imaging technologies served as the platform for this integration, using specific physiological mechanisms relevant to crop improvement to guide the exploration of phenotypic diversity and the selection of wild relatives. Notably, the focus was not on conclusively proving that genotypes exhibited a specific tolerance mechanism but rather on providing a starting point and an indication that a potential trait of interest was present within the population. Nonetheless, detailed physiological studies are needed to validate and confirm these findings (Figure 7.1).

The study demonstrated that while CTD is strongly correlated with instantaneous transpiration rates (Figure 3.5), different levels of CTD do not always translate into biomass declines or predictions of WUE by the end of the experiment. Reduced stomatal density, stomatal sensitivity to light and temperature, and low residual transpiration are drought avoidance traits that help explain the low CTD of *de novo* domesticated line 199_BC2F3_2 and insignificant biomass loss compared to its cultivated parent, La Trobe. However, complementary (high-throughput) measurements, like stomatal counts and residual transpiration assessments, would further clarify underlying physiological mechanisms and enhance thermal data interpretation (Hasanuzzaman *et al.*, 2023a; Pathoumthong *et al.*, 2023). While these traits have been extensively studied at the physiological and molecular levels (Hasanuzzaman *et al.*, 2023a; Xu *et al.*, 2024), their application in large-scale screening for drought tolerance remains to be exploited. Applied to large-scale screening experiments, these recently developed techniques will strengthen the selection of wild candidates and improve germplasm explorations.

Glasshouse phenotyping experiments in this study incorporated a time dimension component with a special emphasis on lines that reduced stomatal conductance faster than others to avoid water depletion. The was justified based on the tendency of drought stress to intensify under conditions of elevated temperatures and high radiation (Wang *et al.*, 2020; Vialet-Chabrand *et al.*, 2021). However, studies on transgenic drought-tolerant wheat challenge this approach, advocating instead for lines that maintain stomatal conductance unchanged (González *et al.*, 2019; Gupta, 2024). This perspective stems from agricultural systems facing moderate to mild droughts more frequently than severe ones. Mild drought conditions significantly affect crop production by inducing stomatal limitations on carbon assimilation, as plants naturally reduce stomatal opening in response to water deficits without necessarily experiencing physiological decline. This breeding approach maximises water use. While in some cases this may lead to water depletion and potential crop failure, in most current agricultural scenarios it is beneficial and unlikely to compromise long-term crop performance (Blum, 2009; Vadez *et al.*, 2024).

With climate change, extreme droughts are expected to become more frequent and severe, potentially becoming the norm (Naumann *et al.*, 2018). Under these conditions, selection strategies that prioritise rapid stomatal closure and water conservation early in the season will become increasingly critical for developing drought-tolerant crops adapted to harsher climates. To fully harness this latter breeding approach, however, it is crucial to complement prompt stomatal closure with mechanisms that protect photosynthetic capacity under high canopy temperatures (Chapter 2).

Notably, this lack of consensus regarding selection criteria early in pre-breeding research highlights the importance of employing unbiased clustering methods based on the entire phenotypic space as undertaken in Chapter 4. This unbiased selection is also intended to avoid assuming that all other factors remain constant when looking for either fast or delayed changes in stomatal conductance, which is never the case. Ensuring a diverse selection of genotypes avoids the risk of narrowing the breeding pool to a small number of stress tolerance mechanisms.

7.4 Towards elucidating the genetic basis of iTE index under drought

The iTE index proposed in this study demonstrates the successful integration of thermal and high-throughput imaging techniques to improve the identification of drought-tolerant wheat varieties under field conditions (Chapter 2). Measuring iTE at the vegetative stage can predict yield declines later in the season, and this merits further investigation to unravel the genetic and physiological basis of iTE.

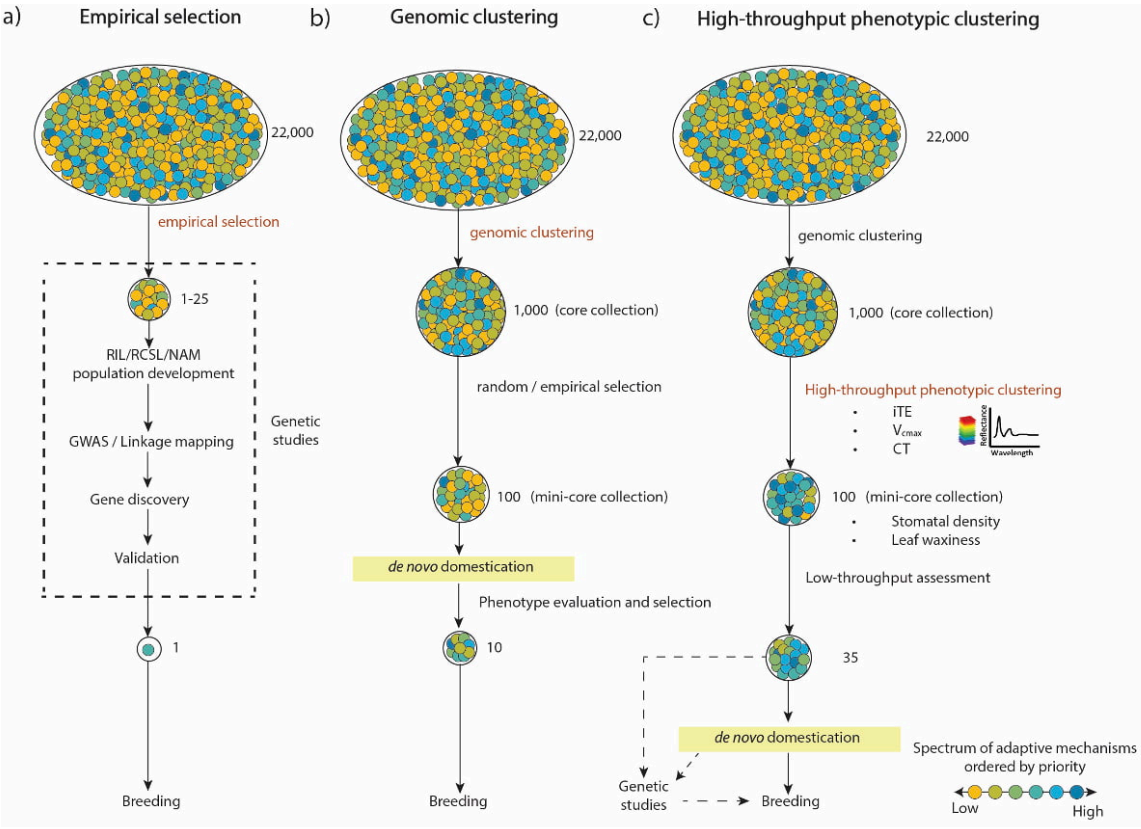

Figure 7.1. Evolution of germplasm evaluation and selection strategies in pre-breeding research. a) Traditional selection based on empirical observations does not ensure optimal genotype capture; b) Advances in bioinformatics enable core collections based on genetic diversity metrics based on genomic data. However, due to large collection sizes, smaller subsets for *de novo* domestication are required. Current methods for mini-core collection assembly, often random or empirical, lack precision and risk overlooking valuable adaptive traits; c) The proposed method uses high-throughput phenotyping via imaging to construct mini-core collections, increasing the chance of identifying genotypes with priority traits for *de novo* domestication, such as sustained carbon fixation under drought stress.

I hypothesise that the rapid depletion of soil moisture during short periods of no rainfall, especially under high VPD conditions, severely disrupted reactive oxygen species (ROS) homeostasis and led to irreversible photodamage (Phua *et al.*, 2021), from which the plants could not recover. Therefore, the identification of genetic factors underlying iTE may be constrained by the occurrence and severity of short and acute field drought conditions at a specific phenological stage of the plant. Barley populations with available genotypic data are ideal for Marker-trait association studies, including linkage mapping and genome-wide association studies (GWAS)which could be used to identify genetic loci linked to phenotypic variation in iTE.

7.5 More severe drought stress for maximising genotypic differences in tolerance traits

Soil water content in glasshouse experiments were carefully controlled to maintain uniform drying rates, ensuring that CTD reflected only the plant physiology rather than soil moisture levels. The overall drying rates for the trial had to be adjusted to compensate for the slow drying rates of certain genotypes due to smaller plant size or narrower leaves. As a result, the intensity and duration of drought stress may have been insufficient, as frequent watering was required for higher-transpiring genotypes. Future experiments could explore the combination of polyethylene glycol (PEG) and controlled water depletion rates to impose a more rapid and severe drought stress to ensure differences in plant health declines.

7.6 A high-precision thermal imaging platform

This study supports the development of large-scale phenotyping platforms capable of capturing high-resolution thermal images multiple times daily with the precision needed to detect genotypic differences in CTD contrasts. While multipurpose phenotyping platforms exist, none are specifically designed to detect changes in transpiration pattern with the precision needed for CTD-based genetic studies (Tardieu *et al.*, 2017). Laboratory protocols can measure small, time-dependent stomatal conductance changes under controlled conditions (Xu *et al.*, 2024), but they are small-scale, inaccessible to breeders, and lack agronomic relevance for large-scale germplasm screening.

While CTD showed a strong empirical relationship with stomatal conductance (Figure 3.5), the low precision hindered the identification of genotypic differences with high confidence. Statistical interactions among time (days after sowing), genotype, and treatment were consistently non-significant across all three phenotyping experiments. As a result, the hypothesised ability of certain lines to close their stomata earlier in development could not be inferred or validated using CTD measurements. This absence of significant interactions between DAS (days after sowing), genotype, and treatment factors likely reflects limitations in the thermal imaging phenotyping platform rather than a lack of true genotypic differences observed in other studies (Xu *et al.*, 2024). As the instantaneous balance between incoming and outgoing energy fluxes (Gutschick, 2016), CTD was highly influenced by ambient temperature and incoming radiation under the tested conditions. Fluctuations in ambient temperature increased the phenotypic variation captured by the thermal camera, potentially reducing statistical power for detecting significant genotypic differences (Falconer & Mackay, 1996).

To improve precision, phenotyping platforms should integrate thermal sensors and ambient temperature probes capable of detecting temperature variations as small as 0.1±0.01°C. Additionally, these platforms should monitor spatial variability and track temporal changes throughout plant development to capture CTD dynamic responses to environmental fluctuations. Minimising the unintended environmental variations, such as ambient temperature and light, would improve repeatability and establish a controlled framework for developing mechanistic or empirical models to translate CTD (°C) into stomatal conductance (mol H_2O $m^{-2}s^{-1}$).

Capturing thermal images multiple times per day throughout the plant's lifecycle, as required to analyse CTD dynamics in response to water depletion and other environmental factors over time, significantly increases data volume and complexity. Thermal imaging, in particular, presents unique challenges due to the use of a single (broad) spectral band of low resolution in the long-wave infrared (LWIR) range (8–14 μm). This limitation complicates automatic background removal and segmentation, particularly in pot experiments where poor contrast between vegetation and background is common. Computer vision techniques could help overcome this challenge and enhance efficient image processing (Tardieu *et al.*, 2017).

Addressing these constraints would enable the development of large-scale, highly controlled experiments capable of identifying key stomatal traits in wild and cultivated populations with greater precision and accuracy. Implementing a high-precision thermal imaging platform would allow for the identification of accessions with reduced sensitivity to light and temperature fluctuations—traits associated with stomatal regulation mechanisms that mitigate water loss under high vapor pressure deficit (VPD) conditions. Ultimately, a systematic approach for the routine exploration of these mechanisms would reduce the reliance on serendipitous discoveries and the dependence on genetic diversity metrics to select wild relatives (Langridge & Waugh, 2019).

7.7 Optimising *de novo* domestication

This study has demonstrated that *de novo* domestication can successfully preserve quantitative traits from wild relatives. This was more evident in spectrally-derived pigment traits like chlorophyll and flavonoid content (Figure 6.13). However, this outcome was not consistent across all measured variables. Notably, in traits such as dry weight (DW), some *de novo*-domesticated lines continued to exhibit cultivated phenotypes even after three hybridisation cycles with wild lines as the recurrent parent (Figure 6.6), suggesting that certain wild phenotypes are more challenging to retain than others. This may be attributed to genetic dominance, epistatic interactions, or the influence of major genes from the cultivated parent, which could override the

expression of wild traits despite repeated backcrossing. In addition to these factors, the extent to which specific quantitative traits are retained depended on the genetic architecture, the number of backcross cycles, the number of genes introgressed and the number of self-pollination events to achieve high levels of homozygosity. This highlights the importance of implementing additional screening steps before conducting *de novo*-domestication to maximise the successful retention of key tolerance mechanisms through refined selection criteria, as outlined in Chapters 2 and Chapter 4. Without such targeted selection, large-scale *de novo* domestication efforts risk expending significant resources on wild lines that may ultimately lack both agronomic value and relevance for in-depth physiological and genetic studies. Future research should focus on optimising *de novo* domestication strategies to enhance efficiency, with an emphasis on integrating gene editing technologies to accelerate the process and improve trait retention.

Unlike marker-assisted backcrossing (MABC), which relies on recombination and selection over multiple generations, gene-editing multiplex platforms could facilitate a more direct path to domestication by inducing loss-of-function mutations in several domestication genes simultaneously (Yu *et al.*, 2021). This would be particularly advantageous for genomic regions with low recombination (King *et al.*, 2007; Neeraja *et al.*, 2007; Zsögön *et al.*, 2018). However, the feasibility of gene-editing for *de novo* domestication relies on prior knowledge of the underlying genes controlling domestication traits. While some domestication genes have been well-characterised, others, such as the *Thresh1* locus associated with grain threshability (Schmalenbach *et al.*, 2011), have only been mapped as QTLs. Precise gene-editing for every domestication trait will become possible as these loci are characterised at the gene level. Additionally, gene-editing technologies could see broader application in crop improvement programs as regulatory frameworks evolve to fully realise their potential (Palmgren *et al.*, 2015). In the meantime, MABC remains the more practical approach for advancing *de novo*-domesticated lines towards commercial viability.

References

Abdolshahi R, Nazari M, Safarian A, Sadathossini TS, Salarpour M, Amiri H. 2015. Integrated selection criteria for drought tolerance in wheat (*Triticum aestivum L.*) breeding programs using discriminant analysis. *Field Crops Research* **174**: 20-29.

Adam D. 2021. How far will global population rise? Researchers can't agree. *Nature: International weekly journal of science* **597**(7877): 462-465.

Agati G, Azzarello E, Pollastri S, Tattini M. 2012. Flavonoids as antioxidants in plants: location and functional significance. *Plant Science* **196**: 67-76.

Agre P, Asibe F, Darkwa K, Edemodu A, Bauchet G, Asiedu R, Adebola P, Asfaw A. 2019. Phenotypic and molecular assessment of genetic structure and diversity in a panel of winged yam (Dioscorea alata) clones and cultivars. *Scientific Reports* **9**(1).

Agurla S, Gahir S, Munemasa S, Murata Y, Raghavendra AS 2018. Mechanism of Stomatal Closure in Plants Exposed to Drought and Cold Stress. In: Iwaya-Inoue M, Sakurai M, Uemura M eds. *Survival Strategies in Extreme Cold and Desiccation: Adaptation Mechanisms and Their Applications*. Singapore: Springer Singapore, 215-232.

Al Abdallat AM, Ayad JY, Abu Elenein JM, Al Ajlouni Z, Harwood WA. 2014. Overexpression of the transcription factor *HvSNAC1* improves drought tolerance in barley (*Hordeum vulgare* L.). *Molecular breeding* **33**(2): 401-414.

Ali F, Kanwal N, Ahsan M, Ali Q, Bibi I, Niazi NK. 2015. Multivariate analysis of grain yield and its attributing traits in different maize hybrids grown under heat and drought stress. *Scientifica* **2015**(1): 563869.

Aliniaeifard S, van Meeteren U. 2014. Natural variation in stomatal response to closing stimuli among *Arabidopsis thaliana* accessions after exposure to low VPD as a tool to recognize the mechanism of disturbed stomatal functioning. *Journal of Experimental Botany* **65**(22): 6529-6542.

Amiri M, Abolhasan M, Shariati N, Lipman J. 2021. Soil moisture remote sensing using SIW cavity based metamaterial perfect absorber. *Scientific Reports* **11**(1): 1-17.

An N, Tang C-S, Xu S-K, Gong X-P, Shi B, Inyang HI. 2018. Effects of soil characteristics on moisture evaporation. *Engineering geology* **239**: 126-135.

Andrade-Sanchez P, Gore MA, Heun JT, Thorp KR, Carmo-Silva AE, French AN, Salvucci ME, White JW. 2013. Development and evaluation of a field-based high-throughput phenotyping platform. *Functional Plant Biology* **41**(1): 68-79.

Araus JL, Kefauver SC, Zaman-Allah M, Olsen MS, Cairns JE. 2018. Translating High-Throughput Phenotyping into Genetic Gain. *Trends in Plant Science* **23**(5): 451-466.

Bacon M, ed. 2004. *Water use efficiency in plant biology*. Biological Sciences. Oxford, UK: Blackwell.

Baker NR, Rosenqvist E. 2004. Applications of chlorophyll fluorescence can improve crop production strategies: an examination of future possibilities. *Journal of Experimental Botany* **55**(403): 1607-1621.

Ballabio C, Sterlacchini S. 2012. Support vector machines for landslide susceptibility mapping: the Staffora River Basin case study, Italy. *Mathematical geosciences* **44**: 47-70.

Bao X, Hou X, Duan W, Yin B, Ren J, Wang Y, Liu X, Gu L, Zhen W. 2023. Screening and evaluation of drought resistance traits of winter wheat in the North China Plain. *FRONTIERS IN PLANT SCIENCE* **14**.

Barati M, Majidi MM, Pirnajmedin F, Mirlohi A, Sarfaraz D, Osivand A. 2020. Drought Tolerance in Cultivated and Wild Barley Genotypes: The Role of Root System Characteristics. *JOURNAL OF AGRICULTURAL SCIENCE AND TECHNOLOGY* **22**(5): 1359-1370.

Bates D, Mächler M, Bolker B, Walker S. 2015. Fitting Linear Mixed-Effects Models Using lme4. *Journal of Statistical Software* **67**(1): 1 - 48.

Bazzaz MM, Khaliq QA, Karim MA, Al-Mahmud A, Khan MSA. 2015. Canopy temperature and yield based selection of wheat genotypes for water deficit environment. *Open Access Library Journal* **2**(10): 1-11.

Benjamini Y, Yekutieli D. 2001. The control of the false discovery rate in multiple testing under dependency. *The Annals of Statistics* **29**(4): 1165-1188, 1124.

Bennani, Nsarellah, Jlibene, Tadesse, Birouk, Ouabbou. 2017. Efficiency of drought tolerance indices under different stress severities for bread wheat selection. *Australian Journal of Crop Science* **11**(4): 395-iii.

Bernardo R. 2016. Genomewide predictions for backcrossing a quantitative trait from an exotic to an adapted line. *Crop science* **56**(3): 1067-1075.

Bertolino LT, Caine RS, Gray JE. 2019. Impact of Stomatal Density and Morphology on Water-Use Efficiency in a Changing World. *Frontiers in Plant Science* **10**: 1-11.

Bivand RS, Wong DWS. 2018. Comparing implementations of global and local indicators of spatial association. *TEST* **27**(3): 716-748.

Blashfield RK. 1976. Mixture model tests of cluster analysis: Accuracy of four agglomerative hierarchical methods. *Psychological Bulletin* **83**(3): 377-388.

Blum A. 2009. Effective use of water (EUW) and not water-use efficiency (WUE) is the target of crop yield improvement under drought stress. *Field Crops Research* **112**(2): 119-123.

Bose J, Rodrigo-Moreno A, Shabala S. 2014. ROS homeostasis in halophytes in the context of salinity stress tolerance. *Journal of Experimental Botany* **65**: 1241-1257.

Busch FA, Ainsworth EA, Amtmann A, Cavanagh AP, Driever SM, Ferguson JN, Kromdijk J, Lawson T, Leakey AD, Matthews JS. 2024. A guide to photosynthetic gas exchange measurements: Fundamental principles, best practice and potential pitfalls. *Plant, Cell & Environment*.

Cai K, Chen X, Han Z, Wu X, Zhang S, Li Q, Nazir MM, Zhang G, Zeng F. 2020. Screening of Worldwide Barley Collection for Drought Tolerance: The Assessment of Various Physiological Measures as the Selection Criteria. **11**(1159).

Camino C, Gonzalez-Dugo V, Hernandez P, Zarco-Tejada PJ. 2019. Radiative transfer Vcmax estimation from hyperspectral imagery and SIF retrievals to assess photosynthetic performance in rainfed and irrigated plant phenotyping trials. *Remote Sensing of Environment* **231**: 1-15.

Cartelat A, Cerovic ZG, Goulas Y, Meyer S, Lelarge C, Prioul JL, Barbottin A, Jeuffroy HM, Gate P, Agati G. 2005. Optically assessed contents of leaf polyphenolics and chlorophyll as indicators of nitrogen deficiency in wheat (Triticum aestivum L.). *Field Crops Research* **91**(1 p.35-49): 49-35.

Celestina C, Hunt J, Brown H, Huth N, Andreucci M, Hochman Z, Bloomfield MH, Porker K, McCallum M, Harris F, et al. 2023. Scales of development for wheat and barley specific to either single culms or a population of culms. *European Journal of Agronomy* **147**.

Cerovic ZG, Masdoumier G, Ghozlen NB, Latouche G. 2012. A new optical leaf-clip meter for simultaneous non-destructive assessment of leaf chlorophyll and epidermal flavonoids. *Physiologia plantarum* **146**(3 p.251-260): 260-251.

Condon A, Richards R. 1992. Broad sense heritability and genotype x environment interaction for carbon isotope discrimination in field-grown wheat. *Australian Journal of Agricultural Research* **43**(5): 921-934.

Condon AG, Richards RA, Rebetzke GJ, Farquhar GD. 2002. Improving Intrinsic Water-Use Efficiency and Crop Yield. *Crop Science* **42**(1): 122-131.

Crain J, Reynolds M, Poland J. 2017. Utilizing High-Throughput Phenotypic Data for Improved Phenotypic Selection of Stress-Adaptive Traits in Wheat. *Crop science* **57**(2 p.648-659): 659-648.

Crossa J, Montesinos-López OA, Pérez-Rodríguez P, Costa-Neto G, Fritsche-Neto R, Ortiz R, Martini JWR, Lillemo M, Montesinos-López A, Jarquin D, et al. 2022. Genome and Environment Based Prediction Models and Methods of Complex Traits Incorporating Genotype × Environment Interaction. In: Ahmadi N, Bartholomé J eds. *Prediction of Complex Traits Methods and Protocols*: Springer, 245-283.

Darkwa K, Agre P, Olasanmi B, Iseki K, Matsumoto R, Powell A, Bauchet G, De Koeyer D, Muranaka S, Adebola P, et al. 2020. Comparative assessment of genetic diversity matrices and clustering methods in white Guinea yam (Dioscorea rotundata) based on morphological and molecular markers. *Scientific Reports* **10**(1): 13191.

Das S, Christopher J, Apan A, Roy Choudhury M, Chapman S, Menzies NW, Dang YP. 2021. UAV-Thermal imaging and agglomerative hierarchical clustering techniques to evaluate and rank physiological performance of wheat genotypes on sodic soil. *ISPRS Journal of Photogrammetry and Remote Sensing* **173**: 221-237.

Dechant B, Cuntz M, Vohland M, Schulz E, Doktor D. 2017. Estimation of photosynthesis traits from leaf reflectance spectra: Correlation to nitrogen content as the dominant mechanism. *Remote Sensing of Environment* **196**: 279-292.

Deery DM, Rebetzke GJ, Jimenez-Berni JA, James RA, Condon AG, Bovill WD, Hutchinson P, Scarrow J, Davy R, Furbank RT. 2016. Methodology for High-Throughput Field Phenotyping of Canopy Temperature Using Airborne Thermography. *Frontiers in Plant Science* **7**: 1-13.

Demidchik V. 2015. Mechanisms of oxidative stress in plants: From classical chemistry to cell biology. *Environmental and Experimental Botany* **109**: 212-228.

DeWitt N, Lyerly J, Guedira M, Holland JB, Murphy JP, Ward BP, Boyles RE, Mergoum M, Babar MA, Shakiba E, et al. 2023. Bearded or smooth? Awns improve yield when wheat experiences heat stress during grain fill in the southeastern United States. *Journal of Experimental Botany* **74**(21): 6749-6759.

Doebley JF, Gaut BS, Smith BD. 2006. The Molecular Genetics of Crop Domestication. *Cell* **127**(7): 1309-1321.

Driesen E, Van den Ende W, De Proft M, Saeys W. 2020. Influence of environmental factors light, CO2, temperature, and relative humidity on stomatal opening and development: A review. *Agronomy* **10**(12): 1975.

Duursma RA. 2015. Plantecophys-an R package for analysing and modelling leaf gas exchange data. *PLoS ONE* **10**(11): e0143346.

Elston RC, Stewart J. 1973. THE ANALYSIS OF QUANTITATIVE TRAITS FOR SIMPLE GENETIC MODELS FROM PARENTAL, F1 AND BACKCROSS DATA. *Genetics* **73**(4): 695-711.

Falconer DS, Mackay TFC. 1996. *Introduction to quantitative genetics*: Longman.

Farquhar GD, Richards RA. 1984. Isotopic Composition of Plant Carbon Correlates With Water-Use Efficiency of Wheat Genotypes. *Functional Plant Biology* **11**(6): 539-552.

Farquhar GD, von Caemmerer S, Berry JA. 1980. A biochemical model of photosynthetic CO_2 assimilation in leaves of C_3 species. *Planta* **149**(1): 78-90.

Fernie AR, Yan J. 2019. De Novo Domestication: An Alternative Route toward New Crops for the Future. *Molecular Plant* **12**(5): 615-631.

Ferreyra MLF, Serra P, Casati P. 2021. Recent advances on the roles of flavonoids as plant protective molecules after UV and high light exposure. *Physiologia plantarum* **173**(3): 736-749.

Flexas J. 2008. Diffusive and Metabolic Limitations to Photosynthesis under Drought and Salinity in C3 Plants. *Plant Biology* **6**(3): 269-279.

Flohr BM, Hunt JR, Kirkegaard JA, Evans JR, Swan A, Rheinheimer B. 2018. Genetic gains in NSW wheat cultivars from 1901 to 2014 as revealed from synchronous flowering during the optimum period. *European Journal of Agronomy* **98**: 1-13.

French RJ, Schultz JE. 1984. Water use efficiency of wheat in a Mediterranean-type environment. I. The relation between yield, water use and climate. *Australian Journal of Agricultural Research* **35**(6): 743-764.

Gálvez S, Mérida-García R, Camino C, Borrill P, Abrouk M, Ramírez-González RH, Biyiklioglu S, Amil-Ruiz F, Dorado G, Budak H, et al. 2019. Hotspots in the genomic architecture of field drought responses in wheat as breeding targets. *Functional & Integrative Genomics* **19**(2): 295-309.

González FG, Capella M, Ribichich KF, Curín F, Giacomelli JI, Ayala F, Watson G, Otegui ME, Chan RL. 2019. Field-grown transgenic wheat expressing the sunflower gene HaHB4 significantly outyields the wild type. *Journal of Experimental Botany* **70**(5): 1669-1681.

Gonzalez-Dugo V, Lopez-Lopez M, Espadafor M, Orgaz F, Testi L, Zarco-Tejada P, Lorite IJ, Fereres E. 2019. Transpiration from canopy temperature: Implications for the assessment of crop yield in almond orchards. *European Journal of Agronomy* **105**: 78-85.

Gould A. 2022. *Taming wild barley: expanding crop genetic diversity with beneficial traits for agriculture.* Honours, The University of Melbourne Victoria, Australia.

Grant OM, Chaves MM, Jones HG. 2006. Optimizing thermal imaging as a technique for detecting stomatal closure induced by drought stress under greenhouse conditions. *Physiologia plantarum* **127**(3 p.507-518): 518-507.

Gregersen PL, Culetic A, Boschian L, Krupinska K. 2013. Plant senescence and crop productivity. *Plant Molecular Biology* **82**(6): 603-622.

Grossiord C, Buckley TN, Cernusak LA, Novick KA, Poulter B, Siegwolf RT, Sperry JS, McDowell NG. 2020. Plant responses to rising vapor pressure deficit. *new phytologist* **226**(6): 1550-1566.

Guadarrama-Escobar LM, Hunt J, Gurung A, Zarco-Tejada PJ, Shabala S, Camino C, Hernandez P, Pourkheirandish M. 2024. Back to the future for drought tolerance. *new phytologist* **242**(2 p.372-383): 383-372.

Gupta PK. 2024. Drought-tolerant transgenic wheat HB4®: a hope for the future. *Trends in Biotechnology* **42**(7): 807-809.

Gutschick VP. 2016. Leaf energy balance: basics, and modeling from leaves to canopies. *Canopy photosynthesis: From basics to applications*: 23-58.

Haas M, Schreiber M, Mascher M. 2019. Domestication and crop evolution of wheat and barley: Genes, genomics, and future directions. *Journal of integrative plant biology* **61**(3 p.204-225): 225-204.

Hanak T, Janjić J, Hay FR, Brinch-Pedersen H. 2023. Genome editing to re-domesticate and accelerate use of barley crop wild relatives. *Frontiers in Sustainable Food Systems* **7**: 1331577.

Handley LL, Nevo E, Raven JA, Martínez-Carrasco R, Scrimgeour CM, Pakniyat H, Forster BP 1994. Chromosome 4 controls potential water use efficiency ($\delta^{13}C$) in barley. *Journal of Experimental Botany*. 1661-1663.

Hasanuzzaman M, Bhuyan MB, Parvin K, Bhuiyan TF, Anee TI, Nahar K, Hossen MS, Zulfiqar F, Alam MM, Fujita M. 2020. Regulation of ROS metabolism in plants under environmental stress: A review of recent experimental evidence. *INTERNATIONAL JOURNAL OF MOLECULAR SCIENCES* **21**(22): 8695.

Hasanuzzaman M, Chakraborty K, Zhou M, Shabala S. 2023a. Measuring residual transpiration in plants: a comparative analysis of different methods. *Functional Plant Biology* **50**(12): 983-992.

Hasanuzzaman M, Shabala L, Brodribb TJ, Zhou M, Shabala S. 2017. Assessing the suitability of various screening methods as a proxy for drought tolerance in barley. *Functional Plant Biology* **44**(2 p.253-266): 266-253.

Hasanuzzaman M, Zhou M, Shabala S. 2023b. How Does Stomatal Density and Residual Transpiration Contribute to Osmotic Stress Tolerance? *Plants* **12**(3): 1-19.

Havrlentová M, Kraic J, Gregusová V, Kovácsová B. 2021. Drought Stress in Cereals – A Review. *Agriculture (Pol'nohospodárstvo)* **67**(2): 47-60.

He X, Zeng J, Cao F, Ahmed Imrul M, Zhang G, Vincze E, Wu F. 2015. *HvEXPB7* , a novel β-expansin gene revealed by the root hair transcriptome of Tibetan wild barley, improves root hair growth under drought stress. *Journal of Experimental Botany* **66**(22): 7405-7419.

Hepworth C, Doheny-Adams T, Hunt L, D. Cameron D, E. Gray J. 2015. Manipulating stomatal density enhances drought tolerance without deleterious effect on nutrient uptake. *New Phytologist* **208**: 336-341.

Honsdorf N, March TJ, Berger B, Tester M, Pillen K. 2014. High-Throughput Phenotyping to Detect Drought Tolerance QTL in Wild Barley Introgression Lines. *PLoS ONE* **9**(5): 1-13.

Hughes J, Hepworth C, Dutton C, Dunn Jessica A, Hunt L, Stephens J, Waugh R, Cameron Duncan D, Gray Julie E. 2017. Reducing Stomatal Density in Barley Improves Drought Tolerance without Impacting on Yield. *Plant Physiology* **174**(2): 776-787.

Hummer KE, Hancock JF. 2015. Vavilovian centers of plant diversity: Implications and impacts. *HortScience* **50**(6): 780-783.

Ivandic V, Hackett CA, Zhang ZJ, Staub JE, Nevo E, Thomas WTB, Forster BP. 2000. Phenotypic responses of wild barley to experimentally imposed water stress. *Journal of Experimental Botany* **51**(353): 2021-2029.

Jacquemoud S, Verhoef W, Baret F, Bacour C, Zarco-Tejada PJ, Asner GP, François C, Ustin SL. 2009. PROSPECT+SAIL models: A review of use for vegetation characterization. *Remote Sensing of Environment* **113**: S56-S66.

Jayakodi M, Lu Q, Pidon H, Rabanus-Wallace MT, Bayer M, Lux T, Guo Y, Jaegle B, Badea A, Bekele W, et al. 2024. Structural variation in the pangenome of wild and domesticated barley. *Nature* **636**(8043): 654-662.

Jayakodi M, Padmarasu S, Haberer G, Bonthala VS, Gundlach H, Monat C, Lux T, Kamal N, Lang D, Himmelbach A, et al. 2020. The barley pan-genome reveals the hidden legacy of mutation breeding. *Nature* **588**(7837): 284-289.

Jian L, Yan J, Liu J. 2022. De novo domestication in the multi-omics era. *Plant and Cell Physiology* **63**(11): 1592-1606.

Jones HG 2014. Plants and microclimate : a quantitative approach to environmental plant physiology / Hamlyn G. Jones, professor emeritus, Division of Plant Science, University of Dundee at the James Hutton Institute, Invergowrie, Dundee, DD2 5DA, UK. and adjunct professor of plant biology, University of Western Australia: Cambridge University Press.

Jou Y-J, Huang C-CL, Cho H-J. 2014. A VIF-based optimization model to alleviate collinearity problems in multiple linear regression. *Computational Statistics* **29**: 1515-1541.

Kang J, Yue L, Wang S, Zhao W, Bao A. 2016. Na compound fertilizer stimulates growth and alleviates water deficit in the succulent xerophyte *Nitraria tangutorum* (Bobr) after breaking seed dormancy. *Soil Science and Plant Nutrition* **62**(5-6): 489-499.

Kar S, Tanaka R, Korbu LB, Kholová J, Iwata H, Durbha SS, Adinarayana J, Vadez V. 2020. Automated discretization of 'transpiration restriction to increasing VPD' features from outdoors high-throughput phenotyping data. *Plant Methods* **16**(1): 140.

Khadka K, Raizada MN, Navabi A. 2020. Recent Progress in Germplasm Evaluation and Gene Mapping to Enable Breeding of Drought-Tolerant Wheat. *Frontiers in Plant Science* **11**: 1-18.

Khazaei H, Street K, Bari A, Mackay M, Stoddard FL. 2013. The FIGS (Focused Identification of Germplasm Strategy) approach identifies traits related to drought adaptation in Vicia faba genetic resources. *PLoS ONE* **8**(5): e63107.

Khoury CK, Brush S, Costich DE, Curry HA, Haan S, Engels JMM, Guarino L, Hoban S, Mercer KL, Miller AJ, et al. 2021. Crop genetic erosion: understanding and responding to loss of crop diversity. *new phytologist* **233**: 84-118.

Kim G, Ryu H, Sung J. 2022. Hormonal Crosstalk and Root Suberization for Drought Stress Tolerance in Plants. *Biomolecules* **12**(6): 1-16.

King J, Armstead IP, Donnison SI, Roberts LA, Harper JA, Skot K, Elborough K, King IP 2007. Comparative analyses between Lolium/Festuca introgression lines and rice reveal the major fraction of functionally annotated gene models is located in recombination-poor/very recombination-poor regions of the genome. United States: GENETICS SOCIETY OF AMERICA. 597-606.

Kornelia G, Justyna G-W, Agnieszka J, Michał AD, Agnieszka O, Katarzyna H, Barbara J, Katarzyna Ż, Daria G, Joanna Ś, et al. 2018. Prioritization of Candidate Genes in QTL Regions for Physiological and Biochemical Traits Underlying Drought Response in Barley (*Hordeum vulgare* L.). *Frontiers in Plant Science* **9**: 1-26.

Kostaki KI, Coupel-Ledru A, Bonnell VC, Gustavsson M, Sun P, McLaughlin FJ, Fraser DP, McLachlan DH, Hetherington AM, Franklin KA, Dodd AN. 2020. Guard cells integrate light and temperature signals to control stomatal aperture. *Plant Physiology* **182**(3): 1404-1419.

Langridge P, Waugh R. 2019. Harnessing the potential of germplasm collections. *Nature Genetics* **51**(2): 200-201.

Lee SH, van der Werf JHJ. 2016. MTG2: an efficient algorithm for multivariate linear mixed model analysis based on genomic information. *Bioinformatics* **32**(9 p.1420-1422): 1422-1420.

Lenth RV, Bolker B, Buerkner P, Giné-Vázquez I, Herve M, Jung M, Love J, Miguez F, Riebl H, Singmann H 2024. emmeans: Estimated Marginal Means, aka Least-Squares Means.

Lever J, Krzywinski M, Altman N. 2017. Points of significance: Principal component analysis. *Nature methods* **14**(7): 641-643.

Li H, Shao L, Liu X, Sun H, Chen S, Zhang X. 2023. What matters more, biomass accumulation or allocation, in yield and water productivity improvement for winter wheat during the past two decades？. *European Journal of Agronomy* **149**: 126910.

Liller CB, Walla A, Boer MP, Hedley P, Macaulay M, Effgen S, von Korff M, van Esse GW, Koornneef M. 2017. Fine mapping of a major QTL for awn length in barley using a multiparent mapping population. *Theoretical and Applied Genetics: International Journal of Plant Breeding Research* **130**(2): 269-281.

Lim CW, Baek W, Jung J, Kim JH, Lee SC. 2015. Function of ABA in Stomatal Defense against Biotic and Drought Stresses. *Int J Mol Sci* **16**(7): 15251-15270.

Liu H, Zhang J. 2022. Is the Mutation Rate Lower in Genomic Regions of Stronger Selective Constraints? *Molecular Biology and Evolution* **39**(8): msac169.

Liu Q, Gu X, Chen X, Mumtaz F, Liu Y, Wang C, Yu T, Zhang Y, Wang D, Zhan Y. 2022. Soil Moisture Content Retrieval from Remote Sensing Data by Artificial Neural Network Based on Sample Optimization. *Sensors* **22**(4): 1-21.

Long Stephen P, Marshall-Colon A, Zhu X-G. 2015. Meeting the Global Food Demand of the Future by Engineering Crop Photosynthesis and Yield Potential. *Cell* **161**(1): 56-66.

Lukac M, Gooding MJ, Griffiths S, Jones HE. 2012. Asynchronous flowering and within-plant flowering diversity in wheat and the implications for crop resilience to heat. *Annals of Botany* **109**(4): 843-850.

Maia RF, Lurbe CB, Hornbuckle J. 2022. Machine learning approach to estimate soil matric potential in the plant root zone based on remote sensing data. *Frontiers in Plant Science* **13**: 1-16.

Majic P, Payne JL. 2023. Developmental Selection and the Perception of Mutation Bias. *Molecular Biology and Evolution* **40**(8): msad179.

Mammadov J, Buyyarapu R, Guttikonda SK, Parliament K, Abdurakhmonov IY, Kumpatla SP. 2018. Wild Relatives of Maize, Rice, Cotton, and Soybean: Treasure Troves for Tolerance to Biotic and Abiotic Stresses. *Frontiers in Plant Science* **9**: 1-21.

Marchin RM, Ossola A, Leishman MR, Ellsworth DS. 2020. A Simple Method for Simulating Drought Effects on Plants. *Frontiers in Plant Science* **10**.

Maurel C, Boursiac Y, Luu D-T, Santoni V, Shahzad Z, Verdoucq L. 2015. Aquaporins in Plants. *Physiological Reviews* **95**(4): 1321-1358.

McCouch S, Baute GJ, Bradeen J, Bramel P, Bretting PK, Buckler E, Burke JM, Charest D, Cloutier S, Cole G, et al. 2013. Feeding the future. *Nature* **499**(7456): 23-24.

Merzlyak MN, Melø TB, Naqvi KR. 2008. Effect of anthocyanins, carotenoids, and flavonols on chlorophyll fluorescence excitation spectra in apple fruit: signature analysis, assessment, modelling, and relevance to photoprotection. *Journal of Experimental Botany* **59**(2): 349-359.

Mikołajczak K, Kuczyńska A, Krajewski P, Sawikowska A, Surma M, Ogrodowicz P, Adamski T, Krystkowiak K, Górny AG, Kempa M, et al. 2017. Quantitative trait loci for plant height in Maresi × CamB barley population and their associations with yield-related traits under different water regimes. *Journal of Applied Genetics: Microorganisms and Organelles* **58**(1): 23 -35.

Milner SG, Jost M, Taketa S, Mazón ER, Himmelbach A, Oppermann M, Weise S, Knüpffer H, Basterrechea M, König P, et al. 2019. Genebank genomics highlights the diversity of a global barley collection. *Nature Genetics* **51**(2): 319-326.

Mirzaghaderi G, Abdolmalaki Z, Ebrahimzadegan R, Bahmani F, Orooji F, Majdi M, Mozafari A-A. 2020. Production of synthetic wheat lines to exploit the genetic diversity of emmer wheat and D genome containing Aegilops species in wheat breeding. *Scientific Reports* **10**(1): 19698.

Mishina K, Suzuki T, Oono Y, Yamashita Y, Zhu H, Ogawa T, Ohta M, Doman K, Xu W, Takahashi D, et al. 2023. Wheat *Ym2* originated from *Aegilops sharonensis* and confers resistance to soil-borne *Wheat yellow mosaic virus* infection to the roots. *Proceedings of the National Academy of Sciences* **120**(11): 1-11.

Monroe JG, Srikant T, Carbonell-Bejerano P, Becker C, Lensink M, Exposito-Alonso M, Klein M, Hildebrandt J, Neumann M, Kliebenstein D, et al. 2022. Mutation bias reflects natural selection in Arabidopsis thaliana. *Nature* **602**(7895): 101-105.

Moore CE, Meacham-Hensold K, Lemonnier P, Slattery RA, Benjamin C, Bernacchi CJ, Lawson T, Cavanagh AP. 2021. The effect of increasing temperature on crop photosynthesis: from enzymes to ecosystems. *Journal of Experimental Botany* **72**: 2822-2844.

Mora F, Quitral YA, Matus I, Russell J, Waugh R, del Pozo A. 2016. SNP-Based QTL Mapping of 15 Complex Traits in Barley under Rain-Fed and Well-Watered Conditions by a Mixed Modeling Approach. *FRONTIERS IN PLANT SCIENCE* **7**.

Morton MJL, Awlia M, Al-Tamimi N, Saade S, Pailles Y, Negrão S, Tester M. 2019. Salt stress under the scalpel – dissecting the genetics of salt tolerance. *Plant Journal* **97**(1 p.148-163): 163-148.

Mulero G, Jiang D, Bonfil DJ, Helman D. 2023. Use of thermal imaging and the photochemical reflectance index (PRI) to detect wheat response to elevated CO₂ and drought. *Plant, cell & environment* **46**(1): 76-92.

Murakami A, Kim E, Minagawa J, Takizawa K. 2024. How much heat does non-photochemical quenching produce? *FRONTIERS IN PLANT SCIENCE* **15**: 1367795.

Murchie EH, Lawson T. 2013. Chlorophyll fluorescence analysis: a guide to good practice and understanding some new applications. *Journal of Experimental Botany* **64**(13): 3983-3998.

Nakazawa M. 2018. fmsb: Functions for medical statistics book with some demographic data. *R package version 0.6* **3**(3).

Naumann G, Alfieri L, Wyser K, Mentaschi L, Betts RA, Carrao H, Spinoni J, Vogt J, Feyen L. 2018. Global changes in drought conditions under different levels of warming. *Geophysical Research Letters* **45**(7): 3285-3296.

Neeraja CN, Maghirang-Rodriguez R, Pamplona A, Heuer S, Collard BC, Septiningsih EM, Vergara G, Sanchez D, Xu K, Ismail AM. 2007. A marker-assisted backcross approach for developing submergence-tolerant rice cultivars. *Theoretical and applied genetics* **115**: 767-776.

Neff MM, Turk E, Kalishman M. 2002. Web-based primer design for single nucleotide polymorphism analysis. *TRENDS in Genetics* **18**(12): 613-615.

Nevo E, Chen G. 2010. Drought and salt tolerances in wild relatives for wheat and barley improvement. *Plant, cell and environment* **33**(4 p.670-685): 685-670.

Nguyen GN, Norton SL. 2020. Genebank Phenomics: A Strategic Approach to Enhance Value and Utilization of Crop Germplasm. *PLANTS-BASEL* **9**(7): 817.

Nguyen N-K 1983. Gendex DOE toolkit.

Ogrodowicz P, Adamski T, Mikołajczak K, Kuczyńska A, Surma M, Krajewski P, Sawikowska A, Górny AG, Gudyś K, Szarejko I, et al. 2017. QTLs for earliness and yield-forming traits in the Lubuski × CamB barley RIL population under various water regimes. *Journal of Applied Genetics: Microorganisms and Organelles* **58**(1): 49-65.

Olivares-Villegas JJ, Reynolds MP, McDonald GK 2007. Drought-adaptive attributes in the Seri/Babax hexaploid wheat population. Australia: CSIRO PUBLISHING. 189-203.

Palmgren MG, Edenbrandt AK, Vedel SE, Andersen MM, Landes X, Østerberg JT, Falhof J, Olsen LI, Christensen SB, Sandøe P, et al. 2015. Are we ready for back-to-nature crop breeding? *Trends in Plant Science* **20**(3): 155-164.

Pathoumthong P, Zhang Z, Roy SJ, El Habti A. 2023. Rapid non-destructive method to phenotype stomatal traits. *Plant Methods* **19**(1): 36.

Perich G, Hund A, Anderegg J, Roth L, Boer MP, Walter A, Liebisch F, Aasen H. 2020. Assessment of multi-image unmanned aerial vehicle based high-throughput field phenotyping of canopy temperature. *FRONTIERS IN PLANT SCIENCE* **11**: 150.

Pham A-T, Maurer A, Pillen K, Brien C, Dowling K, Berger B, Eglinton JK, March TJ. 2019. Genome-wide association of barley plant growth under drought stress using a nested association mapping population. *BMC Plant Biology* **19**(1): 134.

Phathutshedzo-Eugene R, Mohamed AMAE, Elhadi A, Johannes George C, Gang L, Eric Benjamin E. 2023. Determination of Soil Electrical Conductivity and Moisture on Different Soil Layers Using Electromagnetic Techniques in Irrigated Arid Environments in South Africa. *Water* **15**: 1-23.

Phua SY, De Smet B, Remacle C, Chan KX, Van Breusegem F. 2021. Reactive oxygen species and organellar signaling. *Journal of Experimental Botany* **72**(16): 5807-5824.

Pourkheirandish M, Hensel G, Kilian B, Senthil N, Chen G, Sameri M, Azhaguvel P, Sakuma S, Dhanagond S, Sharma R, et al. 2015. Evolution of the Grain Dispersal System in Barley. *Cell* **162**(3): 527-539.

Purcell S, Neale B, Todd-Brown K, Thomas L, Ferreira MA, Bender D, Maller J, Sklar P, de Bakker PI, Daly MJ, Sham PC. 2007. PLINK: a tool set for whole-genome association and population-based linkage analyses. *Am J Hum Genet* **81**(3): 559-575.

Qaseem MF, Qureshi R, Illyas N, Jalal-Ud-Din SG. 2017. Multivariate statistical analysis for yield and yield components in bread wheat planted under rainfed conditions. *Pakistan journal of botany* **49**(6): 2445-2450.

Rahman MM, Crain J, Haghighattalab A, Singh RP, Poland J. 2021. Improving Wheat Yield Prediction Using Secondary Traits and High-Density Phenotyping Under Heat-Stressed Environments. *FRONTIERS IN PLANT SCIENCE* **12**.

Razzaq A, Wani SH, Saleem F, Yu M, Zhou M, Shabala S. 2021. Rewilding crops for climate resilience: economic analysis and *de novo* domestication strategies. *Journal of Experimental Botany* **72**(18): 6123-6139.

Rebetzke GJ, Condon AG, Richards RA, Farquhar GD. 2002. Selection for Reduced Carbon Isotope Discrimination Increases Aerial Biomass and Grain Yield of Rainfed Bread Wheat. *Crop science* **42**(3): 745-739.

Rebetzke GJ, Rattey AR, Farquhar GD, Richards RA, Condon AG 2013. Genomic regions for canopy temperature and their genetic association with stomatal conductance and grain yield in wheat. Australia: CSIRO PUBLISHING. 14.

Resende RT, Piepho H-P, Rosa GJM, Silva-Junior OB, e Silva FF, de Resende MDV, Grattapaglia D. 2021. Enviromics in breeding: applications and perspectives on envirotypic-assisted selection. *Theoretical and Applied Genetics* **134**(1): 95-112.

Richards RA 2022. Drought. In: Reynolds MP, Braun H-J eds. *Wheat improvement : food security in a changing climate* Springer, 417-432.

Rischbeck P, Cardellach P, Mistele B, Schmidhalter U. 2017. Thermal phenotyping of stomatal sensitivity in spring barley. *Journal of agronomy and crop science* **203**(6 p.483-493): 493-483.

Robertson BC, He T, Li C. 2021. The Genetic Control of Stomatal Development in Barley: New Solutions for Enhanced Water-Use Efficiency in Drought-Prone Environments. *Agronomy* **11**(8): 1-24.

Sales CRG, Molero G, Evans JR, Taylor SH, Joynson R, Furbank RT, Hall A, Carmo-Silva E. 2022. Phenotypic variation in photosynthetic traits in wheat grown under field versus glasshouse conditions. *Journal of Experimental Botany*.

Sato K, Yamane M, Yamaji N, Kanamori H, Tagiri A, Schwerdt JG, Fincher GB, Matsumoto T, Takeda K, Komatsuda T. 2016. Alanine aminotransferase controls seed dormancy in barley. *Nature Communications* **7**(1): 11625.

Schmalenbach I, March TJ, Pillen K, Waugh R, Bringezu T. 2011. High-resolution genotyping of wild barley introgression lines and fine-mapping of the threshability locus *thresh-1* using the illumina goldengate assay. *G3: Genes, Genomes, Genetics* **1**(3): 187-196.

Serbin SP, Dillaway DN, Kruger EL, Townsend PA 2012. Leaf optical properties reflect variation in photosynthetic metabolism and its sensitivity to temperature. *Journal of Experimental Botany*. 489-502.

Sexton TM, Steber CM, Cousins AB. 2021. Leaf temperature impacts canopy water use efficiency independent of changes in leaf level water use efficiency. *Journal of Plant Physiology* **258-259**: 1-10.

Shabala S. 2013. Learning from halophytes: physiological basis and strategies to improve abiotic stress tolerance in crops. *Annals of Botany* **112**(7): 1209-1221.

Sharkey TD, Bernacchi CJ, Farquhar GD, Singsaas EL. 2007. Fitting photosynthetic carbon dioxide response curves for C_3 leaves. *Plant, Cell & Environment* **30**(9): 1040-1035.

Sharma D, Jaiswal J, Singh N, Chauhan A, Gahtyari NC. 2018. Developing a selection criterion for terminal heat tolerance in bread wheat based on various mopho-physiological traits. *International journal of current microbiology and applied sciences* **7**(7): 2716-2726.

Sharma S, Upadhyaya H, Varshney R, Gowda C. 2013. Pre-breeding for diversification of primary gene pool and genetic enhancement of grain legumes. *FRONTIERS IN PLANT SCIENCE* **4**.

Shavrukov Y. 2016. CAPS markers in plant biology. *Russian Journal of Genetics: Applied Research* **6**: 279-287.

Shekoofa A, Sinclair TR. 2018. Aquaporin Activity to Improve Crop Drought Tolerance. *Cells* **7**(9): 123.

Silva-Perez V, Molero G, Serbin SP, Condon AG, Reynolds MP, Furbank RT, Evans JR 2018. Hyperspectral reflectance as a tool to measure biochemical and physiological traits in wheat. Great Britain: Oxford University Press. 483-496.

Singh S, Jighly A, Sehgal D, Burgueño J, Joukhadar R, Singh SK, Sharma A, Vikram P, Sansaloni CP, Govindan V, et al. 2021. Direct introgression of untapped diversity into elite wheat lines. *Nature Food* **2**(10): 819-827.

Sirault XRR, James RA, Furbank RT. 2009. A new screening method for osmotic component of salinity tolerance in cereals using infrared thermography. *Functional Plant Biology* **36**(10-11 p.970-977): 977-970.

Slafer GA, Savin R, Sadras VO. 2023. Wheat yield is not causally related to the duration of the growing season. *European Journal of Agronomy* **148**: 1-8.

Sobejano-Paz V, Mikkelsen TN, Baum A, Mo X, Liu S, Köppl CJ, Johnson MS, Gulyas L, García M. 2020. Hyperspectral and Thermal Sensing of Stomatal Conductance,

Transpiration, and Photosynthesis for Soybean and Maize under Drought. *Remote Sensing* **12**(19).

Sofi PA, Ara A, Gull M, Rehman K. 2019. Canopy Temperature Depression as an Effective Physiological Trait for Drought Screening. *Drought - Detection and Solutions*.

Stenberg JA, Ortiz R. 2021. Focused Identification of Germplasm Strategy (FIGS): polishing a rough diamond. *Curr Opin Insect Sci* **45**: 1-6.

Stinziano JR, Roback C, Sargent D, Murphy BK, Hudson PJ, Muir CD. 2021. Principles of resilient coding for plant ecophysiologists. *AoB Plants* **13**(5): plab059.

Street K, Bari A, Mackay M, Amri A 2016. How the Focused Identification of Germplasm Strategy (FIGS) is used to mine plant genetic resources collections for adaptive traits. In: Maxted N, Dulloo ME, Ford-Lloyd BV eds. *Enhancing crop genepool use: capturing wild relative and landrace diversity for crop improvement.* . Wallingford, Oxfordshire, UK: CABI.

Suarez L, González-Dugo V, Camino C, Hornero A, Zarco-Tejada PJ. 2021. Physical model inversion of the green spectral region to track assimilation rate in almond trees with an airborne nano-hyperspectral imager. *Remote Sensing of Environment* **252**: 1-16.

Tamura K, Stecher G, Kumar S. 2021. MEGA11: Molecular Evolutionary Genetics Analysis Version 11. *Mol Biol Evol* **38**(7): 3022-3027.

Tardieu F, Cabrera-Bosquet L, Pridmore T, Bennett M. 2017. Plant phenomics, from sensors to knowledge. *Current Biology* **27**(15): R770-R783.

Thāpā S, Rudd JC, Jessup KE, Liu S, Baker JA, Devkota RN, Xue Q. 2022. Middle portion of the wheat culm remobilizes more carbon reserve to grains under drought. *Journal of agronomy and crop science* **208**(6 p.795-804): 804-795.

Therneau T, Atkinson B, Ripley B, Ripley MB. 2015. Package 'rpart'. *Available online: cran. ma. ic. ac. uk/web/packages/rpart/rpart. pdf (accessed on 20 April 2016)*.

Trojak M, Skowron E. 2023. Growth Light Quality Influences Leaf Surface Temperature by Regulating the Rate of Non-Photochemical Quenching Thermal Dissipation and Stomatal Conductance. *INTERNATIONAL JOURNAL OF MOLECULAR SCIENCES* **24**(23): 16911.

Turner NC. 2019. Imposing and maintaining soil water deficits in drought studies in pots. *Plant and Soil* **439**(1/2): 45-55.

ur Rehman A, Belhaouari SB. 2021. Unsupervised outlier detection in multidimensional data. *Journal of Big Data* **8**(1).

Ustin SL, Gitelson AA, Jacquemoud S, Schaepman M, Asner GP, Gamon JA, Zarco-Tejada P. 2009. Retrieval of foliar information about plant pigment systems from high resolution spectroscopy. *Remote Sensing of Environment* **113**: S67-S77.

Vadez V, Grondin A, Chenu K, Henry A, Laplaze L, Millet EJ, Carminati A. 2024. Crop traits and production under drought. *Nature Reviews Earth & Environment* **5**(3): 211-225.

van der Tol C, Verhoef W, Rosema A. 2009. A model for chlorophyll fluorescence and photosynthesis at leaf scale. *Agricultural and Forest Meteorology* **149**(1): 96-105.

VanRaden PM. 2008. Efficient methods to compute genomic predictions. *J Dairy Sci* **91**(11): 4414-4423.

Velasco S, Román F, White J. 2009. On the Clausius–Clapeyron vapor pressure equation. *Journal of Chemical Education* **86**(1): 106.

Vialet-Chabrand S, Matthews JS, Lawson T. 2021. Light, power, action! Interaction of respiratory energy-and blue light-induced stomatal movements. *new phytologist* **231**(6): 2231-2246.

Visscher PM, Hill WG, Wray NR. 2008. Heritability in the genomics era — concepts and misconceptions. *Nature Reviews Genetics* **9**(4): 255-266.

Wang F, Robson TM, Casal JJ, Shapiguzov A, Aphalo PJ. 2020. Contributions of cryptochromes and phototropins to stomatal opening through the day. *Functional Plant Biology* **47**(3): 226-238.

Wickham H. 2014. Tidy Data. *Journal of Statistical Software* **59**(10): undefined-undefined.

Williams M. 2022. *Waking up Wild Barley: Manipulating Natural Mechanisms to Break Grain Dormancy.* Honours, The University of Melbourne Victoria, Australia.

Wright K. 2022. Will the Real Hopkins Statistic Please Stand Up? *R Journal* **14**(3): 282-292.

Xi J-J, Chen H-Y, Bai W-P, Yang R-C, Yang P-Z, Chen R-J, Hu T-M, Wang S-M. 2018. Sodium-Related Adaptations to Drought: New Insights From the Xerophyte Plant Zygophyllum xanthoxylum. *Frontiers in Plant Science* **9**: 1-15.

Xiaoyu Z, Sean Reynolds M-R, Alex W, Andries P, Andrew B, Colleen H, David J, Yan Z, Scott C, Graeme H, Barbara G-J. 2022. Estimating Photosynthetic Attributes from High-Throughput Canopy Hyperspectral Sensing in Sorghum. *Plant Phenomics* **2022**: 1-18.

Xu X, Liu H, Praat M, Pizzio GA, Jiang Z, Driever SM, Wang R, Van De Cotte B, Villers SL, Gevaert K. 2024. Stomatal opening under high temperatures is controlled by the OST1-regulated TOT3–AHA1 module. *Nature Plants*: 1-13.

Xu Y 2010. Molecular plant breeding / Yunbi Xu: CABI.

Xu Y. 2016. Envirotyping for deciphering environmental impacts on crop plants. *Theoretical and Applied Genetics* **129**(4): 653-673.

Yang B, Chen N, Dang Y, Wang Y, Wen H, Zheng J, Zheng X, Zhao J, Lu J, Qiao L. 2022. Identification and validation of quantitative trait loci for chlorophyll content of flag leaf in wheat under different phosphorus treatments. *FRONTIERS IN PLANT SCIENCE* **13**: 1019012.

Yang C, Zhang D, Li X, Shi Y, Shao Y, Fang B, Yue J, Wang H, Qin F, Cheng H. 2021. Drought effects on photosynthetic performance of two wheat cultivars contrasting in drought. *New Zealand Journal of Crop and Horticultural Science* **49**(1 p.17-29): 29-17.

Ye M, Peng Z, Tang D, Yang Z, Li D, Xu Y, Zhang C, Huang S. 2018. Generation of self-compatible diploid potato by knockout of S-RNase. *Nature Plants* **4**(9): 651-654.

Yu H, Lin T, Meng X, Du H, Zhang J, Liu G, Chen M, Jing Y, Kou L, Li X. 2021. A route to de novo domestication of wild allotetraploid rice. *Cell* **184**(5): 1156-1170. e1114.

Zarco-Tejada PJ, Camino C, Beck PSA, Calderon R, Hornero A, Hernández-Clemente R, Kattenborn T, Montes-Borrego M, Susca L, Morelli M, et al. 2018. Previsual symptoms of Xylella fastidiosa infection revealed in spectral plant-trait alterations. *Nature Plants* **4**(7): 432-439.

Zarco-Tejada PJ, Miller JR, Mohammed GH, Noland TL. 2000a. Chlorophyll fluorescence effects on vegetation apparent reflectance: I. Leaf-level measurements and model simulation. *Remote Sensing of Environment* **74**(3): 582-595.

Zarco-Tejada PJ, Miller JR, Mohammed GH, Noland TL, Sampson PH. 2000b. Chlorophyll fluorescence effects on vegetation apparent reflectance: II. Laboratory and airborne canopy-level measurements with hyperspectral data. *Remote Sensing of Environment* **74**(3): 596-608.

Zarco-Tejada PJ, Poblete T, Camino C, Gonzalez-Dugo V, Calderon R, Hornero A, Hernandez-Clemente R, Román-Écija M, Velasco-Amo MP, Landa BB, et al. 2021. Divergent abiotic spectral pathways unravel pathogen stress signals across species. *Nature Communications* **12**(1).

Zhang K, Fang Z, Liang Y, Tian J. 2009. Genetic dissection of chlorophyll content at different growth stages in common wheat. *Journal of genetics* **88**: 183-189.

Zhao J, Sun H, Dai H, Zhang G, Wu F. 2010. Difference in response to drought stress among Tibet wild barley genotypes. *Euphytica: International Journal of Plant Breeding* **172**(3): 395-403.

Zsögön A, Čermák T, Naves ER, Notini MM, Edel KH, Weinl S, Freschi L, Voytas DF, Kudla J, Peres LEP. 2018. De novo domestication of wild tomato using genome editing. *Nature Biotechnology* **36**(12): 1211-1216.

Appendices

Appendix 2.1. Physiological traits and yield data for six commercial wheat varieties (Triticum spp.) obtained via hyperspectral and thermal imaging at the stem elongation stage of the Santaella experiment from (Camino *et al.*, 2019).

Wheat variety	Replicate	Treatment	Yield (Kg ha^{-1})	CWSI	1-CWSI	V_{cmax}
Var1	1	Rainfed	5,108	0.57	0.43	20.85
Var1	2	Rainfed	5,802	0.47	0.53	82.74
Var1	3	Rainfed	6,873	0.39	0.61	161.93
Var3	1	Rainfed	5,234	0.5	0.5	46.51
Var3	2	Rainfed	5,251	0.56	0.44	104.4
Var3	3	Rainfed	7,222	0.32	0.68	70.08
Var4	1	Rainfed	6,103	0.65	0.35	140.63
Var4	2	Rainfed	5,093	0.58	0.42	265.4
Var5	1	Rainfed	5,850	0.56	0.44	65.64
Var5	2	Rainfed	7,225	0.37	0.63	106.48
Var5	3	Rainfed	7,516	0.44	0.56	25.3
Var5	4	Rainfed	6,120	0.59	0.41	97.62
Var6	1	Rainfed	4,699	0.52	0.48	26.06
Var6	2	Rainfed	4,488	0.5	0.5	15.8
Var6	3	Rainfed	6,543	0.42	0.58	81.89
Var2	1	Rainfed	6,361	0.54	0.46	17.13
Var2	2	Rainfed	6,088	0.69	0.31	48.08
Var2	3	Rainfed	7,109	0.65	0.35	72.66
Var2	4	Rainfed	6,636	0.53	0.47	15.31
Var2	5	Rainfed	6,057	0.61	0.39	64
Var2	6	Rainfed	5,238	0.51	0.49	138.97
Var2	7	Rainfed		0.69	0.31	76.41
Var2	1	Irrigated	8,322	0.13	0.87	243.17
Var6	1	Irrigated	9,199	0.06	0.94	182.84
Var1	1	Irrigated	8,069	-0.06	1.06	258.71
Var3	1	Irrigated	8,439	0.01	0.99	235.49
Var5	1	Irrigated	9,171	0	1	233.57
Var5	2	Irrigated	8,999	-0.05	1.05	205.47
Var3	2	Irrigated	8,100	0.07	0.93	208.05
Var2	2	Irrigated	7,168	0.11	0.89	76.36
Var6	2	Irrigated	7,843	0.01	0.99	147.65
Var1	2	Irrigated	7,561	0	1	184.42
Var1	3	Irrigated	8,333	-0.06	1.06	264.2
Var2	3	Irrigated	7,698	0.1	0.9	117.53
Var3	3	Irrigated	8,732	-0.08	1.08	264.41
Var6	3	Irrigated	8,991	-0.11	1.11	257.87
Var4	1	Irrigated	6,103	-0.12	1.12	286.95
Var4	2	Irrigated	5,093	-0.02	1.02	244.9

V_{cmax} = Photosynthetic capacity (μmol m^{-1} s^{-1})

CWSI = Crop Water Stress Index (unitless)

1-CWSI = Transpiration rates (unitless)

Appendix 3.1. Heritability (H^2) of Canopy Temperature Depression (CTD) for each DAS and irrigation Treatments.

	CTD											
	22 DAS		26 DAS		28 DAS		31 DAS		33 DAS		35 DAS	
Components	**Var**	**%**	**Var**	**%**	**Var**	**%**	**Var**	**%**	**Var**	**%**	**Var**	**%**
Irrigated treatment												
Genotype	0.1	24%	0.04	10%	0.24	37%	0.13	18%	0.1	22%	0.4	50%
Residual	0.32	76%	0.39	90%	0.41	63%	0.6	82%	0.36	78%	0.39	50%
Total variance	0.42	100%	0.43	100%	0.65	100%	0.72	100%	0.46	100%	0.79	100%
Phenotypic variance	0.21		0.17		0.38		0.33		0.22		0.53	
Heritability (H^2) %	49%		25%		64%		39%		46%		75%	
Drought treatment												
Genotype	0.33	51%	0.29	44%	0.54	60%	0.1	14%	0.01	1%	0	0%
Residual	0.32	49%	0.38	56%	0.35	40%	0.65	86%	0.52	99%	0.88	100%
Total variance	0.64	100%	0.67	100%	0.89	100%	0.75	100%	0.52	100%	0.88	100%
Phenotypic variance	0.43		0.42		0.65		0.32		0.18		0.29	
Heritability (H^2) %	75%		70%		82%		32%		4%		0%	

(continuation)

	CTD									
	39 DAS		41 DAS		48 DAS		57 DAS		59 DAS	
Components	**Var**	**%**	**Var**	**%**	**Var**	**%**	**Var**	**%**	**Var**	**%**
Irrigated treatment										
Genotype	0.24	26%	0.28	27%	0.03	4%	0.17	18%	0.48	46%
Residual	0.71	74%	0.74	73%	0.7	96%	0.77	82%	0.57	54%
Total variance	0.95	100%	1.02	100%	0.73	100%	0.95	100%	1.05	100%

Phenotypic variance	0.48		0.52		0.26		0.43		0.67	
Heritability (H^2) %	51%		53%		12%		40%		72%	
Drought treatment										
Genotype	0	0%	0.13	12%	0	0%	0.2	19%	0	0%
Residual	0.99	100%	0.91	88%	0.45	100%	0.83	81%	1.02	100%
Total variance	0.99	100%	1.04	100%	0.45	100%	1.03	100%	1.02	100%
Phenotypic variance	0.33		0.43		0.15		0.48		0.34	
Heritability (H^2) %	0%		30%		0%		42%		0%	

CTD Canopy Temperature Depression, *SPAD* Chlorophyll content as SPAD values, *FW* Fresh weight, *DW* Dry Weight; r=3 replicates

Heritability (H^2) of SPAD values, Fresh Weight (FW) and Dry Weight (DW) for each irrigation Treatment.

	SPAD		**FW**		**DW**	
Components	**Var**	**%**	**Var**	**%**	**Var**	**%**
Irrigated treatment						
Genotype	36.25	89.1%	0.04	90.6%	0.05	83.3%
Residual	4.42	10.9%	0.00	9.4%	0.01	16.7%
Total variance	40.68	100.0%	0.04	100.0%	0.07	100.0%
Phenotypic variance	37.73		0.04		0.06	
Heritability (H^2) %	96%		97%		94%	
Drought treatment						
Genotype	13.16	68.7%	0.01	23.3%	0.04	52.9%
Residual	6.00	31.3%	0.02	76.7%	0.03	47.1%
Total variance	19.16	100.0%	0.02	100.0%	0.07	100.0%
Phenotypic variance	15.16		0.01		0.05	
Heritability (H^2) %	87%		48%		77%	

Appendix 4.1. List of genotype included in the study.

Code	Sample ID	Gendex ID	Taxon	Origin	Status
208	SAMEA111361044	82	*Hordeum vulgare subsp. spontaneum*	Uzbekistan, Toshkent	Wild
213	SAMEA111360925	87	*Hordeum vulgare subsp. spontaneum*	Uzbekistan, Samarqand	Wild
214	SAMEA111360926	88	*Hordeum vulgare subsp. spontaneum*	Uzbekistan, Samarqand	Wild
119	SAMEA111360872	43	*Hordeum vulgare subsp. spontaneum*	Uzbekistan, Jizzax	Wild
209	SAMEA111360922	83	*Hordeum vulgare subsp. spontaneum*	Uzbekistan, Jizzax	Wild
210	SAMEA111360923	84	*Hordeum vulgare subsp. spontaneum*	Uzbekistan, Jizzax	Wild
211	SAMEA111360924	85	*Hordeum vulgare subsp. spontaneum*	Uzbekistan, Jizzax	Wild
212	SAMEA111361045	86	*Hordeum vulgare subsp. spontaneum*	Uzbekistan, Jizzax	Wild
207	SAMEA111361043	81	*Hordeum vulgare subsp. spontaneum*	Uzbekistan, Farg‘ona	Wild
117	SAMEA111360871	42	*Hordeum vulgare subsp. spontaneum*	Turkmenistan, Balkan	Wild
215	SAMEA111361046	89	*Hordeum vulgare subsp. spontaneum*	Turkmenistan, Balkan	Wild
329	SAMEA111361072	114	*Hordeum vulgare subsp. spontaneum*	Turkmenistan, Balkan	Wild
330	SAMEA111360989	115	*Hordeum vulgare subsp. spontaneum*	Turkmenistan, Balkan	Wild
331	SAMEA111360990	116	*Hordeum vulgare subsp. spontaneum*	Turkmenistan, Balkan	Wild
332	SAMEA111360991	117	*Hordeum vulgare subsp. spontaneum*	Turkmenistan, Balkan	Wild
204	SAMEA111360920	79	*Hordeum vulgare subsp. spontaneum*	Turkmenistan, Ahal	Wild
216	SAMEA111360927	90	*Hordeum vulgare subsp. spontaneum*	Turkmenistan, Ahal	Wild
326	SAMEA111361071	113	*Hordeum vulgare subsp. spontaneum*	Turkmenistan, Ahal	Wild
020	SAMEA111360821	4	*Hordeum vulgare subsp. spontaneum*	Turkey, Şanlıurfa	Wild
056	SAMEA111360843	16	*Hordeum vulgare subsp. spontaneum*	Turkey, Kilis	Wild
190	SAMEA111360911	70	*Hordeum vulgare subsp. spontaneum*	Turkey, Kilis	Wild
048	SAMEA111360838	15	*Hordeum vulgare subsp. spontaneum*	Turkey, Hakkâri	Wild
188	SAMEA111361036	69	*Hordeum vulgare subsp. spontaneum*	Turkey, Gaziantep	Wild
192	SAMEA111360912	71	*Hordeum vulgare subsp. spontaneum*	Turkey, Gaziantep	Wild
120	SAMEA111360873	44	*Hordeum vulgare subsp. spontaneum*	Tajikistan, Sughd	Wild
221	SAMEA111360930	94	*Hordeum vulgare subsp. spontaneum*	Tajikistan, Sughd	Wild
026	SAMEA111360826	8	*Hordeum vulgare subsp. spontaneum*	Tajikistan, Khatlon	Wild
106	SAMEA111361014	36	*Hordeum vulgare subsp. spontaneum*	Syria, Tarţūs	Wild
057	SAMEA111360844	17	*Hordeum vulgare subsp. spontaneum*	Syria, Rīf Dimashq	Wild
066	SAMEA111361004	23	*Hordeum vulgare subsp. spontaneum*	Syria, Rīf Dimashq	Wild
069	-	25	*Hordeum vulgare subsp. spontaneum*	Syria, Rīf Dimashq	Wild
108	-	38	*Hordeum vulgare subsp. spontaneum*	Syria, Rīf Dimashq	Wild
111	SAMEA111360866	40	*Hordeum vulgare subsp. spontaneum*	Syria, Rīf Dimashq	Wild
112	SAMEA111360867	41	*Hordeum vulgare subsp. spontaneum*	Syria, Rīf Dimashq	Wild
306	SAMEA111360982	110	*Hordeum vulgare subsp. spontaneum*	Syria, Rīf Dimashq	Wild
064	SAMEA111361003	21	*Hordeum vulgare subsp. spontaneum*	Syria, Idlib	Wild
201	SAMEA111360917	76	*Hordeum vulgare subsp. spontaneum*	Syria, Idlib	Wild
202	SAMEA111360918	77	*Hordeum vulgare subsp. spontaneum*	Syria, Idlib	Wild

203	SAMEA111360919	78	*Hordeum vulgare subsp. spontaneum*	Syria, Idlib	Wild
107	SAMEA111360864	37	*Hordeum vulgare subsp. spontaneum*	Syria, Ḥimş	Wild
198	SAMEA111360915	73	*Hordeum vulgare subsp. spontaneum*	Syria, Ḥimş	Wild
314	SAMEA111360986	111	*Hordeum vulgare subsp. spontaneum*	Syria, Ḥimş	Wild
065	-	22	*Hordeum vulgare subsp. spontaneum*	Syria, Ḥamāh	Wild
199	SAMEA111360916	74	*Hordeum vulgare subsp. spontaneum*	Syria, Ḥamāh	Wild
200	SAMEA111361041	75	*Hordeum vulgare subsp. spontaneum*	Syria, Ḥamāh	Wild
001	SAMEA111360804	1	*Hordeum vulgare subsp. spontaneum*	Syria, Ḥalab	Wild
002	SAMEA111360805	2	*Hordeum vulgare subsp. spontaneum*	Syria, Ḥalab	Wild
062	SAMEA111360847	19	*Hordeum vulgare subsp. spontaneum*	Syria, Ḥalab	Wild
063	SAMEA111360848	20	*Hordeum vulgare subsp. spontaneum*	Syria, Ḥalab	Wild
151	SAMEA111360888	62	*Hordeum vulgare subsp. spontaneum*	Syria, Ḥalab	Wild
197	SAMEA111360914	72	*Hordeum vulgare subsp. spontaneum*	Syria, Ḥalab	Wild
299	SAMEA111361060	108	*Hordeum vulgare subsp. spontaneum*	Syria, Ḥalab	Wild
300	SAMEA111360980	109	*Hordeum vulgare subsp. spontaneum*	Syria, Ḥalab	Wild
130	SAMEA111361018	49	*Hordeum vulgare subsp. spontaneum*	Syria, Dar'ā	Wild
068	SAMEA111360849	24	*Hordeum vulgare subsp. spontaneum*	Syria, As Suwaydā'	Wild
110	SAMEA111360865	39	*Hordeum vulgare subsp. spontaneum*	Syria, As Suwaydā'	Wild
127	SAMEA111361017	48	*Hordeum vulgare subsp. spontaneum*	Syria, As Suwaydā'	Wild
317	SAMEA111361066	112	*Hordeum vulgare subsp. spontaneum*	Syria, Ar Raqqah	Wild
167	SAMEA111360895	64	*Hordeum vulgare subsp. spontaneum*	Syria, Al Ḥasakah	Wild
205	SAMEA111361042	80	*Hordeum vulgare subsp. spontaneum*	Russian Federation, Dagestan, Respublika	Wild
025	SAMEA111360825	7	*Hordeum vulgare subsp. spontaneum*	Pakistan, Balochistan	Wild
074	SAMEA111360850	26	*Hordeum vulgare subsp. spontaneum*	Libya	Wild
075	SAMEA111361009	27	*Hordeum vulgare subsp. spontaneum*	Libya	Wild
132	SAMEA111360880	50	*Hordeum vulgare subsp. spontaneum*	Lebanon, Béqaa	Wild
136	SAMEA111361021	51	*Hordeum vulgare subsp. spontaneum*	Lebanon, Béqaa	Wild
137	SAMEA111360881	52	*Hordeum vulgare subsp. spontaneum*	Lebanon, Béqaa	Wild
140	SAMEA111361023	53	*Hordeum vulgare subsp. spontaneum*	Lebanon, Béqaa	Wild
142	SAMEA111360883	54	*Hordeum vulgare subsp. spontaneum*	Lebanon, Béqaa	Wild
143	SAMEA111361024	55	*Hordeum vulgare subsp. spontaneum*	Lebanon, Béqaa	Wild
145	SAMEA111360884	56	*Hordeum vulgare subsp. spontaneum*	Lebanon, Béqaa	Wild
170	SAMEA111360897	65	*Hordeum vulgare subsp. spontaneum*	Lebanon, Béqaa	Wild
126	SAMEA111361016	47	*Hordeum vulgare subsp. spontaneum*	Lebanon, Al Janūb	Wild
218	-	92	*Hordeum vulgare subsp. spontaneum*	Kazakhstan, Zhambyl oblysy	Wild
219	SAMEA111360928	93	*Hordeum vulgare subsp. spontaneum*	Kazakhstan, Ongtüstik Qazaqstan oblysy	Wild
260	SAMEA111360950	102	*Hordeum vulgare subsp. spontaneum*	Jordan, Ma'ān	Wild
262	-	103	*Hordeum vulgare subsp. spontaneum*	Jordan, Ma'ān	Wild
079	SAMEA111360852	28	*Hordeum vulgare subsp. spontaneum*	Jordan, Jarash	Wild
080	SAMEA111360853	29	*Hordeum vulgare subsp. spontaneum*	Jordan, Irbid	Wild
246	SAMEA111360942	99	*Hordeum vulgare subsp. spontaneum*	Jordan, Irbid	Wild
247	SAMEA111360943	100	*Hordeum vulgare subsp. spontaneum*	Jordan, Irbid	Wild

255	SAMEA111360949	101	*Hordeum vulgare subsp. spontaneum*	Jordan, Irbid	Wild
093	SAMEA111360859	33	*Hordeum vulgare subsp. spontaneum*	Jordan, Az Zarqā’	Wild
092	SAMEA111360858	32	*Hordeum vulgare subsp. spontaneum*	Jordan, Al Mafraq	Wild
095	SAMEA111360979	34	*Hordeum vulgare subsp. spontaneum*	Jordan, Al Karak	Wild
104	SAMEA111361013	35	*Hordeum vulgare subsp. spontaneum*	Jordan, Al Karak	Wild
085	SAMEA111360856	31	*Hordeum vulgare subsp. spontaneum*	Jordan, Al Balqā’	Wild
082	SAMEA111360855	30	*Hordeum vulgare subsp. spontaneum*	Jordan, ‘Ajlūn	Wild
038	SAMEA111360834	12	*Hordeum vulgare subsp. spontaneum*	Israel, Yerushalayim	Wild
291	SAMEA111360972	107	*Hordeum vulgare subsp. spontaneum*	Israel, Yerushalayim	Wild
287	SAMEA111361058	106	*Hordeum vulgare subsp. spontaneum*	Israel, West Bank	Wild
030	SAMEA111360994	9	*Hordeum vulgare subsp. spontaneum*	Israel, HaTsafon	Wild
043	SAMEA111360997	14	*Hordeum vulgare subsp. spontaneum*	Israel, HaTsafon	Wild
281	SAMEA111360963	104	*Hordeum vulgare subsp. spontaneum*	Israel, HaTsafon	Wild
283	SAMEA111360965	105	*Hordeum vulgare subsp. spontaneum*	Israel, HaTsafon	Wild
034	SAMEA111360832	10	*Hordeum vulgare subsp. spontaneum*	Israel, HaMerkaz	Wild
041	SAMEA111360996	13	*Hordeum vulgare subsp. spontaneum*	Israel, HaDarom	Wild
349	SAMEA111361087	118	*Hordeum vulgare subsp. spontaneum*	Israel	Wild
354	SAMEA111361089	119	*Hordeum vulgare subsp. spontaneum*	Israel	Wild
177	SAMEA111360901	68	*Hordeum vulgare subsp. spontaneum*	Iraq, Nīnawá	Wild
021	SAMEA111360822	5	*Hordeum vulgare subsp. spontaneum*	Iraq, Diyālá	Wild
152	SAMEA111361027	63	*Hordeum vulgare subsp. spontaneum*	Iran, Tehrān	Wild
122	SAMEA111360875	45	*Hordeum vulgare subsp. spontaneum*	Iran, Lorestān	Wild
124	-	46	*Hordeum vulgare subsp. spontaneum*	Iran, Kermānshāh	Wild
023	SAMEA111360824	6	*Hordeum vulgare subsp. spontaneum*	Iran, Īlām	Wild
172	SAMEA111360898	66	*Hordeum vulgare subsp. spontaneum*	Iran, Hamadān	Wild
173	SAMEA111360899	67	*Hordeum vulgare subsp. spontaneum*	Iran, Hamadān	Wild
150	SAMEA111360887	61	*Hordeum vulgare subsp. spontaneum*	Iran, Āẕārbāyjān-e Shārqī	Wild
019	SAMEA111360820	3	*Hordeum vulgare subsp. spontaneum*	Iran, Āẕārbāyjān-e Ghārbī	Wild
146	SAMEA111360885	57	*Hordeum vulgare subsp. spontaneum*	Iran, Āẕārbāyjān-e Ghārbī	Wild
147	SAMEA111361025	58	*Hordeum vulgare subsp. spontaneum*	Iran, Āẕārbāyjān-e Ghārbī	Wild
148	SAMEA111360886	59	*Hordeum vulgare subsp. spontaneum*	Iran, Āẕārbāyjān-e Ghārbī	Wild
149	SAMEA111361026	60	*Hordeum vulgare subsp. spontaneum*	Iran, Āẕārbāyjān-e Ghārbī	Wild
058	SAMEA111361002	18	*Hordeum vulgare subsp. spontaneum*	Cyprus, Ammochostos	Wild
227	-	95	*Hordeum vulgare subsp. spontaneum*	Azerbaijan	Wild
229	-	96	*Hordeum vulgare subsp. spontaneum*	Azerbaijan	Wild
230	-	97	*Hordeum vulgare subsp. spontaneum*	Azerbaijan	Wild
232	SAMEA111360932	98	*Hordeum vulgare subsp. spontaneum*	Azerbaijan	Wild
355	SAMEA111361090	120	*Hordeum vulgare subsp. spontaneum*	Azerbaijan	Wild
217	SAMEA111361047	91	*Hordeum vulgare subsp. spontaneum*	Armenia, Erevan	Wild
036	SAMEA111360833	11	*Hordeum vulgare subsp. spontaneum*	Afghanistan, Herāt	Wild
LTR	-	121	*Hordeum vulgare subsp. Vulgare*		Domesticated
BEA	-	122	*Hordeum vulgare subsp. Vulgare*		Domesticated

FLE	-	123	*Hordeum vulgare subsp. Vulgare*	Domesticated
FRA	-	125	*Hordeum vulgare subsp. Vulgare*	Domesticated
GPR	-	124	*Hordeum vulgare subsp. Vulgare*	Domesticated
RGT	-	126	*Hordeum vulgare subsp. Vulgare*	Domesticated

Appendix 4.2. Gendex alpha-lattice design.

Trial 1						Trial 2						Trial 3					
Block1		Block2		Block3		Block1		Block2		Block3		Block1		Block2		Block3	
IR	DR	IR	DR	IR	DR	IR	DR	IR	DR	IR	DR	IR	DR	IR	DR	IR	DR
7	7	108	108	73	73	1	1	63	63	59	59	10	10	67	67	13	13
49	49	61	61	83	83	65	65	101	101	18	18	3	3	98	98	121	121
63	63	75	75	97	97	118	118	66	66	4	4	97	97	4	4	82	82
95	95	21	21	44	44	103	103	112	112	105	105	47	47	111	111	24	24
81	81	89	89	109	109	44	44	74	74	20	20	31	31	93	93	70	70
84	84	96	96	114	114	27	27	22	22	94	94	92	92	77	77	37	37
29	29	70	70	125	125	114	114	34	34	9	9	103	103	32	32	63	63
10	10	59	59	26	26	62	62	92	92	61	61	54	54	51	51	114	114
31	31	11	11	4	4	111	111	97	97	80	80	69	69	20	20	46	46
107	107	1	1	9	9	16	16	107	107	40	40	85	85	113	113	26	26
22	22	23	23	52	52	13	13	85	85	52	52	50	50	101	101	65	65
20	20	6	6	28	28	90	90	25	25	49	49	14	14	117	117	126	126
102	102	111	111	24	24	125	125	19	19	2	2	100	100	86	86	75	75
112	112	79	79	64	64	5	5	8	8	26	26	71	71	74	74	105	105
69	69	14	14	106	106	3	3	126	126	121	121	94	94	1	1	33	33
18	18	34	34	76	76	24	24	54	54	77	77	110	110	11	11	96	96
116	116	16	16	71	71	117	117	42	42	69	69	89	89	60	60	102	102
45	45	82	82	12	12	106	106	1	1	98	98	6	6	95	95	30	30
119	119	25	25	35	35	67	67	76	76	70	70	106	106	107	107	78	78
88	88	122	122	94	94	36	36	82	82	56	56	76	76	15	15	21	21

5	5	100	100	101	101	95	95	29	29	43	43	8	8	17	17	43	43
36	36	50	50	46	46	53	53	12	12	116	116	59	59	39	39	119	119
58	58	54	54	87	87	41	41	45	45	86	86	16	16	9	9	2	2
41	41	32	32	19	19	91	91	55	55	108	108	83	83	48	48	99	99
72	72	67	67	15	15	50	50	33	33	93	93	38	38	72	72	88	88
85	85	104	104	2	2	60	60	51	51	31	31	61	61	52	52	35	35
103	103	120	120	40	40	28	28	58	58	89	89	44	44	125	125	115	115
93	93	124	124	56	56	100	100	109	109	15	15	28	28	34	34	5	5
98	98	78	78	90	90	122	122	79	79	30	30	27	27	23	23	91	91
121	121	86	86	33	33	99	99	68	68	75	75	41	41	29	29	108	108
13	13	113	113	80	80	73	73	72	72	124	124	56	56	104	104	68	68
53	53	91	91	68	68	32	32	123	123	48	48	116	116	81	81	58	58
57	57	117	117	60	60	11	11	96	96	23	23	124	124	84	84	79	79
110	110	66	66	105	105	7	7	38	38	113	113	19	19	57	57	109	109
74	74	99	99	118	118	57	57	88	88	64	64	122	122	62	62	18	18
39	39	8	8	123	123	21	21	14	14	102	102	80	80	42	42	7	7
126	126	43	43	38	38	84	84	17	17	83	83	66	66	123	123	40	40
3	3	42	42	62	62	81	81	115	115	120	120	22	22	64	64	87	87
77	77	48	48	92	92	78	78	119	119	35	35	120	120	118	118	55	55
65	65	55	55	51	51	87	87	104	104	10	10	112	112	90	90	49	49
47	47	30	30	17	17	37	37	47	47	39	39	36	36	45	45	12	12
27	27	37	37	115	115	46	46	6	6	110	110	73	73	25	25	53	53

Appendix 4.3. Soil drying rates for Trial 1, Trial 2 and Trial 3.

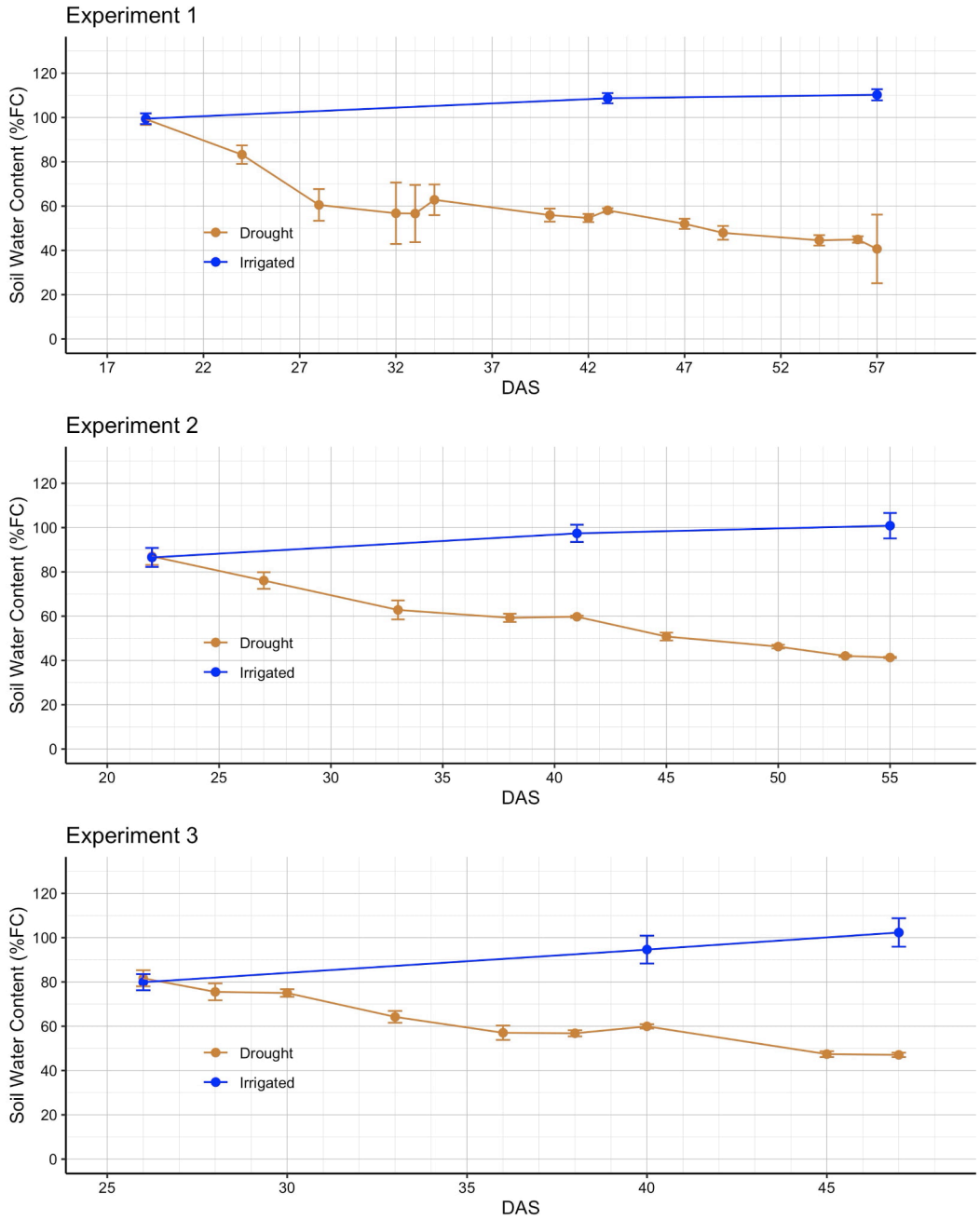

Appendix 4.4. 3D linear trend surfaces.

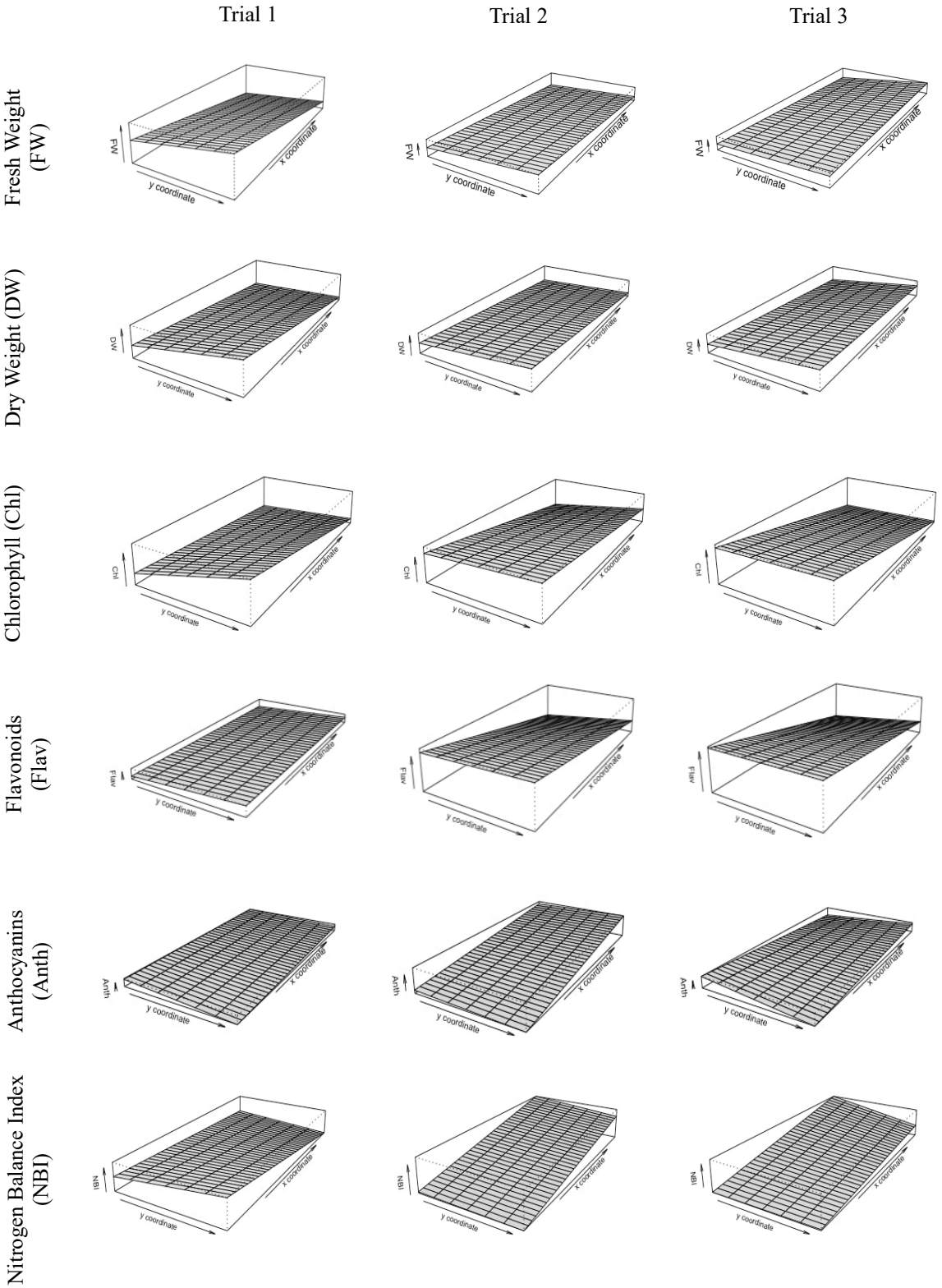

Appendix 4.5. 2D Residual raster plots for biomass and pigment traits.

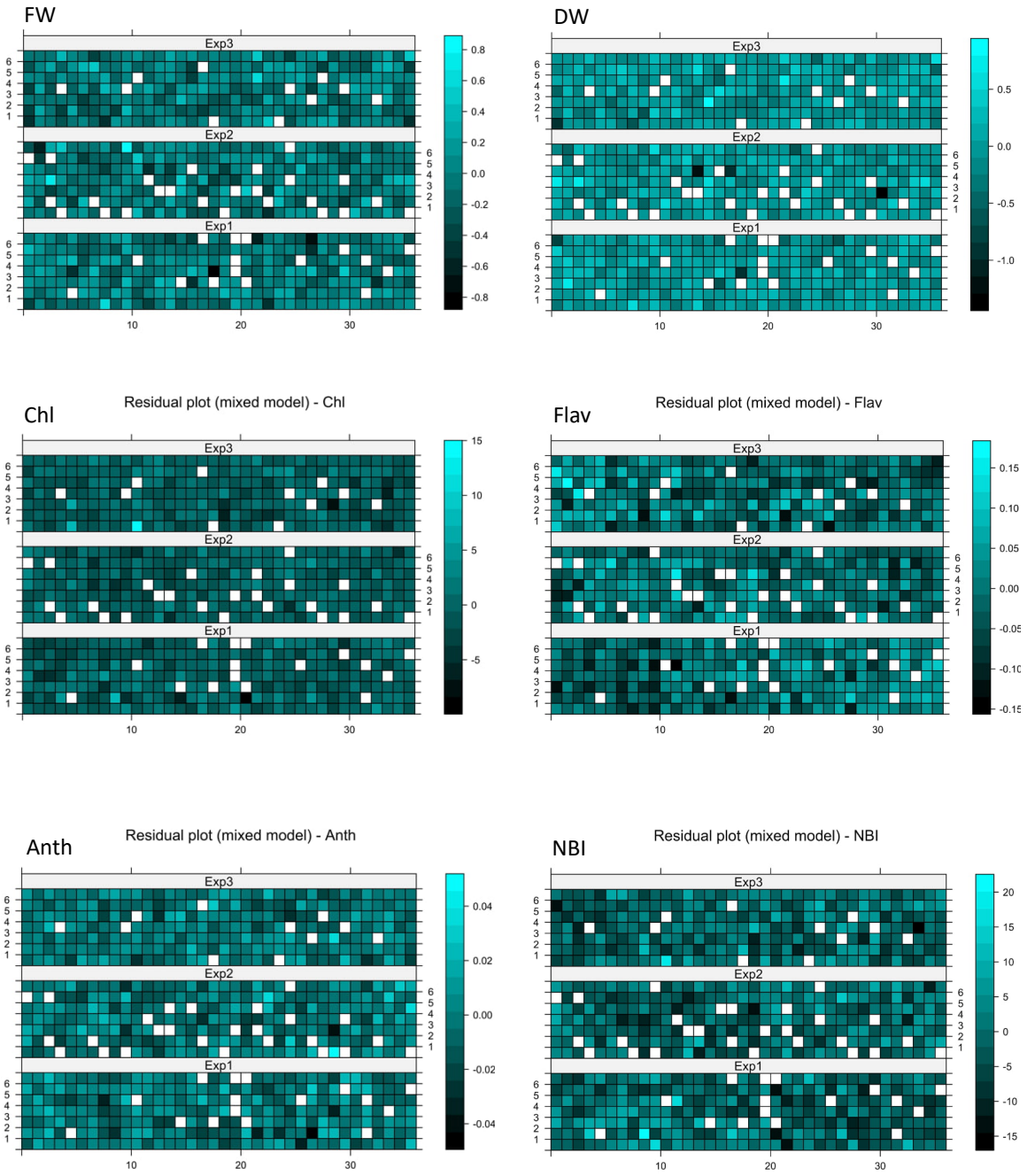

Appendix 4.6. Value distribution as density plots for primary traits.

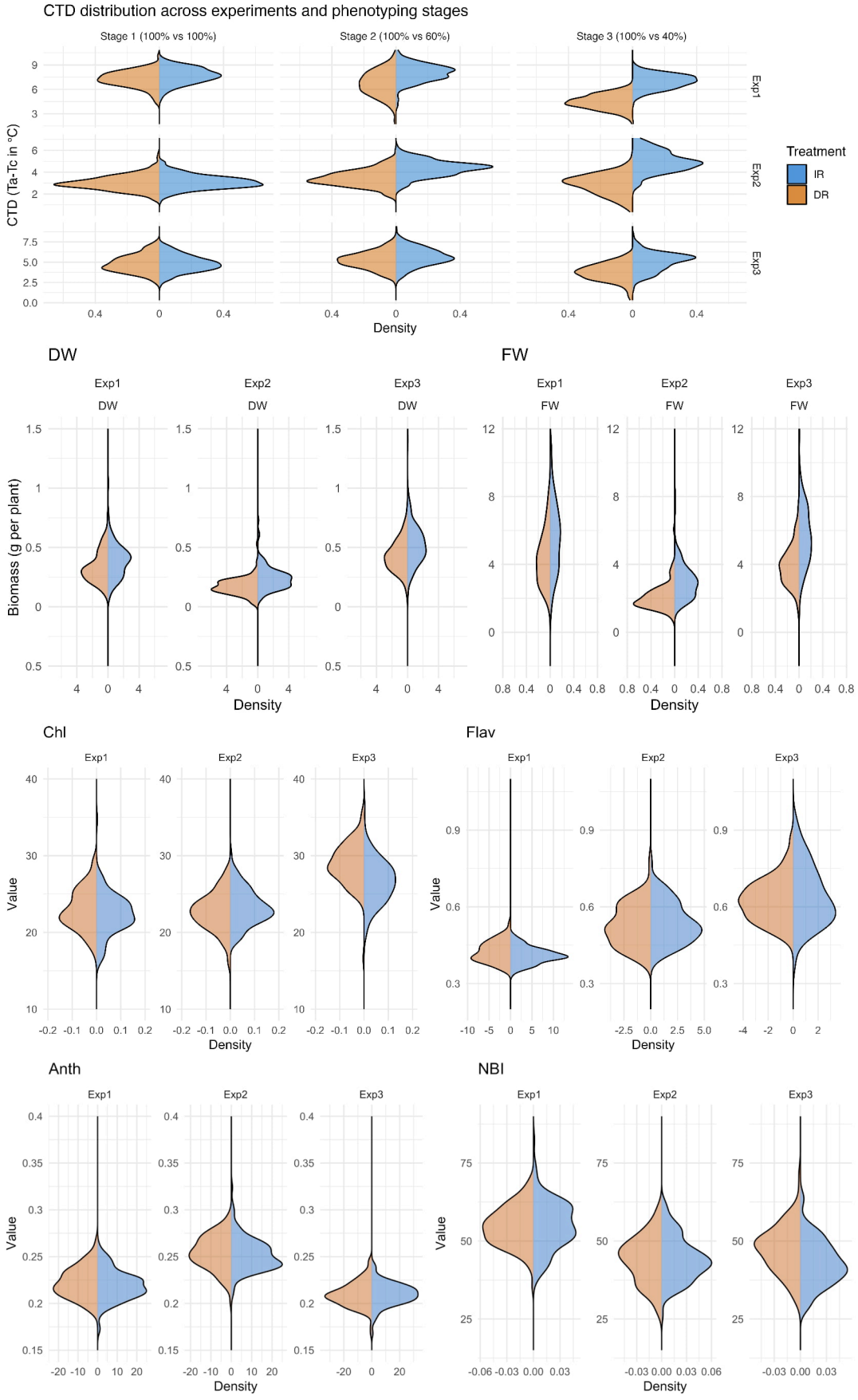

Appendix 4.7. Statistical analyses.

	CTD				
Source of variance	**df1**	**df2⁺**	**F.ratio**	**p-value**	
Ta	1	Inf	1615.5	<.0001	***
Treatment	1	Inf	52.3	<.0001	***
Stage	2	Inf	231.7	<.0001	***
Genotype	123	Inf	2.9	<.0001	***
Treatment:Stage	2	Inf	659.9	<.0001	***
Treatment:Genotype	123	Inf	0.6	0.9997	
Stage:Genotype	246	Inf	2	<.0001	***
Treatment:Stage:Genotype	246	Inf	1.4	<.0001	***

, **,*: Significance at P< 0.05, P<0.01 or P<0.001, respectively. ⁺df2 = denominator degrees of freedom is assumed infinite due to the large number of observations (>6000). The z-distribution is used instead of the t-distribution for p-value calculations.*

	FW					DW				
Source of variance	**df1**	**df2⁺**	**F.ratio**	**p-value**		**df1**	**df2⁺**	**F.ratio**	**p-value**	
x coordinate	1	5.1	28.5	0.0029	**	1	5.4	59.3	0.0004	***
y coordinate	1	448.3	29.7	<.0001	***	1	448.8	46.7	<.0001	***
Genotype	123	448.2	2.8	<.0001	***	123	448.6	2.9	<.0001	***
Treatment	1	415.1	215.7	<.0001	***	1	364.6	86.5	<.0001	***
Experiment	2	448	438.2	<.0001	***	2	448.5	512	<.0001	***
Genotype:Treatment	123	447.9	0.8	0.9546		123	448.3	0.8	0.9644	

*, **,***: Significance at P< 0.05, P<0.01 or P<0.001, respectively. ⁺df2 = denominator degrees of freedom approximated with Satterwaitte's method.

	Chl					Flav				
Source of variance	**df1**	**df2⁺**	**F.ratio**	**p-value**		**df1**	**df2⁺**	**F.ratio**	**p-value**	
x coordinate	1	4.7	52.8	0.001	**	1	5.3	65.4	0.0003	***
y coordinate	1	448.4	11.9	0.0006	***	1	446.7	20.4	<.0001	***
Genotype	123	447.5	1.9	<.0001	***	123	446.3	2	<.0001	***
Treatment	1	264.8	20.2	<.0001	***	1	370.1	0.2	0.6642	
Experiment	2	448	315.9	<.0001	***	2	446.5	710.8	<.0001	***
Genotype:Treatment	123	447.8	0.7	0.9942		123	446.3	0.9	0.7846	

*, **,***: Significance at P< 0.05, P<0.01 or P<0.001, respectively. ⁺df2 = denominator degrees of freedom approximated with Satterwaitte's method.

	Anth					NBI				
Source of variance	**df1**	**df2⁺**	**F.ratio**	**p-value**		**df1**	**df2⁺**	**F.ratio**	**p-value**	
x coordinate	1	6.2	8.7	0.0247		1	5.9	3.7	0.104	
y coordinate	1	448.4	1.5	0.2186		1	447.1	1.9	0.1679	
Genotype	123	442.3	1.2	0.1502		123	446.6	2.1	<.0001	***
Treatment	1	225.1	0.7	0.404		1	347	6.1	0.0141	
Experiment	2	448.1	492.5	<.0001	***	2	446.9	185.2	<.0001	***
Genotype:Treatment	123	447.8	1.1	0.3419		123	446.6	1	0.4403	

*, **,***: Significance at P< 0.05, P<0.01 or P<0.001, respectively. ⁺df2 = denominator degrees of freedom approximated with Satterwaitte's method.

Appendix 5.1. Barley pangenome V1 passport data (Jayakodi *et al.*, 2020).

Group	Subspecies (ssp)	Accession	Name	Status	Country of origin	Row type	Awn roughness
pangenome_V1	*vulgare*	HOR_10596	Igri	cultivar	DEU	2-rowed	rough
pangenome_V1	*vulgare*	HOR_12046	Akashinriki	cultivar	JPN	6-rowed	rough
pangenome_V1	*vulgare*	HOR_13170	Barke	cultivar	DEU	2-rowed	rough
pangenome_V1	*vulgare*	HOR_13821	ESKISHEHIR	landrace	TUR	2-rowed	rough
pangenome_V1	*vulgare*	HOR_13942	BAEZA	landrace	ESP	6-rowed	rough
pangenome_V1	*vulgare*	HOR_3081	Slaski II	cultivar	POL	6-rowed	rough
pangenome_V1	*vulgare*	HOR_3365		landrace	RUS	6-rowed	rough
pangenome_V1	*vulgare*	HOR_7552		landrace	PAK	6-rowed	rough
pangenome_V1	*vulgare*	HOR_9043		landrace	ETH	6-rowed	rough
pangenome_V1	*vulgare*	BCC_906	Morex	cultivar	USA	6-rowed	smooth
pangenome_V1	*vulgare*	HOR_21599	ICARDA 64 SP, P	landrace	SYR	2-rowed	smooth
pangenome_V1	*vulgare*	HOR_8148		landrace	TUR	2-rowed	smooth
pangenome_V1	*vulgare*	BCC_1382	Golden Promise	cultivar	GBR	2-rowed	unkown
pangenome_V1	*vulgare*	OUN333	Chame 1	landrace	NPL	intermedium	unkown
pangenome_V1	*vulgare*	HOR_10350		landrace	ETH	6-rowed	unkown
pangenome_V1	*vulgare*	ZDM01467	dulihuang	landrace	CHN	6-rowed	unkown
pangenome_V1	*vulgare*	ZDM02064	ciba damai	landrace	CHN	6-rowed	unkown
pangenome_V1	*vulgare*	SFR85-014	RGT Planet	cultivar	DEU	2-rowed	unkown
pangenome_V1	*vulgare*	Hockett		cultivar	USA	2-rowed	unkown
pangenome_V1	*spontaneum*	FT11	B1K-04-12	wild	ISR	2-rowed	rough

Appendix 5.2. Sequence alignment of the 19 barley accessions in the pangenome V1 (Jayakodi *et al.*, 2020).

The alignment shows a SNP in position 1,898 bp of the *ROUGH AWN1* locus. The common name of each accession is enclosed in parenthesis.

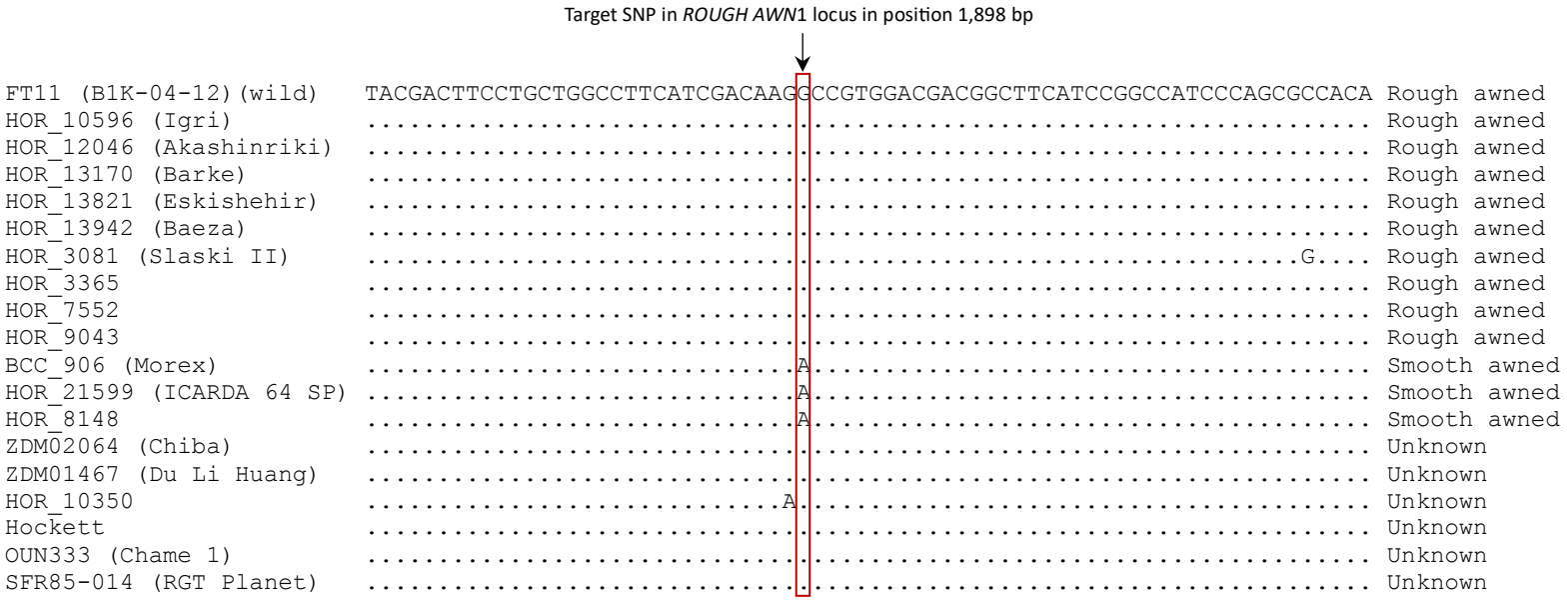

Appendix 5.3. Sequence alignment of the 19 barley accessions in the pangenome V1 (Jayakodi *et al.*, 2020).

The alignment shows a SNP in position 2,373 bp of the *ROUGH AWN1* locus. The common name of each accession is enclosed in parenthesis.

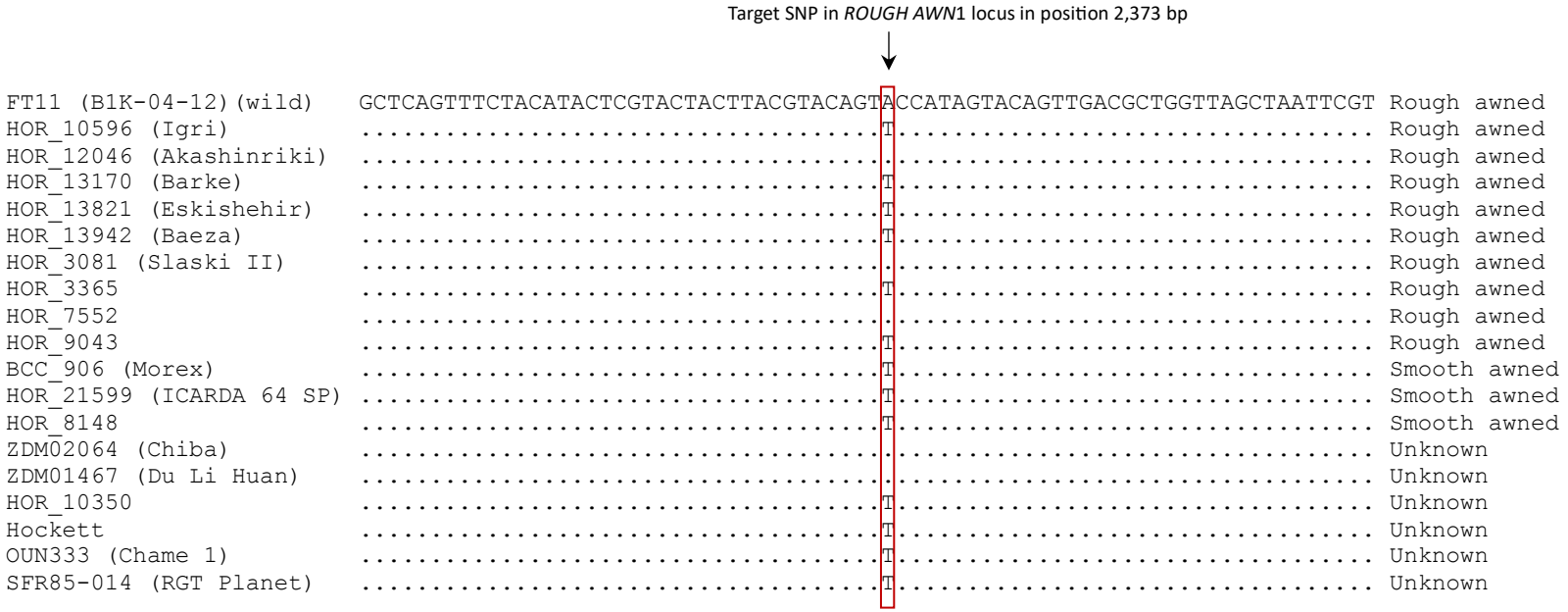

Appendix 5.4. HORVU.MOREX.r3.5HG0502720 gene.

Informative polymorphisms of the smooth awn trait are bold-highlighted. Exons are grey shaded.

>primary_assembly:MorexV3_pseudomolecules_assembly:5H:509668541:509671971:1

AGGATCACCCGGTTCCGGTTCCATCCTCAACTAAACACTGGAATGATGGACTGCGGACGGAATCAACCCGTCTCGTGCAAGTATATCC
TTAAAGCAAACACACCCTGAAACGAGTGGATGGACCACAGTAAACGTAGCTTTGCACTAGATAGCTAGTCCTACCACTTGGCTACACG
CTTTGCATGCCTCGACGGACGGCGAGTTGAAGTATCAACGCGTATATTCAAGTCACTGGAATGGAGGCACCCGTCAAAAAACATAAAG
GTCACCGGAGTAGTACCACGGGATGGGAGGCAGGCAGCTCAGCTAGGTCATAACAGCTAGTAGCTGTGAGGAAGCTACCACAGCTAAG
CTACGACGTACCCTCCCTGATTGGACGGGCGTCCGGTCTAGCGTTTCGGACTGACCGCCCGGGGCGGCCATGCATAGCGCCGGTATGT
ACCCCACGTATATACACATGCTCAATCGATCTATCAGACAGAGAGAGAGAGAGTTCACTGCGGTAAAACAAACACTTGTACTCCAGTT
GGTAGTGTACCATTCATCACGAACTCCTGTTGGCACGCCATGATATATACCCATCCATCCTTCTGCCCTGCCGGCACCCGGCTCGACG
CTTCCTTGCTACAAGTCGCCACCGGCACCACAACTGCTTTCCTTCCTCTCCACGCCCGGTACGCAGGGCAGTCGGCGGCTGAGCTAGC
TAGGAGGCATGCAGGGCGACGGCGGAGGGATGGAGGAGACAGCGGCGGCGGGCCAGGGCCGCAGCGGCGGCGGTGCTGCTGAGGGCGC
CGCCGTGGTGGTGCAGGAGGGGCCTCGGTTCCGGCGGGTGTGCGTGTTCTGCGGGAGCAGCTCCGGGAAGCGCAGCAGCTACCGCGAC
GCCGCCGTCGAGCTCGGCAAGGAGCTGGTACGTACGCAACCCACGGTCAAGCTAATCACACACGTTTTGTGCATGATGTTTGGTTAGT
TAGTTACCCAATTAGTTAAGCATGTGGATCATGCGTGTGTGGTGGCAGGTTGCTCGTCGGATGGATCTGGTGTACGGCGGGGGCAGCC
TGGGGCTCATGGGGGAGGTCTCGGAGGCCGTCCACAAGGCCGGCGGCCACGTTATCGGGGTGAGTCGATCCGTGCACGCACGCACGCAC
CTACGTACGTACACACCCTCTGCTTGCATTATTGTCATCGGCCCGGCCATCGTGTGCTTCTTTTCTCTCTTATTCTACTGGATCTACT
GTAGCCACCTTTCTGTCGACACTGAAGTTTCTCCGACTGGCTTAACAGTATCCTTGCCCAACTTGCTCACGACAGTCGCCTTCTGCTT
TTTCTTTTGATGTGCAGCGTCATACCTACCACTCTCATGGGCAAGGAGGTACGTGCAACACGATTGAGATCGATGCATCGACACCACA
TACCCCCAACCACAGGACAGGAGTAGACTGTGCATGCATGCATGCTTGCATGCAGTAGCGGAGTAGCCGTAGCTTGTACACTAATGTA
GTGTACTGACAAACTAATGTAATTCATGCATGCAAAATGGAACAGATCACGGGGGAGACGGTGGGGGAGGTGGCGGCGGTGTCGGGGA
TGCACGAGCGGAAGGCGGCGATGGCGCGCAACGCCGACGCCTTCATCGCGCTGCCGGGAGGCTACGGCACCCTGGACGAGCTGCTGGA
GGTCATCGCCTGGGCGCAGCTCGGCATCCACACAAAACCAGTTAAGCAGCTATATATGATATATATACTGTACAGTATTCATCAATCG
ACTTGCCTAGCTAACCCATTGGCCGTAGTACGTAGCTATTTAGCTTTGCTGATGGCGGATGGATGGGTGCATGCATGCAGGTGGGGCT
GCTGAACGTGGAGGGGTACTACGACTTCCTGCTGGCCTTCATCGACAAGACCGTGGACGACGGCTTCATCCGGCCATCCCAGCGCCAC
ATCTTCGTCAGCGCGCCCGACGCCAGGGACCTCGTCCACAAGCTCGAGGTAACTATCTAACTGATGATCAATCACCATCTCTCGCTCT
TCACATCTTTCATGCATGCACCCATCCCAGCGCCACATCTTTCATGCATGCACGGTGGTTACCATCTCAGTCACATGACTTGTCCCTG
TCTGGGTCTCCCTCCGTTTCCGTGTGCACAACGGCATGCATGCATCTGCTTCCACGGAGTAATTCCCACCCAGTTCCGGGCTCGTTGT
GCCTACTCTAGCTAGTAGAGTCGTGCTGGTCCTAGCTAGCTAGCGGGCAGCACGTGTCGAGCTGCAACCTGCAAGTTGGAAGTTTCTC
GGCCATCGGCTGTGTACCCATCCACCAAAAGTTTCCACGACGCCACAGCTCAGTTTCTACATACTCGTACTACTTACGTACAGTTTCCA
TAGTACAGTTGACGCTGGTTAGCTAATTCGTTTGGGGTTGCAGGAGTACGTGGCGGTGGAGGAGGAGGACCCGGCGACGCCCAAGCTG
CGGTGGGAGATCGAGCAGGTCGGCTACAACGCCACGCTCCAGGCAGAGATCGCCCGCTGATCCACCTACGACTTGGTTAAATTACTGG
TCCTATAGTGGATGGGACCAACTGGTTACTGGTCCGCTCCGCTAGTGGTTAATTAAGTACACTAGTTTAATGCTACTACCGCACGTAC
GGCATGCATGCATGCATGTGTAAGAAGGGCACGTTACAGTTTGTGCTTGCTAAAAAACTTTAGTGGTACTACTCCTGTTGGCTGACGA
ATGGGTGTGTGTAATAGCGTGTGTATTTTGATGATGTACTACTACCTGGCTGGAACAGTGCGTGGTGTGTGTGGCGCGTATATGCAAT
AATTGTTCCTTCAGCATTTGTCCGGAATAATTTGTGCAATGCGTTTTTCTTTCTCTTGCTTCTTTGACGGGATATTTACGCTGTGAGT
TTGTGCTGAAGCTATAGTTAGTTGTTGTTCTAGTTTGACCTCCATCTACGCTCGATCGAATTGATCCCGTCAGTGCTAGTTTTGGTTG
CTAGTTGGATAGTTAATTTGTTCGAATTAGCTAGAGGTGAGTTTCCTGATTTTAGAATTTGGGTCAGTTGATACGGGGCAGAAAAAAG
CAGGTGAGAAGGCACAACACACCAAGGCAGCTAATGACGGCGTCGAGGCGACCATAGTGAGGCCTCACCCATGAACGAGCCACAGTCG
GTGCTGAGCCAACTGAGGCGAGTTCGAAGACCAACGAGTGTGGCTGCAGGGGCGGGAGCTGCTAGCTTCTGAATTGGAAGTCAGCAGA
GGAAAAAGGGTGGAAGGGAGAGCAGAGCGATGAGGCTGACGCAGGAGCATCGACGGTCAAGGGCAGTCAACTTAACATTCAAGAAAGC
ATAGGCTTTGATACACCTTCTTATATCCCGACATTTAAGAACTTTTGTATTTTTTGTTTCTTTCACATAAAACAACATATGGATTTT

Appendix 5.5. Python script for the analysis of recognition sites across several accessions.

The script iterates through a list of DNA sequences and a list of recognition sites, searching for each recognition site within each DNA sequence. For each sequence, it records the number of occurrences of the recognition site and calculates the corresponding number of fragments generated. The results, along with the positions of the recognition sites, are compiled into a formatted string and appended to a list.

Inputs are provided in three separate files in plain text format:

1. A list of DNA sequences → rough_awn_list_forward_strand.txt
2. A list of Genotypes → genotypes_list.txt
3. A list of Recognition sites (in IUPAC code) → recognition_sites.txt

The script returns the number of fragments and the position of the recognition pattern in the DNA sequence.

```
############################## Start ############################
### Import libraries
import Bio
import numpy as np
import os
from Bio.Seq import Seq
from Bio.SeqUtils import nt_search

### Load text files
mylist = open('rough_awn_list_forward_strand.txt').read().splitlines()
mylist_genotype = open('genotypes_list.txt').read().splitlines()
recognition_sites_list = open('recognition_sites.txt').read().splitlines() #This
recognition sites match with the file "dCAPs enzyme options.xlsx"

### Initialise master list and append heading
master_list = []
first_list = ["Genotype", "Enzyme recognition pattern (before dCAPs)", "DNA Sequence",
"No. of fragments", "Position_1",Position_2", "Position_3"]
master_list.append(str(first_list).lstrip('[').rstrip(']'))

### Main loop
for pattern in recognition_sites_list:
    pattern_seq = Seq(pattern)
    j = 0
    for DNA in mylist:
        second_list = []
        results = nt_search(str(DNA), pattern_seq)
        second_list.append(mylist_genotype[j])
        second_list.append(results[0])
        second_list.append(DNA)
        if len(results) > 1:
            num_frag = len(results[1:]) + 1 #For n pattern, there are n + 1 fragments.
            second_list.append(num_frag)
            for i in range(1, len(results)):
                second_list.append(results[i] + 1) # Adjusts the position by adding 1
        else:
            num_frag = len(results[1:]) + 1
            second_list.append(num_frag)
            second_list.append("none")
        third_list = ", ".join(repr(e) for e in second_list)

        master_list.append(third_list)
        j += 1
my_array = np.array(master_list)
       np.savetxt("restriction_sites_ForwardStrand.csv", my_array, delimiter=",",
fmt='%s')

############################## End ############################
```

Appendix 5.6. Summary of marker details and PCR reaction conditions of *Btr1*, *Qsd1,* and *ROUGH AWN1* markers.

Gene locus	Ensemble Gene ID	Marker	Primer ID	Primer sequence (5' to 3')†	PCR Annealing temperature	Restriction enzyme	IUPAC recognition pattern	Type	Mismatch change	Restriction pattern and total amplicon size	Resolving gel
Btr1	HORVU.MOREX.r3.3 HG0235600	M1	KR813338F247G264	TCGAGCACGCATCCGAC**G**GC	65 °C	HaeIII	GGCC	dCAPS	T>G	La Trobe: 80+44+14+13+ 7=158 Wild: 62+44+19+14+ 13+7=159	agarose 4%
			KR813338R388	TCAGAGCGAGCCACTCGT					-		
Qsd1	HORVU.MOREX.r3.5 HG0481320	M6	LC054183F2030	TTCCGGGATTTATGATCACC	60 °C	Taq1-v2	TCGA	CAPS	n/a	La Trobe: 75+133= 208 Wild: 57+18+133=20 8	agarose 3% + MetaPhor 1%
			LC054184R2218	AAAGTGGGAGTGCGTGTAGG							
ROUGH AWN1	HORVU.MOREX.r3.5 HG0502720	M4	5HG0502720-F1902	TGAAGCCGTCGTCCA**G**GG	62 °C	EcoO109I	RGGNCC Y	dCAPS	C>G	La Trobe: 72 Wild: 18+54=72	agarose 4%
			5HG0502720-R1847	CTGCTGAACGTGGAGGGGTA					-		

† Mismatch is highligthed in bold. No mismatch is required for CAPS marker *Qsd1* M6.

Appendix 5.7. Restriction patterns of the three molecular markers used for genotyping.

LTR and wild present homozygous alleles, whereas F1 hybrids are heterozygous. Dark bands are distinguishable in electrophoresis gel. Light grey bands are less visible due to the short fragment size.

ROUGH AWN1

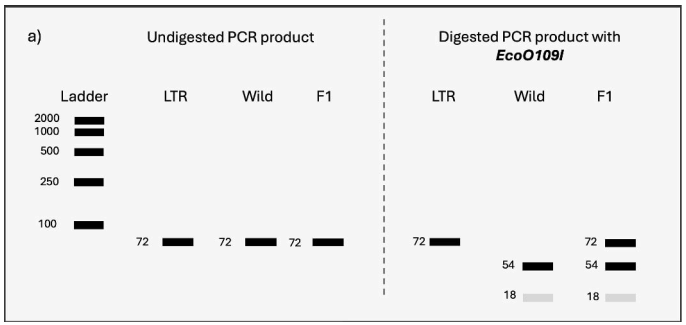

Qsd1

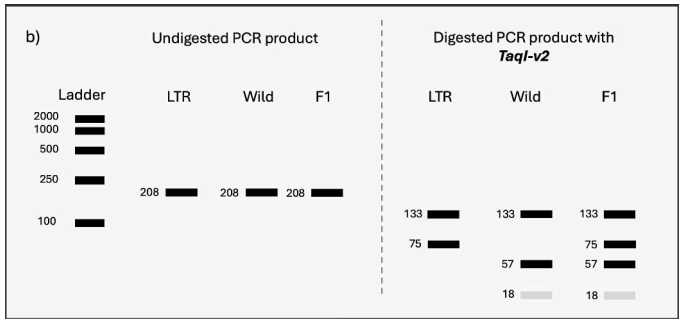

Btr1

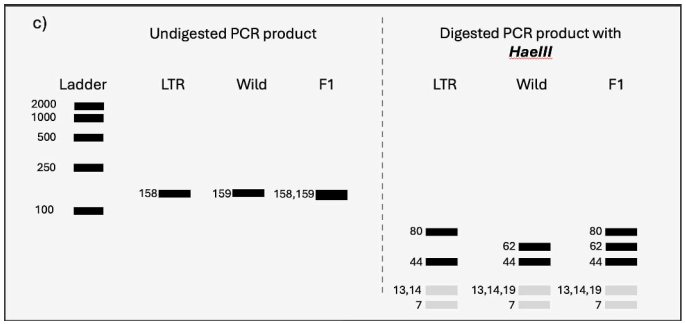

Appendix 5.8. Electrophoresis gels showing digested fragments of the *ROUGH AWN1*, *Qsd1*, and *Btr1* markers. A total of 31 plates were genotyped for each marker throughout the MABC program, with this figure displaying the results for plate number 4 of the BC2F1 generation. This figure serves as a visual reference for the appearance of the digested fragments on the gel.

ROUGH AWN1

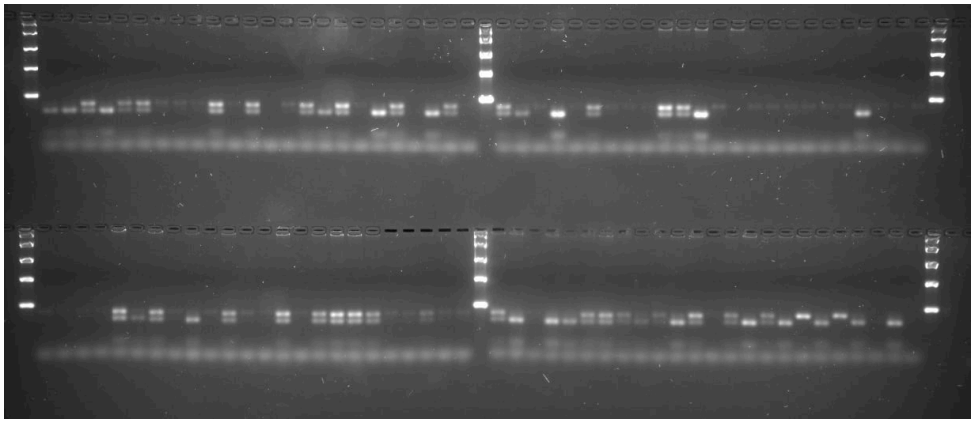

Qsd1

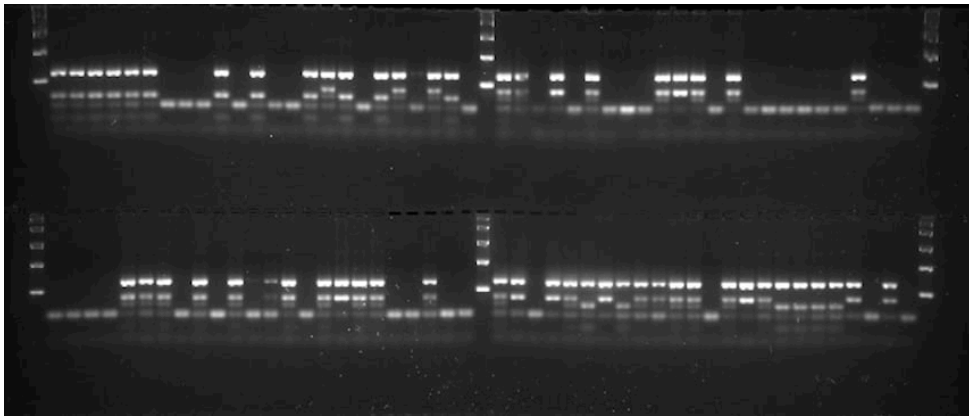

Btr1

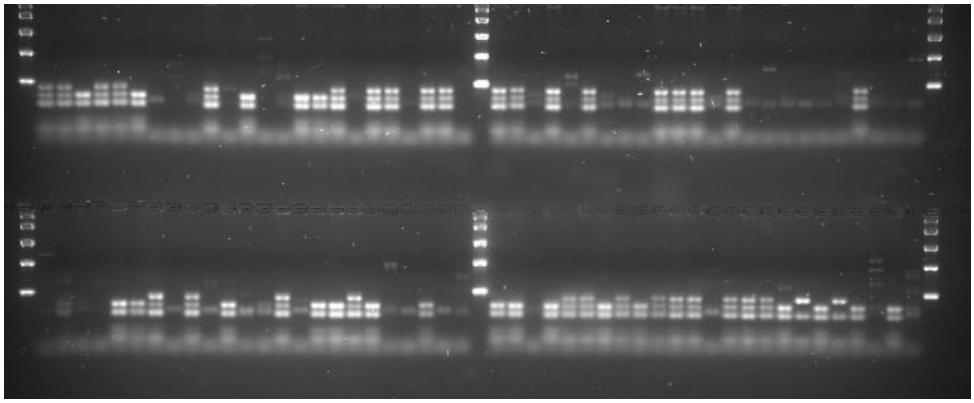

Appendix 5.9. Primer sequences for the amplification of a region spanning the causal SNP for awn roughness trait within the *ROUGH AWN1 l*ocus. The table includes primer pairs (1–5) with their respective forward and reverse primer sequences numerated from 1 to 9, template strand orientation, primer length, melting temperature (Tm), GC content, and the length of the amplified product.

Primer pair	Primer number	Primer ID	Sequence (5'->3')	Template strand	Primer length	Tm (°C)	GC%	Product length
1	P1	G0502720_F1614	AACGCCGACGCCTTCAT	Plus	17	59.7	58.8	706
	P5	G0502720_R2381	AGCTAACCAGCGTCAACTGT	Minus	20	59.6	50.0	
2	P1	G0502720_F1614	AACGCCGACGCCTTCAT	Plus	17	59.7	58.8	495
	P6	G0502720_R2086	GACAAGTCATGTGACTGAGATGG	Minus	23	59.1	47.8	
3	P2	G0502720_F1694	CGGCATCCACACAAAACCAG	Plus	20	60.0	55.0	897
	P7	G0502720_R2571	AGCGGACCAGTAACCAGTTG	Minus	20	60.0	55.0	
4	P4	G0502720_F1333	TGCAGCGTCATACCTACCAC	Plus	20	59.8	55.0	787
	P9	G0502720_R2100	ACCCAGACAGGGACAAGTCA	Minus	20	60.4	55.0	

Genotyping results of progeny from the BC1F1, BC2F1, and BC2F2 generations. HOW = Homozygous Wild, HOC = Homozygous Cultivated, HET= Heterozygous.

Progeny number per generation	Genotyping generation	Wild line	Genotyping ID			*ROUGH AWN1*	*Qsd1*	*Btr1*	Selection
			BC1F1	BC2F1	BC2F2				
1	BC1F1	WBDC-117	P1-A01	-	-	HOW	missing	missing	
2	BC1F1	WBDC-117	P1-B01	-	-	HOW	missing	missing	
3	BC1F1	WBDC-117	P1-C01	-	-	HET	missing	missing	
4	BC1F1	WBDC-117	P1-D01	-	-	HET	missing	missing	
5	BC1F1	WBDC-117	P1-E01	-	-	HOW	HOW	missing	
6	BC1F1	WBDC-117	P1-F01	-	-	HOW	HOW	missing	
7	BC1F1	WBDC-117	P1-G01	-	-	HET	HET	HET	
8	BC1F1	WBDC-117	P1-H01	-	-	HET	HET	HOW	
9	BC1F1	WBDC-117	P1-A02	-	-	HOW	missing	HET	
10	BC1F1	WBDC-117	P1-B02	-	-	HET	missing	HOW	
11	BC1F1	WBDC-117	P1-C02	-	-	HOW	HOW	HET	
12	BC1F1	WBDC-117	P1-D02	-	-	HOW	HOW	missing	
13	BC1F1	WBDC-117	P1-E02	-	-	HOW	HOW	HET	
14	BC1F1	WBDC-117	P1-F02	-	-	HOW	HOW	HOW	
15	BC1F1	WBDC-117	P1-G02	-	-	HET	HET	HET	
16	BC1F1	WBDC-117	P1-H02	-	-	HET	HOW	HET	
17	BC1F1	WBDC-117	P1-A03	-	-	missing	missing	HOW	
18	BC1F1	WBDC-117	P1-B03	-	-	HET	missing	HET	
19	BC1F1	WBDC-117	P1-C03	-	-	HOW	HET	HET	
20	BC1F1	WBDC-117	P1-D03	-	-	HET	HET	HET	Selected
21	BC1F1	WBDC-117	P1-E03	-	-	HET	HOW	HET	
22	BC1F1	WBDC-117	P1-F03	-	-	missing	HOW	HOW	
23	BC1F1	WBDC-117	P1-G03	-	-	HET	HOW	missing	
24	BC1F1	WBDC-117	P1-H03	-	-	HET	HOW	HOW	
25	BC1F1	WBDC-117	P1-A04	-	-	HET	HOW	HET	
26	BC1F1	WBDC-117	P1-B04	-	-	HOW	HET	HET	
27	BC1F1	WBDC-117	P1-C04	-	-	HOW	HET	HOW	
28	BC1F1	WBDC-117	P1-D04	-	-	HET	HET	HET	Selected
29	BC1F1	WBDC-117	P1-E04	-	-	HET	missing	HET	
30	BC1F1	WBDC-117	P1-F04	-	-	HET	HOW	HOW	
31	BC1F1	WBDC-117	P1-G04	-	-	HET	HOW	HOW	
32	BC1F1	WBDC-117	P1-H04	-	-	HOW	HET	HET	
33	BC1F1	WBDC-117	P1-A05	-	-	HET	HOW	missing	
34	BC1F1	WBDC-117	P1-B05	-	-	HOW	HOW	HET	
35	BC1F1	WBDC-117	P1-C05	-	-	HET	HET	HET	Selected

36	BC1F1	WBDC-117	P1-D05	-	-	HOW	HET	HOW
37	BC1F1	WBDC-117	P1-E05	-	-	HET	HOW	HOW
38	BC1F1	WBDC-117	P1-F05	-	-	HET	HOW	HOW
39	BC1F1	WBDC-117	P1-G05	-	-	HET	HET	HET
40	BC1F1	WBDC-117	P1-H05	-	-	HOW	HET	HET
41	BC1F1	WBDC-117	P1-A06	-	-	HET	HOW	HOW
42	BC1F1	WBDC-117	P1-B06	-	-	HET	HOW	HOW
43	BC1F1	WBDC-117	P1-C06	-	-	HET	HOW	HOW
44	BC1F1	WBDC-117	P1-D06	-	-	HOW	HET	HOW
45	BC1F1	WBDC-117	P1-E06	-	-	HOW	HET	HET
46	BC1F1	WBDC-117	P1-F06	-	-	HET	HET	HET
47	BC1F1	WBDC-117	P1-G06	-	-	HET	HET	HET
48	BC1F1	WBDC-117	P1-H06	-	-	HOW	HOW	HET
49	BC1F1	WBDC-117	P1-A07	-	-	HET	HET	HET
50	BC1F1	WBDC-117	P1-B07	-	-	HOW	HOW	HOW
51	BC1F1	WBDC-117	P1-C07	-	-	HET	HET	HET
52	BC1F1	WBDC-117	P1-D07	-	-	HET	HOW	HET
53	BC1F1	WBDC-117	P1-E07	-	-	HET	HET	HOW
54	BC1F1	WBDC-117	P1-F07	-	-	HOW	HOW	HET
55	BC1F1	WBDC-117	P1-G07	-	-	HET	HOW	missing
56	BC1F1	WBDC-117	P1-A08	-	-	HET	HET	HET
57	BC1F1	WBDC-117	P1-B08	-	-	HET	HOW	HET
58	BC1F1	WBDC-117	P1-C08	-	-	HET	HOW	HET
59	BC1F1	WBDC-117	P1-D08	-	-	HET	HET	HET
60	BC1F1	WBDC-117	P1-E08	-	-	HOW	HOW	HOW
61	BC1F1	WBDC-117	P1-F08	-	-	HET	HOW	HOW
62	BC1F1	WBDC-117	P1-G08	-	-	HOW	HOW	HOW
63	BC1F1	WBDC-117	P1-A09	-	-	HOW	HET	HOW
64	BC1F1	WBDC-117	P1-B09	-	-	HOW	HET	HOW
65	BC1F1	WBDC-117	P1-C09	-	-	HOW	HET	HET
66	BC1F1	WBDC-117	P1-D09	-	-	HOW	HOW	HOW
67	BC1F1	WBDC-117	P1-E09	-	-	HOW	HET	HET
68	BC1F1	WBDC-117	P1-F09	-	-	HOW	HOW	HOW
69	BC1F1	WBDC-117	P1-G09	-	-	HOW	HET	HOW
70	BC1F1	WBDC-117	P1-A10	-	-	HET	HET	HOW
71	BC1F1	WBDC-117	P1-B10	-	-	HOW	HET	HET
72	BC1F1	WBDC-117	P1-C10	-	-	HOW	HOW	HOW
73	BC1F1	WBDC-117	P1-D10	-	-	HOW	HOW	HET
74	BC1F1	WBDC-117	P1-E10	-	-	HET	HOW	HET
75	BC1F1	WBDC-117	P1-F10	-	-	HOW	HET	HOW
76	BC1F1	WBDC-117	P1-G10	-	-	HOW	HOW	HET
77	BC1F1	WBDC-117	P1-A11	-	-	HOW	HOW	HET
78	BC1F1	WBDC-117	P1-B11	-	-	HOW	HOW	HET

79	BC1F1	WBDC-117	P1-C11	-	-	HET	missing	HOW
80	BC1F1	WBDC-117	P1-D11	-	-	HET	HOW	HET
81	BC1F1	WBDC-117	P1-E11	-	-	HOW	HOW	missing
82	BC1F1	WBDC-117	P1-F11	-	-	HET	HOW	HOW
83	BC1F1	WBDC-117	P1-G11	-	-	HOW	HOW	HET
84	BC1F1	WBDC-117	P1-A12	-	-	missing	HOW	HOW
85	BC1F1	WBDC-117	P1-B12	-	-	HOW	missing	HET
86	BC1F1	WBDC-117	P1-C12	-	-	missing	HET	missing
87	BC1F1	WBDC-117	P1-D12	-	-	HET	HET	HET
88	BC1F1	WBDC-117	P1-E12	-	-	HET	missing	HET
89	BC1F1	WBDC-117	P1-F12	-	-	HET	HOW	HET
90	BC1F1	WBDC-117	P1-G12	-	-	missing	HOW	HET
91	BC1F1	WBDC-020	P2-A01	-	-	missing	HOC	missing
92	BC1F1	WBDC-020	P2-B01	-	-	HET	HOC	HOW
93	BC1F1	WBDC-020	P2-C01	-	-	HOW	HOC	HOW
94	BC1F1	WBDC-020	P2-D01	-	-	HET	HOC	HOW
95	BC1F1	WBDC-020	P2-E01	-	-	HET	HOC	HOW
96	BC1F1	WBDC-020	P2-F01	-	-	missing	HOC	missing
97	BC1F1	WBDC-020	P2-G01	-	-	HOW	HOC	HET
98	BC1F1	WBDC-020	P2-H01	-	-	HET	HOC	missing
99	BC1F1	WBDC-020	P2-A02	-	-	HOW	HOC	HOW
100	BC1F1	WBDC-020	P2-B02	-	-	HET	HOC	missing
101	BC1F1	WBDC-020	P2-C02	-	-	HET	HOC	missing
102	BC1F1	WBDC-020	P2-D02	-	-	HET	HOC	HOW
103	BC1F1	WBDC-020	P2-E02	-	-	missing	HOC	HOW
104	BC1F1	WBDC-020	P2-F02	-	-	HOW	HOC	HOW
105	BC1F1	WBDC-020	P2-G02	-	-	HOW	HOC	HET
106	BC1F1	WBDC-020	P2-H02	-	-	HET	HOC	HOW
107	BC1F1	WBDC-020	P2-A03	-	-	HOW	HOC	HOW
108	BC1F1	WBDC-020	P2-B03	-	-	missing	HOC	missing
109	BC1F1	WBDC-020	P2-C03	-	-	HOW	HOC	HOW
110	BC1F1	WBDC-020	P2-D03	-	-	missing	HOC	HET
111	BC1F1	WBDC-020	P2-E03	-	-	HET	HOC	HET
112	BC1F1	WBDC-020	P2-F03	-	-	HOW	HOC	HET
113	BC1F1	WBDC-020	P2-G03	-	-	HOW	HOC	HOW
114	BC1F1	WBDC-020	P2-H03	-	-	HET	HOC	HET
115	BC1F1	WBDC-020	P2-A04	-	-	HOW	HOC	HOW
116	BC1F1	WBDC-020	P2-B04	-	-	HET	HOC	HOW
117	BC1F1	WBDC-020	P2-C04	-	-	HOW	HOC	HOW
118	BC1F1	WBDC-020	P2-D04	-	-	HOW	HOC	HOW
119	BC1F1	WBDC-020	P2-E04	-	-	HET	HOC	HET
120	BC1F1	WBDC-020	P2-F04	-	-	HET	HOC	HOW
121	BC1F1	WBDC-020	P2-G04	-	-	HET	HOC	HOW

122	BC1F1	WBDC-020	P2-H04	-	-	HET	HOC	HET
123	BC1F1	WBDC-020	P2-A05	-	-	HET	HOC	HET
124	BC1F1	WBDC-020	P2-B05	-	-	HET	HOC	HET
125	BC1F1	WBDC-020	P2-C05	-	-	HOW	HOC	HET
126	BC1F1	WBDC-020	P2-D05	-	-	HET	HOC	HET
127	BC1F1	WBDC-020	P2-E05	-	-	HET	HOC	HET
128	BC1F1	WBDC-020	P2-F05	-	-	HET	HOC	HET
129	BC1F1	WBDC-020	P2-G05	-	-	HET	HOC	HET
130	BC1F1	WBDC-020	P2-H05	-	-	HET	HOC	HOW
131	BC1F1	WBDC-020	P2-A06	-	-	HET	HOC	missing
132	BC1F1	WBDC-020	P2-B06	-	-	HOW	HOC	HOW
133	BC1F1	WBDC-020	P2-C06	-	-	HOW	HOC	HET
134	BC1F1	WBDC-020	P2-D06	-	-	HET	HOC	HET
135	BC1F1	WBDC-020	P2-E06	-	-	HOW	HOC	HET
136	BC1F1	WBDC-020	P2-F06	-	-	HOW	HOC	HOW
137	BC1F1	WBDC-020	P2-G06	-	-	HOW	HOC	HET
138	BC1F1	WBDC-020	P2-H06	-	-	HOW	HOC	HOW
139	BC1F1	WBDC-020	P2-A07	-	-	HOW	HOC	missing
140	BC1F1	WBDC-020	P2-B07	-	-	HET	HOC	HOW
141	BC1F1	WBDC-020	P2-C07	-	-	HOW	HOC	HOW
142	BC1F1	WBDC-020	P2-D07	-	-	HOW	HOC	HOW
143	BC1F1	WBDC-020	P2-E07	-	-	missing	HOC	missing
144	BC1F1	WBDC-020	P2-F07	-	-	missing	HOC	HOW
145	BC1F1	WBDC-020	P2-G07	-	-	HET	HOC	HET
146	BC1F1	WBDC-020	P2-A08	-	-	HET	HOC	missing
147	BC1F1	WBDC-020	P2-B08	-	-	HET	HOC	HET
148	BC1F1	WBDC-020	P2-C08	-	-	HET	HOC	HET
149	BC1F1	WBDC-020	P2-D08	-	-	missing	HOC	HOW
150	BC1F1	WBDC-020	P2-E08	-	-	HET	HOC	HET
151	BC1F1	WBDC-020	P2-F08	-	-	HET	HOC	HOW
152	BC1F1	WBDC-020	P2-G08	-	-	HOW	HOC	HET
153	BC1F1	WBDC-020	P2-A09	-	-	HOW	HOC	HET
154	BC1F1	WBDC-020	P2-B09	-	-	HET	HOC	HOW
155	BC1F1	WBDC-020	P2-C09	-	-	HET	HOC	HOW
156	BC1F1	WBDC-020	P2-D09	-	-	HET	HOC	missing
157	BC1F1	WBDC-020	P2-E09	-	-	HOW	HOC	missing
158	BC1F1	WBDC-020	P2-F09	-	-	HET	HOC	HET
159	BC1F1	WBDC-020	P2-G09	-	-	HOW	HOC	HOW
160	BC1F1	WBDC-020	P2-A10	-	-	HOW	HOC	HET
161	BC1F1	WBDC-020	P2-B10	-	-	HOW	HOC	HOW
162	BC1F1	WBDC-020	P2-C10	-	-	HOW	HOC	HET
163	BC1F1	WBDC-020	P2-D10	-	-	HET	HOC	HOW
164	BC1F1	WBDC-020	P2-E10	-	-	HET	HOC	HET

165	BC1F1	WBDC-020	P2-F10	-	-	missing	HOC	missing	
166	BC1F1	WBDC-020	P2-G10	-	-	HET	HOC	HOW	
167	BC1F1	WBDC-020	P2-A11	-	-	HOW	HOC	HET	
168	BC1F1	WBDC-020	P2-B11	-	-	HOW	HOC	HOW	
169	BC1F1	WBDC-020	P2-C11	-	-	HET	HOC	HET	
170	BC1F1	WBDC-020	P2-D11	-	-	HET	HOC	HOW	
171	BC1F1	WBDC-020	P2-E11	-	-	HET	HOC	HOW	
172	BC1F1	WBDC-020	P2-F11	-	-	HET	HOC	HET	
173	BC1F1	WBDC-020	P2-G11	-	-	HET	HOC	HET	
174	BC1F1	WBDC-020	P2-A12	-	-	HET	HOC	HOW	
175	BC1F1	WBDC-020	P2-B12	-	-	HET	HOC	HOW	
176	BC1F1	WBDC-020	P2-C12	-	-	HET	HOC	HOW	
177	BC1F1	WBDC-020	P2-D12	-	-	HET	HOC	HOW	
178	BC1F1	WBDC-020	P2-E12	-	-	HET	HOC	HET	
179	BC1F1	WBDC-020	P2-F12	-	-	missing	HOC	HET	
180	BC1F1	WBDC-020	P2-G12	-	-	HOW	HOC	HET	
181	BC1F1	WBDC-038	P3-A09	-	-	HET	HET	HET	Selected
182	BC1F1	WBDC-038	P3-B12	-	-	HET	HET	HET	Selected
183	BC1F1	WBDC-038	P3-D01	-	-	HET	HET	HET	Selected
184	BC1F1	WBDC-038	P3-D04	-	-	HET	HET	HET	Selected
185	BC1F1	WBDC-038	P3-D05	-	-	HET	HET	HET	Selected
186	BC1F1	WBDC-038	P3-E12	-	-	HET	HET	HET	Selected
187	BC1F1	WBDC-199	P3-G12	-	-	HOW	HET	HET	
188	BC1F1	WBDC-199	P3-G05	-	-	HOW	HOW	HET	
189	BC1F1	WBDC-199	P3-G06	-	-	HET	HOW	HET	
190	BC1F1	WBDC-199	P3-H01	-	-	HOW	HOW	HET	
191	BC1F1	WBDC-199	P3-H04	-	-	HOW	HOW	HET	
192	BC1F1	WBDC-199	P3-H05	-	-	HET	HOW	HET	
193	BC1F1	WBDC-038	P3-A01	-	-	HET	HOW	HET	
194	BC1F1	WBDC-038	P3-A02	-	-	HET	HOW	HET	
195	BC1F1	WBDC-038	P3-A03	-	-	HOW	HET	HET	
196	BC1F1	WBDC-038	P3-A04	-	-	HET	HOW	HET	
197	BC1F1	WBDC-038	P3-A05	-	-	HET	HOW	HOW	
198	BC1F1	WBDC-038	P3-A06	-	-	HET	HET	HOW	
199	BC1F1	WBDC-038	P3-A07	-	-	HOW	HOW	HOW	
200	BC1F1	WBDC-038	P3-A08	-	-	HOW	HET	HET	
201	BC1F1	WBDC-038	P3-A10	-	-	HOW	HOW	HET	
202	BC1F1	WBDC-038	P3-A11	-	-	HOW	HET	HOW	
203	BC1F1	WBDC-038	P3-A12	-	-	HOW	HOW	HET	
204	BC1F1	WBDC-038	P3-B01	-	-	HOW	HOW	HOW	
205	BC1F1	WBDC-038	P3-B02	-	-	HOW	HOW	HET	
206	BC1F1	WBDC-038	P3-B03	-	-	HOW	HET	HOW	
207	BC1F1	WBDC-038	P3-B04	-	-	HET	HET	HOW	

208	BC1F1	WBDC-038	P3-B05	-	-	HET	HOW	HOW
209	BC1F1	WBDC-038	P3-B06	-	-	HOW	HOW	HET
210	BC1F1	WBDC-038	P3-B07	-	-	HOW	HOW	HOW
211	BC1F1	WBDC-038	P3-B08	-	-	HOW	HOW	HOW
212	BC1F1	WBDC-038	P3-B09	-	-	HOW	HET	HOW
213	BC1F1	WBDC-038	P3-B10	-	-	HET	HOW	HET
214	BC1F1	WBDC-038	P3-B11	-	-	HOW	HET	HOW
215	BC1F1	WBDC-038	P3-C01	-	-	HOW	HOW	HOW
216	BC1F1	WBDC-038	P3-C02	-	-	missing	missing	missing
217	BC1F1	WBDC-038	P3-C03	-	-	HOW	HOW	HET
218	BC1F1	WBDC-038	P3-C04	-	-	missing	missing	missing
219	BC1F1	WBDC-038	P3-C05	-	-	HET	HOW	HET
220	BC1F1	WBDC-038	P3-C06	-	-	missing	missing	missing
221	BC1F1	WBDC-038	P3-C07	-	-	HOW	HOW	HOW
222	BC1F1	WBDC-038	P3-C08	-	-	HOW	HOW	HOW
223	BC1F1	WBDC-038	P3-C09	-	-	HOW	HOW	HOW
224	BC1F1	WBDC-038	P3-C10	-	-	HOW	HET	HET
225	BC1F1	WBDC-038	P3-C11	-	-	HOW	HOW	HOW
226	BC1F1	WBDC-038	P3-C12	-	-	HET	HOW	HET
227	BC1F1	WBDC-038	P3-D02	-	-	HOW	HET	HOW
228	BC1F1	WBDC-038	P3-D03	-	-	HET	HOW	HET
229	BC1F1	WBDC-038	P3-D06	-	-	HET	HET	HOW
230	BC1F1	WBDC-038	P3-D07	-	-	HOW	HOW	HOW
231	BC1F1	WBDC-038	P3-D08	-	-	HOW	HOW	HOW
232	BC1F1	WBDC-038	P3-D09	-	-	HET	HET	HOW
233	BC1F1	WBDC-038	P3-D10	-	-	HOW	HET	HOW
234	BC1F1	WBDC-038	P3-D11	-	-	HOW	HET	HET
235	BC1F1	WBDC-038	P3-D12	-	-	HET	HOW	HOW
236	BC1F1	WBDC-038	P3-E01	-	-	HOW	HOW	HET
237	BC1F1	WBDC-038	P3-E02	-	-	missing	HOW	missing
238	BC1F1	WBDC-038	P3-E03	-	-	HET	HOW	HOW
239	BC1F1	WBDC-038	P3-E04	-	-	HOW	HET	HOW
240	BC1F1	WBDC-038	P3-E05	-	-	HET	HET	HOW
241	BC1F1	WBDC-038	P3-E06	-	-	HOW	HOW	HOW
242	BC1F1	WBDC-038	P3-E07	-	-	HET	HOW	HOW
243	BC1F1	WBDC-038	P3-E08	-	-	HOW	HET	HOW
244	BC1F1	WBDC-038	P3-E09	-	-	HOW	HOW	HOW
245	BC1F1	WBDC-038	P3-E10	-	-	HOW	HOW	HOW
246	BC1F1	WBDC-038	P3-E11	-	-	HOW	HOW	HET
247	BC1F1	WBDC-038	P3-F01	-	-	HOW	HOW	missing
248	BC1F1	WBDC-038	P3-F02	-	-	HOW	HOW	HOW
249	BC1F1	WBDC-038	P3-F03	-	-	missing	missing	missing
250	BC1F1	WBDC-038	P3-F04	-	-	missing	missing	missing

251	BC1F1	WBDC-038	P3-F05	-	-	HET	HOW	HET	
252	BC1F1	WBDC-038	P3-F06	-	-	HET	HET	HOW	
253	BC1F1	WBDC-038	P3-F07	-	-	HET	HOW	HOW	
254	BC1F1	WBDC-038	P3-F08	-	-	HET	HOW	HOW	
255	BC1F1	WBDC-038	P3-F09	-	-	HOW	HET	HET	
256	BC1F1	WBDC-038	P3-F10	-	-	HOW	HET	HOW	
257	BC1F1	WBDC-038	P3-F11	-	-	HOW	HOW	HOW	
258	BC1F1	WBDC-038	P3-F12	-	-	HOW	HET	HET	
259	BC1F1	WBDC-038	P3-G01	-	-	HET	HET	HOW	
260	BC1F1	WBDC-038	P3-G02	-	-	HET	HOW	HET	
261	BC1F1	WBDC-199	P3-G03	-	-	HET	HET	HOW	
262	BC1F1	WBDC-199	P3-G04	-	-	HET	HET	HOW	
263	BC1F1	WBDC-199	P3-G07	-	-	HOW	HET	HOW	
264	BC1F1	WBDC-199	P3-G08	-	-	HOW	HET	HOW	
265	BC1F1	WBDC-199	P3-G09	-	-	HOW	HOW	HOW	
266	BC1F1	WBDC-199	P3-G10	-	-	HET	HET	HOW	
267	BC1F1	WBDC-199	P3-G11	-	-	HET	HET	HOW	
268	BC1F1	WBDC-199	P3-H02	-	-	HOW	HOW	HOW	
269	BC1F1	WBDC-199	P3-H03	-	-	HET	HET	HOW	
270	BC1F1	WBDC-199	P3-H06	-	-	HET	HOW	HOW	
271	BC1F1	WBDC-199	P4-A01	-	-	HOW	HOW	HOW	
272	BC1F1	WBDC-199	P4-A02	-	-	HET	HOW	HOW	
273	BC1F1	WBDC-199	P4-A03	-	-	HOW	HOW	HOW	
274	BC1F1	WBDC-199	P4-A04	-	-	HOW	HOW	HOW	
275	BC1F1	WBDC-199	P4-A05	-	-	HOW	HET	HOW	
276	BC1F1	WBDC-199	P4-A06	-	-	HET	HOW	HOW	
277	BC1F1	WBDC-199	P4-A07	-	-	HET	HET	HOW	
278	BC1F1	WBDC-199	P4-A08	-	-	HET	HET	HET	Selected
279	BC1F1	WBDC-199	P4-A09	-	-	HOW	HOW	HET	
280	BC1F1	WBDC-199	P4-A10	-	-	HOW	HET	HET	
281	BC1F1	WBDC-199	P4-A11	-	-	HET	HET	HET	Selected
282	BC1F1	WBDC-199	P4-A12	-	-	HET	HOW	HOW	
283	BC1F1	WBDC-199	P4-B01	-	-	HET	HOW	HET	
284	BC1F1	WBDC-199	P4-B02	-	-	HOW	HET	HOW	
285	BC1F1	WBDC-199	P4-B03	-	-	HET	HET	HET	Selected
286	BC1F1	WBDC-199	P4-B04	-	-	HET	HET	HET	Selected
287	BC1F1	WBDC-199	P4-B05	-	-	missing	missing	missing	
288	BC1F1	WBDC-199	P4-B06	-	-	missing	missing	missing	
289	BC1F1	WBDC-199	P4-B07	-	-	HET	HET	HET	Selected
290	BC1F1	WBDC-199	P4-B08	-	-	HET	HET	HET	Selected
291	BC1F1	WBDC-199	P4-B09	-	-	missing	missing	missing	
292	BC1F1	WBDC-199	P4-B10	-	-	HET	HOW	HET	
293	BC1F1	WBDC-199	P4-B11	-	-	HET	HOW	HOW	

294	BC1F1	WBDC-199	P4-B12	-	-	HET	HET	HOW	
295	BC1F1	WBDC-199	P4-C01	-	-	HET	HET	HOW	
296	BC1F1	WBDC-199	P4-C02	-	-	HOW	HET	HOW	
297	BC1F1	WBDC-199	P4-C03	-	-	HOW	HOW	HET	
298	BC1F1	WBDC-199	P4-C04	-	-	HET	HET	HET	Selected
299	BC1F1	WBDC-199	P4-C05	-	-	missing	missing	missing	
300	BC1F1	WBDC-199	P4-C06	-	-	HET	HET	HOW	
301	BC1F1	WBDC-199	P4-C07	-	-	HET	HET	HOW	
302	BC1F1	WBDC-199	P4-C08	-	-	HET	HET	HET	Selected
303	BC1F1	WBDC-199	P4-C09	-	-	HET	HOW	HET	
304	BC1F1	WBDC-199	P4-C10	-	-	HET	HET	HOW	
305	BC1F1	WBDC-199	P4-C11	-	-	HOW	HOW	HET	
306	BC1F1	WBDC-199	P4-C12	-	-	HET	HET	HET	Selected
307	BC1F1	WBDC-199	P4-D01	-	-	HET	HET	HOW	
308	BC1F1	WBDC-199	P4-D02	-	-	HOW	HOW	HOW	
309	BC1F1	WBDC-199	P4-D03	-	-	HOW	HOW	HET	
310	BC1F1	WBDC-199	P4-D04	-	-	HOW	HOW	HOW	
311	BC1F1	WBDC-199	P4-D05	-	-	HET	HOW	HET	
312	BC1F1	WBDC-199	P4-D06	-	-	HOW	HOW	HOW	
313	BC1F1	WBDC-199	P4-D07	-	-	HET	HET	HOW	
314	BC1F1	WBDC-199	P4-D08	-	-	HET	HET	HET	Selected
315	BC1F1	WBDC-199	P4-D09	-	-	HOW	HOW	HET	
316	BC1F1	WBDC-199	P4-D10	-	-	HOW	HET	HET	
317	BC1F1	WBDC-199	P4-D11	-	-	HET	HET	HOW	
318	BC1F1	WBDC-199	P4-D12	-	-	HET	HET	HET	Selected
319	BC1F1	WBDC-048	P4-E01	-	-	HET	HOW	missing	
320	BC1F1	WBDC-048	P4-E02	-	-	HET	HET	missing	
321	BC1F1	WBDC-048	P4-E03	-	-	HET	HOW	HET	Selected
322	BC1F1	WBDC-048	P4-E04	-	-	HOW	HOW	HOW	
323	BC1F1	WBDC-048	P4-E05	-	-	HOW	HOW	HOW	
324	BC1F1	WBDC-048	P4-E06	-	-	HOW	HOW	HET	
325	BC1F1	WBDC-048	P4-E07	-	-	HOW	HOW	HOW	
326	BC1F1	WBDC-048	P4-E08	-	-	HOW	HOW	HET	
327	BC1F1	WBDC-048	P4-E09	-	-	HOW	HET	HET	
328	BC1F1	WBDC-048	P4-E10	-	-	HET	HET	HOW	
329	BC1F1	WBDC-048	P4-E11	-	-	HOW	HET	HOW	
330	BC1F1	WBDC-048	P4-E12	-	-	HOW	HET	HOW	
331	BC1F1	WBDC-048	P4-F01	-	-	HOW	HOW	missing	
332	BC1F1	WBDC-048	P4-F02	-	-	HOW	HET	HET	
333	BC1F1	WBDC-048	P4-F03	-	-	HET	HOW	HET	Selected
334	BC1F1	WBDC-048	P4-F04	-	-	HET	HOW	HOW	
335	BC1F1	WBDC-048	P4-F05	-	-	HET	HOW	HOW	
336	BC1F1	WBDC-048	P4-F06	-	-	HOW	HET	HET	

337	BC1F1	WBDC-048	P4-F07	-	-	HOW	HET	HET	
338	BC1F1	WBDC-048	P4-F08	-	-	HET	HOW	HET	Selected
339	BC1F1	WBDC-048	P4-F09	-	-	HOW	HOW	HET	
340	BC1F1	WBDC-048	P4-F10	-	-	HOW	HET	HET	
341	BC1F1	WBDC-048	P4-F11	-	-	HET	HOW	HOW	
342	BC1F1	WBDC-048	P4-F12	-	-	HOW	HOW	HET	
343	BC1F1	WBDC-048	P4-G01	-	-	HOW	HET	HET	
344	BC1F1	WBDC-048	P4-G02	-	-	HET	HOW	HET	Selected
345	BC1F1	WBDC-048	P4-G03	-	-	HET	HET	HOW	
346	BC1F1	WBDC-048	P4-G04	-	-	HET	HET	HOW	
347	BC1F1	WBDC-048	P4-G05	-	-	HET	HET	HOW	
348	BC1F1	WBDC-048	P4-G06	-	-	HET	HOW	HOW	
349	BC1F1	WBDC-048	P4-G07	-	-	HOW	HET	HOW	
350	BC1F1	WBDC-048	P4-G08	-	-	HOW	HET	HET	
351	BC1F1	WBDC-048	P4-G09	-	-	HOW	HOW	HOW	
352	BC1F1	WBDC-048	P4-G10	-	-	HET	HET	HOW	
353	BC1F1	WBDC-048	P4-G11	-	-	HET	HOW	HET	
354	BC1F1	WBDC-048	P4-G12	-	-	HOW	HET	HOW	
355	BC1F1	WBDC-048	P4-H01	-	-	HET	HOW	HOW	
356	BC1F1	WBDC-048	P4-H02	-	-	HET	HET	HOW	
357	BC1F1	WBDC-048	P4-H03	-	-	HET	HET	HOW	
358	BC1F1	WBDC-048	P4-H04	-	-	HET	HOW	HOW	
359	BC1F1	WBDC-048	P4-H05	-	-	HET	HOW	HET	
360	BC1F1	WBDC-048	P4-H06	-	-	HET	HOW	HOW	
361	BC1F1	WBDC-048	P5-A01	-	-	missing	HOW	missing	
362	BC1F1	WBDC-048	P5-A02	-	-	HET	HOW	HET	
363	BC1F1	WBDC-048	P5-A03	-	-	HET	HOW	HET	
364	BC1F1	WBDC-048	P5-A04	-	-	HET	HOW	HOW	
365	BC1F1	WBDC-048	P5-A05	-	-	HET	HET	HOW	
366	BC1F1	WBDC-048	P5-A06	-	-	HET	HOW	HOW	
367	BC1F1	WBDC-048	P5-A07	-	-	HET	HET	HET	Selected
368	BC1F1	WBDC-048	P5-A08	-	-	HET	HOW	HOW	
369	BC1F1	WBDC-048	P5-A09	-	-	HET	HET	HET	Selected
370	BC1F1	WBDC-048	P5-A10	-	-	HET	HOW	HET	
371	BC1F1	WBDC-048	P5-A11	-	-	HOW	HET	HOW	
372	BC1F1	WBDC-048	P5-A12	-	-	HET	HOW	HET	
373	BC1F1	WBDC-107	P5-B01	-	-	HET	HOW	HET	
374	BC1F1	WBDC-107	P5-B02	-	-	HET	HOW	HET	
375	BC1F1	WBDC-107	P5-B03	-	-	missing	missing	missing	
376	BC1F1	WBDC-107	P5-B04	-	-	HET	HOW	HOW	
377	BC1F1	WBDC-107	P5-B05	-	-	HET	HOW	HOW	
378	BC1F1	WBDC-107	P5-B06	-	-	HET	HOW	HOW	
379	BC1F1	WBDC-107	P5-B07	-	-	HET	HET	HET	Selected

380	BC1F1	WBDC-107	P5-B08	-	-	HET	HET	HET	Selected
381	BC1F1	WBDC-107	P5-B09	-	-	HET	HET	HOW	
382	BC1F1	WBDC-107	P5-B10	-	-	HOW	HOW	HOW	
383	BC1F1	WBDC-107	P5-B11	-	-	HET	HET	HET	Selected
384	BC1F1	WBDC-107	P5-B12	-	-	HET	HET	HET	Selected
385	BC1F1	WBDC-107	P5-C01	-	-	HET	HOW	HOW	
386	BC1F1	WBDC-107	P5-C02	-	-	HOW	HET	HET	
387	BC1F1	WBDC-107	P5-C03	-	-	HOW	HOW	missing	
388	BC1F1	WBDC-107	P5-C04	-	-	HET	HET	HOW	
389	BC1F1	WBDC-107	P5-C05	-	-	HET	HET	HOW	
390	BC1F1	WBDC-107	P5-C06	-	-	HOW	HET	HET	
391	BC1F1	WBDC-107	P5-C07	-	-	HET	HET	HOW	
392	BC1F1	WBDC-107	P5-C08	-	-	HET	HET	HET	Selected
393	BC1F1	WBDC-107	P5-C09	-	-	HET	HET	HOW	
394	BC1F1	WBDC-107	P5-C10	-	-	missing	HOW	HOW	
395	BC1F1	WBDC-107	P5-C11	-	-	HOW	HET	HOW	
396	BC1F1	WBDC-107	P5-C12	-	-	missing	HOW	missing	
397	BC1F1	WBDC-107	P5-D01	-	-	HET	HOW	HOW	
398	BC1F1	WBDC-107	P5-D02	-	-	HOW	HET	HOW	
399	BC1F1	WBDC-107	P5-D03	-	-	HOW	HOW	HET	
400	BC1F1	WBDC-107	P5-D04	-	-	HOW	HOW	HOW	
401	BC1F1	WBDC-107	P5-D05	-	-	missing	missing	missing	
402	BC1F1	WBDC-107	P5-D06	-	-	HET	HOW	HOW	
403	BC1F1	WBDC-107	P5-D07	-	-	HET	HET	HOW	
404	BC1F1	WBDC-107	P5-D08	-	-	HET	HET	HET	Selected
405	BC1F1	WBDC-107	P5-D09	-	-	HET	HET	HET	Selected
406	BC1F1	WBDC-107	P5-D10	-	-	HET	HET	HOW	
407	BC1F1	WBDC-107	P5-D11	-	-	HET	HET	HET	Selected
408	BC1F1	WBDC-107	P5-D12	-	-	missing	HOW	missing	
409	BC1F1	WBDC-107	P5-E01	-	-	HET	HOW	missing	
410	BC1F1	WBDC-107	P5-E02	-	-	HET	HOW	HOW	
411	BC1F1	WBDC-107	P5-E03	-	-	missing	HOW	missing	
412	BC1F1	WBDC-107	P5-E04	-	-	HOW	HET	HOW	
413	BC1F1	WBDC-107	P5-E05	-	-	HOW	HET	HOW	
414	BC1F1	WBDC-107	P5-E06	-	-	HET	HET	HOW	
415	BC1F1	WBDC-107	P5-E07	-	-	HET	HOW	HOW	
416	BC1F1	WBDC-107	P5-E08	-	-	missing	missing	missing	
417	BC1F1	WBDC-107	P5-E09	-	-	missing	missing	missing	
418	BC1F1	WBDC-107	P5-E10	-	-	missing	missing	missing	
419	BC1F1	WBDC-107	P5-E11	-	-	missing	missing	missing	
420	BC1F1	WBDC-107	P5-E12	-	-	missing	missing	missing	
421	BC1F1	WBDC-107	P5-F01	-	-	HET	HOW	missing	
422	BC1F1	WBDC-068	P5-F02	-	-	HET	HOW	HOW	

423	BC1F1	WBDC-068	P5-F03	-	-	HET	HET	HET	Selected
424	BC1F1	WBDC-068	P5-F04	-	-	HOW	HOW	HOW	
425	BC1F1	WBDC-068	P5-F05	-	-	HET	HET	HOW	
426	BC1F1	WBDC-068	P5-F06	-	-	HOW	missing	missing	
427	BC1F1	WBDC-068	P5-F07	-	-	HET	HET	HOW	
428	BC1F1	WBDC-068	P5-F08	-	-	HET	HOW	HOW	
429	BC1F1	WBDC-068	P5-F09	-	-	HET	HET	HET	Selected
430	BC1F1	WBDC-068	P5-F10	-	-	HET	HET	HET	Selected
431	BC1F1	WBDC-068	P5-F11	-	-	HET	HET	HOW	
432	BC1F1	WBDC-068	P5-F12	-	-	HET	HOW	HET	
433	BC1F1	WBDC-068	P5-G01	-	-	HOW	HET	HET	
434	BC1F1	WBDC-068	P5-G02	-	-	HET	HOW	HET	
435	BC1F1	WBDC-068	P5-G03	-	-	HET	HET	HET	Selected
436	BC1F1	WBDC-068	P5-G04	-	-	HET	HET	HET	Selected
437	BC1F1	WBDC-068	P5-G05	-	-	HET	HOW	HOW	
438	BC1F1	WBDC-068	P5-G06	-	-	HOW	HOW	HOW	
439	BC1F1	WBDC-068	P5-G07	-	-	HOW	HOW	HOW	
440	BC1F1	WBDC-068	P5-G08	-	-	HET	HOW	HET	
441	BC1F1	WBDC-068	P5-G09	-	-	HET	HET	HOW	
442	BC1F1	WBDC-068	P5-G10	-	-	HET	HOW	HET	
443	BC1F1	WBDC-068	P5-G11	-	-	HET	HOW	HET	
444	BC1F1	WBDC-068	P5-G12	-	-	HET	HOW	HET	
445	BC1F1	WBDC-068	P5-H01	-	-	HOW	HOW	HOW	
446	BC1F1	WBDC-068	P5-H02	-	-	HET	HET	HOW	
447	BC1F1	WBDC-068	P5-H03	-	-	HOW	HET	HET	
448	BC1F1	WBDC-068	P5-H04	-	-	HET	HET	HOW	
449	BC1F1	WBDC-068	P5-H05	-	-	HOW	HET	HET	
450	BC1F1	WBDC-068	P5-H06	-	-	HOW	HET	HOW	
451	BC1F1	WBDC-068	P6-A01	-	-	HOW	HOW	HOW	
452	BC1F1	WBDC-068	P6-A02	-	-	HET	HOW	HOW	
453	BC1F1	WBDC-068	P6-A03	-	-	HOW	HET	HET	
454	BC1F1	WBDC-068	P6-A04	-	-	HOW	HET	HOW	
455	BC1F1	WBDC-068	P6-A05	-	-	HOW	HOW	HOW	
456	BC1F1	WBDC-068	P6-A06	-	-	HET	HOW	HET	
457	BC1F1	WBDC-068	P6-A07	-	-	HOW	HOW	HET	
458	BC1F1	WBDC-068	P6-A08	-	-	HET	HET	HET	Selected
459	BC1F1	WBDC-068	P6-A09	-	-	HET	HET	HOW	
460	BC1F1	WBDC-068	P6-A10	-	-	HET	HET	HET	Selected
461	BC1F1	WBDC-074	P6-A11	-	-	HET	HET	HET	Selected
462	BC1F1	WBDC-074	P6-A12	-	-	missing	missing	missing	
463	BC1F1	WBDC-074	P6-B01	-	-	HET	HOW	HOW	
464	BC1F1	WBDC-074	P6-B02	-	-	HOW	HOW	HET	
465	BC1F1	WBDC-074	P6-B03	-	-	HET	HOW	HET	

466	BC1F1	WBDC-074	P6-B04	-	-	missing	missing	missing	
467	BC1F1	WBDC-074	P6-B05	-	-	HET	HOW	HOW	
468	BC1F1	WBDC-074	P6-B06	-	-	HOW	HET	HOW	
469	BC1F1	WBDC-074	P6-B07	-	-	HET	HET	HET	Selected
470	BC1F1	WBDC-074	P6-B08	-	-	HOW	HOW	HET	
471	BC1F1	WBDC-074	P6-B09	-	-	missing	missing	missing	
472	BC1F1	WBDC-074	P6-B10	-	-	HOW	HET	HET	
473	BC1F1	WBDC-074	P6-B11	-	-	HET	HET	HOW	
474	BC1F1	WBDC-074	P6-B12	-	-	missing	missing	missing	
475	BC1F1	WBDC-074	P6-C01	-	-	missing	missing	missing	
476	BC1F1	WBDC-074	P6-C02	-	-	HOW	HOW	HET	
477	BC1F1	WBDC-074	P6-C03	-	-	HOW	HET	HET	
478	BC1F1	WBDC-074	P6-C04	-	-	HET	HET	HET	Selected
479	BC1F1	WBDC-074	P6-C05	-	-	HET	HET	HET	Selected
480	BC1F1	WBDC-074	P6-C06	-	-	HOW	HET	HOW	
481	BC1F1	WBDC-074	P6-C07	-	-	HET	HET	HOW	
482	BC1F1	WBDC-074	P6-C08	-	-	HOW	HOW	HOW	
483	BC1F1	WBDC-074	P6-C09	-	-	HOW	HET	HOW	
484	BC1F1	WBDC-074	P6-C10	-	-	missing	missing	missing	
485	BC1F1	WBDC-074	P6-C11	-	-	HET	HET	HET	Selected
486	BC1F1	WBDC-074	P6-C12	-	-	missing	HOW	HOW	
487	BC1F1	WBDC-074	P6-D01	-	-	HOW	HOW	HOW	
488	BC1F1	WBDC-074	P6-D02	-	-	HET	HOW	HOW	
489	BC1F1	WBDC-074	P6-D03	-	-	missing	missing	missing	
490	BC1F1	WBDC-074	P6-D04	-	-	HOW	HET	HOW	
491	BC1F1	WBDC-074	P6-D05	-	-	HET	HET	HET	Selected
492	BC1F1	WBDC-074	P6-D06	-	-	HET	HET	HET	Selected
493	BC1F1	WBDC-074	P6-D07	-	-	HET	HET	HET	Selected
494	BC1F1	WBDC-074	P6-D08	-	-	missing	missing	missing	
495	BC1F1	WBDC-074	P6-D09	-	-	HET	HOW	HOW	
496	BC1F1	WBDC-074	P6-D10	-	-	HET	HOW	HET	
497	BC1F1	WBDC-074	P6-D11	-	-	HOW	HOW	HOW	
498	BC1F1	WBDC-066	P6-D12	-	-	HOW	HOW	HET	
499	BC1F1	WBDC-066	P6-E01	-	-	missing	missing	missing	
500	BC1F1	WBDC-066	P6-E02	-	-	HET	HET	HET	Selected
501	BC1F1	WBDC-066	P6-E03	-	-	HOW	HET	HOW	
502	BC1F1	WBDC-066	P6-E04	-	-	missing	missing	missing	
503	BC1F1	WBDC-066	P6-E05	-	-	HET	HOW	HET	
504	BC1F1	WBDC-066	P6-E06	-	-	HOW	HOW	HET	
505	BC1F1	WBDC-066	P6-E07	-	-	missing	missing	missing	
506	BC1F1	WBDC-066	P6-E08	-	-	missing	missing	missing	
507	BC1F1	WBDC-066	P6-E09	-	-	HOW	HOW	HOW	
508	BC1F1	WBDC-066	P6-E10	-	-	HET	HOW	HET	

509	BC1F1	WBDC-066	P6-E11	-	-	HET	HOW	HOW	
510	BC1F1	WBDC-066	P6-E12	-	-	missing	missing	missing	
511	BC1F1	WBDC-066	P6-F01	-	-	HET	HOW	HOW	
512	BC1F1	WBDC-066	P6-F02	-	-	HOW	HET	HOW	
513	BC1F1	WBDC-066	P6-F03	-	-	missing	missing	missing	
514	BC1F1	WBDC-066	P6-F04	-	-	HOW	HET	HOW	
515	BC1F1	WBDC-066	P6-F05	-	-	HET	HOW	HOW	
516	BC1F1	WBDC-066	P6-F06	-	-	HET	HET	HOW	
517	BC1F1	WBDC-066	P6-F07	-	-	HET	HET	HOW	
518	BC1F1	WBDC-066	P6-F08	-	-	HOW	HET	HET	Selected
519	BC1F1	WBDC-066	P6-F09	-	-	HET	HOW	HET	
520	BC1F1	WBDC-066	P6-F10	-	-	missing	missing	missing	
521	BC1F1	WBDC-066	P6-F11	-	-	HET	HOW	HOW	
522	BC1F1	WBDC-066	P6-F12	-	-	HET	HET	HET	Selected
523	BC1F1	WBDC-066	P6-G01	-	-	HET	HOW	HET	
524	BC1F1	WBDC-066	P6-G02	-	-	HET	HOW	HOW	
525	BC1F1	WBDC-066	P6-G03	-	-	HET	HOW	HET	
526	BC1F1	WBDC-066	P6-G04	-	-	missing	missing	missing	
527	BC1F1	WBDC-066	P6-G05	-	-	HET	HOW	HET	
528	BC1F1	WBDC-314	P6-G06	-	-	HET	HOW	HET	
529	BC1F1	WBDC-314	P6-G07	-	-	HOW	HET	HET	
530	BC1F1	WBDC-314	P6-G08	-	-	HOW	HOW	HET	
531	BC1F1	WBDC-314	P6-G09	-	-	HET	HET	HET	Selected
532	BC1F1	WBDC-314	P6-G10	-	-	HOW	HET	HET	
533	BC1F1	WBDC-314	P6-G11	-	-	HET	HOW	HET	
534	BC1F1	WBDC-314	P6-G12	-	-	HOW	HOW	HOW	
535	BC1F1	WBDC-314	P6-H01	-	-	HET	HOW	HET	
536	BC1F1	WBDC-314	P6-H02	-	-	HET	HET	HOW	
537	BC1F1	WBDC-314	P6-H03	-	-	HET	HET	HOW	
538	BC1F1	WBDC-314	P6-H04	-	-	HET	HET	HOW	
539	BC1F1	WBDC-314	P6-H05	-	-	HOW	HOW	HET	
540	BC1F1	WBDC-314	P6-H06	-	-	HOC	HET	HET	
541	BC1F1	WBDC-314	P7-A01	-	-	HOW	HOW	missing	
542	BC1F1	WBDC-314	P7-A02	-	-	HOW	HET	HOW	
543	BC1F1	WBDC-314	P7-A03	-	-	HET	HET	HET	Selected
544	BC1F1	WBDC-314	P7-A04	-	-	HET	HOW	HOC	
545	BC1F1	WBDC-314	P7-A05	-	-	HET	HOW	HET	
546	BC1F1	WBDC-314	P7-A06	-	-	HOW	HOW	HOW	
547	BC1F1	WBDC-314	P7-A07	-	-	HOW	HET	HET	
548	BC1F1	WBDC-314	P7-A08	-	-	HET	HOW	HET	
549	BC1F1	WBDC-314	P7-A09	-	-	HET	HET	HOW	
550	BC1F1	WBDC-314	P7-A10	-	-	HET	HOW	HOW	
551	BC1F1	WBDC-314	P7-A11	-	-	HET	HOW	HOW	

552	BC1F1	WBDC-314	P7-A12	-	-	missing	missing	missing	
553	BC1F1	WBDC-314	P7-B01	-	-	HET	HOW	missing	
554	BC1F1	WBDC-314	P7-B02	-	-	missing	missing	missing	
555	BC1F1	WBDC-314	P7-B03	-	-	missing	missing	missing	
556	BC1F1	WBDC-317	P7-B04	-	-	HOW	HOW	HOW	
557	BC1F1	WBDC-317	P7-B05	-	-	HET	HET	HOW	
558	BC1F1	WBDC-317	P7-B06	-	-	HET	HOW	HET	
559	BC1F1	WBDC-317	P7-B07	-	-	HET	HOW	HOW	
560	BC1F1	WBDC-317	P7-B08	-	-	HET	HOW	HOW	
561	BC1F1	WBDC-317	P7-B09	-	-	HET	HET	HOW	
562	BC1F1	WBDC-317	P7-B10	-	-	HOC	HOC	HOC	
563	BC1F1	WBDC-317	P7-B11	-	-	HOW	HOW	HET	
564	BC1F1	WBDC-317	P7-B12	-	-	missing	missing	missing	
565	BC1F1	WBDC-317	P7-C01	-	-	HET	HET	HET	Selected
566	BC1F1	WBDC-317	P7-C02	-	-	HET	HET	HOW	
567	BC1F1	WBDC-317	P7-C03	-	-	HET	HOW	HOW	
568	BC1F1	WBDC-317	P7-C04	-	-	HET	HET	HOW	
569	BC1F1	WBDC-317	P7-C05	-	-	HET	HOW	HOW	
570	BC1F1	WBDC-317	P7-C06	-	-	HOW	HOW	HOW	
571	BC1F1	WBDC-317	P7-C07	-	-	HET	HET	HET	Selected
572	BC1F1	WBDC-317	P7-C08	-	-	HET	HOW	HET	
573	BC1F1	WBDC-317	P7-C09	-	-	HET	HET	HOW	
574	BC1F1	WBDC-317	P7-C10	-	-	HOW	HOW	HET	
575	BC1F1	WBDC-317	P7-C11	-	-	HET	HOW	HOW	
576	BC1F1	WBDC-317	P7-C12	-	-	HOW	HOW	HET	
577	BC1F1	WBDC-317	P7-D01	-	-	HOC	HOC	HOC	
578	BC1F1	WBDC-317	P7-D02	-	-	HOW	HOW	HET	
579	BC1F1	WBDC-317	P7-D03	-	-	HOW	HET	HET	
580	BC1F1	WBDC-317	P7-D04	-	-	missing	missing	missing	
581	BC1F1	WBDC-329	P7-D05	-	-	HOW	HET	HOW	
582	BC1F1	WBDC-329	P7-D06	-	-	HOW	HET	HOW	
583	BC1F1	WBDC-329	P7-D07	-	-	HOW	HET	HET	
584	BC1F1	WBDC-329	P7-D08	-	-	HOW	HOW	HET	
585	BC1F1	WBDC-329	P7-D09	-	-	HET	HOW	HOW	
586	BC1F1	WBDC-329	P7-D10	-	-	HET	HET	HET	Selected
587	BC1F1	WBDC-329	P7-D11	-	-	HOW	HOW	HET	
588	BC1F1	WBDC-329	P7-D12	-	-	HOW	HOW	HOW	
589	BC1F1	WBDC-329	P7-E01	-	-	HOW	HOW	HOW	
590	BC1F1	WBDC-329	P7-E02	-	-	HOW	HOW	HOW	
591	BC1F1	WBDC-329	P7-E03	-	-	HET	HET	HOW	
592	BC1F1	WBDC-329	P7-E04	-	-	HET	HOW	HET	Selected
593	BC1F1	WBDC-329	P7-E05	-	-	HOW	HET	HET	
594	BC1F1	WBDC-329	P7-E06	-	-	HOW	HOW	HET	

595	BC1F1	WBDC-329	P7-E07	-	-	missing	missing	missing	
596	BC1F1	WBDC-329	P7-E08	-	-	HET	HET	HOW	
597	BC1F1	WBDC-329	P7-E09	-	-	HOW	HOW	HET	
598	BC1F1	WBDC-329	P7-E10	-	-	HET	HET	HOW	
599	BC1F1	WBDC-329	P7-E11	-	-	HET	HET	HOW	
600	BC1F1	WBDC-329	P7-E12	-	-	HOW	HET	HOW	
601	BC1F1	WBDC-329	P7-F01	-	-	HOW	HOW	HOW	
602	BC1F1	WBDC-075	P7-F02	-	-	HOW	HOW	HOW	
603	BC1F1	WBDC-075	P7-F03	-	-	HET	HET	HOW	
604	BC1F1	WBDC-075	P7-F04	-	-	missing	missing	missing	
605	BC1F1	WBDC-075	P7-F05	-	-	HET	HET	HOW	
606	BC1F1	WBDC-075	P7-F06	-	-	HOW	HOW	HET	
607	BC1F1	WBDC-075	P7-F07	-	-	HET	HOW	HET	Selected
608	BC1F1	WBDC-075	P7-F08	-	-	missing	missing	missing	
609	BC1F1	WBDC-075	P7-F09	-	-	HOW	HOW	HOW	
610	BC1F1	WBDC-075	P7-F10	-	-	HOW	HET	HET	
611	BC1F1	WBDC-075	P7-F11	-	-	HET	HOW	HET	Selected
612	BC1F1	WBDC-075	P7-F12	-	-	missing	missing	missing	
613	BC1F1	WBDC-075	P7-G01	-	-	HOW	HET	HOW	
614	BC1F1	WBDC-075	P7-G02	-	-	HET	HOW	HET	
615	BC1F1	WBDC-075	P7-G03	-	-	HOW	HOW	HET	
616	BC1F1	WBDC-075	P7-G04	-	-	missing	missing	missing	
617	BC1F1	WBDC-075	P7-G05	-	-	HET	HET	HOW	
618	BC1F1	WBDC-075	P7-G06	-	-	HOW	HET	HOW	
619	BC1F1	WBDC-075	P7-G07	-	-	HOW	HET	HOW	
620	BC1F1	WBDC-075	P7-G08	-	-	HOW	HOW	HET	
621	BC1F1	WBDC-075	P7-G09	-	-	missing	missing	missing	
622	BC1F1	WBDC-108	P7-G10	-	-	HOC	HOC	HOC	
623	BC1F1	WBDC-108	P7-G11	-	-	HOW	HOW	HOW	
624	BC1F1	WBDC-108	P7-G12	-	-	HOW	HOW	HET	
625	BC1F1	WBDC-108	P7-H01	-	-	HET	HOW	HOW	
626	BC1F1	WBDC-108	P7-H02	-	-	HET	HET	HOW	
627	BC1F1	WBDC-108	P7-H03	-	-	HET	HOW	HOC	
628	BC1F1	WBDC-108	P7-H04	-	-	HET	HOW	HET	Selected
629	BC1F1	WBDC-108	P7-H05	-	-	HOW	HOW	HOW	
630	BC1F1	WBDC-108	P7-H06	-	-	HOW	HET	HET	
631	BC1F1	WBDC-108	P8-A01	-	-	HOW	HOW	missing	
632	BC1F1	WBDC-108	P8-A02	-	-	HET	HOW	HOW	
633	BC1F1	WBDC-108	P8-A03	-	-	HOW	HET	HOW	
634	BC1F1	WBDC-108	P8-A04	-	-	missing	missing	missing	
635	BC1F1	WBDC-108	P8-A05	-	-	HOW	HET	HOW	
636	BC1F1	WBDC-108	P8-A06	-	-	HOW	HET	HET	
637	BC1F1	WBDC-108	P8-A07	-	-	HOC	HOC	HOC	

638	BC1F1	WBDC-108	P8-A08	-	-	HOC	HET	HOC	
639	BC1F1	WBDC-108	P8-A09	-	-	HET	HET	HET	Selected
640	BC1F1	WBDC-108	P8-A10	-	-	HET	HET	HOW	
641	BC1F1	WBDC-106	P8-A11	-	-	HET	HOW	HOW	
642	BC1F1	WBDC-106	P8-A12	-	-	HET	HET	HET	Selected
643	BC1F1	WBDC-106	P8-B01	-	-	HOW	HOW	missing	
644	BC1F1	WBDC-106	P8-B02	-	-	HOW	HOW	HOW	
645	BC1F1	WBDC-106	P8-B03	-	-	HOW	HOW	HET	
646	BC1F1	WBDC-106	P8-B04	-	-	HOW	HOW	HET	
647	BC1F1	WBDC-106	P8-B05	-	-	HOW	HOW	HOW	
648	BC1F1	WBDC-106	P8-B06	-	-	HOW	HOW	HOW	
649	BC1F1	WBDC-106	P8-B07	-	-	HOW	HOW	HOW	
650	BC1F1	WBDC-106	P8-B08	-	-	HET	HOC	HOW	
651	BC1F1	WBDC-106	P8-B09	-	-	HOW	HOW	HET	
652	BC1F1	WBDC-106	P8-B10	-	-	HET	HET	HET	Selected
653	BC1F1	WBDC-106	P8-B11	-	-	HOW	HOW	HET	
654	BC1F1	WBDC-106	P8-B12	-	-	HET	HET	HOW	
655	BC1F1	WBDC-106	P8-C01	-	-	HOW	HOW	HOW	
656	BC1F1	WBDC-106	P8-C02	-	-	HET	HET	HET	Selected
657	BC1F1	WBDC-106	P8-C03	-	-	HET	HOW	HET	
658	BC1F1	WBDC-106	P8-C04	-	-	HET	HOW	HOW	
659	BC1F1	WBDC-112	P8-C05	-	-	HET	HET	HOW	
660	BC1F1	WBDC-112	P8-C06	-	-	HET	HOW	HOW	
661	BC1F1	WBDC-112	P8-C07	-	-	HOW	HOW	HOW	
662	BC1F1	WBDC-112	P8-C08	-	-	HOW	HET	HOW	
663	BC1F1	WBDC-112	P8-C09	-	-	HOW	HOW	HET	
664	BC1F1	WBDC-112	P8-C10	-	-	HET	HET	HET	Selected
665	BC1F1	WBDC-112	P8-C11	-	-	HOW	HOW	HET	
666	BC1F1	WBDC-112	P8-C12	-	-	missing	missing	missing	
667	BC1F1	WBDC-112	P8-D01	-	-	HOW	HET	HOW	
668	BC1F1	WBDC-112	P8-D02	-	-	HET	HET	HOW	
669	BC1F1	WBDC-112	P8-D03	-	-	HOW	HET	HOW	
670	BC1F1	WBDC-112	P8-D04	-	-	HET	HOW	HET	Selected
671	BC1F1	WBDC-112	P8-D05	-	-	HOW	HET	HOW	
672	BC1F1	WBDC-112	P8-D06	-	-	HOW	HOW	HOW	
673	BC1F1	WBDC-112	P8-D07	-	-	missing	missing	missing	
674	BC1F1	WBDC-210	P8-D08	-	-	HOW	HOW	HET	
675	BC1F1	WBDC-210	P8-D09	-	-	HET	HOW	HET	
676	BC1F1	WBDC-210	P8-D10	-	-	missing	missing	missing	
677	BC1F1	WBDC-210	P8-D11	-	-	HET	HOW	HET	
678	BC1F1	WBDC-210	P8-D12	-	-	HET	HOW	missing	
679	BC1F1	WBDC-210	P8-E01	-	-	HOW	HOW	missing	
680	BC1F1	WBDC-210	P8-E02	-	-	missing	missing	missing	

681	BC1F1	WBDC-210	P8-E03	-	-	missing	missing	missing	
682	BC1F1	WBDC-210	P8-E04	-	-	HET	HET	HET	Selected
683	BC1F1	WBDC-210	P8-E05	-	-	missing	missing	missing	
684	BC1F1	WBDC-210	P8-E06	-	-	HET	HOW	HET	
685	BC1F1	WBDC-210	P8-E07	-	-	missing	missing	missing	
686	BC1F1	WBDC-210	P8-E08	-	-	HET	HET	HET	Selected
687	BC1F1	WBDC-210	P8-E09	-	-	missing	missing	missing	
688	BC1F1	WBDC-210	P8-E10	-	-	missing	missing	missing	
689	BC1F1	WBDC-140	P8-E11	-	-	missing	missing	missing	
690	BC1F1	WBDC-140	P8-E12	-	-	HOW	HOW	HOW	
691	BC1F1	WBDC-140	P8-F01	-	-	missing	missing	missing	
692	BC1F1	WBDC-140	P8-F02	-	-	HOW	HET	HOW	
693	BC1F1	WBDC-140	P8-F03	-	-	HOW	HOW	HET	
694	BC1F1	WBDC-140	P8-F04	-	-	HOW	HET	HET	Selected
695	BC1F1	WBDC-140	P8-F05	-	-	HOW	HET	HOW	
696	BC1F1	WBDC-140	P8-F06	-	-	HOW	missing	missing	
697	BC1F1	WBDC-140	P8-F07	-	-	missing	missing	missing	
698	BC1F1	WBDC-140	P8-F08	-	-	HOW	HET	HOW	
699	BC1F1	WBDC-140	P8-F09	-	-	HET	HET	HOW	
700	BC1F1	WBDC-146	P8-F10	-	-	missing	missing	missing	
701	BC1F1	WBDC-146	P8-F11	-	-	missing	missing	missing	
702	BC1F1	WBDC-146	P8-F12	-	-	missing	missing	missing	
703	BC1F1	WBDC-146	P8-G01	-	-	missing	missing	missing	
704	BC1F1	WBDC-111	P8-G02	-	-	HET	HOW	HOW	
705	BC1F1	WBDC-111	P8-G03	-	-	HOW	HOW	HET	Selected
706	BC1F1	WBDC-111	P8-G04	-	-	HET	HET	HOW	Selected
707	BC1F1	WBDC-117	P8-G05	-	-	HOW	HOW	HOW	
708	BC1F1	WBDC-117	P8-G06	-	-	missing	missing	missing	
709	BC1F1	WBDC-117	P8-G07	-	-	HOW	HOW	HOW	
710	BC1F1	WBDC-117	P8-G08	-	-	HET	HOW	HOW	
711	BC1F1	WBDC-117	P8-G09	-	-	HOW	HOW	HET	
712	BC1F1	WBDC-117	P8-G10	-	-	HOW	HOW	HET	
713	BC1F1	WBDC-117	P8-G11	-	-	HET	HOW	HOW	
714	BC1F1	WBDC-117	P8-G12	-	-	HET	HOW	HET	
715	BC1F1	WBDC-117	P8-H01	-	-	HOW	HOW	HOW	
716	BC1F1	WBDC-117	P8-H02	-	-	HET	HOW	HET	
717	BC1F1	WBDC-117	P8-H03	-	-	HOW	HOW	HOW	
718	BC1F1	WBDC-117	P8-H04	-	-	HET	HOW	HOW	
719	BC1F1	WBDC-117	P8-H05	-	-	HOW	HOW	HET	
720	BC1F1	WBDC-117	P8-H06	-	-	HOC	HOC	HOC	
1	BC2F1	WBDC-329	P7-D10	P1-A01	-	HOW	HET	HET	
2	BC2F1	WBDC-329	P7-D10	P1-B01	-	HOW	HOW	HOW	
3	BC2F1	WBDC-329	P7-D10	P1-A02	-	HET	HET	HET	Selected

4	BC2F1	WBDC-329	P7-D10	P1-B02	-	HOW	HOW	HOW	
5	BC2F1	WBDC-329	P7-D10	P1-A03	-	missing	missing	missing	
6	BC2F1	WBDC-329	P7-D10	P1-B03	-	missing	missing	missing	
7	BC2F1	WBDC-329	P7-D10	P1-A04	-	HOW	HET	HOW	
8	BC2F1	WBDC-329	P7-D10	P1-B04	-	HOW	HOW	HOW	
9	BC2F1	WBDC-329	P7-D10	P1-A05	-	HET	HET	HET	Selected
10	BC2F1	WBDC-329	P7-D10	P1-B05	-	HOW	HET	HOW	
11	BC2F1	WBDC-329	P7-D10	P1-A06	-	HOW	HOW	HOW	
12	BC2F1	WBDC-329	P7-D10	P1-B06	-	HOW	HOW	HET	
13	BC2F1	WBDC-329	P7-D10	P1-A07	-	HOW	HET	HET	
14	BC2F1	WBDC-329	P7-D10	P1-B07	-	HET	HOW	HOW	
15	BC2F1	WBDC-329	P7-D10	P1-A08	-	missing	missing	missing	
16	BC2F1	WBDC-329	P7-D10	P1-B08	-	HOW	HET	HOW	
17	BC2F1	WBDC-329	P7-D10	P1-A09	-	HET	HET	HET	Selected
18	BC2F1	WBDC-329	P7-D10	P1-B09	-	missing	missing	missing	
19	BC2F1	WBDC-329	P7-D10	P1-A10	-	missing	missing	missing	
20	BC2F1	WBDC-329	P7-D10	P1-B10	-	missing	missing	missing	
21	BC2F1	WBDC-329	P7-D10	P1-A11	-	missing	missing	missing	
22	BC2F1	WBDC-329	P7-D10	P1-B11	-	missing	missing	missing	
23	BC2F1	WBDC-329	P7-D10	P1-A12	-	missing	missing	missing	
24	BC2F1	WBDC-329	P7-D10	P1-B12	-	missing	missing	missing	
25	BC2F1	WBDC-329	P7-D10	P1-C01	-	HET	HET	HOW	
26	BC2F1	WBDC-329	P7-D10	P1-D01	-	HET	HET	HOW	
27	BC2F1	WBDC-329	P7-D10	P1-C02	-	HOW	HET	HOW	
28	BC2F1	WBDC-329	P7-D10	P1-D02	-	missing	missing	missing	
29	BC2F1	WBDC-329	P7-D10	P1-C03	-	HOW	HET	HOW	
30	BC2F1	WBDC-329	P7-D10	P1-D03	-	missing	missing	missing	
31	BC2F1	WBDC-329	P7-D10	P1-C04	-	HOW	HET	HET	
32	BC2F1	WBDC-329	P7-D10	P1-D04	-	HET	HET	HET	Selected
33	BC2F1	WBDC-329	P7-D10	P1-C05	-	HET	HOW	HET	
34	BC2F1	WBDC-329	P7-D10	P1-D05	-	missing	missing	missing	
35	BC2F1	WBDC-329	P7-D10	P1-C06	-	HET	HOW	HET	
36	BC2F1	WBDC-329	P7-D10	P1-D06	-	missing	missing	missing	
37	BC2F1	WBDC-329	P7-D10	P1-C07	-	HOW	HOW	HET	
38	BC2F1	WBDC-329	P7-D10	P1-D07	-	HET	HET	HOW	
39	BC2F1	WBDC-329	P7-D10	P1-C08	-	HOW	HET	HET	
40	BC2F1	WBDC-329	P7-D10	P1-D08	-	missing	missing	missing	
41	BC2F1	WBDC-329	P7-D10	P1-C09	-	HOW	HET	HOW	
42	BC2F1	WBDC-329	P7-D10	P1-D09	-	HET	HET	HOW	
43	BC2F1	WBDC-329	P7-D10	P1-C10	-	missing	missing	missing	
44	BC2F1	WBDC-329	P7-D10	P1-D10	-	HOW	HOW	HOW	
45	BC2F1	WBDC-329	P7-D10	P1-C11	-	missing	missing	missing	
46	BC2F1	WBDC-329	P7-D10	P1-D11	-	missing	missing	missing	

47	BC2F1	WBDC-329	P7-D10	P1-C12	-	missing	missing	missing	
48	BC2F1	WBDC-329	P7-D10	P1-D12	-	missing	missing	missing	
49	BC2F1	WBDC-329	P7-D10	P1-E01	-	HOW	HOW	HOW	
50	BC2F1	WBDC-329	P7-D10	P1-F01	-	missing	missing	missing	
51	BC2F1	WBDC-329	P7-D10	P1-E02	-	missing	missing	missing	
52	BC2F1	WBDC-329	P7-D10	P1-F02	-	missing	missing	missing	
53	BC2F1	WBDC-329	P7-D10	P1-E03	-	missing	missing	missing	
54	BC2F1	WBDC-117	P1-D03	P1-F03	-	HOW	HET	HOW	
55	BC2F1	WBDC-329	P7-D10	P1-E04	-	missing	missing	missing	
56	BC2F1	WBDC-117	P1-D03	P1-F04	-	missing	missing	missing	
57	BC2F1	WBDC-329	P7-D10	P1-E05	-	HOW	HET	HET	
58	BC2F1	WBDC-117	P1-D03	P1-F05	-	HOW	HET	HOW	
59	BC2F1	WBDC-329	P7-D10	P1-E06	-	HET	HET	HET	
60	BC2F1	WBDC-117	P1-D03	P1-F06	-	HOW	HET	HOW	
61	BC2F1	WBDC-329	P7-D10	P1-E07	-	missing	missing	missing	
62	BC2F1	WBDC-117	P1-D03	P1-F07	-	missing	missing	missing	
63	BC2F1	WBDC-329	P7-D10	P1-E08	-	missing	missing	missing	
64	BC2F1	WBDC-117	P1-D03	P1-F08	-	missing	missing	missing	
65	BC2F1	WBDC-329	P7-D10	P1-E09	-	missing	missing	missing	
66	BC2F1	WBDC-117	P1-D03	P1-F09	-	HET	HET	HET	Selected
67	BC2F1	WBDC-329	P7-D10	P1-E10	-	missing	missing	missing	
68	BC2F1	WBDC-117	P1-D03	P1-F10	-	missing	missing	missing	
69	BC2F1	WBDC-329	P7-D10	P1-E11	-	missing	missing	missing	
70	BC2F1	WBDC-117	P1-D03	P1-F11	-	missing	missing	missing	
71	BC2F1	WBDC-329	P7-D10	P1-E12	-	HOW	HET	HOW	
72	BC2F1	WBDC-117	P1-D03	P1-F12	-	missing	missing	missing	
73	BC2F1	WBDC-117	P1-D03	P1-G01	-	HET	HET	HOW	
74	BC2F1	WBDC-117	P1-D03	P1-G02	-	HET	HET	HET	Selected
75	BC2F1	WBDC-117	P1-D03	P1-G03	-	missing	missing	missing	
76	BC2F1	WBDC-117	P1-D03	P1-G04	-	missing	missing	missing	
77	BC2F1	WBDC-117	P1-D03	P1-G05	-	HOW	HET	HOW	
78	BC2F1	WBDC-117	P1-D03	P1-G06	-	missing	missing	missing	
79	BC2F1	WBDC-117	P1-D03	P1-G07	-	missing	missing	missing	
80	BC2F1	WBDC-117	P1-D03	P1-G08	-	HET	HET	HOW	
81	BC2F1	WBDC-117	P1-D03	P1-G09	-	missing	missing	missing	
82	BC2F1	WBDC-117	P1-D03	P1-G10	-	HOW	HET	HOW	
83	BC2F1	WBDC-117	P1-D03	P1-G11	-	missing	missing	missing	
84	BC2F1	WBDC-117	P1-D03	P1-G12	-	missing	missing	missing	
85	BC2F1	WBDC-117	P1-D03	P2-A01	-	missing	missing	missing	
86	BC2F1	WBDC-117	P1-D03	P2-B01	-	missing	missing	missing	
87	BC2F1	WBDC-117	P1-D03	P2-A02	-	missing	missing	missing	
88	BC2F1	WBDC-117	P1-D04	P2-B02	-	HET	HET	HET	Selected
89	BC2F1	WBDC-117	P1-D03	P2-A03	-	missing	missing	missing	

90	BC2F1	WBDC-117	P1-D04	P2-B03	-	HOW	HET	HET	
91	BC2F1	WBDC-117	P1-D03	P2-A04	-	HOW	HOW	HET	
92	BC2F1	WBDC-117	P1-D04	P2-B04	-	HET	HET	HOW	
93	BC2F1	WBDC-117	P1-D03	P2-A05	-	HET	HOW	HET	
94	BC2F1	WBDC-117	P1-D04	P2-B05	-	missing	missing	missing	
95	BC2F1	WBDC-117	P1-D03	P2-A06	-	HOW	HET	HOW	
96	BC2F1	WBDC-117	P1-D04	P2-B06	-	missing	missing	missing	
97	BC2F1	WBDC-117	P1-D03	P2-A07	-	missing	missing	missing	
98	BC2F1	WBDC-117	P1-D04	P2-B07	-	missing	missing	missing	
99	BC2F1	WBDC-117	P1-D03	P2-A08	-	missing	missing	missing	
100	BC2F1	WBDC-117	P1-D04	P2-B08	-	missing	missing	missing	
101	BC2F1	WBDC-117	P1-D03	P2-A09	-	missing	missing	missing	
102	BC2F1	WBDC-117	P1-D04	P2-B09	-	HET	HET	HOW	
103	BC2F1	WBDC-117	P1-D03	P2-A10	-	HET	HET	HOW	
104	BC2F1	WBDC-117	P1-D04	P2-B10	-	HOW	HET	HOW	
105	BC2F1	WBDC-117	P1-D03	P2-A11	-	HET	HET	HOW	
106	BC2F1	WBDC-117	P1-D04	P2-B11	-	HET	HET	HOW	
107	BC2F1	WBDC-117	P1-D03	P2-A12	-	HET	HET	HET	Selected
108	BC2F1	WBDC-117	P1-D04	P2-B12	-	missing	missing	missing	
109	BC2F1	WBDC-117	P1-D04	P2-C01	-	missing	missing	missing	
110	BC2F1	WBDC-117	P1-C05	P2-D01	-	missing	missing	missing	
111	BC2F1	WBDC-117	P1-D04	P2-C02	-	missing	missing	missing	
112	BC2F1	WBDC-117	P1-C05	P2-D02	-	HOW	HET	HET	
113	BC2F1	WBDC-117	P1-D04	P2-C03	-	HET	HET	HET	
114	BC2F1	WBDC-117	P1-C05	P2-D03	-	HET	HET	HET	
115	BC2F1	WBDC-117	P1-D04	P2-C04	-	HET	HOW	HOW	
116	BC2F1	WBDC-117	P1-C05	P2-D04	-	HET	HET	HET	
117	BC2F1	WBDC-117	P1-D04	P2-C05	-	missing	missing	missing	
118	BC2F1	WBDC-117	P1-C05	P2-D05	-	missing	missing	missing	
119	BC2F1	WBDC-117	P1-D04	P2-C06	-	HOW	HET	HET	
120	BC2F1	WBDC-117	P1-C05	P2-D06	-	HET	HET	HOW	
121	BC2F1	WBDC-117	P1-D04	P2-C07	-	HOW	HET	HOW	
122	BC2F1	WBDC-117	P1-C05	P2-D07	-	HOW	HET	HET	
123	BC2F1	WBDC-117	P1-D04	P2-C08	-	HET	HET	HET	
124	BC2F1	WBDC-117	P1-C05	P2-D08	-	HOW	HET	HOW	
125	BC2F1	WBDC-117	P1-D04	P2-C09	-	HOW	HOW	HET	
126	BC2F1	WBDC-066	P6-E02	P2-D09	-	HET	HOW	HET	
127	BC2F1	WBDC-117	P1-C05	P2-C10	-	HET	HET	HET	
128	BC2F1	WBDC-066	P6-E02	P2-D10	-	missing	missing	missing	
129	BC2F1	WBDC-117	P1-C05	P2-C11	-	missing	missing	missing	
130	BC2F1	WBDC-066	P6-E02	P2-D11	-	HOW	missing	HET	
131	BC2F1	WBDC-117	P1-C05	P2-C12	-	HOW	missing	HOW	
132	BC2F1	WBDC-066	P6-E02	P2-D12	-	HET	missing	HET	

133	BC2F1	WBDC-066	P6-E02	P2-E01	-	HOW	HOW	HOW	
134	BC2F1	WBDC-066	P6-E02	P2-F01	-	HET	HOW	HOW	
135	BC2F1	WBDC-066	P6-E02	P2-E02	-	HET	HET	HET	Selected
136	BC2F1	WBDC-066	P6-E02	P2-F02	-	HOW	HOW	HET	
137	BC2F1	WBDC-066	P6-E02	P2-E03	-	missing	missing	missing	
138	BC2F1	WBDC-066	P6-E02	P2-F03	-	HET	HET	HOW	
139	BC2F1	WBDC-066	P6-E02	P2-E04	-	HET	HOW	HET	
140	BC2F1	WBDC-066	P6-E02	P2-F04	-	HOW	HOW	HOW	
141	BC2F1	WBDC-066	P6-E02	P2-E05	-	HOW	HOW	HOW	
142	BC2F1	WBDC-066	P6-E02	P2-F05	-	missing	missing	missing	
143	BC2F1	WBDC-066	P6-E02	P2-E06	-	HET	HOW	HET	
144	BC2F1	WBDC-066	P6-E02	P2-F06	-	HOW	HOW	HOW	
145	BC2F1	WBDC-066	P6-E02	P2-E07	-	HOW	HET	HOW	
146	BC2F1	WBDC-066	P6-E02	P2-F07	-	HOW	HOW	HOW	
147	BC2F1	WBDC-066	P6-E02	P2-E08	-	HOW	HOW	HOW	
148	BC2F1	WBDC-066	P6-E02	P2-F08	-	missing	missing	missing	
149	BC2F1	WBDC-066	P6-E02	P2-E09	-	HOW	HET	HOW	
150	BC2F1	WBDC-111	P8-G03	P2-F09	-	HOW	HOW	HET	Selected
151	BC2F1	WBDC-066	P6-E02	P2-E10	-	HOW	HET	HOW	
152	BC2F1	WBDC-111	P8-G03	P2-F10	-	HOW	HOW	HOW	
153	BC2F1	WBDC-066	P6-E02	P2-E11	-	HET	HET	HET	Selected
154	BC2F1	WBDC-111	P8-G03	P2-F11	-	missing	missing	missing	
155	BC2F1	WBDC-066	P6-E02	P2-E12	-	HET	HET	HET	Selected
156	BC2F1	WBDC-111	P8-G03	P2-F12	-	HOW	HOW	HET	Selected
157	BC2F1	WBDC-111	P8-G03	P2-G01	-	missing	missing	missing	
158	BC2F1	WBDC-111	P8-G03	P2-G02	-	missing	missing	missing	
159	BC2F1	WBDC-111	P8-G03	P2-G03	-	missing	missing	missing	
160	BC2F1	WBDC-111	P8-G03	P2-G04	-	HOW	HOW	HET	Selected
161	BC2F1	WBDC-111	P8-G03	P2-G05	-	missing	missing	missing	
162	BC2F1	WBDC-111	P8-G03	P2-G06	-	HOW	HOW	HOW	
163	BC2F1	WBDC-038	P3-A09	P3-A01	-	missing	missing	missing	
164	BC2F1	WBDC-038	P3-A09	P3-B01	-	missing	missing	missing	
165	BC2F1	WBDC-038	P3-A09	P3-A02	-	HOW	HET	HOW	
166	BC2F1	WBDC-038	P3-A09	P3-B02	-	missing	missing	missing	
167	BC2F1	WBDC-038	P3-A09	P3-A03	-	missing	missing	missing	
168	BC2F1	WBDC-038	P3-D01	P3-B03	-	HET	HET	HOW	
169	BC2F1	WBDC-038	P3-A09	P3-A04	-	HET	HET	HOW	
170	BC2F1	WBDC-038	P3-D01	P3-B04	-	missing	missing	missing	
171	BC2F1	WBDC-038	P3-A09	P3-A05	-	missing	missing	missing	
172	BC2F1	WBDC-038	P3-D01	P3-B05	-	HOW	HET	HET	
173	BC2F1	WBDC-038	P3-A09	P3-A06	-	missing	missing	missing	
174	BC2F1	WBDC-038	P3-D01	P3-B06	-	HOW	HOW	HOW	
175	BC2F1	WBDC-038	P3-A09	P3-A07	-	missing	missing	missing	

176	BC2F1	WBDC-038	P3-D01	P3-B07	-	missing	missing	missing	
177	BC2F1	WBDC-038	P3-A09	P3-A08	-	missing	missing	missing	
178	BC2F1	WBDC-038	P3-D01	P3-B08	-	missing	missing	missing	
179	BC2F1	WBDC-038	P3-A09	P3-A09	-	HOW	HET	HET	
180	BC2F1	WBDC-038	P3-D01	P3-B09	-	HET	HET	HET	Selected
181	BC2F1	WBDC-038	P3-A09	P3-A10	-	HOW	HOW	HET	
182	BC2F1	WBDC-038	P3-D01	P3-B10	-	HOW	HET	HOW	
183	BC2F1	WBDC-038	P3-A09	P3-A11	-	HOW	HOW	HET	
184	BC2F1	WBDC-210	P8-E04	P3-B11	-	missing	missing	missing	
185	BC2F1	WBDC-038	P3-A09	P3-A12	-	HOW	HET	HET	
186	BC2F1	WBDC-210	P8-E04	P3-B12	-	HOW	HET	HET	
187	BC2F1	WBDC-210	P8-E04	P3-C01	-	HOW	HOW	HET	
188	BC2F1	WBDC-210	P8-E04	P3-D01	-	HET	HET	HOW	
189	BC2F1	WBDC-210	P8-E04	P3-C02	-	HOW	HET	HET	
190	BC2F1	WBDC-210	P8-E04	P3-D02	-	HET	HET	HET	
191	BC2F1	WBDC-210	P8-E04	P3-C03	-	missing	missing	missing	
192	BC2F1	WBDC-210	P8-E04	P3-D03	-	HOW	HET	HOW	
193	BC2F1	WBDC-210	P8-E04	P3-C04	-	HET	HET	HET	
194	BC2F1	WBDC-210	P8-E04	P3-D04	-	HET	HOW	HOW	
195	BC2F1	WBDC-210	P8-E04	P3-C05	-	missing	missing	missing	
196	BC2F1	WBDC-210	P8-E04	P3-D05	-	HET	HET	HOW	
197	BC2F1	WBDC-210	P8-E04	P3-C06	-	HET	HET	HOW	
198	BC2F1	WBDC-210	P8-E04	P3-D06	-	HET	HET	HET	
199	BC2F1	WBDC-210	P8-E04	P3-C07	-	missing	missing	missing	
200	BC2F1	WBDC-210	P8-E04	P3-D07	-	missing	missing	missing	
201	BC2F1	WBDC-210	P8-E04	P3-C08	-	missing	missing	missing	
202	BC2F1	WBDC-210	P8-E08	P3-D08	-	HOW	HET	HOW	
203	BC2F1	WBDC-210	P8-E04	P3-C09	-	missing	missing	missing	
204	BC2F1	WBDC-210	P8-E08	P3-D09	-	missing	missing	missing	
205	BC2F1	WBDC-210	P8-E04	P3-C10	-	missing	missing	missing	
206	BC2F1	WBDC-210	P8-E08	P3-D10	-	HOW	HET	HOW	
207	BC2F1	WBDC-210	P8-E04	P3-C11	-	missing	missing	missing	
208	BC2F1	WBDC-210	P8-E08	P3-D11	-	missing	missing	missing	
209	BC2F1	WBDC-210	P8-E04	P3-C12	-	missing	missing	missing	
210	BC2F1	WBDC-210	P8-E08	P3-D12	-	missing	missing	missing	
211	BC2F1	WBDC-210	P8-E08	P3-E01	-	HET	HET	HET	
212	BC2F1	WBDC-210	P8-E08	P3-F01	-	HET	HET	HET	
213	BC2F1	WBDC-210	P8-E08	P3-E02	-	missing	missing	missing	
214	BC2F1	WBDC-210	P8-E08	P3-F02	-	HET	HET	HOW	
215	BC2F1	WBDC-210	P8-E08	P3-E03	-	HET	HOW	HET	
216	BC2F1	WBDC-210	P8-E08	P3-F03	-	missing	missing	missing	
217	BC2F1	WBDC-210	P8-E08	P3-E04	-	HET	HET	HOW	
218	BC2F1	WBDC-210	P8-E08	P3-F04	-	missing	missing	missing	

219	BC2F1	WBDC-210	P8-E08	P3-E05	-	HOW	HET	HET	
220	BC2F1	WBDC-210	P8-E08	P3-F05	-	missing	missing	missing	
221	BC2F1	WBDC-210	P8-E08	P3-E06	-	HET	HET	HET	
222	BC2F1	WBDC-210	P8-E08	P3-F06	-	HOW	HET	HET	
223	BC2F1	WBDC-210	P8-E08	P3-E07	-	missing	missing	missing	
224	BC2F1	WBDC-210	P8-E08	P3-F07	-	HET	HOW	HET	
225	BC2F1	WBDC-210	P8-E08	P3-E08	-	HET	HOW	HET	
226	BC2F1	WBDC-020	P2-A05	P3-F08	-	HET	HOC	HET	Selected
227	BC2F1	WBDC-210	P8-E08	P3-E09	-	HOW	HET	HET	
228	BC2F1	WBDC-020	P2-A05	P3-F09	-	HET	HOC	HOW	
229	BC2F1	WBDC-210	P8-E08	P3-E10	-	HET	HET	HET	
230	BC2F1	WBDC-020	P2-A05	P3-F10	-	HET	HOC	HET	
231	BC2F1	WBDC-210	P8-E08	P3-E11	-	missing	missing	missing	
232	BC2F1	WBDC-020	P2-A05	P3-F11	-	HOW	HOC	HET	
233	BC2F1	WBDC-210	P8-E08	P3-E12	-	missing	missing	missing	
234	BC2F1	WBDC-020	P2-A05	P3-F12	-	missing	missing	missing	
235	BC2F1	WBDC-020	P2-A05	P3-G01	-	HOW	HOC	HET	
236	BC2F1	WBDC-020	P2-A05	P3-G02	-	missing	HOC	HOW	
237	BC2F1	WBDC-020	P2-A05	P3-G03	-	HOW	HOC	HOW	
238	BC2F1	WBDC-020	P2-A05	P3-G04	-	HOW	HOC	HOW	
239	BC2F1	WBDC-020	P2-A05	P3-G05	-	HOW	HOC	HET	
240	BC2F1	WBDC-020	P2-A05	P3-G06	-	HOW	HOC	HOW	
241	BC2F1	WBDC-020	P2-A05	P3-G07	-	HOW	HOC	HOW	
242	BC2F1	WBDC-020	P2-A05	P3-G08	-	missing	missing	missing	
243	BC2F1	WBDC-020	P2-A05	P4-A01	-	HOW	HOC	HET	
244	BC2F1	WBDC-020	P2-C11	P4-B01	-	HOW	HOC	HET	
245	BC2F1	WBDC-020	P2-A05	P4-A02	-	HET	HOC	HOW	
246	BC2F1	WBDC-020	P2-C11	P4-B02	-	HOW	HOC	HET	
247	BC2F1	WBDC-020	P2-A05	P4-A03	-	HET	HOC	HET	
248	BC2F1	WBDC-020	P2-C11	P4-B03	-	HET	HOC	HOW	
249	BC2F1	WBDC-020	P2-A05	P4-A04	-	missing	missing	missing	
250	BC2F1	WBDC-020	P2-C11	P4-B04	-	missing	missing	missing	
251	BC2F1	WBDC-020	P2-A05	P4-A05	-	missing	missing	missing	
252	BC2F1	WBDC-020	P2-C11	P4-B05	-	HET	HOC	HET	
253	BC2F1	WBDC-020	P2-A05	P4-A06	-	missing	missing	missing	
254	BC2F1	WBDC-020	P2-C11	P4-B06	-	HET	HOC	HOW	
255	BC2F1	WBDC-020	P2-A05	P4-A07	-	missing	missing	missing	
256	BC2F1	WBDC-199	P4-A08	P4-B07	-	missing	missing	missing	
257	BC2F1	WBDC-020	P2-C11	P4-A08	-	HET	HOC	HOW	
258	BC2F1	WBDC-199	P4-A08	P4-B08	-	HOW	HET	HOW	
259	BC2F1	WBDC-020	P2-C11	P4-A09	-	HET	HOC	HET	Selected
260	BC2F1	WBDC-199	P4-A08	P4-B09	-	missing	missing	missing	
261	BC2F1	WBDC-020	P2-C11	P4-A10	-	HOW	HOC	HET	

262	BC2F1	WBDC-199	P4-A08	P4-B10	-	HET	HET	HET	Selected
263	BC2F1	WBDC-020	P2-C11	P4-A11	-	missing	missing	missing	
264	BC2F1	WBDC-199	P4-A08	P4-B11	-	HOW	HET	HET	
265	BC2F1	WBDC-020	P2-C11	P4-A12	-	HET	HOC	HET	
266	BC2F1	WBDC-199	P4-A08	P4-B12	-	missing	missing	missing	
267	BC2F1	WBDC-199	P4-A08	P4-C01	-	HET	HET	HET	Selected
268	BC2F1	WBDC-199	P4-A11	P4-D01	-	HOW	missing	HET	
269	BC2F1	WBDC-199	P4-A08	P4-C02	-	missing	missing	missing	
270	BC2F1	WBDC-199	P4-A11	P4-D02	-	HOW	HOW	HET	
271	BC2F1	WBDC-199	P4-A08	P4-C03	-	missing	missing	missing	
272	BC2F1	WBDC-199	P4-A11	P4-D03	-	HET	HET	HET	Selected
273	BC2F1	WBDC-199	P4-A08	P4-C04	-	missing	missing	missing	
274	BC2F1	WBDC-199	P4-A11	P4-D04	-	missing	missing	missing	
275	BC2F1	WBDC-199	P4-A08	P4-C05	-	missing	missing	missing	
276	BC2F1	WBDC-199	P4-A11	P4-D05	-	HET	HET	HET	Selected
277	BC2F1	WBDC-199	P4-A08	P4-C06	-	HET	HOW	HET	
278	BC2F1	WBDC-199	P4-A11	P4-D06	-	HOW	HET	HET	
279	BC2F1	WBDC-199	P4-A08	P4-C07	-	missing	missing	missing	
280	BC2F1	WBDC-199	P4-A11	P4-D07	-	missing	HET	HET	
281	BC2F1	WBDC-199	P4-A08	P4-C08	-	missing	missing	missing	
282	BC2F1	WBDC-199	P4-A11	P4-D08	-	missing	missing	missing	
283	BC2F1	WBDC-199	P4-A08	P4-C09	-	missing	missing	missing	
284	BC2F1	WBDC-199	P4-A11	P4-D09	-	missing	missing	missing	
285	BC2F1	WBDC-199	P4-A11	P4-C10	-	missing	missing	missing	
286	BC2F1	WBDC-199	P4-A11	P4-D10	-	missing	missing	missing	
287	BC2F1	WBDC-199	P4-A11	P4-C11	-	HOW	HET	HET	
288	BC2F1	WBDC-199	P4-A11	P4-D11	-	missing	missing	missing	
289	BC2F1	WBDC-199	P4-A11	P4-C12	-	missing	missing	missing	
290	BC2F1	WBDC-199	P4-A11	P4-D12	-	missing	missing	missing	
291	BC2F1	WBDC-199	P4-A11	P4-E01	-	missing	missing	missing	
292	BC2F1	WBDC-199	P4-B03	P4-F01	-	missing	missing	missing	
293	BC2F1	WBDC-199	P4-A11	P4-E02	-	missing	missing	missing	
294	BC2F1	WBDC-199	P4-B03	P4-F02	-	missing	missing	missing	
295	BC2F1	WBDC-199	P4-A11	P4-E03	-	HET	HET	HOW	
296	BC2F1	WBDC-199	P4-B03	P4-F03	-	HOW	HET	HOW	
297	BC2F1	WBDC-199	P4-B03	P4-E04	-	HET	HET	HET	
298	BC2F1	WBDC-199	P4-B03	P4-F04	-	missing	missing	missing	
299	BC2F1	WBDC-199	P4-B03	P4-E05	-	HOW	HET	HET	
300	BC2F1	WBDC-199	P4-B03	P4-F05	-	missing	missing	missing	
301	BC2F1	WBDC-199	P4-B03	P4-E06	-	HET	HET	HOW	
302	BC2F1	WBDC-199	P4-B03	P4-F06	-	missing	missing	missing	
303	BC2F1	WBDC-199	P4-B03	P4-E07	-	missing	missing	HOW	
304	BC2F1	WBDC-199	P4-B03	P4-F07	-	HET	HET	HET	

305	BC2F1	WBDC-199	P4-B03	P4-E08	-	missing	missing	missing	
306	BC2F1	WBDC-199	P4-B03	P4-F08	-	HET	HET	HOW	
307	BC2F1	WBDC-199	P4-B03	P4-E09	-	HET	HOW	HOW	
308	BC2F1	WBDC-199	P4-B04	P4-F09	-	HET	HET	HET	
309	BC2F1	WBDC-199	P4-B03	P4-E10	-	HET	HET	HOW	
310	BC2F1	WBDC-199	P4-B04	P4-F10	-	missing	missing	missing	
311	BC2F1	WBDC-199	P4-B03	P4-E11	-	missing	missing	missing	
312	BC2F1	WBDC-199	P4-B04	P4-F11	-	HET	HET	HOW	
313	BC2F1	WBDC-199	P4-B03	P4-E12	-	missing	missing	missing	
314	BC2F1	WBDC-199	P4-B04	P4-F12	-	missing	missing	missing	
315	BC2F1	WBDC-199	P4-B04	P4-G01	-	HET	HET	HOW	
316	BC2F1	WBDC-199	P4-B04	P4-G02	-	missing	missing	missing	
317	BC2F1	WBDC-199	P4-B04	P4-G03	-	HOW	HET	HET	
318	BC2F1	WBDC-199	P4-B04	P4-G04	-	HET	HOW	HOW	
319	BC2F1	WBDC-199	P4-B04	P4-G05	-	missing	HET	HOW	
320	BC2F1	WBDC-199	P4-B04	P4-G06	-	HOW	HET	HET	
321	BC2F1	WBDC-199	P4-B04	P4-G07	-	missing	missing	missing	
322	BC2F1	WBDC-314	P7-A03	P4-G08	-	HOW	HOW	HET	
323	BC2F1	WBDC-314	P7-A03	P5-A01	-	HOW	HOW	HET	
324	BC2F1	WBDC-314	P7-A03	P5-B01	-	missing	missing	missing	
325	BC2F1	WBDC-314	P7-A03	P5-A02	-	HET	HOW	HET	Selected
326	BC2F1	WBDC-314	P7-A03	P5-B02	-	HOW	HOW	HET	
327	BC2F1	WBDC-314	P7-A03	P5-A03	-	HET	HOW	HET	Selected
328	BC2F1	WBDC-314	P7-A03	P5-B03	-	missing	missing	missing	
329	BC2F1	WBDC-314	P7-A03	P5-A04	-	missing	missing	missing	
330	BC2F1	WBDC-314	P7-A03	P5-B04	-	missing	missing	missing	
331	BC2F1	WBDC-314	P7-A03	P5-A05	-	missing	missing	missing	
332	BC2F1	WBDC-314	P7-A03	P5-B05	-	HOW	HOW	HOW	
333	BC2F1	WBDC-314	P7-A03	P5-A06	-	HOW	HET	HOW	
334	BC2F1	WBDC-314	P7-A03	P5-B06	-	HOW	HOW	HOW	
335	BC2F1	WBDC-314	P7-A03	P5-A07	-	HET	HOW	HOW	
336	BC2F1	WBDC-314	P7-A03	P5-B07	-	missing	missing	missing	
337	BC2F1	WBDC-314	P7-A03	P5-A08	-	missing	missing	missing	
338	BC2F1	WBDC-068	P5-F09	P5-B08	-	missing	missing	missing	
339	BC2F1	WBDC-314	P7-A03	P5-A09	-	HOW	HOW	HOW	
340	BC2F1	WBDC-068	P5-F09	P5-B09	-	HOW	HET	HOW	
341	BC2F1	WBDC-314	P7-A03	P5-A10	-	missing	missing	missing	
342	BC2F1	WBDC-068	P5-F09	P5-B10	-	HET	HET	HET	Selected
343	BC2F1	WBDC-314	P7-A03	P5-A11	-	missing	missing	missing	
344	BC2F1	WBDC-068	P5-F09	P5-B11	-	missing	missing	missing	
345	BC2F1	WBDC-314	P7-A03	P5-A12	-	missing	missing	missing	
346	BC2F1	WBDC-068	P5-F09	P5-B12	-	missing	missing	missing	
347	BC2F1	WBDC-068	P5-F09	P5-C01	-	HET	HOW	HET	

348	BC2F1	WBDC-068	P5-G03	P5-D01	-	missing	missing	missing	
349	BC2F1	WBDC-068	P5-F09	P5-C02	-	missing	missing	missing	
350	BC2F1	WBDC-068	P5-G03	P5-D02	-	missing	missing	missing	
351	BC2F1	WBDC-068	P5-F09	P5-C03	-	HET	HET	HET	Selected
352	BC2F1	WBDC-068	P5-G03	P5-D03	-	missing	missing	missing	
353	BC2F1	WBDC-068	P5-F09	P5-C04	-	HOW	HET	HOW	
354	BC2F1	WBDC-068	P5-G03	P5-D04	-	missing	missing	missing	
355	BC2F1	WBDC-068	P5-F09	P5-C05	-	HET	HET	HOW	
356	BC2F1	WBDC-068	P5-G03	P5-D05	-	missing	missing	missing	
357	BC2F1	WBDC-068	P5-F09	P5-C06	-	HET	HET	HOW	
358	BC2F1	WBDC-068	P5-G03	P5-D06	-	missing	missing	missing	
359	BC2F1	WBDC-068	P5-F09	P5-C07	-	HET	HOW	HOW	
360	BC2F1	WBDC-068	P5-G03	P5-D07	-	missing	missing	missing	
361	BC2F1	WBDC-068	P5-F09	P5-C08	-	HET	HET	HOW	
362	BC2F1	WBDC-068	P5-G03	P5-D08	-	HET	missing	HET	
363	BC2F1	WBDC-068	P5-F09	P5-C09	-	missing	missing	missing	
364	BC2F1	WBDC-068	P5-G03	P5-D09	-	missing	missing	missing	
365	BC2F1	WBDC-068	P5-G03	P5-C10	-	HET	HET	HET	Selected
366	BC2F1	WBDC-068	P5-G03	P5-D10	-	missing	missing	missing	
367	BC2F1	WBDC-068	P5-G03	P5-C11	-	HOW	HET	HET	
368	BC2F1	WBDC-068	P5-G03	P5-D11	-	missing	missing	missing	
369	BC2F1	WBDC-068	P5-G03	P5-C12	-	missing	missing	missing	
370	BC2F1	WBDC-068	P5-G03	P5-D12	-	HOW	HET	HOW	
371	BC2F1	WBDC-068	P5-G03	P5-E01	-	HOW	HET	HET	
372	BC2F1	WBDC-068	P5-G03	P5-F01	-	HET	HET	HET	
373	BC2F1	WBDC-068	P5-G03	P5-E02	-	HOW	HET	HOW	
374	BC2F1	WBDC-068	P5-G03	P5-F02	-	HET	HET	HET	
375	BC2F1	WBDC-068	P5-G03	P5-E03	-	missing	missing	missing	
376	BC2F1	WBDC-068	P5-G04	P5-F03	-	missing	missing	missing	
377	BC2F1	WBDC-068	P5-G03	P5-E04	-	missing	missing	missing	
378	BC2F1	WBDC-068	P5-G04	P5-F04	-	HET	HOW	HET	
379	BC2F1	WBDC-068	P5-G03	P5-E05	-	missing	missing	missing	
380	BC2F1	WBDC-068	P5-G04	P5-F05	-	missing	missing	missing	
381	BC2F1	WBDC-068	P5-G03	P5-E06	-	missing	missing	missing	
382	BC2F1	WBDC-068	P5-G04	P5-F06	-	missing	missing	missing	
383	BC2F1	WBDC-068	P5-G03	P5-E07	-	HOW	HET	HOW	
384	BC2F1	WBDC-068	P5-G04	P5-F07	-	missing	missing	missing	
385	BC2F1	WBDC-068	P5-G03	P5-E08	-	HET	HET	HET	Selected
386	BC2F1	WBDC-068	P5-G04	P5-F08	-	HET	HET	HET	Selected
387	BC2F1	WBDC-068	P5-G03	P5-E09	-	missing	missing	missing	
388	BC2F1	WBDC-068	P5-G04	P5-F09	-	missing	missing	missing	
389	BC2F1	WBDC-068	P5-G03	P5-E10	-	missing	missing	missing	
390	BC2F1	WBDC-068	P5-G04	P5-F10	-	HET	HET	HET	Selected

391	BC2F1	WBDC-068	P5-G03	P5-E11	-	missing	missing	missing	
392	BC2F1	WBDC-068	P5-G04	P5-F11	-	HOW	HOW	HET	
393	BC2F1	WBDC-068	P5-G03	P5-E12	-	HET	HOW	HET	
394	BC2F1	WBDC-068	P5-G04	P5-F12	-	HOW	HOW	HOW	
395	BC2F1	WBDC-068	P5-G04	P5-G01	-	HOW	HET	HOW	
396	BC2F1	WBDC-068	P5-G04	P5-G02	-	HET	HET	HET	
397	BC2F1	WBDC-317	P7-C01	P5-G03	-	HOW	HET	HOW	
398	BC2F1	WBDC-317	P7-C01	P5-G04	-	HET	HET	HET	Selected
399	BC2F1	WBDC-317	P7-C01	P5-G05	-	missing	missing	missing	
400	BC2F1	WBDC-317	P7-C01	P5-G06	-	HET	HOW	HOW	
401	BC2F1	WBDC-317	P7-C01	P5-G07	-	HOW	HOW	HOW	
402	BC2F1	WBDC-317	P7-C01	P5-G08	-	HET	HET	HET	Selected
403	BC2F1	WBDC-317	P7-C01	P6-A01	-	HET	HET	HOW	
404	BC2F1	WBDC-317	P7-C01	P6-B01	-	missing	HET	HOW	
405	BC2F1	WBDC-317	P7-C01	P6-A02	-	missing	missing	missing	
406	BC2F1	WBDC-317	P7-C01	P6-B02	-	missing	HET	HOW	
407	BC2F1	WBDC-317	P7-C01	P6-A03	-	missing	missing	missing	
408	BC2F1	WBDC-317	P7-C01	P6-B03	-	missing	HOW	HET	
409	BC2F1	WBDC-317	P7-C01	P6-A04	-	missing	missing	missing	
410	BC2F1	WBDC-317	P7-C01	P6-B04	-	HOW	HOW	HOW	
411	BC2F1	WBDC-317	P7-C01	P6-A05	-	missing	missing	missing	
412	BC2F1	WBDC-317	P7-C01	P6-B05	-	HOW	HOW	HOW	
413	BC2F1	WBDC-317	P7-C01	P6-A06	-	HET	HET	HOW	
414	BC2F1	WBDC-317	P7-C01	P6-B06	-	missing	missing	missing	
415	BC2F1	WBDC-317	P7-C01	P6-A07	-	HET	HET	HOW	
416	BC2F1	WBDC-317	P7-C01	P6-B07	-	missing	missing	missing	
417	BC2F1	WBDC-317	P7-C01	P6-A08	-	missing	missing	missing	
418	BC2F1	WBDC-317	P7-C01	P6-B08	-	HET	HET	HET	Selected
419	BC2F1	WBDC-317	P7-C01	P6-A09	-	missing	missing	missing	
420	BC2F1	WBDC-317	P7-C01	P6-B09	-	missing	HET	missing	
421	BC2F1	WBDC-317	P7-C01	P6-A10	-	HOW	HET	HET	
422	BC2F1	WBDC-317	P7-C01	P6-B10	-	HET	HET	HET	Selected
423	BC2F1	WBDC-317	P7-C01	P6-A11	-	HOW	HET	HET	
424	BC2F1	WBDC-317	P7-C01	P6-B11	-	HET	HET	HOW	
425	BC2F1	WBDC-317	P7-C01	P6-A12	-	HET	HET	HOW	
426	BC2F1	WBDC-317	P7-C07	P6-B12	-	missing	missing	missing	
427	BC2F1	WBDC-317	P7-C07	P6-C01	-	missing	missing	missing	
428	BC2F1	WBDC-107	P5-B11	P6-D01	-	missing	missing	missing	
429	BC2F1	WBDC-317	P7-C07	P6-C02	-	missing	missing	missing	
430	BC2F1	WBDC-107	P5-B11	P6-D02	-	missing	missing	missing	
431	BC2F1	WBDC-317	P7-C07	P6-C03	-	HOW	HET	HET	
432	BC2F1	WBDC-107	P5-B11	P6-D03	-	HET	HET	HOW	
433	BC2F1	WBDC-317	P7-C07	P6-C04	-	HOW	HET	HOW	

434	BC2F1	WBDC-107	P5-B11	P6-D04	-	missing	missing	missing	
435	BC2F1	WBDC-317	P7-C07	P6-C05	-	missing	missing	missing	
436	BC2F1	WBDC-107	P5-B11	P6-D05	-	missing	missing	missing	
437	BC2F1	WBDC-317	P7-C07	P6-C06	-	missing	missing	missing	
438	BC2F1	WBDC-107	P5-B11	P6-D06	-	missing	missing	missing	
439	BC2F1	WBDC-317	P7-C07	P6-C07	-	missing	missing	missing	
440	BC2F1	WBDC-107	P5-B11	P6-D07	-	missing	missing	missing	
441	BC2F1	WBDC-317	P7-C07	P6-C08	-	HET	HET	HET	
442	BC2F1	WBDC-107	P5-B11	P6-D08	-	missing	missing	missing	
443	BC2F1	WBDC-317	P7-C07	P6-C09	-	HET	HET	HET	
444	BC2F1	WBDC-107	P5-C08	P6-D09	-	HOW	HET	HOW	
445	BC2F1	WBDC-107	P5-B11	P6-C10	-	HET	HET	HET	Selected
446	BC2F1	WBDC-107	P5-C08	P6-D10	-	missing	missing	missing	
447	BC2F1	WBDC-107	P5-B11	P6-C11	-	missing	missing	missing	
448	BC2F1	WBDC-107	P5-C08	P6-D11	-	HOW	HET	HET	
449	BC2F1	WBDC-107	P5-B11	P6-C12	-	missing	missing	missing	
450	BC2F1	WBDC-107	P5-C08	P6-D12	-	HOW	HET	HOW	
451	BC2F1	WBDC-107	P5-C08	P6-E01	-	missing	missing	HOW	
452	BC2F1	WBDC-107	P5-D08	P6-F01	-	HET	HET	HOW	
453	BC2F1	WBDC-107	P5-C08	P6-E02	-	missing	missing	HOW	
454	BC2F1	WBDC-107	P5-D08	P6-F02	-	HET	HOW	HOW	
455	BC2F1	WBDC-107	P5-C08	P6-E03	-	missing	missing	missing	
456	BC2F1	WBDC-107	P5-D08	P6-F03	-	HET	HET	HOW	
457	BC2F1	WBDC-107	P5-C08	P6-E04	-	HET	HET	HET	Selected
458	BC2F1	WBDC-107	P5-D08	P6-F04	-	missing	HOW	HET	
459	BC2F1	WBDC-107	P5-C08	P6-E05	-	missing	missing	missing	
460	BC2F1	WBDC-107	P5-D08	P6-F05	-	HOW	HET	HET	
461	BC2F1	WBDC-107	P5-C08	P6-E06	-	HET	HET	HOW	
462	BC2F1	WBDC-107	P5-D08	P6-F06	-	HOW	HET	HOW	
463	BC2F1	WBDC-107	P5-C08	P6-E07	-	HOW	HOW	HET	
464	BC2F1	WBDC-048	P5-A07	P6-F07	-	missing	missing	missing	
465	BC2F1	WBDC-107	P5-D08	P6-E08	-	HET	HET	HOW	
466	BC2F1	WBDC-048	P5-A07	P6-F08	-	missing	missing	missing	
467	BC2F1	WBDC-107	P5-D08	P6-E09	-	HOW	HET	HOW	
468	BC2F1	WBDC-048	P5-A07	P6-F09	-	missing	missing	missing	
469	BC2F1	WBDC-107	P5-D08	P6-E10	-	missing	HET	HOW	
470	BC2F1	WBDC-048	P5-A07	P6-F10	-	missing	missing	missing	
471	BC2F1	WBDC-107	P5-D08	P6-E11	-	HOW	HET	HOW	
472	BC2F1	WBDC-048	P5-A07	P6-F11	-	missing	missing	missing	
473	BC2F1	WBDC-107	P5-D08	P6-E12	-	HET	HOW	HOW	
474	BC2F1	WBDC-048	P5-A09	P6-F12	-	missing	missing	missing	
475	BC2F1	WBDC-048	P5-A09	P6-G01	-	missing	HET	HOW	
476	BC2F1	WBDC-048	P5-A09	P6-G02	-	missing	HET	HOW	

477	BC2F1	WBDC-048	P5-A09	P6-G03	-	missing	missing	missing	
478	BC2F1	WBDC-048	P5-A09	P6-G04	-	HOW	HET	HOW	
479	BC2F1	WBDC-048	P5-A09	P6-G05	-	missing	missing	missing	
480	BC2F1	WBDC-048	P5-A09	P6-G06	-	HET	HET	HET	Selected
481	BC2F1	WBDC-048	P5-A09	P6-G07	-	HOW	HET	HET	
482	BC2F1	WBDC-048	P5-A09	P6-G08	-	missing	missing	missing	
1	BC2F2	WBDC-117	P1-D04	P2-B02	Tray 3-A01	missing	missing	missing	
2	BC2F2	WBDC-117	P1-D04	P2-B02	Tray 3-B01	HOW	HET	HOC	
3	BC2F2	WBDC-117	P1-D04	P2-B02	Tray 3-C01	HOC	HET	HET	
4	BC2F2	WBDC-117	P1-D04	P2-B02	Tray 3-D01	missing	missing	missing	
5	BC2F2	WBDC-117	P1-D04	P2-B02	Tray 3-E01	HET	HET	HOC	
6	BC2F2	WBDC-117	P1-D04	P2-B02	Tray 3-F01	HET	HET	HET	
7	BC2F2	WBDC-117	P1-D04	P2-B02	Tray 3-G01	HOC	HET	HOC	Selected
8	BC2F2	WBDC-117	P1-D04	P2-B02	Tray 3-H01	HOC	HET	HOW	
9	BC2F2	WBDC-117	P1-D04	P2-B02	Tray 3-A02	missing	HOC	missing	
10	BC2F2	WBDC-117	P1-D04	P2-B02	Tray 3-B02	HOC	HET	HOW	
11	BC2F2	WBDC-117	P1-D04	P2-B02	Tray 3-C02	missing	HET	missing	
12	BC2F2	WBDC-117	P1-D04	P2-B02	Tray 3-D02	HET	HET	HOW	
13	BC2F2	WBDC-117	P1-D04	P2-B02	Tray 3-E02	HET	HOC	HET	
14	BC2F2	WBDC-117	P1-D04	P2-B02	Tray 3-F02	HET	HOC	HOC	Selected
15	BC2F2	WBDC-117	P1-D04	P2-B02	Tray 3-G02	HET	HET	HET	
16	BC2F2	WBDC-117	P1-D04	P2-B02	Tray 3-H02	HOW	HET	HOC	
17	BC2F2	WBDC-117	P1-D04	P2-B02	Tray 3-A03	missing	HOC	missing	
18	BC2F2	WBDC-117	P1-D04	P2-B02	Tray 3-B03	HET	HET	HET	
19	BC2F2	WBDC-117	P1-D04	P2-B02	Tray 3-C03	HET	HET	HET	
20	BC2F2	WBDC-117	P1-D04	P2-B02	Tray 3-D03	HET	HET	HET	
21	BC2F2	WBDC-117	P1-D04	P2-B02	Tray 3-E03	HET	HET	HOW	
22	BC2F2	WBDC-117	P1-D04	P2-B02	Tray 3-F03	HOC	HET	HET	
23	BC2F2	WBDC-117	P1-D04	P2-B02	Tray 3-G03	missing	missing	missing	
24	BC2F2	WBDC-117	P1-D04	P2-B02	Tray 3-H03	HET	HET	HET	
25	BC2F2	WBDC-117	P1-D04	P2-B02	Tray 3-A04	missing	HOC	missing	
26	BC2F2	WBDC-117	P1-D04	P2-B02	Tray 3-B04	HET	HOC	HET	
27	BC2F2	WBDC-117	P1-D04	P2-B02	Tray 3-C04	HOW	HET	HOC	
28	BC2F2	WBDC-117	P1-D04	P2-B02	Tray 3-D04	HET	HET	HOW	
29	BC2F2	WBDC-117	P1-D04	P2-B02	Tray 3-E04	HET	HET	HET	
30	BC2F2	WBDC-117	P1-D04	P2-B02	Tray 3-F04	HOW	HET	HET	
31	BC2F2	WBDC-117	P1-D04	P2-B02	Tray 3-G04	HOC	HET	HOC	Selected
32	BC2F2	WBDC-117	P1-D04	P2-B02	Tray 3-H04	HOW	HET	HOW	
33	BC2F2	WBDC-117	P1-D04	P2-B02	Tray 3-A05	missing	HET	missing	
34	BC2F2	WBDC-117	P1-D04	P2-B02	Tray 3-B05	HOC	HOC	HET	
35	BC2F2	WBDC-117	P1-D04	P2-B02	Tray 3-C05	HET	HET	HOW	
36	BC2F2	WBDC-117	P1-D04	P2-B02	Tray 3-D05	HET	HET	HET	
37	BC2F2	WBDC-117	P1-D04	P2-B02	Tray 3-E05	HET	HOC	HOC	Selected

38	BC2F2	WBDC-117	P1-D04	P2-B02	Tray 3-F05	HOW	HOC	HOW	
39	BC2F2	WBDC-117	P1-D04	P2-B02	Tray 3-G05	HET	HOC	HOC	Selected
40	BC2F2	WBDC-117	P1-D04	P2-B02	Tray 3-A06	missing	HET	missing	
41	BC2F2	WBDC-117	P1-D04	P2-B02	Tray 3-B06	HET	HET	HOC	
42	BC2F2	WBDC-117	P1-D04	P2-B02	Tray 3-C06	HOC	HET	HET	
43	BC2F2	WBDC-117	P1-D04	P2-B02	Tray 3-D06	HOC	HOC	HET	
44	BC2F2	WBDC-117	P1-D04	P2-B02	Tray 3-E06	HOC	HOC	HET	
45	BC2F2	WBDC-117	P1-D04	P2-B02	Tray 3-F06	HET	HET	HET	
46	BC2F2	WBDC-117	P1-D04	P2-B02	Tray 3-G06	HET	HET	HET	
47	BC2F2	WBDC-117	P1-D04	P2-B02	Tray 3-A07	missing	HET	missing	
48	BC2F2	WBDC-117	P1-D04	P2-B02	Tray 3-B07	HOC	HOC	HET	
49	BC2F2	WBDC-117	P1-D04	P2-B02	Tray 3-C07	missing	missing	missing	
50	BC2F2	WBDC-117	P1-D04	P2-B02	Tray 3-D07	HET	HET	HET	
51	BC2F2	WBDC-117	P1-D04	P2-B02	Tray 3-E07	HET	HOC	HOW	
52	BC2F2	WBDC-117	P1-D04	P2-B02	Tray 3-F07	HET	HOW	HOC	
53	BC2F2	WBDC-117	P1-D04	P2-B02	Tray 3-G07	HET	HOC	HET	
54	BC2F2	WBDC-117	P1-D04	P2-B02	Tray 3-A08	missing	HOC	missing	
55	BC2F2	WBDC-117	P1-D04	P2-B02	Tray 3-B08	HOW	HOC	HET	
56	BC2F2	WBDC-117	P1-D04	P2-B02	Tray 3-C08	HOW	HOC	HOC	
57	BC2F2	WBDC-117	P1-D04	P2-B02	Tray 3-D08	missing	missing	HOC	
58	BC2F2	WBDC-117	P1-D04	P2-B02	Tray 3-E08	HOC	HET	HET	
59	BC2F2	WBDC-117	P1-D04	P2-B02	Tray 3-F08	HOC	HOC	HET	
60	BC2F2	WBDC-117	P1-D04	P2-B02	Tray 3-G08	HOC	HET	HET	
61	BC2F2	WBDC-117	P1-D04	P2-B02	Tray 3-A09	missing	HET	missing	
62	BC2F2	WBDC-117	P1-D04	P2-B02	Tray 3-B09	HET	HOC	HOW	
63	BC2F2	WBDC-117	P1-D04	P2-B02	Tray 3-C09	missing	missing	missing	
64	BC2F2	WBDC-117	P1-D04	P2-B02	Tray 3-D09	missing	missing	HOC	
65	BC2F2	WBDC-117	P1-D04	P2-B02	Tray 3-E09	HOC	HOW	HET	
66	BC2F2	WBDC-117	P1-D04	P2-B02	Tray 3-F09	missing	HET	HET	
67	BC2F2	WBDC-117	P1-D04	P2-B02	Tray 3-G09	HET	HET	HOW	
68	BC2F2	WBDC-117	P1-D04	P2-B02	Tray 3-A10	missing	HET	missing	
69	BC2F2	WBDC-117	P1-D04	P2-B02	Tray 3-B10	HOC	HOC	HET	
70	BC2F2	WBDC-117	P1-D04	P2-B02	Tray 3-C10	HET	HOC	HOW	
71	BC2F2	WBDC-117	P1-D04	P2-B02	Tray 3-D10	HET	HET	HOC	
72	BC2F2	WBDC-117	P1-D04	P2-B02	Tray 3-E10	missing	missing	missing	
73	BC2F2	WBDC-117	P1-D04	P2-B02	Tray 3-F10	missing	missing	missing	
74	BC2F2	WBDC-117	P1-D04	P2-B02	Tray 3-G10	missing	missing	missing	
75	BC2F2	WBDC-117	P1-D04	P2-B02	Tray 3-A11	missing	HOC	missing	
76	BC2F2	WBDC-117	P1-D04	P2-B02	Tray 3-B11	HOW	HET	HET	
77	BC2F2	WBDC-117	P1-D04	P2-B02	Tray 3-C11	missing	missing	missing	
78	BC2F2	WBDC-117	P1-D04	P2-B02	Tray 3-D11	HET	HET	HOC	
79	BC2F2	WBDC-117	P1-D04	P2-B02	Tray 3-E11	missing	missing	HET	
80	BC2F2	WBDC-117	P1-D04	P2-B02	Tray 3-F11	missing	missing	missing	

81	BC2F2	WBDC-117	P1-D04	P2-B02	Tray 3-G11	HET	HET	HET	
82	BC2F2	WBDC-117	P1-D04	P2-B02	Tray 3-A12	missing	HET	missing	
83	BC2F2	WBDC-117	P1-D04	P2-B02	Tray 3-B12	HET	HET	HET	
84	BC2F2	WBDC-117	P1-D04	P2-B02	Tray 3-C12	HOC	HET	HOC	Selected
85	BC2F2	WBDC-117	P1-D04	P2-B02	Tray 3-D12	missing	missing	missing	
86	BC2F2	WBDC-117	P1-D04	P2-B02	Tray 3-E12	missing	missing	missing	
87	BC2F2	WBDC-117	P1-D04	P2-B02	Tray 3-F12	missing	HOC	HET	
88	BC2F2	WBDC-117	P1-D04	P2-B02	Tray 3-G12	HET	HET	HOW	
89	BC2F2	WBDC-199	P4-A11	P4-D05	Tray_10-A01	missing	missing	missing	
90	BC2F2	WBDC-199	P4-A11	P4-D05	Tray_10-B01	HET	HET	HOW	
91	BC2F2	WBDC-199	P4-A11	P4-D05	Tray_10-C01	HOC	HOW	HET	
92	BC2F2	WBDC-199	P4-A11	P4-D05	Tray_10-D01	HOW	HOW	HOW	
93	BC2F2	WBDC-199	P4-A11	P4-D05	Tray_10-E01	missing	missing	missing	
94	BC2F2	WBDC-199	P4-A11	P4-D05	Tray_10-F01	HOC	HET	HET	
95	BC2F2	WBDC-199	P4-A11	P4-D05	Tray_10-G01	missing	missing	missing	
96	BC2F2	WBDC-199	P4-A11	P4-D05	Tray_10-H01	missing	missing	missing	
97	BC2F2	WBDC-199	P4-A11	P4-D05	Tray_10-A02	HET	HET	HET	
98	BC2F2	WBDC-199	P4-A11	P4-D05	Tray_10-B02	HET	HOW	HOC	
99	BC2F2	WBDC-199	P4-A11	P4-D05	Tray_10-C02	HET	HOW	missing	
100	BC2F2	WBDC-199	P4-A11	P4-D05	Tray_10-D02	HET	missing	missing	
101	BC2F2	WBDC-199	P4-A11	P4-D05	Tray_10-E02	missing	missing	missing	
102	BC2F2	WBDC-199	P4-A11	P4-D05	Tray_10-F02	missing	missing	missing	
103	BC2F2	WBDC-199	P4-A11	P4-D05	Tray_10-G02	HET	missing	missing	
104	BC2F2	WBDC-199	P4-A11	P4-D05	Tray_10-H02	missing	missing	missing	
105	BC2F2	WBDC-199	P4-A11	P4-D05	Tray_10-A03	HET	HET	HOC	
106	BC2F2	WBDC-199	P4-A11	P4-D05	Tray_10-B03	HOW	HET	HOC	
107	BC2F2	WBDC-199	P4-A11	P4-D05	Tray_10-C03	HOW	HOW	HET	
108	BC2F2	WBDC-199	P4-A11	P4-D05	Tray_10-D03	missing	missing	missing	
109	BC2F2	WBDC-199	P4-A11	P4-D05	Tray_10-E03	HOW	HOW	HET	
110	BC2F2	WBDC-199	P4-A11	P4-D05	Tray_10-F03	HET	HET	HOC	
111	BC2F2	WBDC-199	P4-A11	P4-D05	Tray_10-G03	HET	HET	HOC	
112	BC2F2	WBDC-199	P4-A11	P4-D05	Tray_10-H03	missing	missing	missing	
113	BC2F2	WBDC-199	P4-A11	P4-D05	Tray_10-A04	HOW	HET	HET	
114	BC2F2	WBDC-199	P4-A11	P4-D05	Tray_10-B04	HOC	HET	HET	
115	BC2F2	WBDC-199	P4-A11	P4-D05	Tray_10-C04	HET	HOC	HOW	
116	BC2F2	WBDC-199	P4-A11	P4-D05	Tray_10-D04	HET	HET	HET	
117	BC2F2	WBDC-199	P4-A11	P4-D05	Tray_10-E04	HET	HOC	HOW	
118	BC2F2	WBDC-199	P4-A11	P4-D05	Tray_10-F04	missing	missing	missing	
119	BC2F2	WBDC-199	P4-A11	P4-D05	Tray_10-G04	HET	HET	HET	
120	BC2F2	WBDC-199	P4-A11	P4-D05	Tray_10-H04	missing	missing	missing	
121	BC2F2	WBDC-199	P4-A11	P4-D05	Tray_10-A05	HOW	HET	HOC	
122	BC2F2	WBDC-199	P4-A11	P4-D05	Tray_10-B05	HET	HET	HET	
123	BC2F2	WBDC-199	P4-A11	P4-D05	Tray_10-C05	missing	missing	missing	

124	BC2F2	WBDC-199	P4-A11	P4-D05	Tray_10-D05	HOW	HOW	HET	
125	BC2F2	WBDC-199	P4-A11	P4-D05	Tray_10-E05	HOC	HET	HOW	
126	BC2F2	WBDC-199	P4-A11	P4-D05	Tray_10-F05	missing	missing	missing	
127	BC2F2	WBDC-199	P4-A11	P4-D05	Tray_10-G05	HOW	HET	HET	
128	BC2F2	WBDC-199	P4-A11	P4-D05	Tray_10-A06	HOC	HET	HET	
129	BC2F2	WBDC-199	P4-A11	P4-D05	Tray_10-B06	HET	HOC	HET	
130	BC2F2	WBDC-199	P4-A11	P4-D05	Tray_10-C06	HOC	HET	HOC	Selected
131	BC2F2	WBDC-199	P4-A11	P4-D05	Tray_10-D06	HET	HET	HET	
132	BC2F2	WBDC-199	P4-A11	P4-D05	Tray_10-E06	missing	missing	missing	
133	BC2F2	WBDC-199	P4-A11	P4-D05	Tray_10-F06	HOW	HET	HOC	
134	BC2F2	WBDC-199	P4-A11	P4-D05	Tray_10-G06	missing	missing	missing	
135	BC2F2	WBDC-199	P4-A11	P4-D05	Tray_10-A07	missing	missing	missing	
136	BC2F2	WBDC-199	P4-A11	P4-D05	Tray_10-B07	missing	missing	missing	
137	BC2F2	WBDC-199	P4-A11	P4-D05	Tray_10-C07	missing	missing	missing	
138	BC2F2	WBDC-199	P4-A11	P4-D05	Tray_10-D07	HOW	HOC	HOC	
139	BC2F2	WBDC-199	P4-A11	P4-D05	Tray_10-E07	missing	missing	missing	
140	BC2F2	WBDC-199	P4-A11	P4-D05	Tray_10-F07	missing	missing	missing	
141	BC2F2	WBDC-199	P4-A11	P4-D05	Tray_10-G07	HOC	missing	missing	
142	BC2F2	WBDC-199	P4-A11	P4-D05	Tray_10-A08	HOW	HOW	HET	
143	BC2F2	WBDC-199	P4-A11	P4-D05	Tray_10-B08	missing	missing	missing	
144	BC2F2	WBDC-199	P4-A11	P4-D05	Tray_10-C08	HOC	HET	HET	
145	BC2F2	WBDC-199	P4-A11	P4-D05	Tray_10-D08	HET	HET	HET	
146	BC2F2	WBDC-199	P4-A11	P4-D05	Tray_10-E08	missing	missing	missing	
147	BC2F2	WBDC-199	P4-A11	P4-D05	Tray_10-F08	missing	missing	missing	
148	BC2F2	WBDC-199	P4-A11	P4-D05	Tray_10-G08	missing	missing	missing	
149	BC2F2	WBDC-199	P4-A11	P4-D05	Tray_10-A09	HOC	HOC	HOC	Selected
150	BC2F2	WBDC-199	P4-A11	P4-D05	Tray_10-B09	HET	missing	missing	
151	BC2F2	WBDC-199	P4-A11	P4-D05	Tray_10-C09	HET	HOC	HOC	Selected
152	BC2F2	WBDC-199	P4-A11	P4-D05	Tray_10-D09	HET	HOC	HOW	
153	BC2F2	WBDC-199	P4-A11	P4-D05	Tray_10-E09	missing	missing	missing	
154	BC2F2	WBDC-199	P4-A11	P4-D05	Tray_10-F09	HOW	HOW	HET	
155	BC2F2	WBDC-199	P4-A11	P4-D05	Tray_10-G09	missing	missing	missing	
156	BC2F2	WBDC-199	P4-A11	P4-D05	Tray_10-A10	HET	HET	HET	
157	BC2F2	WBDC-199	P4-A11	P4-D05	Tray_10-B10	HOC	HOC	HET	
158	BC2F2	WBDC-199	P4-A11	P4-D05	Tray_10-C10	HOC	missing	missing	
159	BC2F2	WBDC-199	P4-A11	P4-D05	Tray_10-D10	HET	HET	HET	
160	BC2F2	WBDC-199	P4-A11	P4-D05	Tray_10-E10	HOC	missing	missing	
161	BC2F2	WBDC-199	P4-A11	P4-D05	Tray_10-F10	HOC	HOC	HET	
162	BC2F2	WBDC-199	P4-A11	P4-D05	Tray_10-G10	HET	missing	missing	
163	BC2F2	WBDC-199	P4-A11	P4-D05	Tray_10-A11	HET	missing	missing	
164	BC2F2	WBDC-199	P4-A11	P4-D05	Tray_10-B11	HET	missing	missing	
165	BC2F2	WBDC-199	P4-A11	P4-D05	Tray_10-C11	HOW	HOW	HET	
166	BC2F2	WBDC-199	P4-A11	P4-D05	Tray_10-D11	HOC	missing	missing	

167	BC2F2	WBDC-199	P4-A11	P4-D05	Tray_10-E11	missing	missing	missing
168	BC2F2	WBDC-199	P4-A11	P4-D05	Tray_10-F11	missing	missing	missing
169	BC2F2	WBDC-199	P4-A11	P4-D05	Tray_10-G11	HET	HET	HOW
170	BC2F2	WBDC-199	P4-A11	P4-D05	Tray_10-A12	HET	HOC	HET
171	BC2F2	WBDC-199	P4-A11	P4-D05	Tray_10-B12	HET	HOC	HOW
172	BC2F2	WBDC-199	P4-A11	P4-D05	Tray_10-C12	HOW	HOC	HOW
173	BC2F2	WBDC-199	P4-A11	P4-D05	Tray_10-D12	HET	HET	HOW
174	BC2F2	WBDC-199	P4-A11	P4-D05	Tray_10-E12	missing	missing	missing
175	BC2F2	WBDC-199	P4-A11	P4-D05	Tray_10-F12	HET	missing	missing
176	BC2F2	WBDC-199	P4-A11	P4-D05	Tray_10-G12	HET	HOW	HOC
177	BC2F2	WBDC-329	P7-D10	P1-D04	Tray_14-A01	HET	HOC	HOC
178	BC2F2	WBDC-329	P7-D10	P1-D04	Tray_14-B01	HET	HET	HET
179	BC2F2	WBDC-329	P7-D10	P1-D04	Tray_14-C01	HET	HET	HET
180	BC2F2	WBDC-329	P7-D10	P1-D04	Tray_14-D01	HET	HET	HET
181	BC2F2	WBDC-329	P7-D10	P1-D04	Tray_14-E01	HOC	HOC	HET
182	BC2F2	WBDC-329	P7-D10	P1-D04	Tray_14-F01	HET	HET	HOC
183	BC2F2	WBDC-329	P7-D10	P1-D04	Tray_14-G01	HOC	HOW	HOW
184	BC2F2	WBDC-329	P7-D10	P1-D04	Tray_14-H01	missing	missing	missing
185	BC2F2	WBDC-329	P7-D10	P1-D04	Tray_14-A02	missing	missing	missing
186	BC2F2	WBDC-329	P7-D10	P1-D04	Tray_14-B02	HOW	HET	HOC
187	BC2F2	WBDC-329	P7-D10	P1-D04	Tray_14-C02	HOW	HOW	HET
188	BC2F2	WBDC-329	P7-D10	P1-D04	Tray_14-D02	missing	missing	missing
189	BC2F2	WBDC-329	P7-D10	P1-D04	Tray_14-E02	HET	HOC	HOW
190	BC2F2	WBDC-329	P7-D10	P1-D04	Tray_14-F02	HET	HET	HET
191	BC2F2	WBDC-329	P7-D10	P1-D04	Tray_14-G02	HOW	missing	HOW
192	BC2F2	WBDC-329	P7-D10	P1-D04	Tray_14-H02	HOC	HET	HOW
193	BC2F2	WBDC-329	P7-D10	P1-D04	Tray_14-A03	HET	HOC	HOW
194	BC2F2	WBDC-329	P7-D10	P1-D04	Tray_14-B03	HOC	HET	HOW
195	BC2F2	WBDC-329	P7-D10	P1-D04	Tray_14-C03	HOC	HET	HOW
196	BC2F2	WBDC-329	P7-D10	P1-D04	Tray_14-D03	HOW	HOC	HOC
197	BC2F2	WBDC-329	P7-D10	P1-D04	Tray_14-E03	HET	HOW	HOC
198	BC2F2	WBDC-329	P7-D10	P1-D04	Tray_14-F03	HET	HET	HET
199	BC2F2	WBDC-329	P7-D10	P1-D04	Tray_14-G03	missing	missing	missing
200	BC2F2	WBDC-329	P7-D10	P1-D04	Tray_14-H03	missing	missing	missing
201	BC2F2	WBDC-329	P7-D10	P1-D04	Tray_14-A04	HET	HET	HOC
202	BC2F2	WBDC-329	P7-D10	P1-D04	Tray_14-B04	HET	missing	HOW
203	BC2F2	WBDC-329	P7-D10	P1-D04	Tray_14-C04	HET	HOC	HET
204	BC2F2	WBDC-329	P7-D10	P1-D04	Tray_14-D04	missing	missing	missing
205	BC2F2	WBDC-329	P7-D10	P1-D04	Tray_14-E04	HOW	HET	HOC
206	BC2F2	WBDC-329	P7-D10	P1-D04	Tray_14-F04	HET	HOC	HET
207	BC2F2	WBDC-329	P7-D10	P1-D04	Tray_14-G04	HET	HOC	HOC
208	BC2F2	WBDC-329	P7-D10	P1-D04	Tray_14-H04	HET	HOW	HET
209	BC2F2	WBDC-329	P7-D10	P1-D04	Tray_14-A05	missing	missing	missing

210	BC2F2	WBDC-329	P7-D10	P1-D04	Tray_14-B05	HET	HET	HET	
211	BC2F2	WBDC-329	P7-D10	P1-D04	Tray_14-C05	HOW	HET	HET	
212	BC2F2	WBDC-329	P7-D10	P1-D04	Tray_14-D05	HOC	HET	HET	
213	BC2F2	WBDC-329	P7-D10	P1-D04	Tray_14-E05	missing	missing	missing	
214	BC2F2	WBDC-329	P7-D10	P1-D04	Tray_14-F05	HOW	HET	HOC	
215	BC2F2	WBDC-329	P7-D10	P1-D04	Tray_14-G05	HET	HET	HOC	
216	BC2F2	WBDC-329	P7-D10	P1-D04	Tray_14-A06	HET	HOC	HOW	
217	BC2F2	WBDC-329	P7-D10	P1-D04	Tray_14-B06	HET	HET	HOW	
218	BC2F2	WBDC-329	P7-D10	P1-D04	Tray_14-C06	HET	HET	missing	
219	BC2F2	WBDC-329	P7-D10	P1-D04	Tray_14-D06	HET	HOW	HET	
220	BC2F2	WBDC-329	P7-D10	P1-D04	Tray_14-E06	HOC	HOW	HOC	
221	BC2F2	WBDC-329	P7-D10	P1-D04	Tray_14-F06	HOW	HET	HOW	
222	BC2F2	WBDC-329	P7-D10	P1-D04	Tray_14-G06	HOC	HOC	HOC	Selected
223	BC2F2	WBDC-329	P7-D10	P1-D04	Tray_14-A07	HOW	HOC	HET	
224	BC2F2	WBDC-329	P7-D10	P1-D04	Tray_14-B07	HET	HET	HET	
225	BC2F2	WBDC-329	P7-D10	P1-D04	Tray_14-C07	HOW	HOW	HOC	
226	BC2F2	WBDC-329	P7-D10	P1-D04	Tray_14-D07	HOW	HOC	HET	
227	BC2F2	WBDC-329	P7-D10	P1-D04	Tray_14-E07	HET	HET	HET	
228	BC2F2	WBDC-329	P7-D10	P1-D04	Tray_14-F07	HET	HET	HOC	
229	BC2F2	WBDC-329	P7-D10	P1-D04	Tray_14-G07	missing	missing	missing	
230	BC2F2	WBDC-329	P7-D10	P1-D04	Tray_14-A08	HOW	HET	HET	
231	BC2F2	WBDC-329	P7-D10	P1-D04	Tray_14-B08	HOW	HOW	HOW	
232	BC2F2	WBDC-329	P7-D10	P1-D04	Tray_14-C08	HET	HOW	HET	
233	BC2F2	WBDC-329	P7-D10	P1-D04	Tray_14-D08	HET	HOC	HET	
234	BC2F2	WBDC-329	P7-D10	P1-D04	Tray_14-E08	HET	HOW	HOW	
235	BC2F2	WBDC-329	P7-D10	P1-D04	Tray_14-F08	HET	HOC	HET	
236	BC2F2	WBDC-329	P7-D10	P1-D04	Tray_14-G08	HET	HET	HET	
237	BC2F2	WBDC-329	P7-D10	P1-D04	Tray_14-A09	HET	HOW	HET	
238	BC2F2	WBDC-329	P7-D10	P1-D04	Tray_14-B09	HOW	HOW	HET	
239	BC2F2	WBDC-329	P7-D10	P1-D04	Tray_14-C09	HET	HOW	HET	
240	BC2F2	WBDC-329	P7-D10	P1-D04	Tray_14-D09	HET	HOW	HOW	
241	BC2F2	WBDC-329	P7-D10	P1-D04	Tray_14-E09	missing	missing	missing	
242	BC2F2	WBDC-329	P7-D10	P1-D04	Tray_14-F09	HOW	HOW	HOC	
243	BC2F2	WBDC-329	P7-D10	P1-D04	Tray_14-G09	missing	missing	missing	
244	BC2F2	WBDC-329	P7-D10	P1-D04	Tray_14-A10	missing	missing	missing	
245	BC2F2	WBDC-329	P7-D10	P1-D04	Tray_14-B10	missing	missing	missing	
246	BC2F2	WBDC-329	P7-D10	P1-D04	Tray_14-C10	missing	missing	missing	
247	BC2F2	WBDC-329	P7-D10	P1-D04	Tray_14-D10	missing	missing	missing	
248	BC2F2	WBDC-329	P7-D10	P1-D04	Tray_14-E10	missing	missing	missing	
249	BC2F2	WBDC-329	P7-D10	P1-D04	Tray_14-F10	HOW	HOW	HOC	
250	BC2F2	WBDC-329	P7-D10	P1-D04	Tray_14-G10	missing	missing	missing	
251	BC2F2	WBDC-329	P7-D10	P1-D04	Tray_14-A11	missing	missing	missing	
252	BC2F2	WBDC-329	P7-D10	P1-D04	Tray_14-B11	missing	missing	missing	

253	BC2F2	WBDC-329	P7-D10	P1-D04	Tray_14-C11	missing	missing	missing	
254	BC2F2	WBDC-329	P7-D10	P1-D04	Tray_14-D11	missing	missing	missing	
255	BC2F2	WBDC-329	P7-D10	P1-D04	Tray_14-E11	missing	missing	missing	
256	BC2F2	WBDC-329	P7-D10	P1-D04	Tray_14-F11	missing	missing	missing	
257	BC2F2	WBDC-329	P7-D10	P1-D04	Tray_14-G11	missing	missing	missing	
258	BC2F2	WBDC-329	P7-D10	P1-D04	Tray_14-A12	missing	missing	missing	
259	BC2F2	WBDC-329	P7-D10	P1-D04	Tray_14-B12	missing	missing	missing	
260	BC2F2	WBDC-329	P7-D10	P1-D04	Tray_14-C12	missing	missing	missing	
261	BC2F2	WBDC-329	P7-D10	P1-D04	Tray_14-D12	missing	missing	missing	
262	BC2F2	WBDC-329	P7-D10	P1-D04	Tray_14-E12	HET	missing	missing	
263	BC2F2	WBDC-329	P7-D10	P1-D04	Tray_14-F12	missing	missing	missing	
264	BC2F2	WBDC-329	P7-D10	P1-D04	Tray_14-G12	missing	missing	missing	
265	BC2F2	WBDC-038	P3-D01	P3-B09	Tray_9-A01	HET	HET	HOW	
266	BC2F2	WBDC-038	P3-D01	P3-B09	Tray_9-B01	HET	HOC	HET	
267	BC2F2	WBDC-038	P3-D01	P3-B09	Tray_9-C01	HET	HET	HOW	
268	BC2F2	WBDC-038	P3-D01	P3-B09	Tray_9-D01	HET	HOC	HOC	
269	BC2F2	WBDC-038	P3-D01	P3-B09	Tray_9-E01	HOC	HOC	HET	
270	BC2F2	WBDC-038	P3-D01	P3-B09	Tray_9-F01	HET	HET	HET	
271	BC2F2	WBDC-038	P3-D01	P3-B09	Tray_9-G01	HOW	HOC	HET	
272	BC2F2	WBDC-038	P3-D01	P3-B09	Tray_9-H01	HOW	missing	HOW	
273	BC2F2	WBDC-038	P3-D01	P3-B09	Tray_9-A02	HET	HET	HOC	
274	BC2F2	WBDC-038	P3-D01	P3-B09	Tray_9-B02	HET	HET	HET	
275	BC2F2	WBDC-038	P3-D01	P3-B09	Tray_9-C02	HET	HOC	HET	
276	BC2F2	WBDC-038	P3-D01	P3-B09	Tray_9-D02	HOC	HET	HOC	
277	BC2F2	WBDC-038	P3-D01	P3-B09	Tray_9-E02	HOW	HET	HET	
278	BC2F2	WBDC-038	P3-D01	P3-B09	Tray_9-F02	HET	HET	HOW	
279	BC2F2	WBDC-038	P3-D01	P3-B09	Tray_9-G02	HET	HOC	HET	
280	BC2F2	WBDC-038	P3-D01	P3-B09	Tray_9-H02	HET	HET	HOC	
281	BC2F2	WBDC-038	P3-D01	P3-B09	Tray_9-A03	HET	HET	HOC	
282	BC2F2	WBDC-038	P3-D01	P3-B09	Tray_9-B03	HOC	HET	HET	
283	BC2F2	WBDC-038	P3-D01	P3-B09	Tray_9-C03	HET	HET	HOC	
284	BC2F2	WBDC-038	P3-D01	P3-B09	Tray_9-D03	HOC	HOC	HET	
285	BC2F2	WBDC-038	P3-D01	P3-B09	Tray_9-E03	HET	HET	HOC	
286	BC2F2	WBDC-038	P3-D01	P3-B09	Tray_9-F03	HOC	HOC	HOW	
287	BC2F2	WBDC-038	P3-D01	P3-B09	Tray_9-G03	HET	HET	HET	
288	BC2F2	WBDC-038	P3-D01	P3-B09	Tray_9-H03	missing	HOC	HET	
289	BC2F2	WBDC-038	P3-D01	P3-B09	Tray_9-A04	HET	HET	HOC	
290	BC2F2	WBDC-038	P3-D01	P3-B09	Tray_9-B04	HET	HET	HET	
291	BC2F2	WBDC-038	P3-D01	P3-B09	Tray_9-C04	HOW	HET	HOW	
292	BC2F2	WBDC-038	P3-D01	P3-B09	Tray_9-D04	HOC	HOC	HOW	
293	BC2F2	WBDC-038	P3-D01	P3-B09	Tray_9-E04	HOC	HOC	HOC	Selected
294	BC2F2	WBDC-038	P3-D01	P3-B09	Tray_9-F04	HET	HET	HET	
295	BC2F2	WBDC-038	P3-D01	P3-B09	Tray_9-G04	HOW	HOW	HOW	

296	BC2F2	WBDC-038	P3-D01	P3-B09	Tray_9-H04	HET	HET	HET	
297	BC2F2	WBDC-038	P3-D01	P3-B09	Tray_9-A05	HOW	HET	HOW	
298	BC2F2	WBDC-038	P3-D01	P3-B09	Tray_9-B05	HET	HOW	HET	
299	BC2F2	WBDC-038	P3-D01	P3-B09	Tray_9-C05	HET	HOC	HOW	
300	BC2F2	WBDC-038	P3-D01	P3-B09	Tray_9-D05	HET	HET	HET	
301	BC2F2	WBDC-038	P3-D01	P3-B09	Tray_9-E05	HET	HET	HOW	
302	BC2F2	WBDC-038	P3-D01	P3-B09	Tray_9-F05	HET	HOW	HOC	
303	BC2F2	WBDC-038	P3-D01	P3-B09	Tray_9-G05	HET	HOC	HOW	
304	BC2F2	WBDC-038	P3-D01	P3-B09	Tray_9-A06	HET	HET	HET	
305	BC2F2	WBDC-038	P3-D01	P3-B09	Tray_9-B06	HET	HOW	HOC	
306	BC2F2	WBDC-038	P3-D01	P3-B09	Tray_9-C06	HOW	HET	HOW	
307	BC2F2	WBDC-038	P3-D01	P3-B09	Tray_9-D06	HET	HET	HET	
308	BC2F2	WBDC-038	P3-D01	P3-B09	Tray_9-E06	HET	HOW	HET	
309	BC2F2	WBDC-038	P3-D01	P3-B09	Tray_9-F06	HOC	HOC	HOC	Selected
310	BC2F2	WBDC-038	P3-D01	P3-B09	Tray_9-G06	HOW	HET	HET	
311	BC2F2	WBDC-038	P3-D01	P3-B09	Tray_9-A07	HOC	missing	HOW	
312	BC2F2	WBDC-038	P3-D01	P3-B09	Tray_9-B07	HET	HOC	HOC	Selected
313	BC2F2	WBDC-038	P3-D01	P3-B09	Tray_9-C07	HOW	HOC	HET	
314	BC2F2	WBDC-038	P3-D01	P3-B09	Tray_9-D07	HET	HET	HET	
315	BC2F2	WBDC-038	P3-D01	P3-B09	Tray_9-E07	HOW	HOW	HOC	
316	BC2F2	WBDC-038	P3-D01	P3-B09	Tray_9-F07	missing	missing	missing	
317	BC2F2	WBDC-038	P3-D01	P3-B09	Tray_9-G07	HOC	HOW	HET	
318	BC2F2	WBDC-038	P3-D01	P3-B09	Tray_9-A08	HET	HOC	HOC	
319	BC2F2	WBDC-038	P3-D01	P3-B09	Tray_9-B08	HET	HOW	HET	
320	BC2F2	WBDC-038	P3-D01	P3-B09	Tray_9-C08	HOW	HOC	HOC	
321	BC2F2	WBDC-038	P3-D01	P3-B09	Tray_9-D08	HOC	HET	HET	
322	BC2F2	WBDC-038	P3-D01	P3-B09	Tray_9-E08	HOC	HOW	HET	
323	BC2F2	WBDC-038	P3-D01	P3-B09	Tray_9-F08	HOW	HOW	HET	
324	BC2F2	WBDC-038	P3-D01	P3-B09	Tray_9-G08	HOC	HOC	HOW	
325	BC2F2	WBDC-038	P3-D01	P3-B09	Tray_9-A09	HET	HOW	HET	
326	BC2F2	WBDC-038	P3-D01	P3-B09	Tray_9-B09	HOW	HOW	HET	
327	BC2F2	WBDC-038	P3-D01	P3-B09	Tray_9-C09	HET	HOC	HOC	
328	BC2F2	WBDC-038	P3-D01	P3-B09	Tray_9-D09	HOC	HET	HET	
329	BC2F2	WBDC-038	P3-D01	P3-B09	Tray_9-E09	HOW	HOC	HET	
330	BC2F2	WBDC-038	P3-D01	P3-B09	Tray_9-F09	HOC	HET	HOC	
331	BC2F2	WBDC-038	P3-D01	P3-B09	Tray_9-G09	HET	HOC	HOW	
332	BC2F2	WBDC-038	P3-D01	P3-B09	Tray_9-A10	HOW	HOC	HET	
333	BC2F2	WBDC-038	P3-D01	P3-B09	Tray_9-B10	HET	HOW	HET	
334	BC2F2	WBDC-038	P3-D01	P3-B09	Tray_9-C10	HOC	HOC	HOC	Selected
335	BC2F2	WBDC-038	P3-D01	P3-B09	Tray_9-D10	HET	HET	HET	
336	BC2F2	WBDC-038	P3-D01	P3-B09	Tray_9-E10	HOW	HET	HET	
337	BC2F2	WBDC-038	P3-D01	P3-B09	Tray_9-F10	HOC	HET	HOC	
338	BC2F2	WBDC-038	P3-D01	P3-B09	Tray_9-G10	HET	HET	HOW	

339	BC2F2	WBDC-038	P3-D01	P3-B09	Tray_9-A11	HOC	HET	HET
340	BC2F2	WBDC-038	P3-D01	P3-B09	Tray_9-B11	HOC	missing	HOW
341	BC2F2	WBDC-038	P3-D01	P3-B09	Tray_9-C11	HOW	HET	HOC
342	BC2F2	WBDC-038	P3-D01	P3-B09	Tray_9-D11	HET	HOW	HET
343	BC2F2	WBDC-038	P3-D01	P3-B09	Tray_9-E11	HET	HET	HOC
344	BC2F2	WBDC-038	P3-D01	P3-B09	Tray_9-F11	HET	HET	HOC
345	BC2F2	WBDC-038	P3-D01	P3-B09	Tray_9-G11	HET	HET	HET
346	BC2F2	WBDC-038	P3-D01	P3-B09	Tray_9-A12	HET	HET	HET
347	BC2F2	WBDC-038	P3-D01	P3-B09	Tray_9-B12	HOW	HOC	HOC
348	BC2F2	WBDC-038	P3-D01	P3-B09	Tray_9-C12	HET	HOW	HET
349	BC2F2	WBDC-038	P3-D01	P3-B09	Tray_9-D12	HET	HET	HOC
350	BC2F2	WBDC-038	P3-D01	P3-B09	Tray_9-E12	HOW	HET	HET
351	BC2F2	WBDC-038	P3-D01	P3-B09	Tray_9-F12	HET	HET	HET
352	BC2F2	WBDC-038	P3-D01	P3-B09	Tray_9-G12	HOW	missing	HET
353	BC2F2	WBDC-117	P1-D04	P2-B02	Tray 3-A01	missing	missing	missing
354	BC2F2	WBDC-117	P1-D04	P2-B02	Tray_6-A02	HET	HOC	HOW
355	BC2F2	WBDC-117	P1-D04	P2-B02	Tray_6-D08	HOC	HOW	HET
356	BC2F2	WBDC-117	P1-D04	P2-B02	Tray 3-A02	HOC	HOC	HET
357	BC2F2	WBDC-117	P1-D04	P2-B02	Tray_6-A03	HOC	HOC	HOW
358	BC2F2	WBDC-117	P1-D04	P2-B02	Tray_6-E02	HOC	HOC	HOW
359	BC2F2	WBDC-117	P1-D04	P2-B02	Tray 3-A03	HET	HOC	HET
360	BC2F2	WBDC-117	P1-D04	P2-B02	Tray_6-A04	HET	HET	HOW
361	BC2F2	WBDC-117	P1-D04	P2-B02	Tray_6-E03	HOC	HOC	missing
362	BC2F2	WBDC-117	P1-D04	P2-B02	Tray 3-A04	HET	HOC	HET
363	BC2F2	WBDC-117	P1-D04	P2-B02	Tray_6-B02	HET	HET	HET
364	BC2F2	WBDC-117	P1-D04	P2-B02	Tray_6-E07	HOW	HET	HET
365	BC2F2	WBDC-117	P1-D04	P2-B02	Tray 3-A05	HOW	HET	HET
366	BC2F2	WBDC-117	P1-D04	P2-B02	Tray_6-B03	HOW	HET	HET
367	BC2F2	WBDC-117	P1-D04	P2-B02	Tray_6-E08	HET	HOC	HET
368	BC2F2	WBDC-117	P1-D04	P2-B02	Tray 3-A06	HET	HET	HET
369	BC2F2	WBDC-117	P1-D04	P2-B02	Tray_6-B04	HET	HET	HOC
370	BC2F2	WBDC-117	P1-D04	P2-B02	Tray_6-G02	HET	HET	HET
371	BC2F2	WBDC-117	P1-D04	P2-B02	Tray 3-A07	HET	HET	HET
372	BC2F2	WBDC-117	P1-D04	P2-B02	Tray_6-C02	HET	HOW	HET
373	BC2F2	WBDC-117	P1-D04	P2-B02	Tray_6-H03	HET	HOW	HET
374	BC2F2	WBDC-117	P1-D04	P2-B02	Tray 3-A08	HET	HOC	HET
375	BC2F2	WBDC-117	P1-D04	P2-B02	Tray_6-C03	HOC	HOC	HOW
376	BC2F2	WBDC-117	P1-D04	P2-B02	Tray_6-H04	HET	HOW	HOC
377	BC2F2	WBDC-117	P1-D04	P2-B02	Tray 3-A09	HET	HET	HET
378	BC2F2	WBDC-117	P1-D04	P2-B02	Tray_6-C07	HOW	HET	HET
379	BC2F2	WBDC-117	P1-D04	P2-B02	Tray 3-A10	HET	HET	HET
380	BC2F2	WBDC-117	P1-D04	P2-B02	Tray_6-C09	HET	HET	HET
381	BC2F2	WBDC-117	P1-D04	P2-B02	Tray 3-A11	HOC	HOC	HET

382	BC2F2	WBDC-117	P1-D04	P2-B02	Tray_6-D02	HET	HOW	HOC	
383	BC2F2	WBDC-117	P1-D04	P2-B02	Tray 3-A12	HET	HET	HET	
384	BC2F2	WBDC-117	P1-D04	P2-B02	Tray_6-D07	HOC	HET	HET	
385	BC2F2	WBDC-068	P5-G03	P5-E08	Tray 1-A01	HET	HET	missing	
386	BC2F2	WBDC-068	P5-G03	P5-E08	Tray 1-B01	HET	HOW	HET	
387	BC2F2	WBDC-068	P5-G03	P5-E08	Tray 1-C01	HET	HET	missing	
388	BC2F2	WBDC-068	P5-G03	P5-E08	Tray 1-D01	HOW	HET	HOW	
389	BC2F2	WBDC-068	P5-G03	P5-E08	Tray 1-E01	missing	HET	missing	
390	BC2F2	WBDC-068	P5-G03	P5-E08	Tray 1-F01	HOC	HOC	HET	
391	BC2F2	WBDC-068	P5-G03	P5-E08	Tray 1-G01	missing	missing	HOW	
392	BC2F2	WBDC-068	P5-G03	P5-E08	Tray 1-H01	HOW	HOW	HET	
393	BC2F2	WBDC-068	P5-G03	P5-E08	Tray 1-A02	missing	missing	missing	
394	BC2F2	WBDC-068	P5-G03	P5-E08	Tray 1-B02	missing	missing	missing	
395	BC2F2	WBDC-068	P5-G03	P5-E08	Tray 1-C02	HOC	HET	HET	
396	BC2F2	WBDC-068	P5-G03	P5-E08	Tray 1-D02	HET	HET	missing	
397	BC2F2	WBDC-068	P5-G03	P5-E08	Tray 1-E02	missing	HET	missing	
398	BC2F2	WBDC-068	P5-G03	P5-E08	Tray 1-F02	HOW	HET	HET	
399	BC2F2	WBDC-068	P5-G03	P5-E08	Tray 1-G02	missing	missing	missing	
400	BC2F2	WBDC-068	P5-G03	P5-E08	Tray 1-H02	HET	missing	missing	
401	BC2F2	WBDC-068	P5-G03	P5-E08	Tray 1-A03	missing	missing	missing	
402	BC2F2	WBDC-068	P5-G03	P5-E08	Tray 1-B03	missing	missing	missing	
403	BC2F2	WBDC-068	P5-G03	P5-E08	Tray 1-C03	missing	missing	missing	
404	BC2F2	WBDC-068	P5-G03	P5-E08	Tray 1-D03	HET	HOC	HET	
405	BC2F2	WBDC-068	P5-G03	P5-E08	Tray 1-E03	missing	HET	missing	
406	BC2F2	WBDC-068	P5-G03	P5-E08	Tray 1-F03	HET	HOW	HET	
407	BC2F2	WBDC-068	P5-G03	P5-E08	Tray 1-G03	missing	missing	missing	
408	BC2F2	WBDC-068	P5-G03	P5-E08	Tray 1-H03	HOC	missing	missing	
409	BC2F2	WBDC-068	P5-G03	P5-E08	Tray 1-A04	missing	missing	missing	
410	BC2F2	WBDC-068	P5-G03	P5-E08	Tray 1-B04	missing	missing	missing	
411	BC2F2	WBDC-068	P5-G03	P5-E08	Tray 1-C04	missing	missing	missing	
412	BC2F2	WBDC-068	P5-G03	P5-E08	Tray 1-D04	HOW	HET	HOC	
413	BC2F2	WBDC-068	P5-G03	P5-E08	Tray 1-E04	missing	missing	missing	
414	BC2F2	WBDC-068	P5-G03	P5-E08	Tray 1-F04	HET	HOC	HET	
415	BC2F2	WBDC-068	P5-G03	P5-E08	Tray 1-G04	HET	HOC	HET	
416	BC2F2	WBDC-068	P5-G03	P5-E08	Tray 1-H04	missing	missing	missing	
417	BC2F2	WBDC-068	P5-G03	P5-E08	Tray 1-A05	missing	missing	missing	
418	BC2F2	WBDC-068	P5-G03	P5-E08	Tray 1-B05	missing	missing	missing	
419	BC2F2	WBDC-068	P5-G03	P5-E08	Tray 1-C05	HOC	HOC	HOC	Selected
420	BC2F2	WBDC-068	P5-G03	P5-E08	Tray 1-D05	HOW	HOC	HOW	
421	BC2F2	WBDC-068	P5-G03	P5-E08	Tray 1-E05	HET	HET	HOW	
422	BC2F2	WBDC-068	P5-G03	P5-E08	Tray 1-F05	HET	HOW	HOW	
423	BC2F2	WBDC-068	P5-G03	P5-E08	Tray 1-G05	HOW	HOC	HOC	
424	BC2F2	WBDC-068	P5-G03	P5-E08	Tray 1-A06	HOW	HET	HET	

425	BC2F2	WBDC-068	P5-G03	P5-E08	Tray 1-B06	HET	HOC	HOW	
426	BC2F2	WBDC-068	P5-G03	P5-E08	Tray 1-C06	HET	HET	HOC	
427	BC2F2	WBDC-068	P5-G03	P5-E08	Tray 1-D06	HET	HOW	HET	
428	BC2F2	WBDC-068	P5-G03	P5-E08	Tray 1-E06	HOC	HOC	HOC	Selected
429	BC2F2	WBDC-068	P5-G03	P5-E08	Tray 1-F06	HOW	HOC	HOW	
430	BC2F2	WBDC-068	P5-G03	P5-E08	Tray 1-G06	HOW	HET	HOC	
431	BC2F2	WBDC-068	P5-G03	P5-E08	Tray 1-A07	HOW	HET	HOC	
432	BC2F2	WBDC-068	P5-G03	P5-E08	Tray 1-B07	HOW	HET	HET	
433	BC2F2	WBDC-068	P5-G03	P5-E08	Tray 1-C07	HET	HOW	HOW	
434	BC2F2	WBDC-068	P5-G03	P5-E08	Tray 1-D07	HET	HET	HET	
435	BC2F2	WBDC-068	P5-G03	P5-E08	Tray 1-E07	HOW	HOC	HET	
436	BC2F2	WBDC-068	P5-G03	P5-E08	Tray 1-F07	HET	HET	HOC	
437	BC2F2	WBDC-068	P5-G03	P5-E08	Tray 1-G07	HET	HOC	HOW	
438	BC2F2	WBDC-068	P5-G03	P5-E08	Tray 1-A08	HET	HET	missing	
439	BC2F2	WBDC-068	P5-G03	P5-E08	Tray 1-B08	HOW	HOC	HET	
440	BC2F2	WBDC-068	P5-G03	P5-E08	Tray 1-C08	HET	HOC	HET	
441	BC2F2	WBDC-068	P5-G03	P5-E08	Tray 1-D08	HET	HET	HET	
442	BC2F2	WBDC-068	P5-G03	P5-E08	Tray 1-E08	HOW	HOC	HOW	
443	BC2F2	WBDC-068	P5-G03	P5-E08	Tray 1-F08	HET	HOC	HET	
444	BC2F2	WBDC-068	P5-G03	P5-E08	Tray 1-G08	HOC	HOC	HOW	
445	BC2F2	WBDC-068	P5-G03	P5-E08	Tray 1-A09	HET	HOW	HOC	
446	BC2F2	WBDC-068	P5-G03	P5-E08	Tray 1-B09	HET	HET	HOC	
447	BC2F2	WBDC-068	P5-G03	P5-E08	Tray 1-C09	missing	missing	missing	
448	BC2F2	WBDC-068	P5-G03	P5-E08	Tray 1-D09	HET	HOC	HOW	
449	BC2F2	WBDC-068	P5-G03	P5-E08	Tray 1-E09	HET	HOW	HOW	
450	BC2F2	WBDC-068	P5-G03	P5-E08	Tray 1-F09	HET	HOW	HOC	
451	BC2F2	WBDC-068	P5-G03	P5-E08	Tray 1-G09	HET	HOW	HOW	
452	BC2F2	WBDC-068	P5-G03	P5-E08	Tray 1-A10	missing	missing	missing	
453	BC2F2	WBDC-068	P5-G03	P5-E08	Tray 1-B10	missing	missing	missing	
454	BC2F2	WBDC-068	P5-G03	P5-E08	Tray 1-C10	HET	HET	HOC	
455	BC2F2	WBDC-068	P5-G03	P5-E08	Tray 1-D10	HOW	HET	HET	
456	BC2F2	WBDC-068	P5-G03	P5-E08	Tray 1-E10	HOW	HOW	HET	
457	BC2F2	WBDC-068	P5-G03	P5-E08	Tray 1-F10	HOC	HOC	HOC	Selected
458	BC2F2	WBDC-068	P5-G03	P5-E08	Tray 1-G10	HET	HOC	HET	
459	BC2F2	WBDC-068	P5-G03	P5-E08	Tray 1-A11	HET	HOW	HET	
460	BC2F2	WBDC-068	P5-G03	P5-E08	Tray 1-B11	missing	missing	missing	
461	BC2F2	WBDC-068	P5-G03	P5-E08	Tray 1-C11	HET	HET	HOW	
462	BC2F2	WBDC-068	P5-G03	P5-E08	Tray 1-D11	HOW	HOW	HET	
463	BC2F2	WBDC-068	P5-G03	P5-E08	Tray 1-E11	HET	HET	HET	
464	BC2F2	WBDC-068	P5-G03	P5-E08	Tray 1-F11	HOW	HET	HOC	
465	BC2F2	WBDC-068	P5-G03	P5-E08	Tray 1-G11	HET	HET	HOW	
466	BC2F2	WBDC-068	P5-G03	P5-E08	Tray 1-A12	HET	HOC	HOC	Selected
467	BC2F2	WBDC-068	P5-G03	P5-E08	Tray 1-B12	HOC	HET	HOC	

468	BC2F2	WBDC-068	P5-G03	P5-E08	Tray 1-C12	missing	missing	missing	
469	BC2F2	WBDC-068	P5-G03	P5-E08	Tray 1-D12	HET	HET	HET	
470	BC2F2	WBDC-068	P5-G03	P5-E08	Tray 1-E12	HET	HET	HOC	
471	BC2F2	WBDC-068	P5-G03	P5-E08	Tray 1-F12	HOC	HET	HOW	
472	BC2F2	WBDC-068	P5-G03	P5-E08	Tray 1-G12	HOW	HET	HOW	
473	BC2F2	WBDC-199	P4-A11	P4-D05	Tray_7-A01	HET	HOC	missing	
474	BC2F2	WBDC-199	P4-A11	P4-D05	Tray_7-B01	HET	HET	HOW	
475	BC2F2	WBDC-199	P4-A11	P4-D05	Tray_7-C01	missing	missing	missing	
476	BC2F2	WBDC-199	P4-A11	P4-D05	Tray_7-D01	missing	missing	missing	
477	BC2F2	WBDC-199	P4-A11	P4-D05	Tray_7-E01	missing	missing	missing	
478	BC2F2	WBDC-199	P4-A11	P4-D05	Tray_7-F01	HOC	HOW	HET	
479	BC2F2	WBDC-199	P4-A11	P4-D05	Tray_7-G01	HET	HET	HOW	
480	BC2F2	WBDC-199	P4-A11	P4-D05	Tray_7-H01	HOC	HET	HOW	
481	BC2F2	WBDC-199	P4-A11	P4-D05	Tray_7-A02	HOC	HET	missing	
482	BC2F2	WBDC-199	P4-A11	P4-D05	Tray_7-B02	HET	HET	HOW	
483	BC2F2	WBDC-199	P4-A11	P4-D05	Tray_7-C02	HET	HET	missing	
484	BC2F2	WBDC-199	P4-A11	P4-D05	Tray_7-D02	HOW	HOW	HET	
485	BC2F2	WBDC-199	P4-A11	P4-D05	Tray_7-E02	HOC	HET	HOW	
486	BC2F2	WBDC-199	P4-A11	P4-D05	Tray_7-F02	HOC	HET	HOW	
487	BC2F2	WBDC-199	P4-A11	P4-D05	Tray_7-G02	missing	missing	missing	
488	BC2F2	WBDC-199	P4-A11	P4-D05	Tray_7-H02	HOC	HOC	HET	
489	BC2F2	WBDC-199	P4-A11	P4-D05	Tray_7-A03	HOC	HOC	HOW	
490	BC2F2	WBDC-199	P4-A11	P4-D05	Tray_7-B03	HET	HOW	HOW	
491	BC2F2	WBDC-199	P4-A11	P4-D05	Tray_7-C03	HET	HET	missing	
492	BC2F2	WBDC-199	P4-A11	P4-D05	Tray_7-D03	HET	HOW	HOC	
493	BC2F2	WBDC-199	P4-A11	P4-D05	Tray_7-E03	HET	HET	HOW	
494	BC2F2	WBDC-199	P4-A11	P4-D05	Tray_7-F03	HET	HOC	HOW	
495	BC2F2	WBDC-199	P4-A11	P4-D05	Tray_7-G03	HET	HOW	HET	
496	BC2F2	WBDC-199	P4-A11	P4-D05	Tray_7-H03	HET	HET	HET	
497	BC2F2	WBDC-199	P4-A11	P4-D05	Tray_7-A04	HOW	HET	HET	
498	BC2F2	WBDC-199	P4-A11	P4-D05	Tray_7-B04	HET	HOC	HOC	Selected
499	BC2F2	WBDC-199	P4-A11	P4-D05	Tray_7-C04	HOW	HET	HET	
500	BC2F2	WBDC-199	P4-A11	P4-D05	Tray_7-D04	HOC	missing	missing	
501	BC2F2	WBDC-199	P4-A11	P4-D05	Tray_7-E04	HOW	HET	missing	
502	BC2F2	WBDC-199	P4-A11	P4-D05	Tray_7-F04	missing	missing	missing	
503	BC2F2	WBDC-199	P4-A11	P4-D05	Tray_7-G04	missing	missing	missing	
504	BC2F2	WBDC-199	P4-A11	P4-D05	Tray_7-H04	HET	HET	HET	
505	BC2F2	WBDC-199	P4-A11	P4-D05	Tray_7-A05	HOC	HET	HET	
506	BC2F2	WBDC-199	P4-A11	P4-D05	Tray_7-B05	missing	missing	missing	
507	BC2F2	WBDC-199	P4-A11	P4-D05	Tray_7-C05	missing	missing	missing	
508	BC2F2	WBDC-199	P4-A11	P4-D05	Tray_7-D05	HOW	HET	missing	
509	BC2F2	WBDC-199	P4-A11	P4-D05	Tray_7-E05	missing	HET	missing	
510	BC2F2	WBDC-199	P4-A11	P4-D05	Tray_7-F05	HET	HOW	missing	

511	BC2F2	WBDC-199	P4-A11	P4-D05	Tray_7-G05	HOC	HET	HET
512	BC2F2	WBDC-199	P4-A11	P4-D05	Tray_7-A06	missing	missing	missing
513	BC2F2	WBDC-199	P4-A11	P4-D05	Tray_7-B06	HET	HOW	HOC
514	BC2F2	WBDC-199	P4-A11	P4-D05	Tray_7-C06	HOC	HET	HET
515	BC2F2	WBDC-199	P4-A11	P4-D05	Tray_7-D06	missing	missing	missing
516	BC2F2	WBDC-199	P4-A11	P4-D05	Tray_7-E06	missing	missing	missing
517	BC2F2	WBDC-199	P4-A11	P4-D05	Tray_7-F06	missing	missing	missing
518	BC2F2	WBDC-199	P4-A11	P4-D05	Tray_7-G06	missing	HOW	missing
519	BC2F2	WBDC-199	P4-A11	P4-D05	Tray_7-A07	HOC	HET	missing
520	BC2F2	WBDC-199	P4-A11	P4-D05	Tray_7-B07	HOC	HOW	HET
521	BC2F2	WBDC-199	P4-A11	P4-D05	Tray_7-C07	HET	HET	HET
522	BC2F2	WBDC-199	P4-A11	P4-D05	Tray_7-D07	HET	HET	missing
523	BC2F2	WBDC-199	P4-A11	P4-D05	Tray_7-E07	HOW	HOW	HET
524	BC2F2	WBDC-199	P4-A11	P4-D05	Tray_7-F07	HET	HET	HET
525	BC2F2	WBDC-199	P4-A11	P4-D05	Tray_7-G07	missing	HOW	missing
526	BC2F2	WBDC-199	P4-A11	P4-D05	Tray_7-A08	HET	HOC	HOW
527	BC2F2	WBDC-199	P4-A11	P4-D05	Tray_7-B08	HET	HET	HET
528	BC2F2	WBDC-199	P4-A11	P4-D05	Tray_7-C08	HET	HOW	HOC
529	BC2F2	WBDC-199	P4-A11	P4-D05	Tray_7-D08	HET	HET	missing
530	BC2F2	WBDC-199	P4-A11	P4-D05	Tray_7-E08	HOW	HOW	HOW
531	BC2F2	WBDC-199	P4-A11	P4-D05	Tray_7-F08	HOW	HOC	HET
532	BC2F2	WBDC-199	P4-A11	P4-D05	Tray_7-G08	missing	missing	missing
533	BC2F2	WBDC-199	P4-A11	P4-D05	Tray_7-A09	missing	missing	missing
534	BC2F2	WBDC-199	P4-A11	P4-D05	Tray_7-B09	HOW	HOC	HOW
535	BC2F2	WBDC-199	P4-A11	P4-D05	Tray_7-C09	missing	HOC	missing
536	BC2F2	WBDC-199	P4-A11	P4-D05	Tray_7-D09	missing	missing	missing
537	BC2F2	WBDC-199	P4-A11	P4-D05	Tray_7-E09	HET	HET	HOC
538	BC2F2	WBDC-199	P4-A11	P4-D05	Tray_7-F09	HOW	HOW	HET
539	BC2F2	WBDC-199	P4-A11	P4-D05	Tray_7-G09	HET	HET	HOW
540	BC2F2	WBDC-199	P4-A11	P4-D05	Tray_7-A10	missing	HOC	missing
541	BC2F2	WBDC-199	P4-A11	P4-D05	Tray_7-B10	missing	missing	missing
542	BC2F2	WBDC-199	P4-A11	P4-D05	Tray_7-C10	HET	HET	HOC
543	BC2F2	WBDC-199	P4-A11	P4-D05	Tray_7-D10	HOC	HET	HOW
544	BC2F2	WBDC-199	P4-A11	P4-D05	Tray_7-E10	HOW	HOW	HET
545	BC2F2	WBDC-199	P4-A11	P4-D05	Tray_7-F10	missing	missing	missing
546	BC2F2	WBDC-199	P4-A11	P4-D05	Tray_7-G10	missing	missing	missing
547	BC2F2	WBDC-199	P4-A11	P4-D05	Tray_7-A11	HET	HET	HOC
548	BC2F2	WBDC-199	P4-A11	P4-D05	Tray_7-B11	missing	missing	missing
549	BC2F2	WBDC-199	P4-A11	P4-D05	Tray_7-C11	HOC	HOC	HOW
550	BC2F2	WBDC-199	P4-A11	P4-D05	Tray_7-D11	missing	missing	missing
551	BC2F2	WBDC-199	P4-A11	P4-D05	Tray_7-E11	HET	HET	HET
552	BC2F2	WBDC-199	P4-A11	P4-D05	Tray_7-F11	HOC	HET	missing
553	BC2F2	WBDC-199	P4-A11	P4-D05	Tray_7-G11	HOC	HET	HOW

554	BC2F2	WBDC-199	P4-A11	P4-D05	Tray_7-A12	HOW	HET	HOW	
555	BC2F2	WBDC-199	P4-A11	P4-D05	Tray_7-B12	HOC	HET	HOC	
556	BC2F2	WBDC-199	P4-A11	P4-D05	Tray_7-C12	HET	HET	HET	
557	BC2F2	WBDC-199	P4-A11	P4-D05	Tray_7-D12	HET	HET	HET	
558	BC2F2	WBDC-199	P4-A11	P4-D05	Tray_7-E12	HET	HOW	HOC	
559	BC2F2	WBDC-199	P4-A11	P4-D05	Tray_7-F12	HOC	HET	HOC	
560	BC2F2	WBDC-199	P4-A11	P4-D05	Tray_7-G12	HET	HET	HOC	
561	BC2F2	WBDC-329	P7-D10	P1-D04	Tray_13-A01	HET	HET	missing	
562	BC2F2	WBDC-329	P7-D10	P1-D04	Tray_13-B01	HET	HOC	HET	
563	BC2F2	WBDC-329	P7-D10	P1-D04	Tray_13-C01	HOW	HOW	HOW	
564	BC2F2	WBDC-329	P7-D10	P1-D04	Tray_13-D01	missing	missing	missing	
565	BC2F2	WBDC-329	P7-D10	P1-D04	Tray_13-E01	HOC	HET	HET	
566	BC2F2	WBDC-329	P7-D10	P1-D04	Tray_13-F01	HET	HET	HOC	
567	BC2F2	WBDC-329	P7-D10	P1-D04	Tray_13-G01	HET	HET	HET	
568	BC2F2	WBDC-329	P7-D10	P1-D04	Tray_13-H01	HOW	HET	HET	
569	BC2F2	WBDC-329	P7-D10	P1-D04	Tray_13-A02	HET	HET	HET	
570	BC2F2	WBDC-329	P7-D10	P1-D04	Tray_13-B02	HET	HOC	HET	
571	BC2F2	WBDC-329	P7-D10	P1-D04	Tray_13-C02	HET	HOC	HOC	
572	BC2F2	WBDC-329	P7-D10	P1-D04	Tray_13-D02	HOW	HET	HOC	
573	BC2F2	WBDC-329	P7-D10	P1-D04	Tray_13-E02	HET	HOC	HET	
574	BC2F2	WBDC-329	P7-D10	P1-D04	Tray_13-F02	HET	HET	HET	
575	BC2F2	WBDC-329	P7-D10	P1-D04	Tray_13-G02	HET	HET	HOW	
576	BC2F2	WBDC-329	P7-D10	P1-D04	Tray_13-H02	HOW	HET	HOC	
577	BC2F2	WBDC-329	P7-D10	P1-D04	Tray_13-A03	HOW	HOW	HOC	
578	BC2F2	WBDC-329	P7-D10	P1-D04	Tray_13-B03	HOW	HOC	HOW	
579	BC2F2	WBDC-329	P7-D10	P1-D04	Tray_13-C03	HET	HOW	HOW	
580	BC2F2	WBDC-329	P7-D10	P1-D04	Tray_13-D03	HET	HOC	HOW	
581	BC2F2	WBDC-329	P7-D10	P1-D04	Tray_13-E03	HOC	HOC	HET	
582	BC2F2	WBDC-329	P7-D10	P1-D04	Tray_13-F03	HET	HOW	HET	
583	BC2F2	WBDC-329	P7-D10	P1-D04	Tray_13-G03	HET	HOC	HET	
584	BC2F2	WBDC-329	P7-D10	P1-D04	Tray_13-H03	HET	HET	HET	
585	BC2F2	WBDC-329	P7-D10	P1-D04	Tray_13-A04	HOC	HOC	HOC	Selected
586	BC2F2	WBDC-329	P7-D10	P1-D04	Tray_13-B04	HOC	HOC	HOW	
587	BC2F2	WBDC-329	P7-D10	P1-D04	Tray_13-C04	HOW	HET	HOW	
588	BC2F2	WBDC-329	P7-D10	P1-D04	Tray_13-D04	HOW	HOW	HOC	
589	BC2F2	WBDC-329	P7-D10	P1-D04	Tray_13-E04	HET	HET	HOC	
590	BC2F2	WBDC-329	P7-D10	P1-D04	Tray_13-F04	HET	HOC	HET	
591	BC2F2	WBDC-329	P7-D10	P1-D04	Tray_13-G04	HET	HOC	HOC	Selected
592	BC2F2	WBDC-329	P7-D10	P1-D04	Tray_13-H04	HET	HET	HOC	
593	BC2F2	WBDC-329	P7-D10	P1-D04	Tray_13-A05	missing	HET	missing	
594	BC2F2	WBDC-329	P7-D10	P1-D04	Tray_13-B05	HOW	HET	missing	
595	BC2F2	WBDC-329	P7-D10	P1-D04	Tray_13-C05	HOW	HOC	HOW	
596	BC2F2	WBDC-329	P7-D10	P1-D04	Tray_13-D05	HOW	HET	HOC	

597	BC2F2	WBDC-329	P7-D10	P1-D04	Tray_13-E05	HET	HOC	HOC	Selected
598	BC2F2	WBDC-329	P7-D10	P1-D04	Tray_13-F05	HOC	HET	HOW	
599	BC2F2	WBDC-329	P7-D10	P1-D04	Tray_13-G05	HOC	HET	HOW	
600	BC2F2	WBDC-329	P7-D10	P1-D04	Tray_13-A06	HOC	HOC	HOW	
601	BC2F2	WBDC-329	P7-D10	P1-D04	Tray_13-B06	HET	HET	HOC	
602	BC2F2	WBDC-329	P7-D10	P1-D04	Tray_13-C06	missing	missing	missing	
603	BC2F2	WBDC-329	P7-D10	P1-D04	Tray_13-D06	HOW	HET	HET	
604	BC2F2	WBDC-329	P7-D10	P1-D04	Tray_13-E06	HOC	HOC	HOW	
605	BC2F2	WBDC-329	P7-D10	P1-D04	Tray_13-F06	HOC	HET	HOC	
606	BC2F2	WBDC-329	P7-D10	P1-D04	Tray_13-G06	HOW	HOW	missing	
607	BC2F2	WBDC-329	P7-D10	P1-D04	Tray_13-A07	HET	HET	HET	
608	BC2F2	WBDC-329	P7-D10	P1-D04	Tray_13-B07	missing	missing	missing	
609	BC2F2	WBDC-329	P7-D10	P1-D04	Tray_13-C07	HET	HET	HOC	
610	BC2F2	WBDC-329	P7-D10	P1-D04	Tray_13-D07	HOC	HOC	HET	
611	BC2F2	WBDC-329	P7-D10	P1-D04	Tray_13-E07	HET	HOC	HET	
612	BC2F2	WBDC-329	P7-D10	P1-D04	Tray_13-F07	HET	HET	HOW	
613	BC2F2	WBDC-329	P7-D10	P1-D04	Tray_13-G07	missing	missing	missing	
614	BC2F2	WBDC-329	P7-D10	P1-D04	Tray_13-A08	HET	HET	HOW	
615	BC2F2	WBDC-329	P7-D10	P1-D04	Tray_13-B08	HET	HET	HET	
616	BC2F2	WBDC-329	P7-D10	P1-D04	Tray_13-C08	missing	missing	missing	
617	BC2F2	WBDC-329	P7-D10	P1-D04	Tray_13-D08	HOC	HOW	HOC	
618	BC2F2	WBDC-329	P7-D10	P1-D04	Tray_13-E08	HOW	HOW	HOW	
619	BC2F2	WBDC-329	P7-D10	P1-D04	Tray_13-F08	HOC	HOC	HET	
620	BC2F2	WBDC-329	P7-D10	P1-D04	Tray_13-G08	HOW	HET	HOW	
621	BC2F2	WBDC-329	P7-D10	P1-D04	Tray_13-A09	HOC	HOC	HET	
622	BC2F2	WBDC-329	P7-D10	P1-D04	Tray_13-B09	HET	HET	HET	
623	BC2F2	WBDC-329	P7-D10	P1-D04	Tray_13-C09	HET	HET	HOW	
624	BC2F2	WBDC-329	P7-D10	P1-D04	Tray_13-D09	missing	missing	missing	
625	BC2F2	WBDC-329	P7-D10	P1-D04	Tray_13-E09	HET	HET	HOC	
626	BC2F2	WBDC-329	P7-D10	P1-D04	Tray_13-F09	HOC	HET	HET	
627	BC2F2	WBDC-329	P7-D10	P1-D04	Tray_13-G09	missing	missing	missing	
628	BC2F2	WBDC-329	P7-D10	P1-D04	Tray_13-A10	HET	HET	HET	
629	BC2F2	WBDC-329	P7-D10	P1-D04	Tray_13-B10	HOC	HET	HET	
630	BC2F2	WBDC-329	P7-D10	P1-D04	Tray_13-C10	missing	missing	missing	
631	BC2F2	WBDC-329	P7-D10	P1-D04	Tray_13-D10	HOW	HET	HOW	
632	BC2F2	WBDC-329	P7-D10	P1-D04	Tray_13-E10	HET	HET	HOW	
633	BC2F2	WBDC-329	P7-D10	P1-D04	Tray_13-F10	HET	HET	HET	
634	BC2F2	WBDC-329	P7-D10	P1-D04	Tray_13-G10	HOC	HOW	HET	
635	BC2F2	WBDC-329	P7-D10	P1-D04	Tray_13-A11	HET	HOC	HOW	
636	BC2F2	WBDC-329	P7-D10	P1-D04	Tray_13-B11	HOW	HET	HET	
637	BC2F2	WBDC-329	P7-D10	P1-D04	Tray_13-C11	missing	missing	missing	
638	BC2F2	WBDC-329	P7-D10	P1-D04	Tray_13-D11	HOC	HET	HOC	
639	BC2F2	WBDC-329	P7-D10	P1-D04	Tray_13-E11	HET	HET	HET	

640	BC2F2	WBDC-329	P7-D10	P1-D04	Tray_13-F11	HET	HOC	HET
641	BC2F2	WBDC-329	P7-D10	P1-D04	Tray_13-G11	missing	missing	missing
642	BC2F2	WBDC-329	P7-D10	P1-D04	Tray_13-A12	HOC	HET	HOC
643	BC2F2	WBDC-329	P7-D10	P1-D04	Tray_13-B12	HET	HET	HOC
644	BC2F2	WBDC-329	P7-D10	P1-D04	Tray_13-C12	HET	missing	HOW
645	BC2F2	WBDC-329	P7-D10	P1-D04	Tray_13-D12	HOC	missing	HET
646	BC2F2	WBDC-329	P7-D10	P1-D04	Tray_13-E12	HET	missing	HET
647	BC2F2	WBDC-329	P7-D10	P1-D04	Tray_13-F12	HET	missing	HET
648	BC2F2	WBDC-329	P7-D10	P1-D04	Tray_13-G12	HET	missing	HOW
649	BC2F2	WBDC-068	P5-F09	P5-B10	Tray_2-A01	missing	missing	missing
650	BC2F2	WBDC-068	P5-F09	P5-B10	Tray_2-B01	HOC	HET	HET
651	BC2F2	WBDC-068	P5-F09	P5-B10	Tray_2-C01	HET	HOC	HET
652	BC2F2	WBDC-068	P5-F09	P5-B10	Tray_2-D01	missing	missing	missing
653	BC2F2	WBDC-068	P5-F09	P5-B10	Tray_2-E01	HET	HET	HET
654	BC2F2	WBDC-068	P5-F09	P5-B10	Tray_2-F01	HOW	HOC	missing
655	BC2F2	WBDC-068	P5-F09	P5-B10	Tray_2-G01	HOW	HET	HOW
656	BC2F2	WBDC-068	P5-F09	P5-B10	Tray_2-H01	HET	HET	HOC
657	BC2F2	WBDC-068	P5-F09	P5-B10	Tray_2-A02	HOC	HET	HET
658	BC2F2	WBDC-068	P5-F09	P5-B10	Tray_2-B02	HET	HOW	HET
659	BC2F2	WBDC-068	P5-F09	P5-B10	Tray_2-C02	missing	HET	missing
660	BC2F2	WBDC-068	P5-F09	P5-B10	Tray_2-D02	HET	HOC	HOW
661	BC2F2	WBDC-068	P5-F09	P5-B10	Tray_2-E02	HET	HOW	HET
662	BC2F2	WBDC-068	P5-F09	P5-B10	Tray_2-F02	missing	missing	missing
663	BC2F2	WBDC-068	P5-F09	P5-B10	Tray_2-G02	HOW	HOC	HET
664	BC2F2	WBDC-068	P5-F09	P5-B10	Tray_2-H02	missing	missing	HOW
665	BC2F2	WBDC-068	P5-F09	P5-B10	Tray_2-A03	missing	missing	missing
666	BC2F2	WBDC-068	P5-F09	P5-B10	Tray_2-B03	missing	missing	missing
667	BC2F2	WBDC-068	P5-F09	P5-B10	Tray_2-C03	missing	missing	missing
668	BC2F2	WBDC-068	P5-F09	P5-B10	Tray_2-D03	missing	HOC	missing
669	BC2F2	WBDC-068	P5-F09	P5-B10	Tray_2-E03	HET	HET	HOC
670	BC2F2	WBDC-068	P5-F09	P5-B10	Tray_2-F03	missing	missing	missing
671	BC2F2	WBDC-068	P5-F09	P5-B10	Tray_2-G03	missing	missing	missing
672	BC2F2	WBDC-068	P5-F09	P5-B10	Tray_2-H03	missing	missing	missing
673	BC2F2	WBDC-068	P5-F09	P5-B10	Tray_2-A04	missing	missing	HET
674	BC2F2	WBDC-068	P5-F09	P5-B10	Tray_2-B04	HET	HOC	HET
675	BC2F2	WBDC-068	P5-F09	P5-B10	Tray_2-C04	missing	HOC	missing
676	BC2F2	WBDC-068	P5-F09	P5-B10	Tray_2-D04	missing	missing	missing
677	BC2F2	WBDC-068	P5-F09	P5-B10	Tray_2-E04	missing	missing	missing
678	BC2F2	WBDC-068	P5-F09	P5-B10	Tray_2-F04	missing	missing	missing
679	BC2F2	WBDC-068	P5-F09	P5-B10	Tray_2-G04	missing	missing	missing
680	BC2F2	WBDC-068	P5-F09	P5-B10	Tray_2-H04	HOC	missing	HET
681	BC2F2	WBDC-068	P5-F09	P5-B10	Tray_2-A05	missing	missing	HOW
682	BC2F2	WBDC-068	P5-F09	P5-B10	Tray_2-B05	HOC	HOC	HOW

683	BC2F2	WBDC-068	P5-F09	P5-B10	Tray_2-C05	HET	HOC	HOC	Selected
684	BC2F2	WBDC-068	P5-F09	P5-B10	Tray_2-D05	HET	HOC	HOW	
685	BC2F2	WBDC-068	P5-F09	P5-B10	Tray_2-E05	HOW	HOW	HOW	
686	BC2F2	WBDC-068	P5-F09	P5-B10	Tray_2-F05	missing	missing	HET	
687	BC2F2	WBDC-068	P5-F09	P5-B10	Tray_2-G05	HOC	HOW	HET	
688	BC2F2	WBDC-068	P5-F09	P5-B10	Tray_2-A06	missing	HET	HET	
689	BC2F2	WBDC-068	P5-F09	P5-B10	Tray_2-B06	missing	missing	missing	
690	BC2F2	WBDC-068	P5-F09	P5-B10	Tray_2-C06	HET	HET	HET	
691	BC2F2	WBDC-068	P5-F09	P5-B10	Tray_2-D06	HET	HET	HOC	Selected
692	BC2F2	WBDC-068	P5-F09	P5-B10	Tray_2-E06	missing	HET	missing	
693	BC2F2	WBDC-068	P5-F09	P5-B10	Tray_2-F06	missing	missing	HET	
694	BC2F2	WBDC-068	P5-F09	P5-B10	Tray_2-G06	HET	HET	HET	
695	BC2F2	WBDC-068	P5-F09	P5-B10	Tray_2-A07	HET	HOW	HET	
696	BC2F2	WBDC-068	P5-F09	P5-B10	Tray_2-B07	HOW	HOW	HET	
697	BC2F2	WBDC-068	P5-F09	P5-B10	Tray_2-C07	missing	missing	missing	
698	BC2F2	WBDC-068	P5-F09	P5-B10	Tray_2-D07	HOW	HET	missing	
699	BC2F2	WBDC-068	P5-F09	P5-B10	Tray_2-E07	HOW	HOW	HET	
700	BC2F2	WBDC-068	P5-F09	P5-B10	Tray_2-F07	HOC	HET	HET	
701	BC2F2	WBDC-068	P5-F09	P5-B10	Tray_2-G07	missing	missing	missing	
702	BC2F2	WBDC-068	P5-F09	P5-B10	Tray_2-A08	HET	HOC	HET	
703	BC2F2	WBDC-068	P5-F09	P5-B10	Tray_2-B08	HOW	HET	HET	
704	BC2F2	WBDC-068	P5-F09	P5-B10	Tray_2-C08	HET	HET	HET	
705	BC2F2	WBDC-068	P5-F09	P5-B10	Tray_2-D08	HET	HET	HET	
706	BC2F2	WBDC-068	P5-F09	P5-B10	Tray_2-E08	missing	missing	missing	
707	BC2F2	WBDC-068	P5-F09	P5-B10	Tray_2-F08	HOW	HET	HOW	
708	BC2F2	WBDC-068	P5-F09	P5-B10	Tray_2-G08	HOC	missing	missing	
709	BC2F2	WBDC-068	P5-F09	P5-B10	Tray_2-A09	HOC	HET	HET	
710	BC2F2	WBDC-068	P5-F09	P5-B10	Tray_2-B09	missing	missing	HOW	
711	BC2F2	WBDC-068	P5-F09	P5-B10	Tray_2-C09	HET	HOW	HET	
712	BC2F2	WBDC-068	P5-F09	P5-B10	Tray_2-D09	HOW	HOC	missing	
713	BC2F2	WBDC-068	P5-F09	P5-B10	Tray_2-E09	missing	missing	HOW	
714	BC2F2	WBDC-068	P5-F09	P5-B10	Tray_2-F09	missing	HOW	missing	
715	BC2F2	WBDC-068	P5-F09	P5-B10	Tray_2-G09	HET	HOW	HOC	
716	BC2F2	WBDC-068	P5-F09	P5-B10	Tray_2-A10	HOW	HOC	HET	
717	BC2F2	WBDC-068	P5-F09	P5-B10	Tray_2-B10	HOW	HOW	HET	
718	BC2F2	WBDC-068	P5-F09	P5-B10	Tray_2-C10	HOW	HET	HET	
719	BC2F2	WBDC-068	P5-F09	P5-B10	Tray_2-D10	HET	HOW	HET	
720	BC2F2	WBDC-068	P5-F09	P5-B10	Tray_2-E10	missing	missing	missing	
721	BC2F2	WBDC-068	P5-F09	P5-B10	Tray_2-F10	missing	missing	missing	
722	BC2F2	WBDC-068	P5-F09	P5-B10	Tray_2-G10	HOW	HOW	HOC	
723	BC2F2	WBDC-068	P5-F09	P5-B10	Tray_2-A11	HET	HOW	HET	
724	BC2F2	WBDC-068	P5-F09	P5-B10	Tray_2-B11	HET	HET	HET	
725	BC2F2	WBDC-068	P5-F09	P5-B10	Tray_2-C11	HET	HOC	HET	

726	BC2F2	WBDC-068	P5-F09	P5-B10	Tray_2-D11	missing	missing	missing	
727	BC2F2	WBDC-068	P5-F09	P5-B10	Tray_2-E11	HOW	HOC	missing	
728	BC2F2	WBDC-068	P5-F09	P5-B10	Tray_2-F11	HOC	HET	HET	
729	BC2F2	WBDC-068	P5-F09	P5-B10	Tray_2-G11	HOW	HET	HET	
730	BC2F2	WBDC-068	P5-F09	P5-B10	Tray_2-A12	HOC	HOW	HET	
731	BC2F2	WBDC-068	P5-F09	P5-B10	Tray_2-B12	missing	missing	missing	
732	BC2F2	WBDC-068	P5-F09	P5-B10	Tray_2-C12	missing	missing	missing	
733	BC2F2	WBDC-068	P5-F09	P5-B10	Tray_2-D12	missing	missing	missing	
734	BC2F2	WBDC-068	P5-F09	P5-B10	Tray_2-E12	missing	missing	missing	
735	BC2F2	WBDC-068	P5-F09	P5-B10	Tray_2-F12	missing	missing	missing	
736	BC2F2	WBDC-068	P5-F09	P5-B10	Tray_2-G12	missing	missing	missing	
737	BC2F2	WBDC-199	P4-A08	P4-B10	Tray_8-A01	HOW	HOC	HET	
738	BC2F2	WBDC-199	P4-A08	P4-B10	Tray_8-B01	HET	HOW	HOC	
739	BC2F2	WBDC-199	P4-A08	P4-B10	Tray_8-C01	HOC	HOC	HOW	
740	BC2F2	WBDC-199	P4-A08	P4-B10	Tray_8-D01	HOC	HET	HOW	
741	BC2F2	WBDC-199	P4-A08	P4-B10	Tray_8-E01	HET	HOC	HOC	
742	BC2F2	WBDC-199	P4-A08	P4-B10	Tray_8-F01	HET	HET	HET	
743	BC2F2	WBDC-199	P4-A08	P4-B10	Tray_8-G01	HOC	HOC	HOW	
744	BC2F2	WBDC-199	P4-A08	P4-B10	Tray_8-H01	HET	HOW	missing	
745	BC2F2	WBDC-199	P4-A08	P4-B10	Tray_8-A02	HET	HOC	HOW	
746	BC2F2	WBDC-199	P4-A08	P4-B10	Tray_8-B02	HOC	HET	HOC	
747	BC2F2	WBDC-199	P4-A08	P4-B10	Tray_8-C02	HET	HET	HOC	
748	BC2F2	WBDC-199	P4-A08	P4-B10	Tray_8-D02	HET	HET	HET	
749	BC2F2	WBDC-199	P4-A08	P4-B10	Tray_8-E02	HET	HOC	HOW	
750	BC2F2	WBDC-199	P4-A08	P4-B10	Tray_8-F02	HOW	HET	HOW	
751	BC2F2	WBDC-199	P4-A08	P4-B10	Tray_8-G02	HET	HOW	HET	
752	BC2F2	WBDC-199	P4-A08	P4-B10	Tray_8-H02	HOW	HET	HET	
753	BC2F2	WBDC-199	P4-A08	P4-B10	Tray_8-A03	HET	HOC	HOC	Selected
754	BC2F2	WBDC-199	P4-A08	P4-B10	Tray_8-B03	missing	missing	missing	
755	BC2F2	WBDC-199	P4-A08	P4-B10	Tray_8-C03	HET	HET	HOC	
756	BC2F2	WBDC-199	P4-A08	P4-B10	Tray_8-D03	HET	HET	HOW	
757	BC2F2	WBDC-199	P4-A08	P4-B10	Tray_8-E03	HOC	HOW	HOW	
758	BC2F2	WBDC-199	P4-A08	P4-B10	Tray_8-F03	HET	HET	HOC	
759	BC2F2	WBDC-199	P4-A08	P4-B10	Tray_8-G03	HOW	HET	HET	
760	BC2F2	WBDC-199	P4-A08	P4-B10	Tray_8-H03	HET	HET	HOC	
761	BC2F2	WBDC-199	P4-A08	P4-B10	Tray_8-A04	HOC	HOC	HOC	Selected
762	BC2F2	WBDC-199	P4-A08	P4-B10	Tray_8-B04	missing	missing	missing	
763	BC2F2	WBDC-199	P4-A08	P4-B10	Tray_8-C04	HOW	HOC	missing	
764	BC2F2	WBDC-199	P4-A08	P4-B10	Tray_8-D04	HET	HET	HOW	
765	BC2F2	WBDC-199	P4-A08	P4-B10	Tray_8-E04	HET	HOW	HOC	
766	BC2F2	WBDC-199	P4-A08	P4-B10	Tray_8-F04	HET	HET	HET	
767	BC2F2	WBDC-199	P4-A08	P4-B10	Tray_8-G04	HOC	HOC	HET	
768	BC2F2	WBDC-199	P4-A08	P4-B10	Tray_8-H04	HET	HET	HET	

769	BC2F2	WBDC-199	P4-A08	P4-B10	Tray_8-A05	missing	missing	missing	
770	BC2F2	WBDC-199	P4-A08	P4-B10	Tray_8-B05	HOW	HET	HET	
771	BC2F2	WBDC-199	P4-A08	P4-B10	Tray_8-C05	missing	missing	HOC	
772	BC2F2	WBDC-199	P4-A08	P4-B10	Tray_8-D05	HET	HOC	HOC	Selected
773	BC2F2	WBDC-199	P4-A08	P4-B10	Tray_8-E05	HOC	HOW	HOC	
774	BC2F2	WBDC-199	P4-A08	P4-B10	Tray_8-F05	HOC	HET	HET	
775	BC2F2	WBDC-199	P4-A08	P4-B10	Tray_8-G05	missing	missing	missing	
776	BC2F2	WBDC-199	P4-A08	P4-B10	Tray_8-A06	HOC	HET	HET	
777	BC2F2	WBDC-199	P4-A08	P4-B10	Tray_8-B06	missing	missing	missing	
778	BC2F2	WBDC-199	P4-A08	P4-B10	Tray_8-C06	missing	missing	missing	
779	BC2F2	WBDC-199	P4-A08	P4-B10	Tray_8-D06	HOC	HET	HET	
780	BC2F2	WBDC-199	P4-A08	P4-B10	Tray_8-E06	HET	HET	HOW	
781	BC2F2	WBDC-199	P4-A08	P4-B10	Tray_8-F06	missing	missing	missing	
782	BC2F2	WBDC-199	P4-A08	P4-B10	Tray_8-G06	missing	missing	missing	
783	BC2F2	WBDC-199	P4-A08	P4-B10	Tray_8-A07	HOC	HOC	HOW	
784	BC2F2	WBDC-199	P4-A08	P4-B10	Tray_8-B07	missing	missing	missing	
785	BC2F2	WBDC-199	P4-A08	P4-B10	Tray_8-C07	HET	HET	HOW	
786	BC2F2	WBDC-199	P4-A08	P4-B10	Tray_8-D07	missing	missing	missing	
787	BC2F2	WBDC-199	P4-A08	P4-B10	Tray_8-E07	HOW	HET	HET	
788	BC2F2	WBDC-199	P4-A08	P4-B10	Tray_8-F07	HET	HET	HET	
789	BC2F2	WBDC-199	P4-A08	P4-B10	Tray_8-G07	missing	missing	missing	
790	BC2F2	WBDC-199	P4-A08	P4-B10	Tray_8-A08	HET	HET	HOC	
791	BC2F2	WBDC-199	P4-A08	P4-B10	Tray_8-B08	missing	missing	missing	
792	BC2F2	WBDC-199	P4-A08	P4-B10	Tray_8-C08	HET	HET	HET	
793	BC2F2	WBDC-199	P4-A08	P4-B10	Tray_8-D08	HOC	HOC	HOW	
794	BC2F2	WBDC-199	P4-A08	P4-B10	Tray_8-E08	HET	HOC	HOC	
795	BC2F2	WBDC-199	P4-A08	P4-B10	Tray_8-F08	HOW	HET	HET	
796	BC2F2	WBDC-199	P4-A08	P4-B10	Tray_8-G08	missing	missing	missing	
797	BC2F2	WBDC-199	P4-A08	P4-B10	Tray_8-A09	HET	HOC	missing	
798	BC2F2	WBDC-199	P4-A08	P4-B10	Tray_8-B09	HET	HET	HET	
799	BC2F2	WBDC-199	P4-A08	P4-B10	Tray_8-C09	missing	missing	missing	
800	BC2F2	WBDC-199	P4-A08	P4-B10	Tray_8-D09	missing	missing	missing	
801	BC2F2	WBDC-199	P4-A08	P4-B10	Tray_8-E09	HET	HOC	HET	
802	BC2F2	WBDC-199	P4-A08	P4-B10	Tray_8-F09	HOC	HOW	HOC	
803	BC2F2	WBDC-199	P4-A08	P4-B10	Tray_8-G09	missing	missing	missing	
804	BC2F2	WBDC-199	P4-A08	P4-B10	Tray_8-A10	HOW	HET	HET	
805	BC2F2	WBDC-199	P4-A08	P4-B10	Tray_8-B10	HET	HOC	HET	
806	BC2F2	WBDC-199	P4-A08	P4-B10	Tray_8-C10	missing	missing	missing	
807	BC2F2	WBDC-199	P4-A08	P4-B10	Tray_8-D10	missing	missing	missing	
808	BC2F2	WBDC-199	P4-A08	P4-B10	Tray_8-E10	HET	HET	HET	
809	BC2F2	WBDC-199	P4-A08	P4-B10	Tray_8-F10	HET	HOW	HOC	
810	BC2F2	WBDC-199	P4-A08	P4-B10	Tray_8-G10	missing	missing	missing	
811	BC2F2	WBDC-199	P4-A08	P4-B10	Tray_8-A11	HET	HET	missing	

812	BC2F2	WBDC-199	P4-A08	P4-B10	Tray_8-B11	missing	missing	missing	
813	BC2F2	WBDC-199	P4-A08	P4-B10	Tray_8-C11	HET	HET	HOW	
814	BC2F2	WBDC-199	P4-A08	P4-B10	Tray_8-D11	missing	missing	missing	
815	BC2F2	WBDC-199	P4-A08	P4-B10	Tray_8-E11	HET	HET	HET	
816	BC2F2	WBDC-199	P4-A08	P4-B10	Tray_8-F11	missing	missing	missing	
817	BC2F2	WBDC-199	P4-A08	P4-B10	Tray_8-G11	missing	missing	missing	
818	BC2F2	WBDC-199	P4-A08	P4-B10	Tray_8-A12	HET	HET	HET	
819	BC2F2	WBDC-199	P4-A08	P4-B10	Tray_8-B12	missing	missing	missing	
820	BC2F2	WBDC-199	P4-A08	P4-B10	Tray_8-C12	missing	missing	missing	
821	BC2F2	WBDC-199	P4-A08	P4-B10	Tray_8-D12	missing	missing	missing	
822	BC2F2	WBDC-199	P4-A08	P4-B10	Tray_8-E12	missing	missing	missing	
823	BC2F2	WBDC-199	P4-A08	P4-B10	Tray_8-F12	missing	missing	missing	
824	BC2F2	WBDC-199	P4-A08	P4-B10	Tray_8-G12	HOW	missing	missing	
825	BC2F2	WBDC-068	P5-F09	P5-B10	Tray_5-A01	HET	HOC	HET	
826	BC2F2	WBDC-068	P5-F09	P5-B10	Tray_5-B01	HET	HOW	HET	
827	BC2F2	WBDC-068	P5-F09	P5-B10	Tray_5-C01	HOC	HOW	HET	
828	BC2F2	WBDC-068	P5-F09	P5-B10	Tray_5-D01	missing	missing	missing	
829	BC2F2	WBDC-068	P5-F09	P5-B10	Tray_5-E01	HET	missing	HET	
830	BC2F2	WBDC-068	P5-F09	P5-B10	Tray_5-F01	missing	missing	missing	
831	BC2F2	WBDC-068	P5-F09	P5-B10	Tray_5-G01	missing	missing	missing	
832	BC2F2	WBDC-068	P5-F09	P5-B10	Tray_5-H01	HOC	HOW	HOC	
833	BC2F2	WBDC-068	P5-F09	P5-B10	Tray_5-A02	HOC	HOC	HOW	
834	BC2F2	WBDC-068	P5-F09	P5-B10	Tray_5-B02	missing	missing	missing	
835	BC2F2	WBDC-068	P5-F09	P5-B10	Tray_5-C02	HOC	missing	HOC	
836	BC2F2	WBDC-068	P5-F09	P5-B10	Tray_5-D02	HOC	HET	HOW	
837	BC2F2	WBDC-068	P5-F09	P5-B10	Tray_5-E02	missing	missing	missing	
838	BC2F2	WBDC-068	P5-F09	P5-B10	Tray_5-F02	missing	missing	missing	
839	BC2F2	WBDC-068	P5-F09	P5-B10	Tray_5-G02	missing	missing	missing	
840	BC2F2	WBDC-068	P5-F09	P5-B10	Tray_5-H02	missing	missing	missing	
841	BC2F2	WBDC-068	P5-F09	P5-B10	Tray_5-A03	HOC	HET	HOC	Selected
842	BC2F2	WBDC-068	P5-F09	P5-B10	Tray_5-B03	missing	missing	missing	
843	BC2F2	WBDC-068	P5-F09	P5-B10	Tray_5-C03	missing	missing	missing	
844	BC2F2	WBDC-068	P5-F09	P5-B10	Tray_5-D03	missing	missing	missing	
845	BC2F2	WBDC-068	P5-F09	P5-B10	Tray_5-E03	missing	missing	missing	
846	BC2F2	WBDC-068	P5-F09	P5-B10	Tray_5-F03	missing	missing	missing	
847	BC2F2	WBDC-068	P5-F09	P5-B10	Tray_5-G03	missing	missing	missing	
848	BC2F2	WBDC-068	P5-F09	P5-B10	Tray_5-H03	missing	missing	missing	
849	BC2F2	WBDC-068	P5-F09	P5-B10	Tray_5-A04	HOC	HOC	HOC	Selected
850	BC2F2	WBDC-068	P5-F09	P5-B10	Tray_5-B04	missing	missing	missing	
851	BC2F2	WBDC-068	P5-F09	P5-B10	Tray_5-C04	missing	missing	missing	
852	BC2F2	WBDC-068	P5-F09	P5-B10	Tray_5-D04	missing	missing	missing	
853	BC2F2	WBDC-068	P5-F09	P5-B10	Tray_5-E04	HET	HOW	HET	
854	BC2F2	WBDC-068	P5-F09	P5-B10	Tray_5-F04	HET	HOW	HET	

855	BC2F2	WBDC-068	P5-F09	P5-B10	Tray_5-G04	missing	missing	missing
856	BC2F2	WBDC-068	P5-F09	P5-B10	Tray_5-H04	HET	HET	HOC
857	BC2F2	WBDC-068	P5-F09	P5-B10	Tray_5-A05	HET	HOC	HET
858	BC2F2	WBDC-068	P5-F09	P5-B10	Tray_5-B05	HET	HET	HET
859	BC2F2	WBDC-068	P5-F09	P5-B10	Tray_5-C05	missing	missing	missing
860	BC2F2	WBDC-068	P5-F09	P5-B10	Tray_5-D05	missing	missing	missing
861	BC2F2	WBDC-068	P5-F09	P5-B10	Tray_5-E05	missing	missing	missing
862	BC2F2	WBDC-068	P5-F09	P5-B10	Tray_5-F05	missing	missing	missing
863	BC2F2	WBDC-068	P5-F09	P5-B10	Tray_5-G05	missing	missing	missing
864	BC2F2	WBDC-068	P5-F09	P5-B10	Tray_5-A06	HOC	HET	HET
865	BC2F2	WBDC-068	P5-F09	P5-B10	Tray_5-B06	missing	missing	missing
866	BC2F2	WBDC-068	P5-F09	P5-B10	Tray_5-C06	missing	missing	missing
867	BC2F2	WBDC-068	P5-F09	P5-B10	Tray_5-D06	missing	missing	missing
868	BC2F2	WBDC-068	P5-F09	P5-B10	Tray_5-E06	missing	missing	missing
869	BC2F2	WBDC-068	P5-F09	P5-B10	Tray_5-F06	missing	missing	missing
870	BC2F2	WBDC-068	P5-F09	P5-B10	Tray_5-G06	HOW	HOC	HOC
871	BC2F2	WBDC-068	P5-F09	P5-B10	Tray_5-A07	missing	missing	missing
872	BC2F2	WBDC-068	P5-F09	P5-B10	Tray_5-B07	missing	missing	missing
873	BC2F2	WBDC-068	P5-F09	P5-B10	Tray_5-C07	missing	missing	missing
874	BC2F2	WBDC-068	P5-F09	P5-B10	Tray_5-D07	missing	missing	missing
875	BC2F2	WBDC-068	P5-F09	P5-B10	Tray_5-E07	missing	missing	missing
876	BC2F2	WBDC-068	P5-F09	P5-B10	Tray_5-F07	HET	HET	HOW
877	BC2F2	WBDC-068	P5-F09	P5-B10	Tray_5-G07	missing	missing	missing
878	BC2F2	WBDC-068	P5-F09	P5-B10	Tray_5-A08	missing	missing	missing
879	BC2F2	WBDC-068	P5-F09	P5-B10	Tray_5-B08	missing	missing	missing
880	BC2F2	WBDC-068	P5-F09	P5-B10	Tray_5-C08	HET	HOC	HET
881	BC2F2	WBDC-068	P5-F09	P5-B10	Tray_5-D08	HET	HET	HET
882	BC2F2	WBDC-068	P5-F09	P5-B10	Tray_5-E08	HET	HET	HOC
883	BC2F2	WBDC-068	P5-F09	P5-B10	Tray_5-F08	HET	HET	HET
884	BC2F2	WBDC-068	P5-F09	P5-B10	Tray_5-G08	HET	HET	HET
885	BC2F2	WBDC-068	P5-F09	P5-B10	Tray_5-A09	missing	missing	missing
886	BC2F2	WBDC-068	P5-F09	P5-B10	Tray_5-B09	missing	missing	missing
887	BC2F2	WBDC-068	P5-F09	P5-B10	Tray_5-C09	missing	missing	missing
888	BC2F2	WBDC-068	P5-F09	P5-B10	Tray_5-D09	missing	missing	missing
889	BC2F2	WBDC-068	P5-F09	P5-B10	Tray_5-E09	missing	missing	missing
890	BC2F2	WBDC-068	P5-F09	P5-B10	Tray_5-F09	missing	missing	missing
891	BC2F2	WBDC-068	P5-F09	P5-B10	Tray_5-G09	HOC	HET	HET
892	BC2F2	WBDC-038	P3-D01	P3-B09	Tray_5-A10	missing	missing	missing
893	BC2F2	WBDC-038	P3-D01	P3-B09	Tray_5-B10	HET	HET	HOC
894	BC2F2	WBDC-038	P3-D01	P3-B09	Tray_5-C10	missing	missing	missing
895	BC2F2	WBDC-038	P3-D01	P3-B09	Tray_5-D10	HOC	HET	HET
896	BC2F2	WBDC-038	P3-D01	P3-B09	Tray_5-E10	missing	missing	missing
897	BC2F2	WBDC-038	P3-D01	P3-B09	Tray_5-F10	HET	missing	HOC

898	BC2F2	WBDC-038	P3-D01	P3-B09	Tray_5-G10	HET	HOC	HOW
899	BC2F2	WBDC-038	P3-D01	P3-B09	Tray_5-A11	missing	missing	missing
900	BC2F2	WBDC-038	P3-D01	P3-B09	Tray_5-B11	HET	HET	HET
901	BC2F2	WBDC-038	P3-D01	P3-B09	Tray_5-C11	missing	missing	missing
902	BC2F2	WBDC-038	P3-D01	P3-B09	Tray_5-D11	missing	missing	missing
903	BC2F2	WBDC-038	P3-D01	P3-B09	Tray_5-E11	missing	missing	missing
904	BC2F2	WBDC-038	P3-D01	P3-B09	Tray_5-F11	missing	missing	missing
905	BC2F2	WBDC-038	P3-D01	P3-B09	Tray_5-G11	missing	missing	missing
906	BC2F2	WBDC-038	P3-D01	P3-B09	Tray_5-A12	missing	missing	missing
907	BC2F2	WBDC-038	P3-D01	P3-B09	Tray_5-B12	HET	HOW	HET
908	BC2F2	WBDC-038	P3-D01	P3-B09	Tray_5-C12	missing	missing	missing
909	BC2F2	WBDC-038	P3-D01	P3-B09	Tray_5-D12	missing	missing	missing
910	BC2F2	WBDC-038	P3-D01	P3-B09	Tray_5-E12	missing	HOW	HOC
911	BC2F2	WBDC-038	P3-D01	P3-B09	Tray_5-F12	missing	missing	missing
912	BC2F2	WBDC-038	P3-D01	P3-B09	Tray_5-G12	HET	HET	HET
913	BC2F2	WBDC-199	P4-A08	P4-B10	Tray_11-A01	HOW	HOW	HOW
914	BC2F2	WBDC-199	P4-A08	P4-B10	Tray_11-B01	HET	HOW	HOC
915	BC2F2	WBDC-199	P4-A08	P4-B10	Tray_11-C01	HET	HET	HOC
916	BC2F2	WBDC-199	P4-A08	P4-B10	Tray_11-D01	HOC	HET	HOW
917	BC2F2	WBDC-199	P4-A08	P4-B10	Tray_11-E01	HOW	HET	HET
918	BC2F2	WBDC-199	P4-A08	P4-B10	Tray_11-F01	HET	HET	HET
919	BC2F2	WBDC-199	P4-A08	P4-B10	Tray_11-G01	HOC	HOW	HOC
920	BC2F2	WBDC-199	P4-A08	P4-B10	Tray_11-H01	HET	HOW	HET
921	BC2F2	WBDC-199	P4-A08	P4-B10	Tray_11-A02	HET	HET	HET
922	BC2F2	WBDC-199	P4-A08	P4-B10	Tray_11-B02	HET	HET	HET
923	BC2F2	WBDC-199	P4-A08	P4-B10	Tray_11-C02	HOW	HET	HOW
924	BC2F2	WBDC-199	P4-A08	P4-B10	Tray_11-D02	HET	HET	HET
925	BC2F2	WBDC-199	P4-A08	P4-B10	Tray_11-E02	HOC	HET	HOC
926	BC2F2	WBDC-199	P4-A08	P4-B10	Tray_11-F02	HOC	HOC	HET
927	BC2F2	WBDC-199	P4-A08	P4-B10	Tray_11-G02	HOW	HOC	HET
928	BC2F2	WBDC-199	P4-A08	P4-B10	Tray_11-H02	HOC	HET	HET
929	BC2F2	WBDC-199	P4-A08	P4-B10	Tray_11-A03	missing	missing	missing
930	BC2F2	WBDC-199	P4-A08	P4-B10	Tray_11-B03	missing	missing	missing
931	BC2F2	WBDC-199	P4-A08	P4-B10	Tray_11-C03	HOC	HOC	HET
932	BC2F2	WBDC-199	P4-A08	P4-B10	Tray_11-D03	HOC	HOC	HOW
933	BC2F2	WBDC-199	P4-A08	P4-B10	Tray_11-E03	HOC	HOC	HET
934	BC2F2	WBDC-199	P4-A08	P4-B10	Tray_11-F03	missing	missing	missing
935	BC2F2	WBDC-199	P4-A08	P4-B10	Tray_11-G03	HOC	HOW	HOW
936	BC2F2	WBDC-199	P4-A08	P4-B10	Tray_11-H03	HET	HET	HOW
937	BC2F2	WBDC-199	P4-A08	P4-B10	Tray_11-A04	HET	HOC	HET
938	BC2F2	WBDC-199	P4-A08	P4-B10	Tray_11-B04	missing	missing	missing
939	BC2F2	WBDC-199	P4-A08	P4-B10	Tray_11-C04	HOC	HET	HET
940	BC2F2	WBDC-199	P4-A08	P4-B10	Tray_11-D04	HOC	HOC	HET

941	BC2F2	WBDC-199	P4-A08	P4-B10	Tray_11-E04	missing	missing	missing	
942	BC2F2	WBDC-199	P4-A08	P4-B10	Tray_11-F04	HET	HET	HOC	
943	BC2F2	WBDC-199	P4-A08	P4-B10	Tray_11-G04	HET	HOC	HET	
944	BC2F2	WBDC-199	P4-A08	P4-B10	Tray_11-H04	HOW	missing	HET	
945	BC2F2	WBDC-199	P4-A08	P4-B10	Tray_11-A05	HOW	HOC	HOC	
946	BC2F2	WBDC-199	P4-A08	P4-B10	Tray_11-B05	missing	missing	missing	
947	BC2F2	WBDC-199	P4-A08	P4-B10	Tray_11-C05	HOC	HOW	HET	
948	BC2F2	WBDC-199	P4-A08	P4-B10	Tray_11-D05	HOC	HOC	HOC	Selected
949	BC2F2	WBDC-199	P4-A08	P4-B10	Tray_11-E05	HOC	HET	HOC	
950	BC2F2	WBDC-199	P4-A08	P4-B10	Tray_11-F05	HOC	HET	HOW	
951	BC2F2	WBDC-199	P4-A08	P4-B10	Tray_11-G05	missing	missing	missing	
952	BC2F2	WBDC-199	P4-A08	P4-B10	Tray_11-A06	HOW	HET	HOW	
953	BC2F2	WBDC-199	P4-A08	P4-B10	Tray_11-B06	missing	missing	missing	
954	BC2F2	WBDC-199	P4-A08	P4-B10	Tray_11-C06	HOC	HET	HOC	
955	BC2F2	WBDC-199	P4-A08	P4-B10	Tray_11-D06	HET	HOW	HOC	
956	BC2F2	WBDC-199	P4-A08	P4-B10	Tray_11-E06	HOC	HET	HOC	
957	BC2F2	WBDC-199	P4-A08	P4-B10	Tray_11-F06	HET	HET	HET	
958	BC2F2	WBDC-199	P4-A08	P4-B10	Tray_11-G06	missing	missing	missing	
959	BC2F2	WBDC-199	P4-A08	P4-B10	Tray_11-A07	HET	HOW	missing	
960	BC2F2	WBDC-199	P4-A08	P4-B10	Tray_11-B07	HOC	HOW	HOC	
961	BC2F2	WBDC-199	P4-A08	P4-B10	Tray_11-C07	HOC	HET	HET	
962	BC2F2	WBDC-199	P4-A08	P4-B10	Tray_11-D07	missing	missing	HOC	
963	BC2F2	WBDC-199	P4-A08	P4-B10	Tray_11-E07	HET	HET	HOC	
964	BC2F2	WBDC-199	P4-A08	P4-B10	Tray_11-F07	HET	HOW	HOC	
965	BC2F2	WBDC-199	P4-A08	P4-B10	Tray_11-G07	HOC	HET	HET	
966	BC2F2	WBDC-199	P4-A08	P4-B10	Tray_11-A08	HET	HET	HOC	
967	BC2F2	WBDC-199	P4-A08	P4-B10	Tray_11-B08	HOW	HET	HOC	
968	BC2F2	WBDC-199	P4-A08	P4-B10	Tray_11-C08	missing	missing	missing	
969	BC2F2	WBDC-199	P4-A08	P4-B10	Tray_11-D08	missing	missing	missing	
970	BC2F2	WBDC-199	P4-A08	P4-B10	Tray_11-E08	HET	HOW	HOC	
971	BC2F2	WBDC-199	P4-A08	P4-B10	Tray_11-F08	HET	HET	HET	
972	BC2F2	WBDC-199	P4-A08	P4-B10	Tray_11-G08	missing	missing	missing	
973	BC2F2	WBDC-199	P4-A08	P4-B10	Tray_11-A09	missing	missing	missing	
974	BC2F2	WBDC-199	P4-A08	P4-B10	Tray_11-B09	HOW	HOW	HOC	
975	BC2F2	WBDC-199	P4-A08	P4-B10	Tray_11-C09	HOC	HET	HOW	
976	BC2F2	WBDC-199	P4-A08	P4-B10	Tray_11-D09	HOC	HET	HOW	
977	BC2F2	WBDC-199	P4-A08	P4-B10	Tray_11-E09	HOC	HET	HET	
978	BC2F2	WBDC-199	P4-A08	P4-B10	Tray_11-F09	HOC	HOC	HOW	
979	BC2F2	WBDC-199	P4-A08	P4-B10	Tray_11-G09	missing	missing	missing	
980	BC2F2	WBDC-199	P4-A08	P4-B10	Tray_11-A10	HOC	HET	HET	
981	BC2F2	WBDC-199	P4-A08	P4-B10	Tray_11-B10	missing	missing	missing	
982	BC2F2	WBDC-199	P4-A08	P4-B10	Tray_11-C10	missing	missing	missing	
983	BC2F2	WBDC-199	P4-A08	P4-B10	Tray_11-D10	HET	HET	HET	

984	BC2F2	WBDC-199	P4-A08	P4-B10	Tray_11-E10	HET	HET	HOC
985	BC2F2	WBDC-199	P4-A08	P4-B10	Tray_11-F10	missing	missing	missing
986	BC2F2	WBDC-199	P4-A08	P4-B10	Tray_11-G10	HET	HET	HET
987	BC2F2	WBDC-199	P4-A08	P4-B10	Tray_11-A11	HOW	HOC	HET
988	BC2F2	WBDC-199	P4-A08	P4-B10	Tray_11-B11	missing	missing	missing
989	BC2F2	WBDC-199	P4-A08	P4-B10	Tray_11-C11	HOW	HET	HOW
990	BC2F2	WBDC-199	P4-A08	P4-B10	Tray_11-D11	HET	HET	HOW
991	BC2F2	WBDC-199	P4-A08	P4-B10	Tray_11-E11	HOC	HET	HOC
992	BC2F2	WBDC-199	P4-A08	P4-B10	Tray_11-F11	HOW	HET	HOC
993	BC2F2	WBDC-199	P4-A08	P4-B10	Tray_11-G11	HET	HOC	HET
994	BC2F2	WBDC-199	P4-A08	P4-B10	Tray_11-A12	HET	HET	HET
995	BC2F2	WBDC-199	P4-A08	P4-B10	Tray_11-B12	HOW	HET	HET
996	BC2F2	WBDC-199	P4-A08	P4-B10	Tray_11-C12	missing	HET	HOW
997	BC2F2	WBDC-199	P4-A08	P4-B10	Tray_11-D12	HET	HET	HET
998	BC2F2	WBDC-199	P4-A08	P4-B10	Tray_11-E12	HOC	HET	HET
999	BC2F2	WBDC-199	P4-A08	P4-B10	Tray_11-F12	HOC	HET	HET
1000	BC2F2	WBDC-199	P4-A08	P4-B10	Tray_11-G12	HET	HOC	HOW

Appendix 6.1. Analysis of Variance for Canopy Temperature Depression (CTD), pigment, biomass and Narrow-Band Hyperspectral Indices (NBHIs).

	CTD				
Source of variance	**df1**	**df2⁺**	**F.ratio**	**p-value**	
Ta (covariate)	1	1315	160.8	<0.001	***
Treatment	1	59	70.3	<0.001	***
Line	9	59	2.4	0.024	*
DAS	5	1296	112.2	<0.001	***
Treatment:Line	9	59	0.3	0.954	
Treatment:DAS	5	1259	65.1	<0.001	***
Line:DAS	45	1259	2.9	<0.001	***
Treatment:Line:DAS	45	1259	1.0	0.437	

, **,*: Significance at P< 0.05, P<0.01 or P<0.001, respectively.*

	Chl				
Source of variance	**df1**	**df2⁺**	**F.ratio**	**p-value**	
Line	9	600	88.1	<0.001	***
Treatment	1	600	65.8	<0.001	***
DAS	9	600	327.8	<0.001	***
Line:Treatment	9	600	4.4	<0.001	***
Line:DAS	81	600	2.2	<0.001	***
Treatment:DAS	9	600	5.0	<0.001	***
Line:Treatment:DAS	81	600	0.5	1.000	

, **,*: Significance at P< 0.05, P<0.01 or P<0.001, respectively.*

	Flav				
Source of variance	**df1**	**df2⁺**	**F.ratio**	**p-value**	
Line	9	599	63.0	<0.001	***
Treatment	1	599	219.4	<0.001	***
DAS	9	599	57.6	<0.001	***
Line:Treatment	9	599	5.0	<0.001	***
Line:DAS	81	599	2.5	<0.001	***
Treatment:DAS	9	599	8.6	<0.001	***
Line:Treatment:DAS	81	599	0.7	0.974	

, **,*: Significance at P< 0.05, P<0.01 or P<0.001, respectively.*

	Anth				
Source of variance	**df1**	**df2⁺**	**F.ratio**	**p-value**	
Line	9	600	70.1	<0.001	***
Treatment	1	600	13.0	<0.001	***
DAS	9	600	276.2	<0.001	***
Line:Treatment	9	600	3.7	<0.001	***
Line:DAS	81	600	1.9	<0.001	***
Treatment:DAS	9	600	2.6	<0.001	***
Line:Treatment:DAS	81	600	0.9	0.818	

, **,*: Significance at P< 0.05, P<0.01 or P<0.001, respectively.*

NBI

Source of variance	df1	df2+	F.ratio	p-value	
Line	9	599	90.9	<0.001	***
Treatment	1	599	219.0	<0.001	***
DAS	9	599	56.5	<0.001	***
Line:Treatment	9	599	4.2	<0.001	***
Line:DAS	81	599	2.4	<0.001	***
Treatment:DAS	9	599	10.4	<0.001	***
Line:Treatment:DAS	81	599	0.6	0.999	

, **,*: Significance at P< 0.05, P<0.01 or P<0.001, respectively.*

DW

Source of variance	df1	df2+	F.ratio	p-value	
Treatment	1	59	39.6	<0.001	***
Line	9	59	6.0	<0.001	***
Block	1	59	0.0	0.965	
Treatment:Line	9	59	1.0	0.448	

, **,*: Significance at P< 0.05, P<0.01 or P<0.001, respectively.*

FW

Source of variance	df1	df2+	F.ratio	p-value	
Treatment	1	59	47.4	<0.001	***
Line	9	59	3.7	<0.001	***
Block	1	59	1.7	0.195	
Treatment:Line	9	59	1.2	0.333	

, **,*: Significance at P< 0.05, P<0.01 or P<0.001, respectively.*

WUE

Source of variance	df1	df2+	F.ratio	p-value	
Treatment	1	59	24.4	<0.001	***
Line	9	59	2.4	<0.05	*
Block	1	59	0.6	0.450	
Treatment:Line	9	59	0.7	0.725	

, **,*: Significance at P< 0.05, P<0.01 or P<0.001, respectively.*

MCARI1

Source of variance	df1	df2+	F.ratio	p-value	
Line	9	60	1.1	0.392	
Treatment	1	60	10.4	<.01	**
Line:Treatment	9	60	0.6	0.761	

, **,*: Significance at P< 0.05, P<0.01 or P<0.001, respectively.*

SRPI

Source of variance	df1	df2+	F.ratio	p-value	
Line	9	60	4.4	<0.001	***
Treatment	1	60	1.1	0.296	
Line:Treatment	9	60	0.3	0.96	

, **,*: Significance at P< 0.05, P<0.01 or P<0.001, respectively.*

NPQI

Source of variance	df1	df2+	F.ratio	p-value	
Line	9	60	2.3	0.026	*
Treatment	1	60	4.5	0.038	*
Line:Treatment	9	60	0.8	0.643	

, **,*: Significance at P< 0.05, P<0.01 or P<0.001, respectively.*

DNCabxc

Source of variance	df1	df2+	F.ratio	p-value	
Line	9	60	3.6	<.01	**
Treatment	1	60	8.7	<.01	**
Line:Treatment	9	60	0.9	0.556	

, **,*: Significance at P< 0.05, P<0.01 or P<0.001, respectively.*

LIC3

Source of variance	df1	df2+	F.ratio	p-value	
Line	9	60	2.6	0.014	*
Treatment	1	60	6.7	0.012	*
Line:Treatment	9	60	1.0	0.461	

, **,*: Significance at P< 0.05, P<0.01 or P<0.001, respectively.*

PRIM2

Source of variance	df1	df2+	F.ratio	p-value	
Line	9	60	1.2	0.294	
Treatment	1	60	4.4	0.041	*
Line:Treatment	9	60	0.8	0.591	

, **,*: Significance at P< 0.05, P<0.01 or P<0.001, respectively.*

PRI.CI

Source of variance	df1	df2+	F.ratio	p-value
Line	9	60	1.2	0.303
Treatment	1	60	0.0	0.976
Line:Treatment	9	60	0.8	0.627

, **,*: Significance at P< 0.05, P<0.01 or P<0.001, respectively.*

B

Source of variance	df1	df2+	F.ratio	p-value
Line	9	60	0.9	0.547
Treatment	1	60	0.4	0.525
Line:Treatment	9	60	0.9	0.521

*, **,***: Significance at P< 0.05, P<0.01 or P<0.001, respectively.*

	BF1				
Source of variance	**df1**	**df2⁺**	**F.ratio**	**p-value**	
Line	9	60	2.5	0.015	*
Treatment	1	60	3.8	0.055	
Line:Treatment	9	60	0.3	0.96	

*, **,***: Significance at P< 0.05, P<0.01 or P<0.001, respectively.*

	CUR				
Source of variance	**df1**	**df2⁺**	**F.ratio**	**p-value**	
Line	9	60	2.4	0.019	*
Treatment	1	60	34.9	<0.001	***
Line:Treatment	9	60	1.5	0.158	

*, **,***: Significance at P< 0.05, P<0.01 or P<0.001, respectively.*

Appendix 6.2. A-Ci curve fitting routine using *photosynthesis* R package

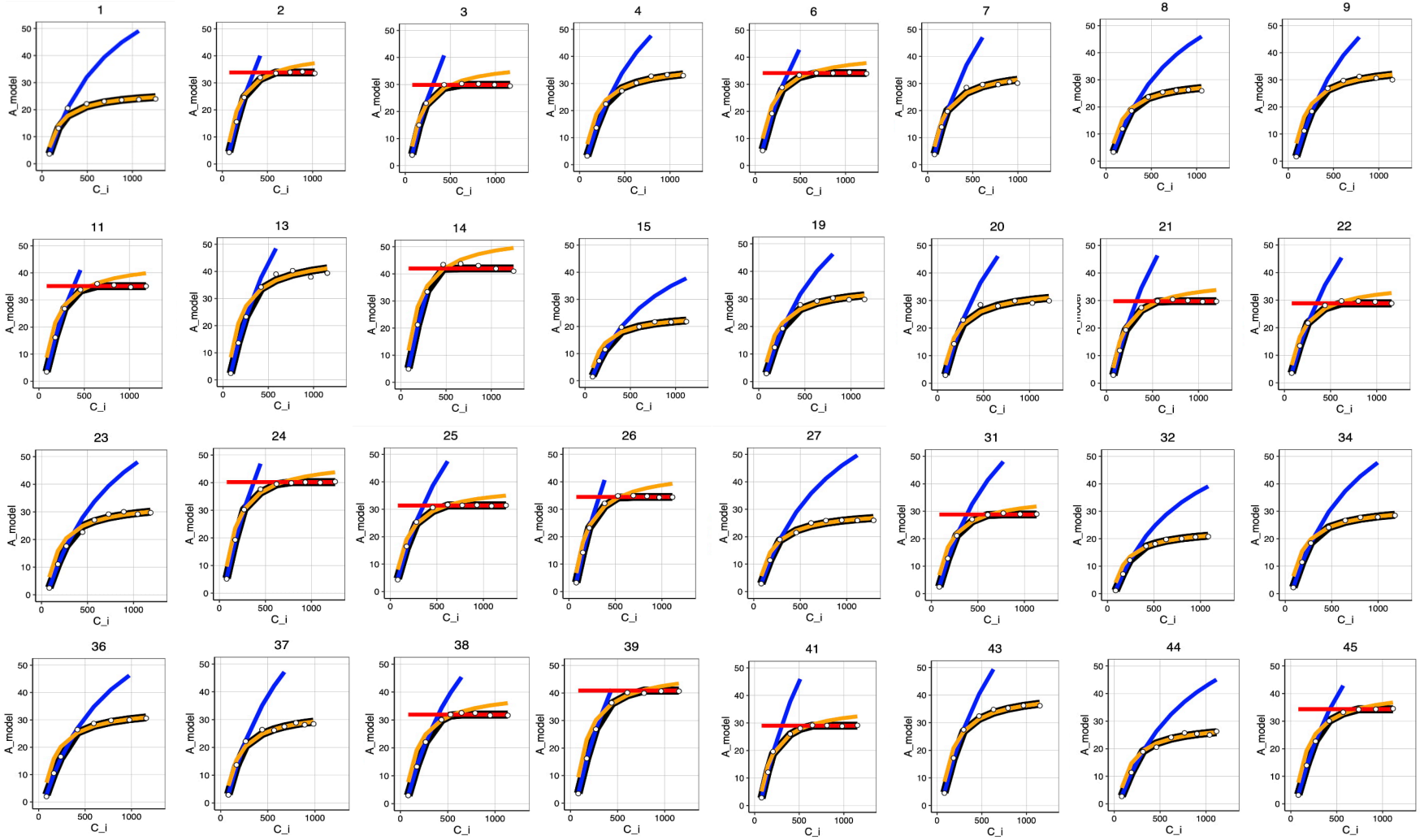

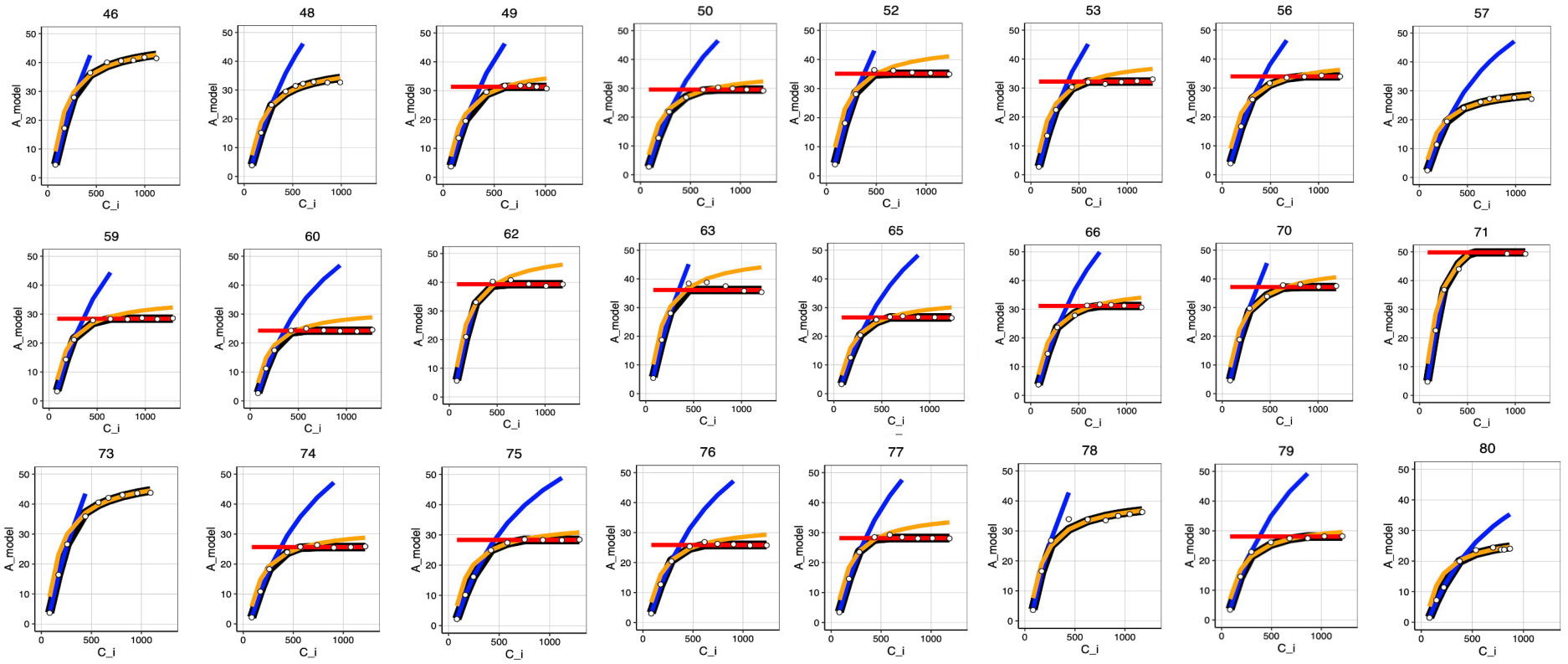
46
48
49
50
52
53
56
57
59
60
62
63
65
66
70
71
73
74
75
76
77
78
79
80
A_model
C_i
0
10
20
30
40
50
500
1000

Appendix 6.3. A-Ci curve fitting routine using *plantecophys* R package.

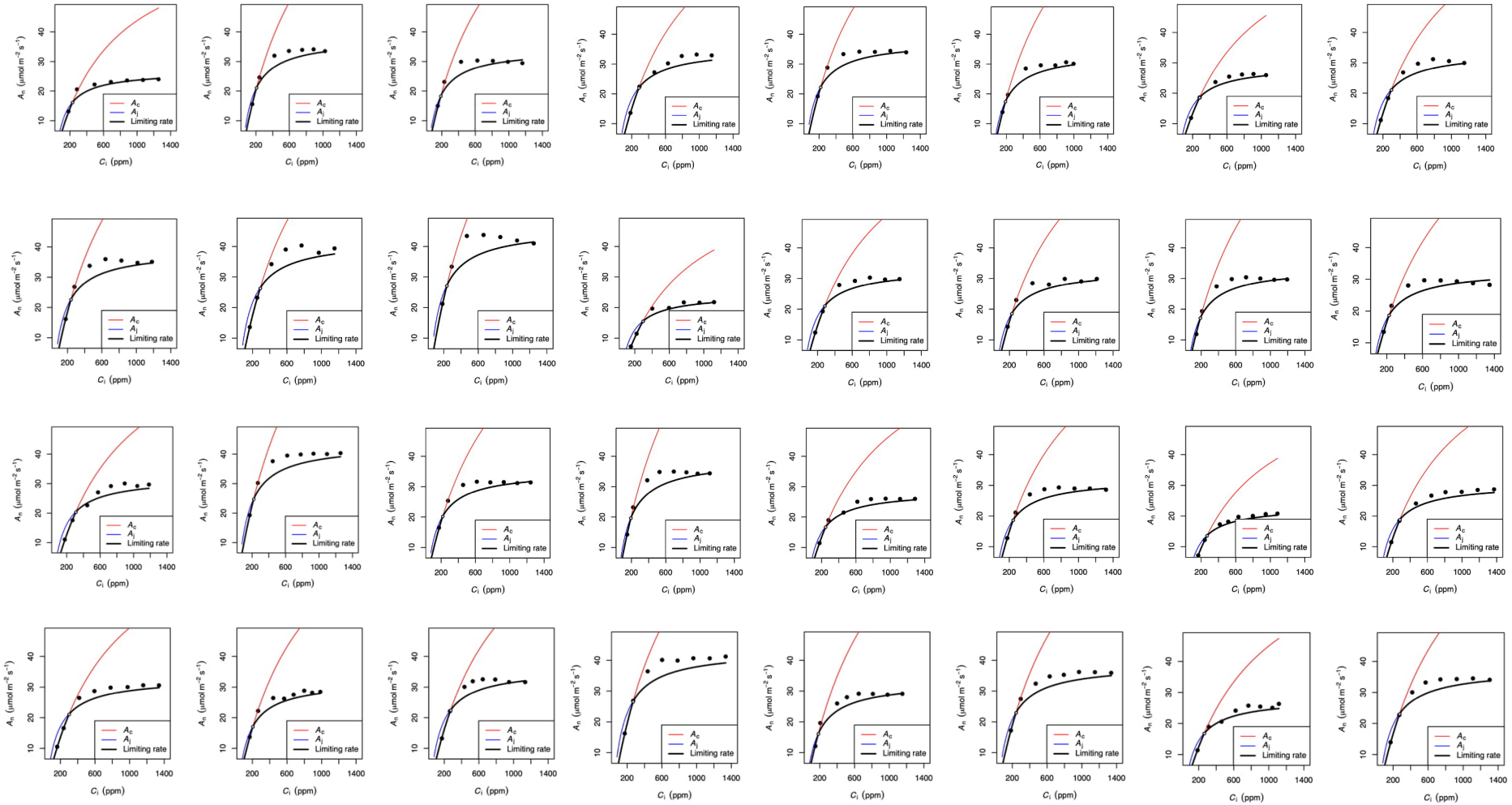

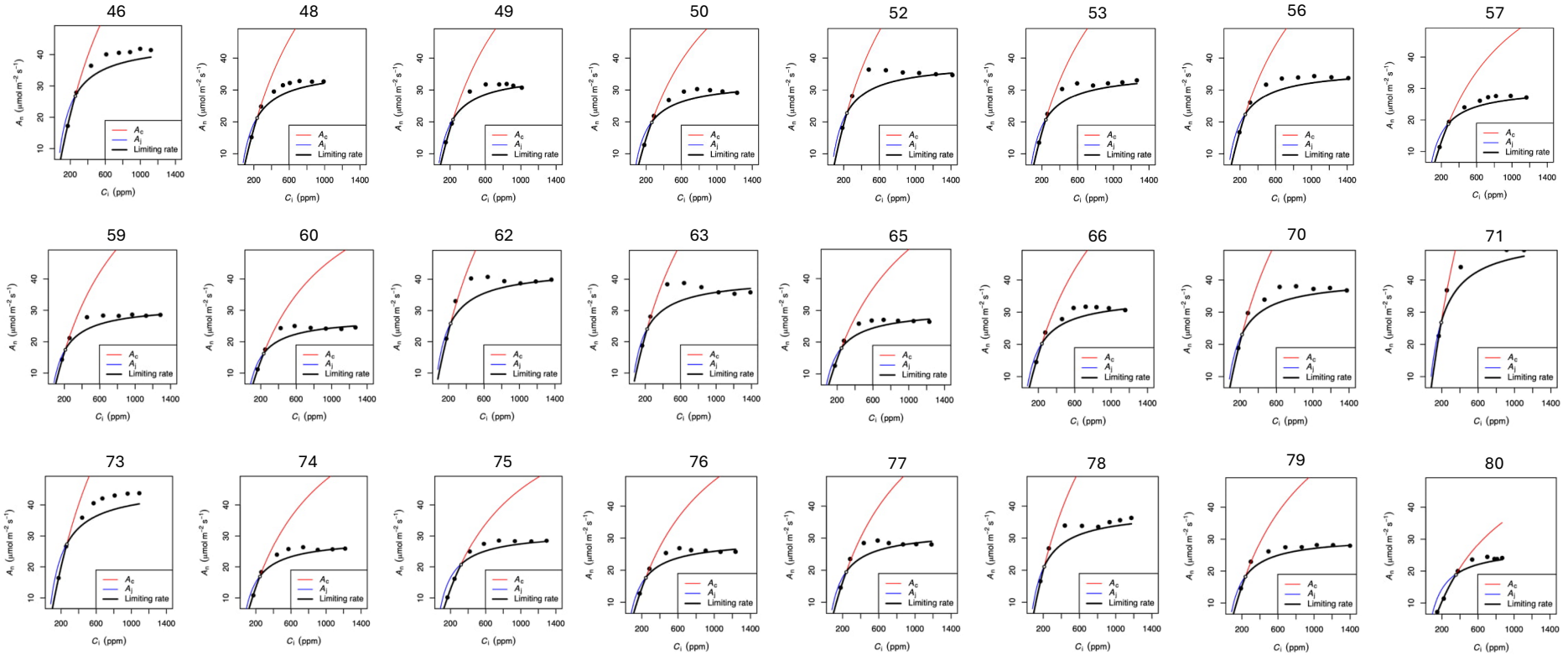
46
48
49
50
52
53
56
57
59
60
62
63
65
66
70
71
73
74
75
76
77
78
79
80
A_n (μmol m^{-2} s^{-1})
C_i (ppm)
A_c
A_j
Limiting rate

Appendix 6.4. Correlation of photosynthesis parameters from two curve fitting routines from *plantecophys* and *photosynthesis* R packages.

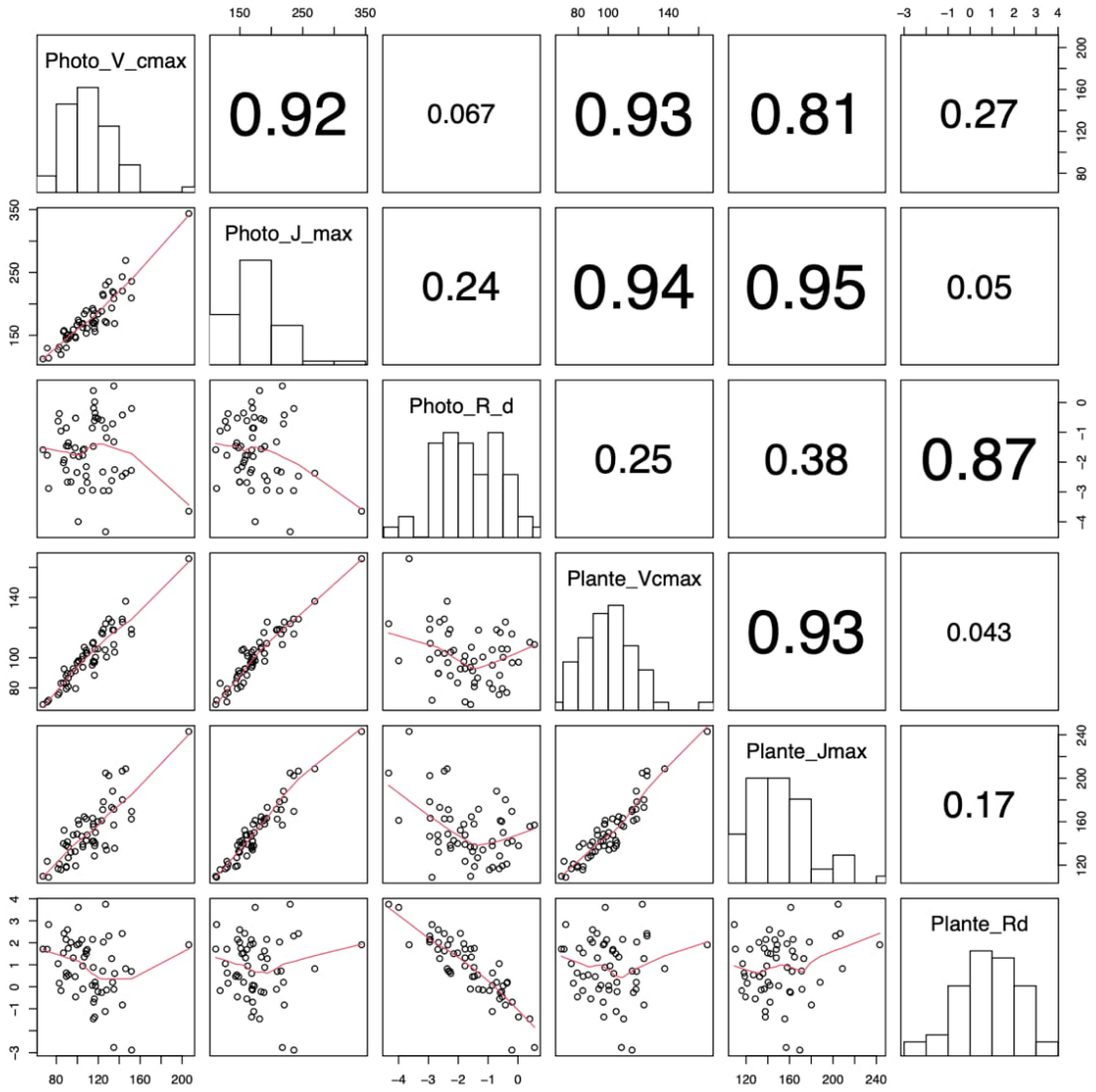

Appendix 6.5. Partial Least Square Regression (PLSR) and Support Vector Regression (SVR) performance metrics for predicting V_{cmax} from spectral data. Input variables for PLSR were raw spectral reflectance. Input variables for SVR were VIF-filtered NBHIs (DNCabxc, BF1, NPQI, SRPI, PRIM2, LIC3, B, PRI.CI, MCARI1, and CUR.

Partial Least Square Regression (PLSR)

Number of components	**MAE**	**RMSE**	**R^2**
5	22.04	28.90	0.0644
10	22.76	31.94	0.0098
20	25.34	33.93	0.0006
30	25.39	33.96	0.0006

Support Vector Regression (SVR)

Data excluded	**MAE**	**RMSE**	**R^2**
No data excluded	21.36	28.09	0.0470
Excluded Data: Day_1	21.19	27.86	0.0518
Excluded Data: Day_2	21.07	27.71	0.0508
Excluded Data: Day_3	22.80	30.25	0.0246
Excluded Data: Day_4	17.59	21.53	0.0001
Excluded Data: Treatment_IR	24.03	32.16	0.0339
Excluded Data: Treatment_DR	17.53	20.91	0.0052

Appendix 6.6. Pigment content contrasts between La Trobe (LTR) against Wild, and the two *de novo*-domesticated lines coded as BC2F3_1 and BC2F3_2.Blue and brown shaded bars correspond to irrigated and drought conditions, respectively.

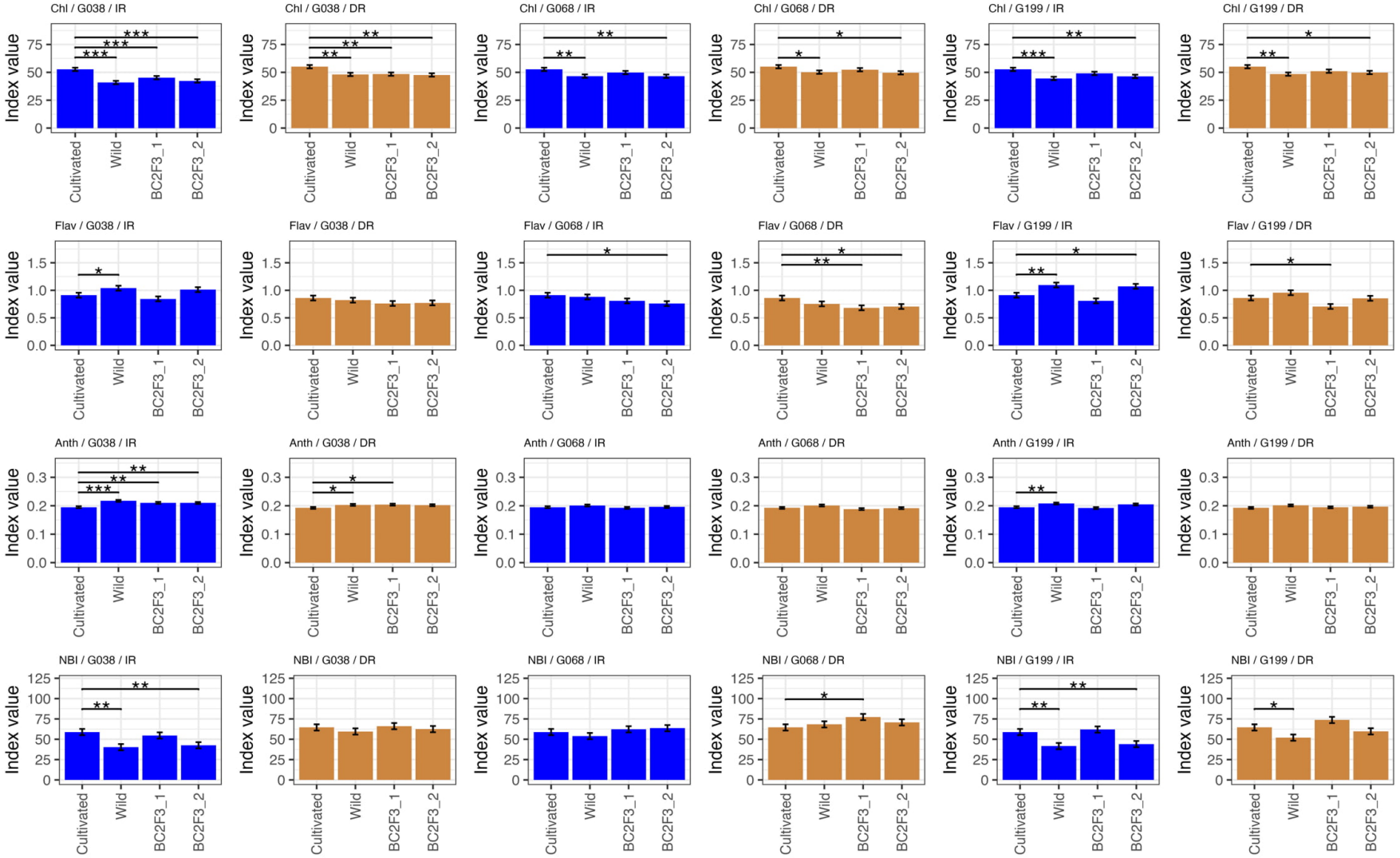

Appendix 6.7. NBHIs contrasts between La Trobe (LTR) against Wild, and the two *de novo*-domesticated lines coded as BC2F3_1 and BC2F3_2. Blue and brown shaded bars correspond to irrigated and drought conditions, respectively.

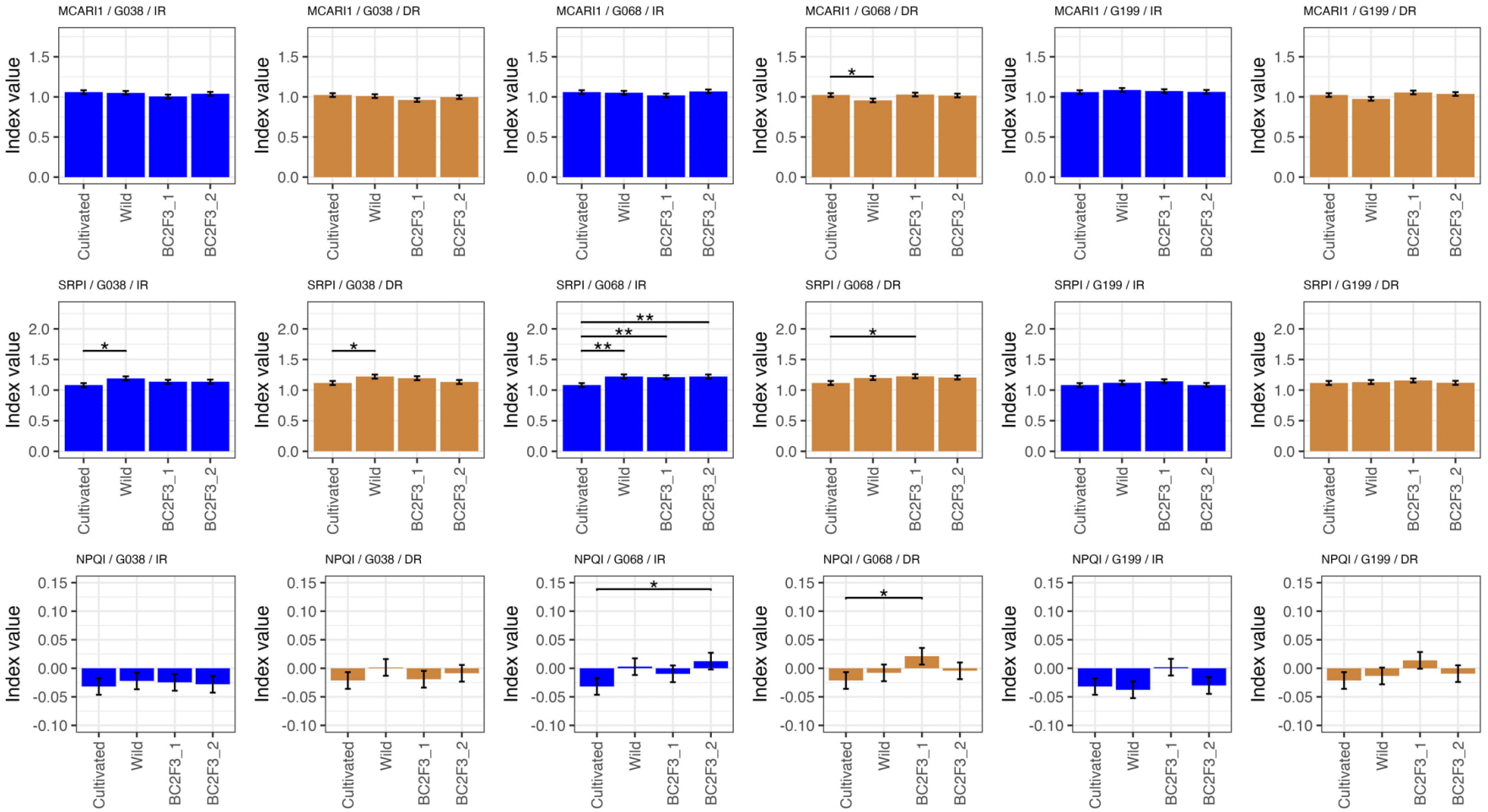

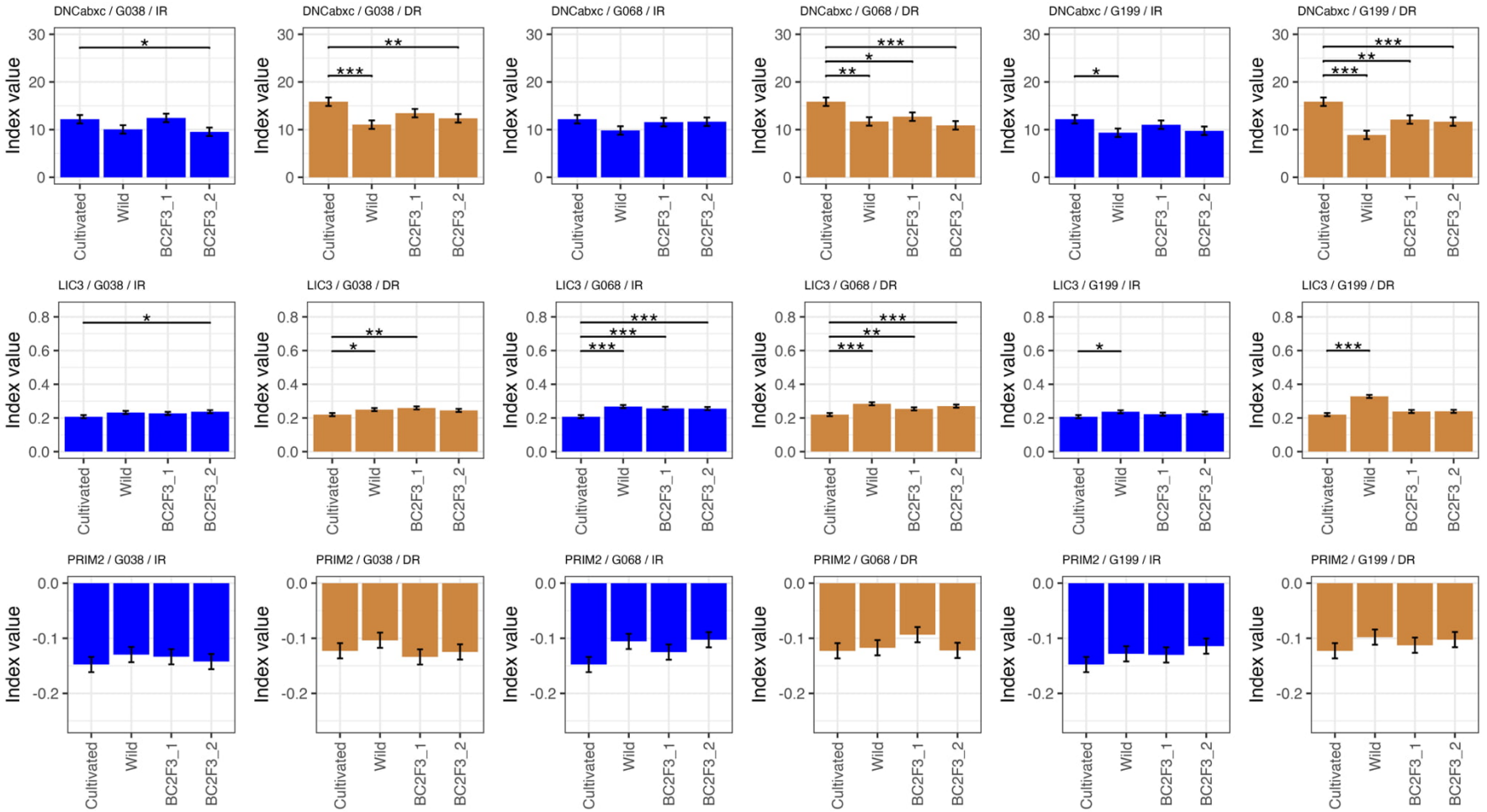
DNCabxc / G038 / IR
DNCabxc / G038 / DR
DNCabxc / G068 / IR
DNCabxc / G068 / DR
DNCabxc / G199 / IR
DNCabxc / G199 / DR
LIC3 / G038 / IR
LIC3 / G038 / DR
LIC3 / G068 / IR
LIC3 / G068 / DR
LIC3 / G199 / IR
LIC3 / G199 / DR
PRIM2 / G038 / IR
PRIM2 / G038 / DR
PRIM2 / G068 / IR
PRIM2 / G068 / DR
PRIM2 / G199 / IR
PRIM2 / G199 / DR
Index value
Cultivated
Wild
BC2F3_1
BC2F3_2

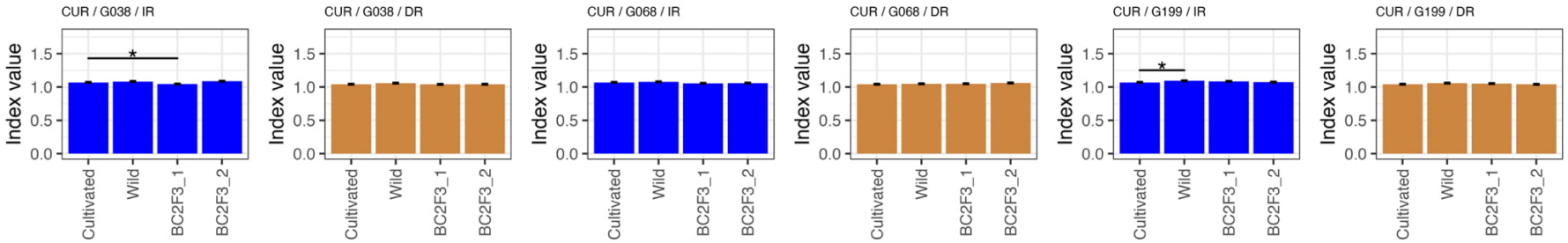
CUR / G038 / IR
CUR / G038 / DR
CUR / G068 / IR
CUR / G068 / DR
CUR / G199 / IR
CUR / G199 / DR
Index value
1.5
1.0
0.5
0.0
*
Cultivated
Wild
BC2F3_1
BC2F3_2

Appendix 6.8. Decision trees for classification across different families (LTR, G038, G068, and G199), irrigation treatment (IR,DR), or lines (L1 to L10) and material type (Wild, Cultivated).

Treatment

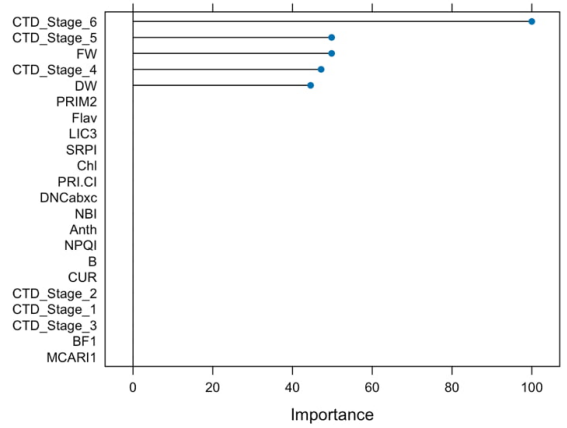

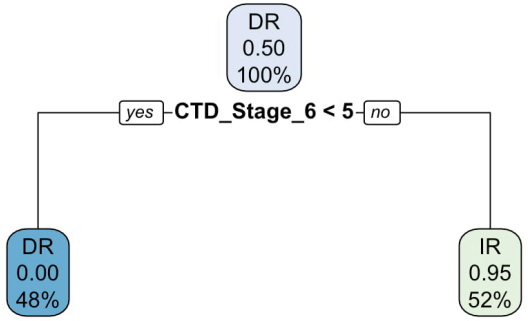

Lines

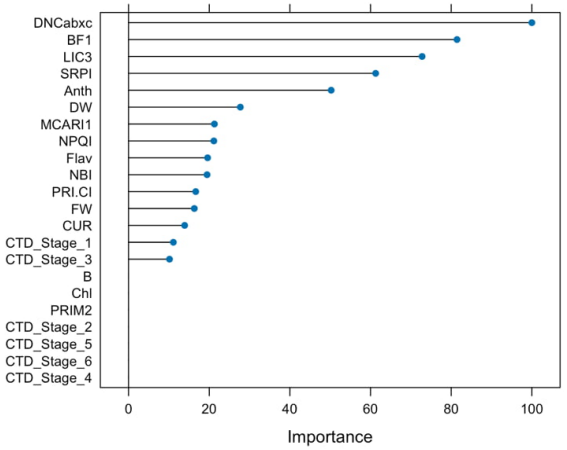

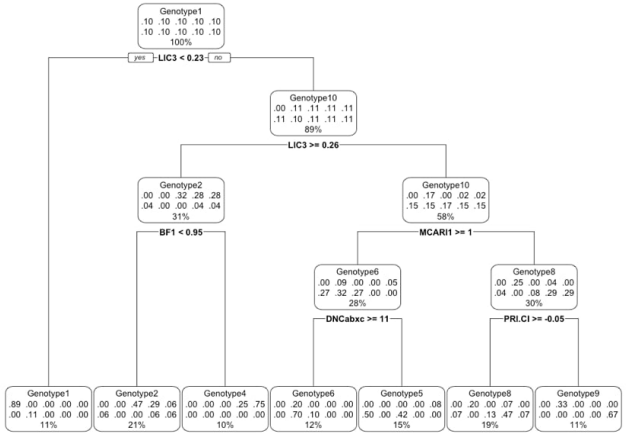

Family background

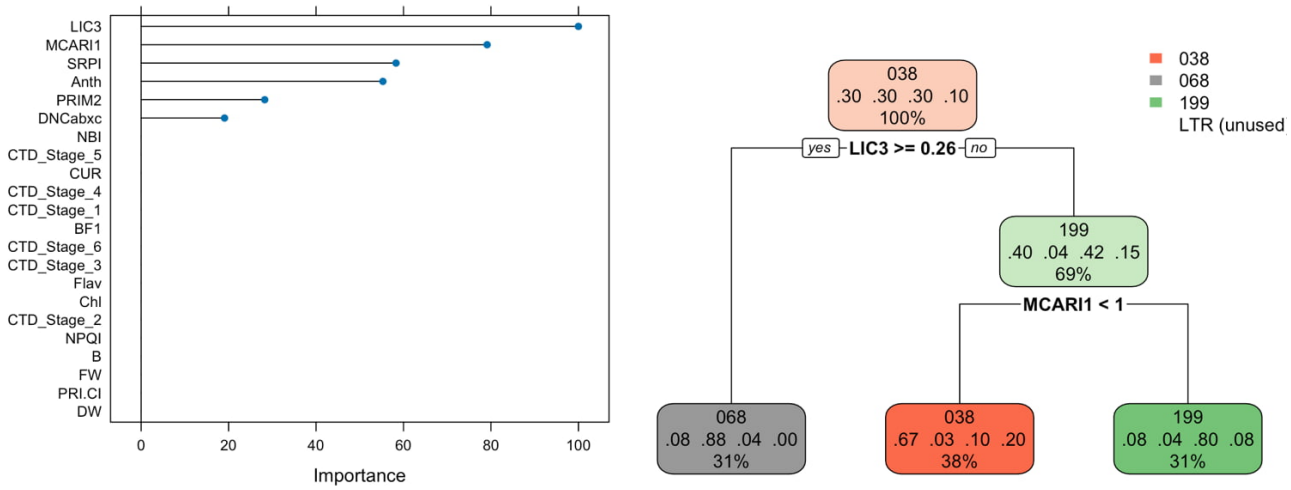

Material type

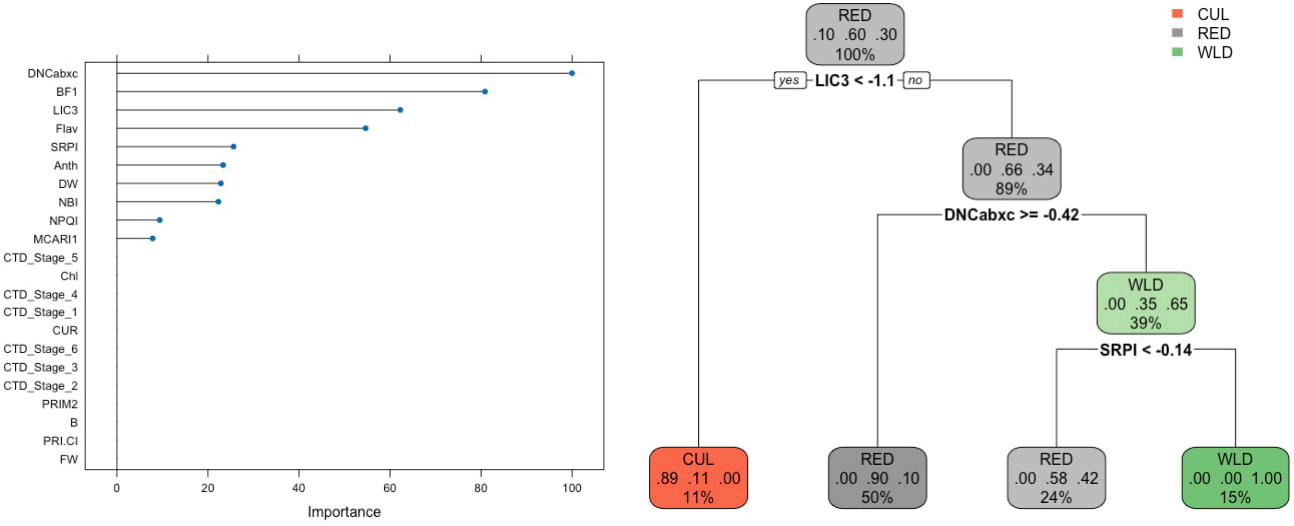

Appendix 6.9. Histogram plots showing the distribution values for all measured traits.

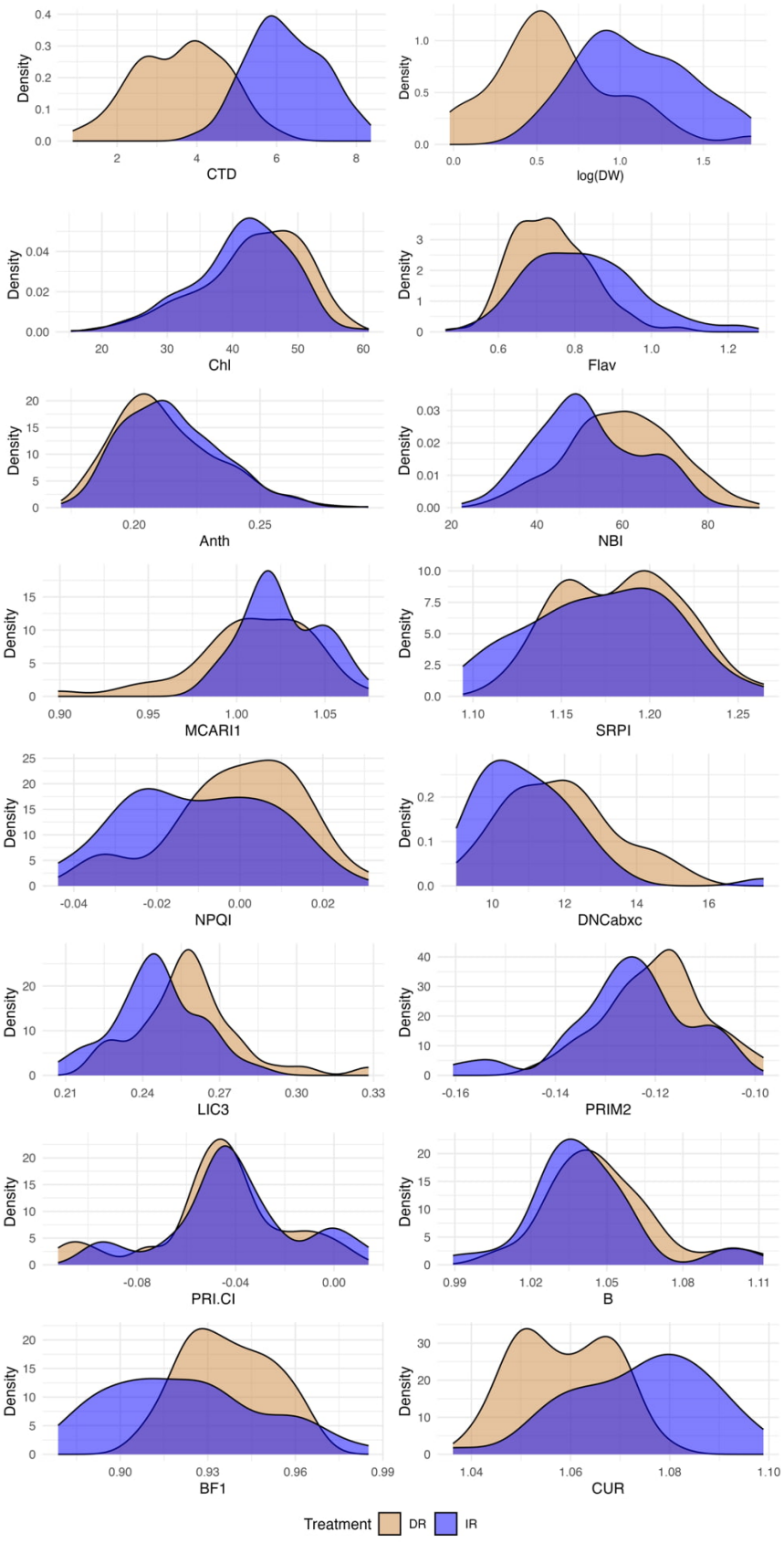

New Phytologist

Forum

Viewpoints

Back to the future for drought tolerance

Summary

Global agriculture faces increasing pressure to produce more food with fewer resources. Drought, exacerbated by climate change, is a major agricultural constraint costing the industry an estimated US $80 billion per year in lost production. Wild relatives of domesticated crops, including wheat (*Triticum* spp.) and barley (*Hordeum vulgare* L.), are an underutilized source of drought tolerance genes. However, managing their undesirable characteristics, assessing drought responses, and selecting lines with heritable traits remains a significant challenge. Here, we propose a novel strategy of using multi-trait selection criteria based on high-throughput spectral images to facilitate the assessment and selection challenge. The importance of measuring plant capacity for sustained carbon fixation under drought stress is explored, and an image-based transpiration efficiency (iTE) index obtained via a combination of hyperspectral and thermal imaging, is proposed. Incorporating iTE along with other drought-related variables in selection criteria will allow the identification of accessions with diverse tolerance mechanisms. A comprehensive approach that merges high-throughput phenotyping and *de novo* domestication is proposed for developing drought-tolerant prebreeding material and providing breeders with access to gene pools containing unexplored drought tolerance mechanisms.

Introduction

The rising global population, projected to peak at 10.9 billion by 2100, along with dietary shifts toward higher meat consumption, reinforces the demand for sustainable food production (Adam, 2021). These challenges are exacerbated by climate change and global warming. Globally, drought is the most damaging abiotic stressor, causing annual losses of US$80 billion per year (Razzaq *et al.*, 2021). Despite past genetic improvements boosting productivity, yield gains for key crops (such as wheat, rice, maize, and barley) are declining, suggesting limitations of current breeding resources and/or selection strategies (Araus *et al.*, 2018).

Crop wild relatives, shaped by countless generations of natural selection, are a reservoir of stress tolerance mechanisms (Langridge & Reynolds, 2021). One of the biggest hurdles to their effective utilization is accurately identifying drought-tolerant accessions within large screening populations. This challenge stems from the complexities of drought tolerance mechanisms, which are closely linked to the severity and timing of water shortage events. For instance, under mild water stress, many xerophytes use Na^+ as a cheap osmoticum to maintain normal stomatal function (Kang *et al.*, 2016; Xi *et al.*, 2018). Under severe stress, plants not only optimize water use efficiency (WUE) by reducing stomatal aperture but also decrease stomatal density to prevent unproductive water loss (Shabala, 2013; Bertolino *et al.*, 2019; Robertson *et al.*, 2021). This can be accompanied by changes in leaf wax composition (Hasanuzzaman *et al.*, 2023), increased root suberization (Kim *et al.*, 2022), and alterations in water channels including aquaporins (Maurel *et al.*, 2015; Shekoofa & Sinclair, 2018). All these processes are controlled by a myriad of signaling molecules and transcription factors that exacerbate the complexity of the already arduous germplasm evaluation, especially during the discovery phase of initial screening.

To overcome these challenges, developing selection criteria suitable for assessing extensive populations of wild germplasm is essential. Our review examines historical and contemporary approaches for drought tolerance breeding, focusing on improving transpiration efficiency (TE), a critical factor in crop WUE. We introduce a novel image-based transpiration efficiency (iTE), designed to identify drought-tolerant accessions based on spectral proxies for physiological traits, including photosynthetic capacity and transpiration rate. While differences in photosynthetic capacity and transpiration rate may appear insignificant across different genotypes, mainly due to the influence of short-term environmental fluctuations, these are crucial components for understanding plants' TE. The time-integrated effect of these subtle yet influential traits throughout the plant lifecycle profoundly impacts the long-term plant productivity. To detect significant variation in photosynthetic capacity and transpiration within a large population, iTE uses state-of-the-art high-throughput phenotyping imaging technologies and should be used alongside suitable experimental field designs and statistical and spatial modeling.

Selection criteria for breeding drought-tolerant cereals

Traditionally, crop improvements in arid environments have emphasized yield increase with limited knowledge of physiological and molecular mechanisms involved (Bacon, 2004; Singh *et al.*, 2021). However, the growing unpredictability of weather patterns due to climate change negatively affecting yield heritability reduces the effectiveness of cultivar selection, especially under field drought conditions (Abdolshahi *et al.*, 2015). The future of crop improvement thus relies on traits with stable heritability – those with genetic factors explaining most of the phenotypic variation – under well-watered and drought conditions.

Using yield performance as the primary selection criterion in wild relatives may inadvertently favor early flowering genotypes

New Phytologist

adapted to Mediterranean climates, which avoid rather than tolerate drought. However, future yield improvements are expected from plants with prolonged reproductive stages that maximize growth and dry matter partitioning during the critical period of grain number determination, and/or exhibit stay-green phenotypes (Gregersen *et al.*, 2013; Flohr *et al.*, 2018; Slafer *et al.*, 2023). Gaining a deeper comprehension of drought response is essential to unlock tolerance mechanisms present in wild relatives, particularly because certain wild lines do not exhibit short life cycles as an adaptation to drought. Drought tolerance mechanisms may not be immediately evident in these genetic resources, and rigorous scientific investigation is required.

Transpiration efficiency

Transpiration efficiency is closely connected to plant physiological processes, making it a promising trait with higher heritability to maintain a high level of carbon assimilation (A) per unit of water transpired (T) (Eqn 1). TE is a subcomponent of WUE – the ratio of grain or biomass accumulated per total water evapotranspiration over the crop life cycle (French & Schultz, 1984) – and can be measured at either the crop or the leaf scale. In contrast to WUE, TE is less prone to the long-term environmental effects, such as variable evaporation and soil characteristics:

$$\mathrm{TE} = A/T \qquad \text{Eqn 1}$$

Unlike yield and harvest index (HI) that have been continuously used in modern breeding since the 1960s to estimate drought tolerance (Long *et al.*, 2015), the full potential of TE for plant breeding remains untapped. This is primarily due to the logistical challenges associated with measuring TE on a large scale.

High TE is desirable for improving drought tolerance in rainfed crops. A plant exhibiting high TE generates a greater amount of biomass per unit of water transpired, in contrast to a plant with lower TE. Due to logistical challenges, TE is typically measured using indirect methods. For instance, carbon isotope discrimination (CID) provides a high-throughput surrogate of TE for inferring TE in large-scale phenotyping experiments (Farquhar & Richards, 1984). CID is based on the differential diffusion of CO_2 isotopes (^{13}C and ^{12}C) through stomata, where ^{13}C is incorporated into the Calvin cycle by Rubisco at a slower rate compared with ^{12}C. CID offers a valuable time-integrated inference of TE, reflecting the long-term equilibrium between carbon gain and water loss. Since carbon isotopes are stable, it enables sampling without concern of negative effects of short-term environmental fluctuations. Due to this time-integrated nature, CID has found most of its success in selecting genotypes that consistently exhibit high TE throughout their lifecycle. However, these lines generally show yield penalties in environments where yield is less constrained by water supply (Condon & Richards, 1992; Bacon, 2004). This dualism has sparked an ongoing discussion among researchers debating the relative importance of high vs low TE for improving cereal crops (Handley *et al.*, 1994; Blum, 2009; Hughes *et al.*, 2017).

Low TE is traditionally considered undesirable in dry environments. A plant with low TE produces less biomass for the amount of water it transpires, compared with one with high TE. Surprisingly, low TE (measured as CID) has been observed in wild barley (*Hordeum vulgare* L. ssp. *spontaneous*) accessions from dry regions, which suggest mechanisms that compensate for the higher water loss or exploit environmental context to achieve high TE (Handley *et al.*, 1994). For instance, TE is highly sensitive to vapor pressure deficit (VPD) and can vary threefold in response to seasonal changes in this climate variable; a response of much greater magnitude than that due to genetic variation (Kar *et al.*, 2020). Wild lines with apparent low TE may in fact have growth and development patterns adapted to endemic seasonal cycles of VPD, and achieve relatively high TE within their local environmental context as a result. Low TE could also be an indication of ephemeral adaptation to maximize carbon uptake following sporadic rainfall (Handley *et al.*, 1994). Hypothetically, accessions that exhibit low TE under low VPD or well-watered conditions but can promptly switch to high TE at the onset of high VPD or drought stress are ideal candidates for agriculture. Wild barley may possess important stomata regulation mechanisms in response to various environmental stimuli. Comprehensive investigations are required to understand the underlying mechanisms which may exist.

New frontiers for improving transpiration efficiency

Optimum TE under nonstressed conditions

Adjustable pores located in the leaf surface called stomata are vital in managing water loss and carbon uptake in plants. Alterations in stomatal conductance (g_s) affect CO_2 and H_2O differently (Fig. 1). Water loss through stomata is more than a hundred times higher than carbon uptake (Bacon, 2004). Typical $CO_2 : H_2O$ ratios in C_3 and C_4 plants are 1 : 600 and 1 : 450, respectively, with C_4 species exhibiting greater efficiency due to Kranz-like anatomy. This inherent dominance of water loss to carbon uptake in C_3 and C_4 plants, largely determined by the concentration gradients and diffusion coefficients of both gases, makes water transpiration (T in Eqn 1) more sensitive to changes in stomatal conductance. Although low stomatal conductance generally reduces carbon assimilation by limiting the diffusion of CO_2 into the carboxylation site, a moderately low supply of CO_2 from the atmosphere can also increase the gradient and driving force of CO_2 diffusion into the leaf interior, while the gradient and driving force for outward H_2O diffusion remains constant. Given the differences in gradient and driving forces of both gases involved in this exchange process, there must exist a lower threshold of g_s where carbon assimilation is only marginally decreased while transpiration is significantly reduced. This has been observed in *Arabidopsis* and barley with reduced stomata density (SD; Hepworth *et al.*, 2015; Hughes *et al.*, 2017), and the same phenomenon could be achieved through an increased sensitivity to closing stimuli (Aliniaeifard & van Meeteren, 2014).

Reduced stomatal density and increased sensitivity to closing stimuli are beneficial traits mainly under nonstressed conditions to reduce the unproductive water losses. However, plants with these

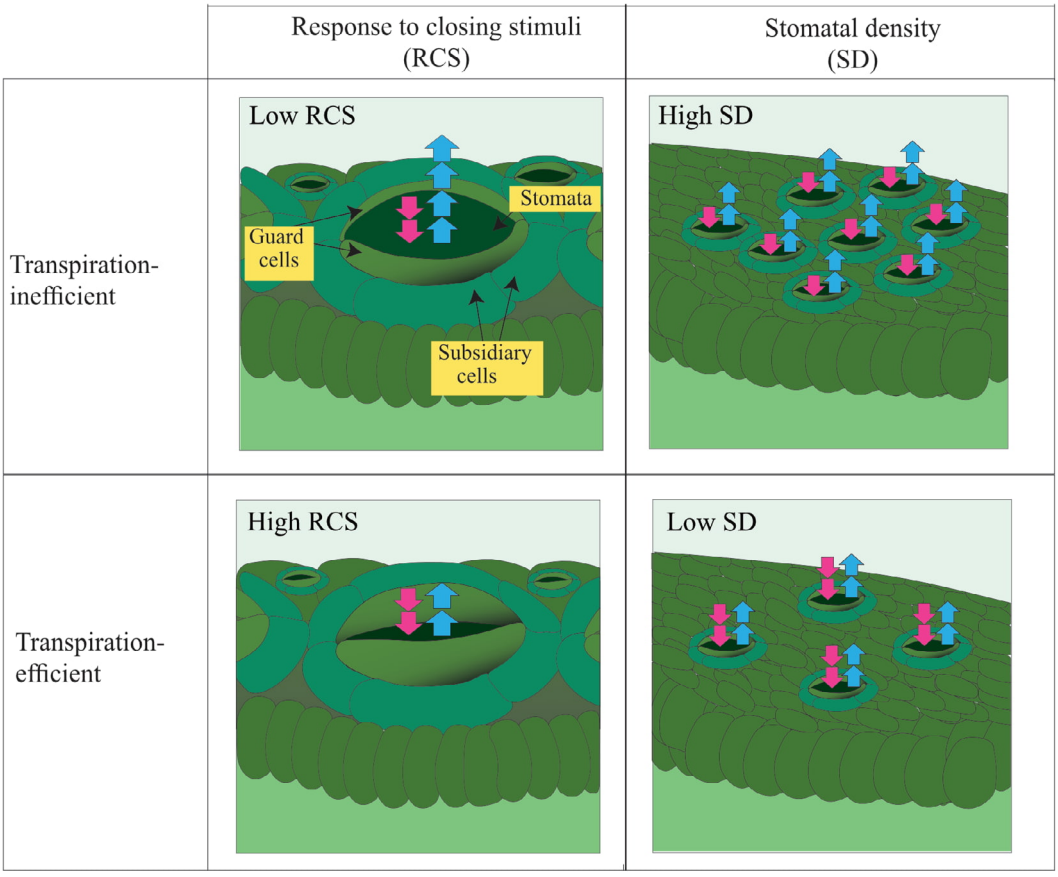

Fig. 1 Influential factors on transpiration efficiency (TE): response to closing stimuli (RCS) and stomata density (SD) in a leaf. The top row presents a transpiration-inefficient genotype with low RCS and high SD, while the bottom row shows a transpiration-efficient genotype with high RCS and low SD. Pink arrows denote CO_2 uptake; blue arrows indicate H_2O transpiration. Reduced stomatal conductance, achieved via high RCS or low SD, increases the CO_2 concentration gradient, maintaining CO_2 uptake rate despite significant reductions in transpiration. In the transpiration-efficient genotype (bottom row), CO_2 uptake remains constant (equal pink arrows), while transpiration halves (fewer blue arrows) relative to the transpiration-inefficient genotype (top row).

characteristics may still experience negative effects on carbon assimilation under severe stress via nonstomatal inhibition (Yang *et al.*, 2021). Overproduction of molecules such as reactive oxygen species (ROS) via the chloroplast Mehler reaction can inhibit carbon assimilation by damaging the photosynthetic machinery and compromising the capacity for carbon fixation (Havrlentová *et al.*, 2021). Appropriate phenotyping methods are then required to distinguish genotypes with high TE while maintaining relatively steady levels of photosynthetic capacity.

Sustained carbon fixation under drought stress

Carbon assimilation and carbon fixation are closely related yet distinct processes in plant physiology. The differentiation between these two concepts is crucial in order to optimize TE under drought scenarios and use it as a target trait in plant breeding. Carbon assimilation (A in Eqn 1) is the broad process of converting atmospheric CO_2 into organic compounds, while carbon fixation is the specific process of converting CO_2 into organic molecules through enzyme-catalyzed reactions in photosynthesis. The carbon assimilation rate is not solely dependent on the capacity for carbon fixation; it is also significantly influenced by the availability of CO_2 in the carboxylation site. Unlike carbon assimilation, carbon fixation can remain stable even when stomata close, preventing CO_2 diffusion, provided the photosynthetic machinery remains intact. Thus, sustained carbon fixation capacity under drought stress does not equal a sustained rate of carbon assimilation. The ability of a plant to sustain carbon fixation under conditions of water scarcity is a crucial trait for retaining crop productivity. By preserving photosynthetic activity during periods of limited water availability, plants can rapidly resume growth and recover upon rehydration.

The capacity for carbon fixation is typically measured as V_{cmax}, a critical component when carbon assimilation is Rubisco-limited (Sharkey *et al.*, 2007). V_{cmax} represents the maximum catalytic rate at which the enzyme Rubisco can carboxylate ribulose-1,5-bisphosphate (RuBP) under conditions of saturated intercellular CO_2 concentration. V_{cmax} is derived from A–C_i curves obtained through gas exchange measurements and is characterized by the initial slope of these curves in combination with a photosynthetic model that accounts for both the carboxylation and oxygenation activities of Rubisco, as well as RuBP regeneration (Farquhar *et al.*, 1980).

Understanding the relative changes in the components of TE is a crucial aspect to identify genotypes with high TE through sustained carbon fixation. In theory, plants can achieve high TE by either (1) maintaining A while T decreases or (2) reducing T to a greater extent than A (Eqn 1). The first approach – where A remains relatively constant compared with a nonstressed baseline – appears advantageous as it seemingly preserves productivity. However, this strategy may not be optimal, particularly under severe drought conditions that depend on water reserves from off-season precipitation. The maintenance of carbon assimilation in this scenario occurs through continued CO_2 diffusion into the leaf, but it inadvertently results in substantial water losses. Consequently, plants adopting this strategy will deplete their water reserves more rapidly compared with those that more efficiently modulate stomatal closure. By contrast, the scenario where T is reduced more significantly than A is a more viable strategy under severe drought conditions. This approach involves maintaining a degree of carbon fixation despite reductions in carbon assimilation and transpiration due to decreased stomatal conductance. It represents a balance between conserving water and sustaining photosynthetic activity (Fig. 2).

Employing CID as a proxy of TE has limitations in identifying genotypes with sustained carbon fixation capacity as it does not provide insights on the relative contributions of A and T, but rather integrates the effects of stomatal and nonstomatal inhibitions into a single value (Farquhar & Richards, 1984; Condon *et al.*, 2002; Sexton *et al.*, 2021). Furthermore, since the heritability of CID significantly decreases under dry conditions (Richards, 2022), breeding selection criteria are generally constrained to performance under well-irrigated conditions, thus overlooking the negative impacts on carbon fixation capacity under drought stress. The deployment of advanced imaging technologies could provide the means to distinguish alterations in carbon-to-transpiration relationship, essential for selecting genotypes that sustain photosynthesis under drought stress.

High-throughput phenotyping

The pursuit of more efficient, scalable, and precise methods for assessing changes in TE under drought scenarios underlines the need for innovations in phenotyping technologies. Traditional approaches for examining key physiological processes, such as transpiration rates and carbon fixation, rely heavily on labor-intensive measurements, often limiting the scope and scalability of germplasm evaluations. For instance, transpiration rate traditionally requires direct measurements of stomatal conductance (g_s) using handheld porometers. Similarly, creating A–C_i curves to derive V_{cmax} is time-consuming, taking more than half an hour per curve, and impractical for extensive germplasm evaluations. Remote sensing techniques offer high-throughput and precise options for estimating plant physiological properties, including transpiration rate and V_{cmax} (Camino *et al.*, 2019). These nondestructive techniques can be used at different developmental stages to monitor the progression of plants' responses to drought stress and allow crops to be phenotyped in replicated field trials at an unprecedented scale and resolution.

Thermal imaging

Thermal imaging consists of collecting the thermal infrared spectral region to derive vegetation canopy temperature (CT). The differences in CT between genotypes can suggest differences in transpiration rates. The Crop Water Stress Index (CWSI) is a valuable tool for quantifying plant transpiration rates by assessing stress levels against established wet and dry baselines in field conditions (Gonzalez-Dugo *et al.*, 2019). Thermal imaging from aerial platforms has become increasingly vital in plant breeding because it enhances the accuracy of measuring CWSI, making it more stable against temporal fluctuations. This improvement increases the heritability of CWSI when contrasted with stomatal conductance measured by handheld porometers (Deery *et al.*, 2016), making it an effective trait for germplasm phenotyping.

While CT can provide valuable insights into the impact of drought stress on the transpiration component of TE, interpretations of field-measured CWSI as proxy of transpiration rates should be approached cautiously. A lower CWSI, indicative of a genotype with higher transpiration rates, does not inherently imply that the genotype uses water inefficiently. Low values of CWSI may also result from enhanced access to subsoil water resources, facilitated by the presence of deep root systems. In this scenario, despite the plant's ability to partially close stomata as a survival mechanism, their effective water uptake allows them to continue transpiring at relatively higher rates than less adapted genotypes. The challenge thus lies in differentiating plants that transpire more when water is scarce from plants that transpire more because they have better access to subsoil water. This ability to maintain higher transpiration rates while still conserving water through stomatal closure can be advantageous for the drought-tolerant plant genotypes as it enables them to continue essential physiological processes. To avoid potential confounding effects of deep rooting and transpiration rates, it is advisable to develop phenotyping platforms that account for the above shortcomings. For instance, thermal imaging from field trials can be complemented with appropriate stress management in glasshouse experiments. Comparing the extent to which genotype differences are consistent between the field and glasshouse can suggest whether a low CT is due to higher water accessibility through deep rooting or differences in SD and aperture.

Hyperspectral imaging

Hyperspectral imaging, also known as imaging spectroscopy, is a method that uses high spectral resolution cameras to create images by capturing the reflected radiation at multiple narrow and contiguous spectral bands. Traits with strong absorption signals such as leaf mass per leaf area and nonphotosynthetic pigments have been used in models such as partial least square regression to empirically derive V_{cmax}, a critical component of photosynthetic capacity when carbon assimilation is Rubisco-limited (Serbin *et al.*, 2012; Dechant *et al.*, 2017; Xiaoyu *et al.*, 2022). However, these empirical models have limited transferability to other species or environmental conditions since the information obtained is not directly related to leaf photosynthesis and are affected by canopy structural and background effects (Suarez *et al.*, 2021).

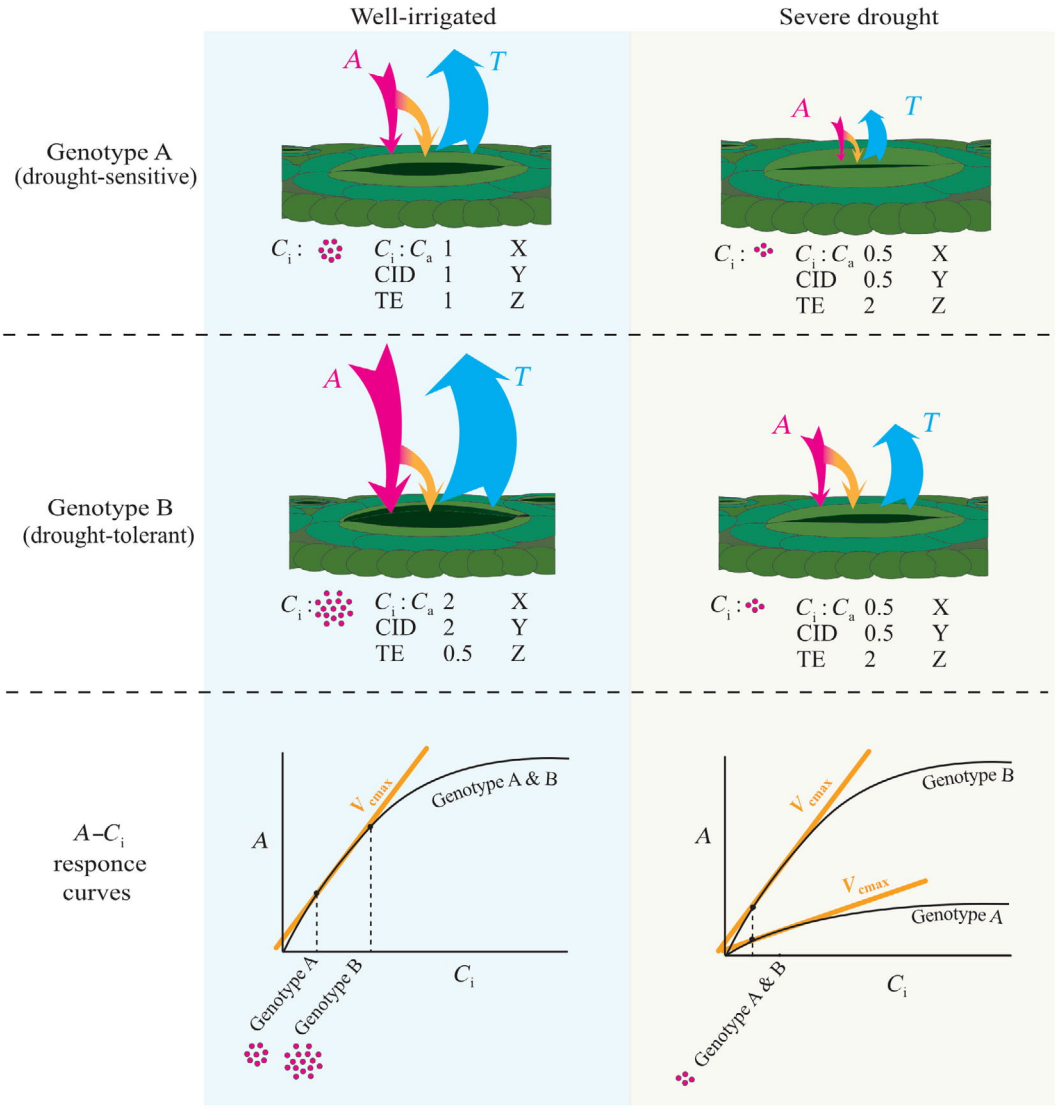

Fig. 2 Impact of severe drought on two hypothetical genotypes. Under well-irrigated conditions, both genotypes exhibit equivalent carbon fixation capacity (V_{cmax}; orange arrows) but differ in carbon assimilation (*A*; pink arrows) and transpiration (*T*; blue arrows). Selections based on carbon isotope discrimination (CID) are generally conducted under well-irrigated conditions given the trait's higher heritability. In this example, Genotype A will be selected based on CID, which exhibits higher TE than Genotype B. Under severe drought, stomata close, increasing both Genotype A and B's transpiration efficiency (TE). The increase in TE occurs due to the significant decrease in transpiration (*T*) than the reduction in carbon assimilation (*A*). This increase in TE is accompanied by changes in the ratio between intercellular and ambient CO_2 ($C_i : C_a$ ratio) reflected in CID. Genotype B maintains a robust carbon fixation capacity, while Genotype A achieves the same $C_i : C_a$ ratio via lower stomatal conductance. Differences in carbon fixation capacity are captured via the initial slope of A–C_i curves (bottom row). Under drought conditions, Genotype B's curve and slope closely resemble those observed under well-irrigated conditions, whereas Genotype A's curve and slope exhibit notable deterioration. Genotype B modulates stomatal conductance more efficiently in response to short-term changes in water availability and other environmental stimuli, including vapor pressure deficit (VPD). This increased responsiveness allows Genotype B to effectively minimize water losses while maintaining high productivity under severe drought.

The development of sophisticated sensors with higher spectral resolution has allowed the detection of the relatively weaker absorption signatures of important photosynthetic and nonphotosynthetic constituents, such as Chl*a*, Chl*b*, carotenoids, anthocyanins, and xanthophylls (Jacquemoud *et al.*, 2009; Ustin *et al.*, 2009). The latter pigments represent a major mechanism for nonenzymatic ROS scavenging and allow plants to reduce the detrimental effects of hydroxyl radicals – the most aggressive form of ROS (Bose *et al.*, 2014; Demidchik, 2015). Mechanistic radiative transfer models, such as the Soil-Canopy Observation of Photosynthesis and Energy (SCOPE) (van der Tol *et al.*, 2009), enables the establishment of a direct relationship between the spectral reflectance captured by an imaging spectrometer and the absorption of these photosynthetic constituents and V_{cmax}. This allows for a more robust determination of plants' carbon fixation capacity than site-specific empirical relationships (Camino *et al.*, 2019; Suarez *et al.*, 2021). Although measured and model-estimated V_{cmax} has yielded a high linear relationship (Camino

et al., 2019), it is important to highlight that the objective is not to achieve absolute quantification of V_{cmax}, which is more accurately determined using low throughput gas exchange systems. Instead, the focus lies on the insights gained from the relative changes in the capacity for carbon fixation under the effects of drought of large germplasms collections. Additionally, like thermal imaging, airborne platforms of hyperspectral imaging offer an even higher throughput phenotyping option than ground-based measurements. Airborne hyperspectral imaging can potentially increase the heritability of V_{cmax} by minimizing the impact of spatial and temporal variability during data acquisition (Gálvez *et al.*, 2019).

An image-based transpiration efficiency index for plant breeding

To quantify the relative changes in the components of TE, we propose combining CWSI and normalized values of V_{cmax} obtained via remote sensing into a unitless iTE index as defined in Eqn 2. The CWSI, serving as a proxy for transpiration rate, requires a linear transformation before inclusion within iTE to preserve the assimilation-to-transpiration ratio (A: T) from Eqn 1; a metric of carbon acquisition relative to water expenditure. The linear transformation necessary for a positive correlation between CWSI and transpiration rate is accomplished by the expression $1 - \text{CWSI}$. Higher values of $1 - \text{CWSI}$ indicate lower levels of crop water stress and consequently higher transpiration rates:

$$\text{iTE} = V_{cmax}/(1-\text{CWSI}) \qquad \text{Eqn 2}$$

We have tested the validity of the proposed iTE by re-analyzing data from Camino *et al.* (2019) across six wheat varieties at the stem elongation stage (Supporting Information Table S1; Methods S1). This re-analysis shows the variable nature of iTE among wheat varieties under irrigated and rainfed conditions (Fig. 3), demonstrating the potential of this index for selecting drought-tolerant genotypes. However, a large population with hundreds of accessions can pose a challenge. The population size may weaken the observed effects of iTE due to the noise in data introduced by the impact of the environment. Several components, including the number of genotypes, replicates, variations introduced by the heterogeneity of natural field conditions, and the intrinsic genetic variation of the germplasm under evaluation, should be carefully considered during the experimental design. The former two generally represent a trade-off between precision and practicality. Including a large number of genotypes enables the incorporation of a broader spectrum of responses and the identification of potentially valuable genetic material, while increasing the number of replicates enhances the statistical robustness. However, increasing either the number of genotypes or replicates requires a greater allocation of resources. Advanced statistical and spatial modeling can help reduce such trade-offs.

The significance of iTE as a trait for drought tolerance improvement lies in the relative changes under drought stress compared with a well-irrigated baseline. Camino *et al.* (2019) successfully demonstrated high correlations between hyperspectrally derived and ground-based measurements of V_{cmax}. However, to draw robust conclusions about the shifts in iTE across the different irrigation treatments, a sufficient number of whole plots are necessary to integrate the hierarchical structure of split-plot designs into the linear model. An appropriate number of whole plots is tightly linked to the number of factors, treatment levels, and replicates of the experimental design. Without an appropriate number of whole plots, the irrigation treatment correlates with the whole plots and the statistical model cannot distinguish variations due to irrigation from those caused by the blocking factor. This is the case of the re-analyzed data from Camino *et al.* (2019). Despite this limitation in the Camino *et al.* (2019) study, we utilized the combined dataset from irrigated and rainfed plots to illustrate the potential of the relative shifts on iTE and its components as a criterion for selecting drought-tolerant wheat varieties (Fig. 4).

High relative iTE values under drought, compared with a well-irrigated baseline, indicate that transpiration is reduced more substantially than photosynthetic capacity (Var4). By contrast, lower relative iTE values indicate a genotype undergoing a more significant decline in photosynthetic activity compared with the decrease in transpiration, potentially suggesting the vulnerability of photosynthetic machinery to drought stress (Var6).

Future research should aim to elucidate the genetic factors underpinning the changes in iTE relative to a well-irrigated baseline. However, the primary significance of iTE in plant breeding lies in its integration with economically relevant traits (Morton *et al.*, 2019). For example, an increase in iTE resulting from a stable V_{cmax} under drought conditions is expected to show a strong correlation with a stress tolerance index derived from the difference between yield under irrigated and yield under drought conditions (TOL index) (Morton *et al.*, 2019). The significant decrease in transpiration during the initial stages of drought stress enables water conservation, while the plant's sustained photosynthetic capacity allows a better recovery upon rehydration, effectively minimizing crop yield losses. Establishing a correlation between the newly proposed iTE index and a range of tolerance indices thus offers a deeper understanding of how iTE variations translate into practical agronomic outcomes (Fig. 5).

Notably, low TOL can stem from the lack of responsiveness to stress-free conditions if a cultivar has a reduced growth/yield under both rainfed and irrigation. Incorporating other productivity measures, such as mean productivity (MP), with TOL can improve the selection criteria for breeding purposes by identifying accessions that achieve low TOL but are also relatively high yielding. This ensures a more accurate and holistic evaluation of their agronomic potential for drought tolerance.

The proposed iTE index is primarily intended for screening wild relatives. It addresses the challenge of directly measuring grain yield in the field, which is often impractical due to the inherent grain shattering in wild accessions. Nonetheless, the iTE index has potential applications within cultivated breeding pools. Empirical breeding frequently encounters a dichotomy: (1) high yields under optimal conditions yet substantial reductions under drought stress, indicative of high MP and high yield losses (high TOL) under drought (Morton *et al.*, 2019) vs (2) yield stability under drought stress (low TOL) accompanied by a substantial yield penalty in well-irrigated scenarios (low MP) (Blum, 2011). Within this

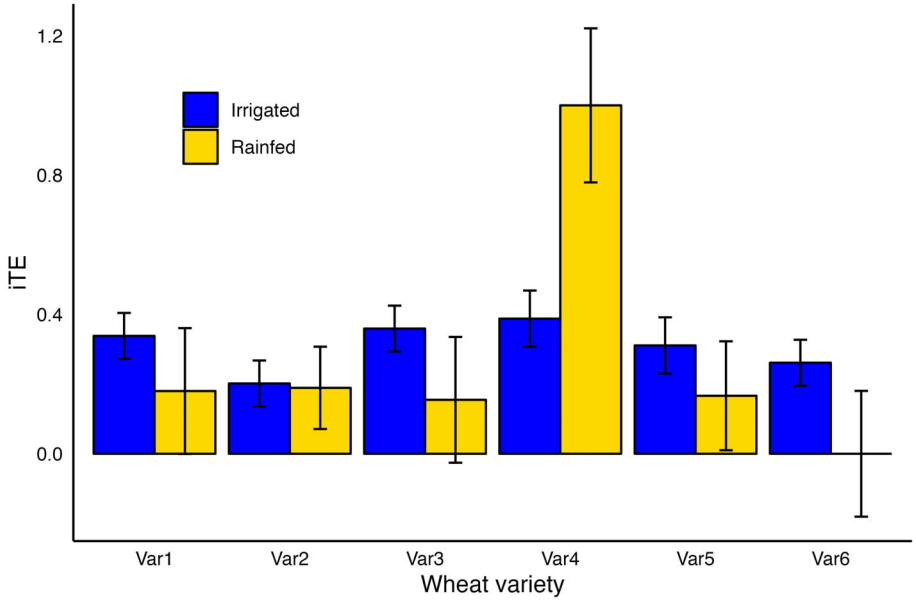

Fig. 3 Comparative analysis of an image-based transpiration efficiency (iTE) index for six wheat varieties (*Triticum* spp.) under irrigated (blue) and rainfed (yellow) conditions from Camino *et al*. (2019) dataset. Data are means ± SE. Most wheat varieties show a decrease in iTE from irrigated to rainfed conditions, while Var4 exhibits a pronounced increase, indicating potential adaptation and tolerance of this variety to water scarcity.

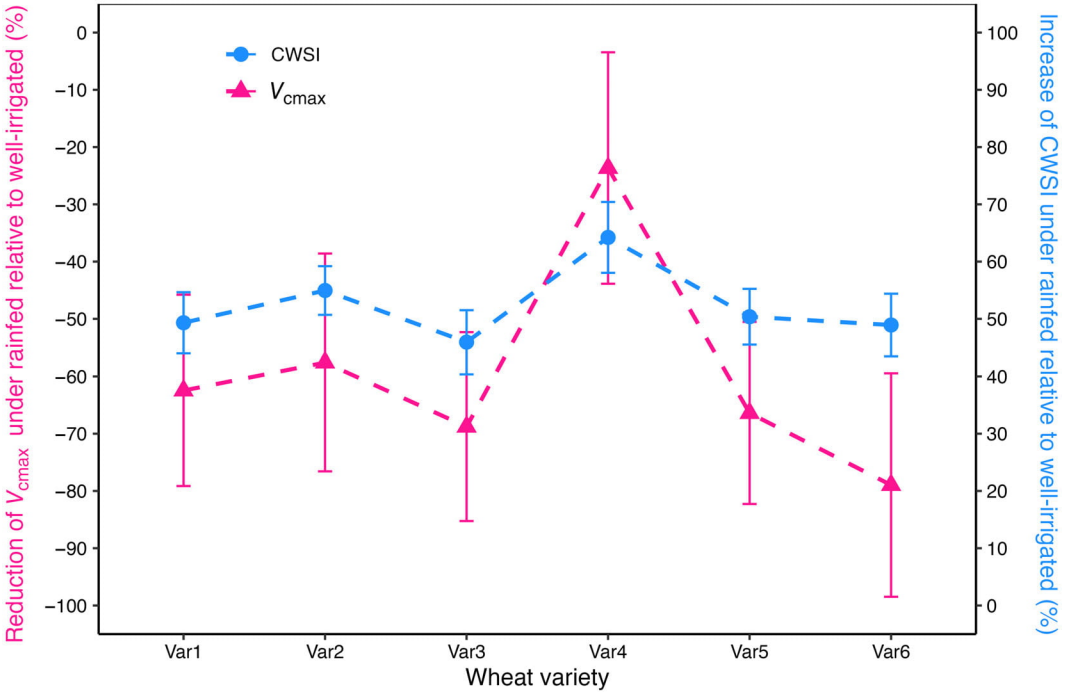

Fig. 4 Changes in Crop Water Stress Index (CWSI) (blue) and V_{cmax} (pink) to drought relative to well-irrigated conditions across six commercial wheat varieties (*Triticum* spp.) re-analyzed by Camino *et al*. (2019). Data are means ± SE. While V_{cmax} typically experiences > 50% decrease in most varieties, Var4 stands out as an exception, maintaining its carbon fixation capacity with only 23% reduction from optimal conditions, despite the significant increase in CWSI. This suggests a potential tolerance mechanism that retains photosynthetic capacity to some extent under drought stress.

framework, elite cultivars with high yields and poor stability might be preferred, if their absolute yield under drought exceeds that of more yield-stable varieties. A deep understanding of the molecular processes that enable photosynthesis to persist under drought stress will lead to the refinement of breeding selection strategies, potentially enhancing the heritability of iTE beyond the limitations imposed by current practices focused exclusively on yield stability (low TOL). This paves the way for integrating the trait of sustained photosynthesis into high-performing elite cultivars. However, before breeders use iTE for crop improvement programs, it is essential to investigate the genetic architecture and heritability of iTE. Comprehensive genomic studies, including genome-wide

New Phytologist

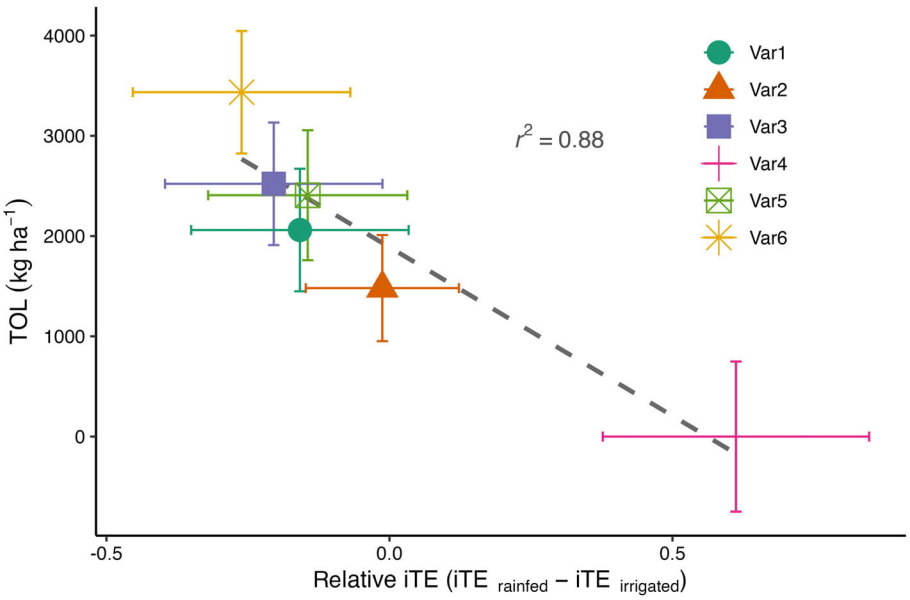

Fig. 5 Correlation analysis illustrating the relationship between the relative change in image-based transpiration efficiency (iTE) from rainfed to irrigated conditions (relative iTE) at the stem elongation stage and the grain yield loss (TOL) for six wheat varieties (*Triticum* spp.) based on re-analyzed data from Camino *et al*. (2019). Lower values of TOL and high values of relative iTE are desired for plant breeding. The dashed grey regression line indicates a strong negative correlation, as denoted by the r^2 value of 0.88, suggesting that variations in iTE significantly predict TOL across these varieties. Each variety is represented by a unique symbol and color. Error bars represent ± SE.

association studies and genomic selection models, are valuable tools to uncover genetic factors and determine the extent to which iTE can be used for trait introgression in plant breeding.

Identification and selection of wild candidate accessions

Phenotyping, clustering, and selection

Preliminary screening experiments aim to enhance breeding pools, and traits amenable to high-throughput measurements are essential for evaluating and selecting outstanding accessions within diverse populations. To maximize the use of diverse populations, selection strategies can be built upon unsupervised machine learning methods, like hierarchical clustering, to identify patterns of phenotypic resemblance across different genotypes (Das *et al*., 2021) (Fig. 6). Wild accessions may have developed a distinct mechanism of drought tolerance. For example, some of them have high TE to modulate stomata conductance at the time of severe drought. However, others with low TE that deplete soil water rapidly probably evolved efficient mechanisms for osmotic adjustment (Handley *et al*., 1994). Improved osmotic adjustment allows accessions with low TE to withstand longer periods of water scarcity.

Clustering also facilitates a more impartial selection process. By identifying and selecting representative accessions from various clusters, we ensure a broad capture of diverse tolerance mechanisms, moving away from oversimplified classifications based on drought-tolerant vs drought-sensitive or high-yielding vs low-yielding. Such binary classifications risk overlooking valuable genetic material, including accessions with low TE well-suited to arid conditions (e.g. wild barley from desertic regions) (Handley *et al*., 1994).

Multi-trait evaluations enhance the value of phenotypic diversity assessments as genotypes can be categorized based on the vast variety of responses. For instance, relative changes in iTE offer insights into the balance between transpiration and photosynthetic capacity. However, it is through the collective analysis of iTE, V_{cmax}, CWSI, and TOL that breeders can differentiate between plants that achieve high iTE either by sustained photosynthesis (type A; Fig. 6) or by significant reductions in transpiration (type C; Fig. 6). While productivity indices like MP can be considered in comprehensive selection criteria, scientists and breeders should prioritize uncovering and understanding various tolerance mechanisms during the prebreeding research, placing less emphasis on aspects of the plant productivity. This approach is crucial for long-term crop improvement, as it lays the foundation for developing robust drought-tolerant varieties. As the breeding process progresses toward commercialization, breeders will prioritize traits that enhance productivity and marketability, including grain yield and quality.

Multi-trait assessments and clustering can reduce the need for multi-environmental trials. Leveraging existing phenotyping technologies can capture a wide spectrum of response mechanisms within a limited set of growing conditions. Incorporating additional measurements to address and adjust for environmental variations is essential for ensuring accuracy and reliability in the selection process. By integrating environmental data, crop prediction models can reflect genetic potential under varying conditions. The result is a focused and resource-efficient initial screening phase.

Envirotyping

Traditionally, conducting multiple trials under a diverse array of representative environments is considered necessary to confidently select potential candidates for breeding. Given the trade-off between achieving detailed data collection and managing limited resources, researchers usually employ categorical classifications of drought conditions to account for G × E interactions. While there

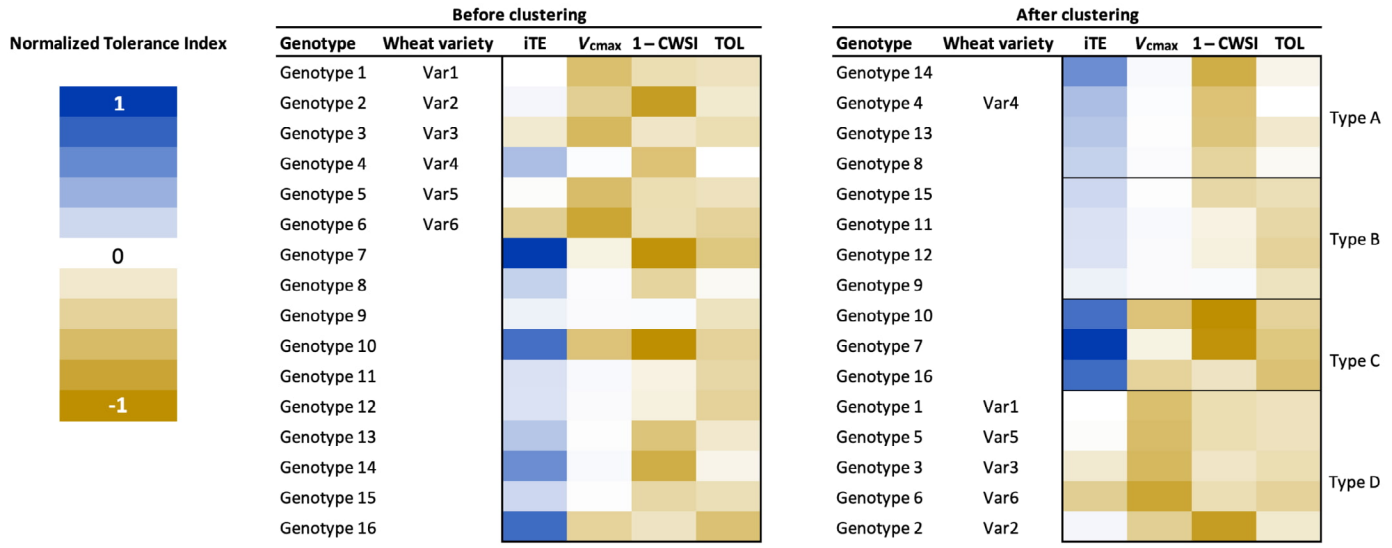

Fig. 6 Representation of a multivariate clustering analysis involving 16 genotypes. Traits included in this representation are image-based transpiration efficiency (iTE), carbon fixation capacity (V_{cmax}), canopy temperature-derived transpiration (1 − CWSI), and the difference in yield (TOL) between irrigated and drought conditions. The left panel shows unclustered data, while the right panel displays the clustered heatmap representing possible selection criteria. Genotypes have been categorized into Types A–D, reflecting distinct drought response behaviors. Genotypes 1 through 6, corresponding to varieties 1 through 6 (*Triticum* spp.), are based on experimental data derived from the 2016 Santaella experiment (Camino *et al*., 2019). The data for Genotypes 7 through 16 are hypothetical and have been constructed to illustrate potential grouping into discrete clusters. The color gradient represents a normalized change in multiple traits under drought stress compared with a well-irrigated reference, with blue indicating a 100% increase (+1) and brown indicating a 100% reduction (−1).

are numerous ways to describe drought events in terms of stress duration, timing, and severity, a general classification can be used as transient and prolonged drought. Transient drought events prompt plants to activate short-term adaptive mechanisms such as stomatal closure. By contrast, prolonged drought, characterized by extended water shortages, requires plants to employ long-term survival strategies. This approach facilitates the assessment of G × E interactions within specific drought conditions. However, categorical classifications alone do not fully account for the environmental variation within trial sites and restricts the ability to accurately predict genotypes' performance in different locations.

As technology advances, there are increasingly more low-cost, accurate, and rapid methods that allow the systematic quantification of environmental factors, known as envirotyping (Xu, 2016; Resende *et al*., 2021). Envirotyping enables researchers to include environmental covariates – a quantitative variable used in statistical analysis to account for potential confounding effects or explain variations in the dependent variable – to enhance the accuracy of model predictions (Crossa *et al*., 2022). To gain accurate insights into the impact of drought stress on TE, it is crucial to quantify soil moisture content at various temporal and spatial points within a trial site. This can be achieved through methods such as remote sensing or the utilization of soil moisture probes. While existing techniques for soil moisture measurement primarily serve large-scale hydrological and geoscience research (Liu *et al*., 2022) or farming decision-making (Maia *et al*., 2022), developing more suitable approaches tailored for plant breeding is essential. The EM38, an electromagnetic induction instrument, offers a noninvasive and rapid approach for measuring soil moisture at multiple soil depths and soil electrical conductivity (Phathutshedzo-Eugene *et al*., 2023), making it promising for incorporation in plant breeding research trials. Accurately measuring soil moisture content will enable the removal of confounding effects and help distinguish whether particularly a low transpiration is attributable to the absence of water or to the physiology of the plant.

Future prospects

High throughput and precise phenotyping based on advanced remote sensing technology, in addition to classical physiological characteristics will facilitate the selection of crop wild relatives for drought tolerance breeding. Once a drought-tolerant accession is identified, the subsequent challenge involves determining the most efficient methods to integrate the tolerance mechanism from the selected accession to the elite cultivar. The employment of wild relatives in modern breeding has been most successful in transferring traits controlled by one or a few major genes through backcrossing methods, such as disease resistance (Mammadov *et al*., 2018; Mishina *et al*., 2023). However, drought tolerance mechanisms are likely to be controlled by hundreds of genes. Thus, the classical method of backcrossing with an elite cultivar as a recurrent parent will not be effective. Instead, most domestication traits are controlled by a single or few genes. It may be more feasible to replace the major domestication genes in the selected wild parent to retain its tolerance mechanism. This is known as *de novo* domestication (Pourkheirandish *et al*., 2020).

De novo domestication is an accelerated version of the artificial selection exerted by humans that has spanned millennia (Langridge & Waugh, 2019). In this method, the aim is to introduce

domestication alleles into a wild genetic background, using either molecular-assisted backcrossing or gene-editing techniques. However, we should be mindful that the *de novo*-domesticated line is not ready for growers to immediately use for commercialization due to the long history of selective breeding on elite cultivars for high yield, grain quality, etc. The basic idea of *de novo* domestication is to convert the drought-tolerant wild accession into prebreeding material rather than the direct development of new commercial cultivars.

Notably, the adoption of *de novo*-domesticated prebreeding material also presents challenges. These include reconciling the differences between wild and cultivated crops in valuable agronomic traits, which is essential for developing commercially viable agricultural products. However, bridging the gap between wild and cultivated crops in terms of grain size, weight, and quality may be more feasible than enhancing these traits starting from an existing cultivated gene pool (Hebelstrup, 2017). The combination of high-throughput image phenotyping and *de novo* domestication constructs a framework where initially, complex but desirable traits for drought tolerance, such as sustained photosynthesis, are integrated into the breeding pool. Subsequently, breeders can fine-tune the selected lines to meet specific market demands and agricultural needs. This strategy can revolutionize crop development to make it more adaptable to the changing climate and capable of meeting the growing global food demand.

Acknowledgements

We express our gratitude to Dr Richard Richards for providing feedback on earlier drafts of this manuscript. We thank the Crop Genetics and Molecular Evolution Lab (GropGEM) at the University of Melbourne for providing invaluable discussions on the conceptual framework of this paper. LMG-E was supported by the Research Training Scholarship provided by the University of Melbourne and the Department of Education of the Australian Government. This paper was partly supported by Australian Research Council grants to MP (DP220102271). PH was supported by project P18-RT-992 (Junta de Andalucia, Spain, co-funded by FEDER). Open access publishing facilitated by The University of Melbourne, as part of the Wiley - The University of Melbourne agreement via the Council of Australian University Librarians.

Competing interests

None declared.

Author contributions

LMG-E and MP conceptualized the idea. LMG-E wrote the first draft of the manuscript with contributions from MP, SS, JH, AG and PJZ-T. CC and PH contributed with the experimental data necessary to validate the proposed approach. All authors revised and approved the final version of the manuscript for publication.

ORCID

Carlos Camino https://orcid.org/0000-0001-5188-4406
Luis M. Guadarrama-Escobar https://orcid.org/0009-0009-5983-0010
Allison Gurung https://orcid.org/0000-0001-5857-5366
Pilar Hernandez https://orcid.org/0000-0001-5166-4454
James Hunt https://orcid.org/0000-0003-2884-5622
Mohammad Pourkheirandish https://orcid.org/0000-0003-4337-3600
Sergey Shabala https://orcid.org/0000-0003-2345-8981
Pablo J. Zarco-Tejada https://orcid.org/0000-0003-1433-6165

Data availability

Data are available in the articles Supporting Information.

Luis M. Guadarrama-Escobar[1], James Hunt[1], Allison Gurung[1], Pablo J. Zarco-Tejada[1,2,3], Sergey Shabala[4,5], Carlos Camino[6], Pilar Hernandez[3] and Mohammad Pourkheirandish[1]*

[1]School of Agriculture, Food and Ecosystem Sciences (SAFES), University of Melbourne, Melbourne, Vic., 3010, Australia; [2]Department of Infrastructure Engineering (IE), Faculty of Engineering and Information Technology (FEIT), University of Melbourne, Melbourne, Vic., 3010, Australia; [3]Institute for Sustainable Agriculture (IAS), Spanish Council for Scientific Research (CSIC), Cordoba, 14004, Spain; [4]School of Biological Sciences, University of Western Australia, Perth, WA, 6009, Australia; [5]International Research Centre for Environmental Membrane Biology, Foshan University, Foshan, 528000, China; [6]Joint Research Centre (JRC), European Commission (EC), Ispra, 21027, Italy
(*Author for correspondence: email: mohammad.p@unimelb.edu.au)

References

Abdolshahi R, Nazari M, Safarian A, Sadathossini TS, Salarpour M, Amiri H. 2015. Integrated selection criteria for drought tolerance in wheat (*Triticum aestivum L.*) breeding programs using discriminant analysis. *Field Crops Research* **174**: 20–29.

Adam D. 2021. How far will global population rise? Researchers can't agree. *Nature* **597**: 462–465.

Aliniaeifard S, van Meeteren U. 2014. Natural variation in stomatal response to closing stimuli among *Arabidopsis thaliana* accessions after exposure to low VPD as a tool to recognize the mechanism of disturbed stomatal functioning. *Journal of Experimental Botany* **65**: 6529–6542.

Araus JL, Kefauver SC, Zaman-Allah M, Olsen MS, Cairns JE. 2018. Translating high-throughput phenotyping into genetic gain. *Trends in Plant Science* **23**: 451–466.

Bacon M, ed. 2004. *Water use efficiency in plant biology. Biological Sciences.* Oxford, UK: Blackwell.

Bertolino LT, Caine RS, Gray JE. 2019. Impact of stomatal density and morphology on water-use efficiency in a changing world. *Frontiers in Plant Science* **10**: 1–11.

Blum A. 2009. Effective use of water (EUW) and not water-use efficiency (WUE) is the target of crop yield improvement under drought stress. *Field Crops Research* **112**: 119–123.

Blum A. 2011. Drought resistance and its improvement. In: *Plant breeding for water-limited environments*. New York, NY, USA: Springer Science+Business Media, 53–152.

Bose J, Rodrigo-Moreno A, Shabala S. 2014. ROS homeostasis in halophytes in the context of salinity stress tolerance. *Journal of Experimental Botany* **65**: 1241–1257.

Camino C, Gonzalez-Dugo V, Hernandez P, Zarco-Tejada PJ. 2019. Radiative transfer Vcmax estimation from hyperspectral imagery and SIF retrievals to assess photosynthetic performance in rainfed and irrigated plant phenotyping trials. *Remote Sensing of Environment* **231**: 1–15.

Condon A, Richards R. 1992. Broad sense heritability and genotype x environment interaction for carbon isotope discrimination in field-grown wheat. *Australian Journal of Agricultural Research* **43**: 921–934.

Condon AG, Richards RA, Rebetzke GJ, Farquhar GD. 2002. Improving intrinsic water-use efficiency and crop yield. *Crop Science* **42**: 122–131.

Crossa J, Montesinos-López OA, Pérez-Rodríguez P, Costa-Neto G, Fritsche-Neto R, Ortiz R, Martini JWR, Lillemo M, Montesinos-López A, Jarquin D *et al.* 2022. Genome and environment based prediction models and methods of complex traits incorporating genotype × environment interaction. In: Ahmadi N, Bartholomé J, eds. *Prediction of complex traits methods and protocols*. Berlin, Germany: Springer, 245–283.

Das S, Christopher J, Apan A, Roy Choudhury M, Chapman S, Menzies NW, Dang YP. 2021. UAV-thermal imaging and agglomerative hierarchical clustering techniques to evaluate and rank physiological performance of wheat genotypes on sodic soil. *ISPRS Journal of Photogrammetry and Remote Sensing* **173**: 221–237.

Dechant B, Cuntz M, Vohland M, Schulz E, Doktor D. 2017. Estimation of photosynthesis traits from leaf reflectance spectra: correlation to nitrogen content as the dominant mechanism. *Remote Sensing of Environment* **196**: 279–292.

Deery DM, Rebetzke GJ, Jimenez-Berni JA, James RA, Condon AG, Bovill WD, Hutchinson P, Scarrow J, Davy R, Furbank RT. 2016. Methodology for high-throughput field phenotyping of canopy temperature using airborne thermography. *Frontiers in Plant Science* **7**: 1–13.

Demidchik V. 2015. Mechanisms of oxidative stress in plants: from classical chemistry to cell biology. *Environmental and Experimental Botany* **109**: 212–228.

Farquhar GD, Richards RA. 1984. Isotopic composition of plant carbon correlates with water-use efficiency of wheat genotypes. *Functional Plant Biology* **11**: 539–552.

Farquhar GD, von Caemmerer S, Berry JA. 1980. A biochemical model of photosynthetic CO_2 assimilation in leaves of C_3 species. *Planta* **149**: 78–90.

Flohr BM, Hunt JR, Kirkegaard JA, Evans JR, Swan A, Rheinheimer B. 2018. Genetic gains in NSW wheat cultivars from 1901 to 2014 as revealed from synchronous flowering during the optimum period. *European Journal of Agronomy* **98**: 1–13.

French RJ, Schultz JE. 1984. Water use efficiency of wheat in a Mediterranean-type environment. I. The relation between yield, water use and climate. *Australian Journal of Agricultural Research* **35**: 743–764.

Gálvez S, Mérida-García R, Camino C, Borrill P, Abrouk M, Ramírez-González RH, Biyiklioglu S, Amil-Ruiz F, Dorado G, Budak H *et al.* 2019. Hotspots in the genomic architecture of field drought responses in wheat as breeding targets. *Functional & Integrative Genomics* **19**: 295–309.

Gonzalez-Dugo V, Lopez-Lopez M, Espadafor M, Orgaz F, Testi L, Zarco-Tejada P, Lorite IJ, Fereres E. 2019. Transpiration from canopy temperature: implications for the assessment of crop yield in almond orchards. *European Journal of Agronomy* **105**: 78–85.

Gregersen PL, Culetic A, Boschian L, Krupinska K. 2013. Plant senescence and crop productivity. *Plant Molecular Biology* **82**: 603–622.

Handley LL, Nevo E, Raven JA, Martínez-Carrasco R, Scrimgeour CM, Pakniyat H, Forster BP. 1994. Chromosome 4 controls potential water use efficiency ($\delta^{13}C$) in barley. *Journal of Experimental Botany* **45**: 1661–1663.

Hasanuzzaman M, Zhou M, Shabala S. 2023. How does stomatal density and residual transpiration contribute to osmotic stress tolerance? *Plants* **12**: 1–19.

Havrlentová M, Kraic J, Gregusová V, Kovácsová B. 2021. Drought stress in cereals – a review. *Agriculture (Pol'nohospodárstvo)* **67**: 47–60.

Hebelstrup KH. 2017. Differences in nutritional quality between wild and domesticated forms of barley and emmer wheat. *Plant Science* **256**: 1–4.

Hepworth C, Doheny-Adams T, Hunt L, Cameron DD, Gray JE. 2015. Manipulating stomatal density enhances drought tolerance without deleterious effect on nutrient uptake. *New Phytologist* **208**: 336–341.

Hughes J, Hepworth C, Dutton C, Dunn Jessica A, Hunt L, Stephens J, Waugh R, Cameron Duncan D, Gray Julie E. 2017. Reducing stomatal density in barley improves drought tolerance without impacting on yield. *Plant Physiology* **174**: 776–787.

Jacquemoud S, Verhoef W, Baret F, Bacour C, Zarco-Tejada PJ, Asner GP, François C, Ustin SL. 2009. PROSPECT+SAIL models: a review of use for vegetation characterization. *Remote Sensing of Environment* **113**: S56–S66.

Kang J, Yue L, Wang S, Zhao W, Bao A. 2016. Na compound fertilizer stimulates growth and alleviates water deficit in the succulent xerophyte *Nitraria tangutorum* (Bobr) after breaking seed dormancy. *Soil Science and Plant Nutrition* **62**: 489–499.

Kar S, Tanaka R, Korbu LB, Kholová J, Iwata H, Durbha SS, Adinarayana J, Vadez V. 2020. Automated discretization of 'transpiration restriction to increasing VPD' features from outdoors high-throughput phenotyping data. *Plant Methods* **16**: 140.

Kim G, Ryu H, Sung J. 2022. Hormonal crosstalk and root suberization for drought stress tolerance in plants. *Biomolecules* **12**: 1–16.

Langridge P, Reynolds M. 2021. Breeding for drought and heat tolerance in wheat. *Theoretical and Applied Genetics* **134**: 1753–1769.

Langridge P, Waugh R. 2019. Harnessing the potential of germplasm collections. *Nature Genetics* **51**: 200–201.

Liu Q, Gu X, Chen X, Mumtaz F, Liu Y, Wang C, Yu T, Zhang Y, Wang D, Zhan Y. 2022. Soil moisture content retrieval from remote sensing data by artificial neural network based on sample optimization. *Sensors* **22**: 1–21.

Long SP, Marshall-Colon A, Zhu X-G. 2015. Meeting the global food demand of the future by engineering crop photosynthesis and yield potential. *Cell* **161**: 56–66.

Maia RF, Lurbe CB, Hornbuckle J. 2022. Machine learning approach to estimate soil matric potential in the plant root zone based on remote sensing data. *Frontiers in Plant Science* **13**: 1–16.

Mammadov J, Buyyarapu R, Guttikonda SK, Parliament K, Abdurakhmonov IY, Kumpatla SP. 2018. Wild relatives of maize, rice, cotton, and soybean: treasure troves for tolerance to biotic and abiotic stresses. *Frontiers in Plant Science* **9**: 1–21.

Maurel C, Boursiac Y, Luu D-T, Santoni V, Shahzad Z, Verdoucq L. 2015. Aquaporins in plants. *Physiological Reviews* **95**: 1321–1358.

Mishina K, Suzuki T, Oono Y, Yamashita Y, Zhu H, Ogawa T, Ohta M, Doman K, Xu W, Takahashi D *et al.* 2023. Wheat *Ym2* originated from *Aegilops sharonensis* and confers resistance to soil-borne *Wheat yellow mosaic virus* infection to the roots. *Proceedings of the National Academy of Sciences, USA* **120**: 1–11.

Morton MJL, Awlia M, Al-Tamimi N, Saade S, Pailles Y, Negrão S, Tester M. 2019. Salt stress under the scalpel – dissecting the genetics of salt tolerance. *The Plant Journal* **97**: 148–163.

Phathutshedzo-Eugene R, Mohamed AMAE, Elhadi A, Johannes George C, Gang L, Eric Benjamin E. 2023. Determination of soil electrical conductivity and moisture on different soil layers using electromagnetic techniques in irrigated arid environments in South Africa. *Water* **15**: 1–23.

Pourkheirandish M, Golicz AA, Bhalla PL, Singh MB. 2020. Global role of crop genomics in the face of climate change. *Frontiers in Plant Science* **11**: 922.

Razzaq A, Wani SH, Saleem F, Yu M, Zhou M, Shabala S. 2021. Rewilding crops for climate resilience: economic analysis and *de novo* domestication strategies. *Journal of Experimental Botany* **72**: 6123–6139.

Resende RT, Piepho H-P, Rosa GJM, Silva-Junior OB, e Silva FF, de Resende MDV, Grattapaglia D. 2021. Enviromics in breeding: applications and perspectives on envirotypic-assisted selection. *Theoretical and Applied Genetics* **134**: 95–112.

Richards RA. 2022. Drought. In: Reynolds MP, Braun H-J, eds. *Wheat improvement: food security in a changing climate*. Berlin, Germany: Springer, 417–432.

Robertson BC, He T, Li C. 2021. The genetic control of stomatal development in barley: new solutions for enhanced water-use efficiency in drought-prone environments. *Agronomy* **11**: 1–24.

Serbin SP, Dillaway DN, Kruger EL, Townsend PA. 2012. Leaf optical properties reflect variation in photosynthetic metabolism and its sensitivity to temperature. *Journal of Experimental Botany* **63**: 489–502.

Sexton TM, Steber CM, Cousins AB. 2021. Leaf temperature impacts canopy water use efficiency independent of changes in leaf level water use efficiency. *Journal of Plant Physiology* **258–259**: 1–10.

Shabala S. 2013. Learning from halophytes: physiological basis and strategies to improve abiotic stress tolerance in crops. *Annals of Botany* **112**: 1209–1221.

Sharkey TD, Bernacchi CJ, Farquhar GD, Singsaas EL. 2007. Fitting photosynthetic carbon dioxide response curves for C_3 leaves. *Plant, Cell & Environment* **30**: 1035–1040.

Shekoofa A, Sinclair TR. 2018. Aquaporin activity to improve crop drought tolerance. *Cell* **7**: 123.

Singh S, Jighly A, Sehgal D, Burgueño J, Joukhadar R, Singh SK, Sharma A, Vikram P, Sansaloni CP, Govindan V *et al.* 2021. Direct introgression of untapped diversity into elite wheat lines. *Nature Food* **2**: 819–827.

Slafer GA, Savin R, Sadras VO. 2023. Wheat yield is not causally related to the duration of the growing season. *European Journal of Agronomy* **148**: 1–8.

Suarez L, González-Dugo V, Camino C, Hornero A, Zarco-Tejada PJ. 2021. Physical model inversion of the green spectral region to track assimilation rate in almond trees with an airborne nano-hyperspectral imager. *Remote Sensing of Environment* **252**: 1–16.

van der Tol C, Verhoef W, Rosema A. 2009. A model for chlorophyll fluorescence and photosynthesis at leaf scale. *Agricultural and Forest Meteorology* **149**: 96–105.

Ustin SL, Gitelson AA, Jacquemoud S, Schaepman M, Asner GP, Gamon JA, Zarco-Tejada P. 2009. Retrieval of foliar information about plant pigment systems from high resolution spectroscopy. *Remote Sensing of Environment* **113**: S67–S77.

Xi J-J, Chen H-Y, Bai W-P, Yang R-C, Yang P-Z, Chen R-J, Hu T-M, Wang S-M. 2018. Sodium-related adaptations to drought: new insights from the xerophyte plant *Zygophyllum xanthoxylum*. *Frontiers in Plant Science* **9**: 1–15.

Xiaoyu Z, Sean Reynolds M-R, Alex W, Andries P, Andrew B, Colleen H, David J, Yan Z, Scott C, Graeme H *et al.* 2022. Estimating photosynthetic attributes from high-throughput canopy hyperspectral sensing in sorghum. *Plant Phenomics* **2022**: 1–18.

Xu Y. 2016. Envirotyping for deciphering environmental impacts on crop plants. *Theoretical and Applied Genetics* **129**: 653–673.

Yang C, Zhang D, Li X, Shi Y, Shao Y, Fang B, Yue J, Wang H, Qin F, Cheng H. 2021. Drought effects on photosynthetic performance of two wheat cultivars contrasting in drought. *New Zealand Journal of Crop and Horticultural Science* **49**: 17–29.

Supporting Information

Additional Supporting Information may be found online in the Supporting Information section at the end of the article.

Methods S1 Statistical analysis of iTE from Camino *et al.* (2019) Santaella experiment.

Table S1 Physiological traits and yield data for six commercial wheat varieties (*Triticum* spp.) obtained via hyperspectral and thermal imaging at the stem elongation stage of the Santaella experiment from Camino *et al.* (2019).

Please note: Wiley is not responsible for the content or functionality of any Supporting Information supplied by the authors. Any queries (other than missing material) should be directed to the *New Phytologist* Central Office.

Key words: *de novo* domestication, high-throughput imaging, stomata, transpiration efficiency, water use efficiency, wild relatives.

Received, 14 August 2023; accepted, 22 January 2024.